

University of Windsor

## Scholarship at UWindor

---

Electronic Theses and Dissertations

Theses, Dissertations, and Major Papers

---

2017

# A Multibody Dynamics Model of a Motorcycle with a Multi-link Front Suspension

Changdong Liu  
*University of Windsor*

Follow this and additional works at: <https://scholar.uwindsor.ca/etd>

---

### Recommended Citation

Liu, Changdong, "A Multibody Dynamics Model of a Motorcycle with a Multi-link Front Suspension" (2017). *Electronic Theses and Dissertations*. 7376.  
<https://scholar.uwindsor.ca/etd/7376>

This online database contains the full-text of PhD dissertations and Masters' theses of University of Windsor students from 1954 forward. These documents are made available for personal study and research purposes only, in accordance with the Canadian Copyright Act and the Creative Commons license—CC BY-NC-ND (Attribution, Non-Commercial, No Derivative Works). Under this license, works must always be attributed to the copyright holder (original author), cannot be used for any commercial purposes, and may not be altered. Any other use would require the permission of the copyright holder. Students may inquire about withdrawing their dissertation and/or thesis from this database. For additional inquiries, please contact the repository administrator via email ([scholarship@uwindsor.ca](mailto:scholarship@uwindsor.ca)) or by telephone at 519-253-3000ext. 3208.

A MULTIBODY DYNAMICS MODEL OF A MOTORCYCLE WITH A MULTI-LINK  
FRONT SUSPENSION

by  
Changdong Liu

A Thesis  
Submitted to the Faculty of Graduate Studies  
through Mechanical Engineering  
in Partial Fulfilment of the Requirements for  
the Degree of Master of Applied Science at the  
University of Windsor

Windsor, Ontario, Canada

©2017 Changdong Liu

A Multibody Dynamics Model of a Motorcycle with a Multi-link Front Suspension

by

Changdong Liu

APPROVED BY

---

S. Cheng  
Department of Civil and Environmental Engineering

---

J. Johrendt  
Department of Mechanical, Automotive, & Materials Engineering

---

B. Minaker, Advisor  
Department of Mechanical, Automotive, & Materials Engineering

November 3, 2017

# Author's Declaration of Originality

I hereby certify that I am the sole author of this thesis and that no part of this thesis has been published or submitted for publication.

I certify that, to the best of my knowledge, my thesis does not infringe upon anyone's copyright nor violate any proprietary rights and that any ideas, techniques, quotations, or any other material from the work of other people included in my thesis, published or otherwise, are fully acknowledged in accordance with the standard referencing practices. Furthermore, to the extent that I have included copyrighted material that surpasses the bounds of fair dealing within the meaning of the Canada Copyright Act, I certify that I have obtained a written permission from the copyright owner(s) to include such material(s) in my thesis and have included copies of such copyright clearances to my appendix.

I declare that this is a true copy of my thesis, including any final revisions, as approved by my thesis committee and the Graduate Studies office, and that this thesis has not been submitted for a higher degree to any other University or Institution.

# Abstract

The development of motorcycles has been around for over a century. Nowadays, it has become one of the most popular means of transportation in the world. It is well known that the telescopic fork is the most widely used front suspension for motorcycles, because the first motorcycle was a bicycle with a small engine attached to the frame. However, there are a number of shortcomings inherent in this design. Therefore, a novel multi-link suspension has been designed for the front assembly of the motorcycle in this research. In order to compare the performance between telescopic fork and multi-link front suspension motorcycles, linear and nonlinear models were built and simulated under a variety of different conditions. Furthermore, an appropriate method of comparison between conventional and multi-link models was developed, and the assessment standard of performance for conventional and multi-link models was explored in this research.

*To my mother,  
for her marvelous love and support.*

# Acknowledgements

This thesis writing is nearing its end. Looking back over the past two years, many people have given me support and made this work possible, it is hard to thank all those people enough for their contributions and advice. I am always grateful for their help.

First and foremost, my deepest gratitude to my advisor Dr. B.P. Minaker, for his excellent erudition, altruism and patience. Under his instruction and help, the last two years of my MASc career is the best experience I have ever had. I am very honored to have an advisor who gave me the freedom to explore and has inspired me to be positive and confident during my demanding MASc student life. His patience and guidance helped me to complete a number of research projects. I am often attracted by his easy to understand and interesting teaching method, which also expanded my knowledge and is very helpful in finishing my thesis. I will never be able to adequately express my gratitude.

I would like to thank my mother, and my family. With their support and encouragement, I can go further along the way of my choice. They give me selfless love; home is always my strongest shield and source of strength. I would also like to express my appreciation to all my friends; it was always a pleasure coming to work every day with such lovely and engaging people.

Moreover, I would like to express my sincere gratitude to my thesis committee members who have offered very valuable opinions and suggestions.

# Contents

Declaration of Originality	iii
Abstract	iv
Dedication	v
Acknowledgements	vi
List of Tables	x
List of Figures	xii
List of Abbreviations	xvi
Nomenclature	xvii
<b>1 Introduction</b>	<b>1</b>
1.1 Background . . . . .	3
1.1.1 Development of the Bicycle . . . . .	3
1.1.2 Development of the Motorcycle . . . . .	7
1.1.3 Motorcycle Front Suspension . . . . .	12
1.1.4 Patent Search . . . . .	16
<b>2 Motivation, Objectives, and Thesis Structure</b>	<b>20</b>
2.1 Motivation . . . . .	20
2.2 Research Objectives . . . . .	21
2.2.1 Comparisons of Simulations and Experiment . . . . .	22
2.3 Thesis Structure . . . . .	24
<b>3 Motorcycle Dynamics and Modeling</b>	<b>26</b>
3.1 Kinematics of Motorcycles . . . . .	26



---

3.1.1	The Geometry of Motorcycles . . . . .	28
3.1.2	Kinematics of the Steering Mechanism . . . . .	30
3.1.3	Roll Motion and Steering . . . . .	32
3.2	Out-of-plane Modes . . . . .	33
3.3	In-plane Modes . . . . .	35
3.3.1	In-plane Dynamics Model . . . . .	35
3.4	Front Suspension Structure and Characteristics . . . . .	38
3.5	Motorcycle Tires . . . . .	43
3.6	Multibody Dynamics . . . . .	47
3.6.1	Model in EoM Software . . . . .	48
3.6.2	Model in Altair MotionView® . . . . .	51
3.7	Generation of a Random Road . . . . .	53
<b>4</b>	<b>Simulation Results</b> . . . . .	<b>55</b>
4.1	Kinematics Simulation . . . . .	55
4.2	Tire Test . . . . .	57
4.3	Out-of-plane Simulation . . . . .	59
4.3.1	Unforced Straight Running Simulation . . . . .	59
4.3.2	Forced Straight Running Simulation . . . . .	66
4.4	In-plane Simulation . . . . .	69
4.4.1	Braking Simulation . . . . .	70
4.4.2	Plank Road Simulation . . . . .	78
4.4.3	Random Road Simulation . . . . .	80
<b>5</b>	<b>Discussion of Results</b> . . . . .	<b>96</b>
5.1	Model Assesment . . . . .	96
5.1.1	Caster Angle and Trail . . . . .	97
5.1.2	Motorcycle Tire . . . . .	97
5.2	Out-of-plane Simulation Analysis . . . . .	97
5.2.1	Unforced Straight Running Simulation Analysis . . . . .	98
5.2.2	Forced Straight Running Simulation Analysis . . . . .	102
5.3	In-plane Simulation Analysis . . . . .	106
5.3.1	Braking Simulation Analysis . . . . .	106
5.3.2	Plank Road Simulation Analysis . . . . .	112
5.3.3	Random Road Simulation Analysis . . . . .	113

---

<b>6</b>	<b>Conclusions, Recommendations, and Contributions</b>	<b>122</b>
6.1	Conclusions . . . . .	122
6.2	Recommendations . . . . .	123
6.3	Contributions . . . . .	124
	<b>References</b>	<b>127</b>
	<b>Appendix A</b>	<b>131</b>
A.1	MATLAB <sup>®</sup> Codes of Random Road . . . . .	131
A.2	MATLAB <sup>®</sup> Codes of Power Spectral Density . . . . .	133
	<b>Appendix B</b>	<b>134</b>
B.1	Eigenvalues, Natural Frequency, Damping Ratio of Telescopic Front Suspension at 5 m/s . .	134
B.2	Eigenvalues, Natural Frequency, Damping Ratio of Telescopic Front Suspension at 10 m/s . .	135
B.3	Eigenvalues, Natural Frequency, Damping Ratio of Telescopic Front Suspension at 40 m/s . .	137
B.4	Eigenvalues, Natural Frequency, Damping Ratio of Multi-link Front Suspension at 5 m/s . .	138
B.5	Eigenvalues, Natural Frequency, Damping Ratio of Multi-link Front Suspension at 10 m/s . .	139
B.6	Eigenvalues, Natural Frequency, Damping Ratio of Multi-link Front Suspension at 40 m/s . .	140
	<b>Appendix C</b>	<b>141</b>
C.1	Braking Simulation Results with 100 Nm Braking Torque . . . . .	141
C.2	Braking Simulation Results with 800 Nm Braking Torque . . . . .	144
	<b>Vita Auctoris</b>	<b>147</b>

# List of Tables

3.1	Degrees of freedom of the basic motorcycle model . . . . .	27
3.2	Degrees of freedom of the advanced motorcycle model . . . . .	27
3.3	Parameters of 180/55 tire . . . . .	46
3.4	Body CG locations and mass . . . . .	49
3.5	Body inertia properties . . . . .	49
3.6	Body CG locations and mass . . . . .	50
3.7	Body inertia properties . . . . .	50
3.8	ISO Road roughness values classification . . . . .	54
4.1	Tire test result . . . . .	58
4.2	Eigenvalues of telescopic front suspension at 25 m/s . . . . .	61
4.3	Natural frequency, damping ratio at 25 m/s . . . . .	61
4.4	Eigenvalues of multi-link front suspension at 25 m/s . . . . .	63
4.5	Natural frequency, damping ratio at 25 m/s . . . . .	63
4.6	Motorcycles performance . . . . .	66
4.7	1 Nm straight running linear analysis . . . . .	68
4.8	Telescopic non-linear yaw result . . . . .	69
4.9	Multi-link non-linear yaw result . . . . .	69
4.10	Telescopic braking results . . . . .	73
4.11	Multi-link braking results . . . . .	74
4.12	Caster angle and trail, telescopic suspension . . . . .	77
4.13	Caster angle and trail, multi-link suspension . . . . .	78
5.1	Frequency of bounce and pitch . . . . .	101
5.2	Frequency of wobble and weave modes . . . . .	101
5.3	Vertical force . . . . .	110
5.4	10 m/s frame height . . . . .	114
5.5	30 m/s frame height . . . . .	115

---

5.6	10 m/s pitch angle . . . . .	116
5.7	30 m/s pitch angle . . . . .	116
5.8	10 m/s suspension travel . . . . .	118
5.9	30 m/s suspension travel . . . . .	118
B.1	Eigenvalues of telescopic front suspension at 5 m/s . . . . .	134
B.2	Natural frequency, damping ratio at 5 m/s . . . . .	135
B.3	Eigenvalues of telescopic front suspension at 10 m/s . . . . .	135
B.4	Natural frequency, damping ratio at 10 m/s . . . . .	136
B.5	Eigenvalues of telescopic front suspension at 40 m/s . . . . .	137
B.6	Natural frequency, damping ratio at 40 m/s . . . . .	137
B.7	Eigenvalues of Multi-link front suspension at 5 m/s . . . . .	138
B.8	Natural frequency, damping ratio at 5 m/s . . . . .	138
B.9	Eigenvalues of Multi-link front suspension at 10 m/s . . . . .	139
B.10	Natural frequency, damping ratio at 10 m/s . . . . .	139
B.11	Eigenvalues of Multi-link front suspension at 40 m/s . . . . .	140
B.12	Natural frequency, damping ratio at 40 m/s . . . . .	140

# List of Figures

1.1	Kinematic structure of a motorcycle . . . . .	1
1.2	Schematic diagram of the multi-link front suspension bike . . . . .	2
1.3	The draisine, or running machine . . . . .	3
1.4	Velocipede by Pierre Michaux et Cie . . . . .	4
1.5	Penny farthing, or ordinary . . . . .	5
1.6	Eigenvalues vs speed . . . . .	6
1.7	Sylvester Roper steam motorcycle . . . . .	8
1.8	Daimler petrol-powered motorcycle . . . . .	9
1.9	The Hildebrand and Wolfmüller motorcycle . . . . .	9
1.10	Suzuki <sup>®</sup> GSX-R1000 . . . . .	10
1.11	Tommy Smith riding . . . . .	11
1.12	Hub-center steering . . . . .	12
1.13	Springer forks . . . . .	13
1.14	Upside-down forks . . . . .	13
1.15	Telelever suspension . . . . .	14
1.16	Doulever forks . . . . .	15
1.17	Big Piston suspension . . . . .	15
1.18	Alternate front suspensions . . . . .	16
1.19	EU patent No. 07122393.7 . . . . .	17
1.20	US patent No. 6, 349, 784 . . . . .	18
1.21	US patent No. 8, 851, 221 . . . . .	18
2.1	Schemes of telescopic forks . . . . .	20
2.2	Model validation . . . . .	23
3.1	Geometry of a motorcycle . . . . .	28
3.2	Positive trail . . . . .	29
3.3	Negative trail . . . . .	30

3.4	The steering mechanism . . . . .	31
3.5	Motorcycle in a curve . . . . .	32
3.6	Capsize . . . . .	34
3.7	Wobble . . . . .	34
3.8	Weave . . . . .	35
3.9	The basic model . . . . .	36
3.10	The bounce and pitch model . . . . .	37
3.11	The four degrees of freedom model . . . . .	38
3.12	Telescopic fork structure . . . . .	39
3.13	Reduced stiffness . . . . .	40
3.14	Multi-link front suspension I . . . . .	41
3.15	Multi-link front suspension II . . . . .	42
3.16	Multi-link front suspension III . . . . .	43
3.17	Tire and road . . . . .	43
3.18	The Magic Formula graph . . . . .	45
3.19	180/55 tire lateral force results . . . . .	46
3.20	Telescopic front suspension motorcycle . . . . .	51
3.21	Multi-link front suspension motorcycle . . . . .	52
4.1	The simple 3D model . . . . .	56
4.2	The caster angle and trail . . . . .	56
4.3	Tire lateral force . . . . .	57
4.4	Tire test result . . . . .	59
4.5	Telescopic eigenvalues vs speed . . . . .	60
4.6	Multi-link eigenvalues vs speed . . . . .	62
4.7	Free response at 40 m/s, telescopic suspension . . . . .	65
4.8	Free response at 40 m/s, multi-link suspension . . . . .	65
4.9	Response to 50 Nm 1 Hz steer torque, telescopic suspension I . . . . .	67
4.10	Response to 50 Nm 1 Hz steer torque, telescopic suspension II . . . . .	67
4.11	Response to 50 Nm 1 Hz steer torque, multi-link suspension . . . . .	68
4.12	Euler parameters principle line . . . . .	70
4.13	Forward velocity, 500 Nm braking torque . . . . .	71
4.14	Euler parameter $E_2$ , 500 Nm braking torque . . . . .	72
4.15	Motorcycle height, 500 Nm braking torque . . . . .	73
4.16	Multi-link caster angle test model . . . . .	75
4.17	Multi-link trail test model . . . . .	75
4.18	Caster angle, 500 Nm braking torque . . . . .	76

---

4.19	Trail, 500 Nm braking torque . . . . .	77
4.20	Plank road definition . . . . .	78
4.21	Pitch angle of plank test . . . . .	79
4.22	Frame height of plank test . . . . .	79
4.23	Suspension travel of plank test . . . . .	80
4.24	Random road classification . . . . .	81
4.25	10 m/s telescopic level 6 random road contact force . . . . .	82
4.26	10 m/s multi-link level 6 random road contact force . . . . .	82
4.27	Level 3 random road . . . . .	83
4.28	10 m/s level 3 frame height . . . . .	84
4.29	10 m/s level 3 pitch angle . . . . .	84
4.30	10 m/s level 3 suspension travel . . . . .	85
4.31	Level 4 random road . . . . .	86
4.32	10 m/s level 4 frame height . . . . .	86
4.33	10 m/s level 4 pitch angle . . . . .	87
4.34	10 m/s level 4 suspension travel . . . . .	87
4.35	Level 5 random road . . . . .	88
4.36	10 m/s level 5 frame height . . . . .	88
4.37	10 m/s level 5 pitch angle . . . . .	89
4.38	10 m/s level 5 suspension travel . . . . .	89
4.39	30 m/s telescopic level 5 random road contact force . . . . .	90
4.40	30 m/s multi-link level 5 random road contact force . . . . .	91
4.41	30 m/s level 3 frame height . . . . .	92
4.42	30 m/s level 3 pitch angle . . . . .	92
4.43	30 m/s level 3 suspension travel . . . . .	93
4.44	30 m/s level 4 frame height . . . . .	94
4.45	30 m/s level 4 pitch angle . . . . .	94
4.46	30 m/s level 4 suspension travel . . . . .	95
5.1	Theoretical unforced straight running result . . . . .	98
5.2	Telescopic suspension linear and non-linear result . . . . .	103
5.3	Multi-link suspension linear and non-linear result . . . . .	103
5.4	Telescopic suspension non-linear result . . . . .	104
5.5	Multi-link suspension non-linear result . . . . .	104
5.6	Braking stop time . . . . .	106
5.7	Braking pitch angle . . . . .	107
5.8	Braking frame height . . . . .	108

---

5.9	500 Nm telescopic vertical forces . . . . .	109
5.10	500 Nm multi-link vertical forces . . . . .	109
5.11	Braking caster angle . . . . .	111
5.12	Braking trail . . . . .	112
5.13	30 m/s level 3 frame height difference . . . . .	115
5.14	30 m/s level 4 pitch angle difference . . . . .	117
5.15	30 m/s level 4 suspension travel difference . . . . .	119
5.16	30 m/s level 4 tire compression . . . . .	120
5.17	30 m/s level 4 tire compression difference . . . . .	120
6.1	Performance assessment method . . . . .	125
6.2	Comparison method . . . . .	126
C.1	Forward velocity, 100 Nm braking torque . . . . .	141
C.2	Euler parameter $E_2$ , 100 Nm braking torque . . . . .	142
C.3	Motorcycle height, 100 Nm braking torque . . . . .	142
C.4	Caster angle, 100 Nm braking torque . . . . .	143
C.5	Trail, 100 Nm braking torque . . . . .	143
C.6	Forward velocity, 800 Nm braking torque . . . . .	144
C.7	Euler parameter $E_2$ , 800 Nm braking torque . . . . .	144
C.8	Motorcycle height, 800 Nm braking torque . . . . .	145
C.9	Caster angle, 800 Nm braking torque . . . . .	145
C.10	Trail, 800 Nm braking torque . . . . .	146



# List of Abbreviations

All abbreviations used in this work are described in this section.

## Abbreviations

Abbreviation	Meaning
MATLAB <sup>®</sup>	Matrix Laboratory software
URB	Unridable Bicycle
TiN	A Chemical Element
EoM	Equation of Motion
BMW <sup>®</sup>	Bavarian Motor Works (the German manufacturer)
CAE	Computer Aided Engineering
DAE	Differential Algebraic Equation
ODE	Ordinary Differential Equation
CG	Center of Gravity
RBT	Roller Bench Test
SAE	Society of Automotive Engineers
PSD	Power Spectral Density
ISO	International Standard Organization
DOF	Degree of Freedom
CAD	Computer Aided Design
3D	Three Dimensional
2D	Two Dimensional

# Nomenclature

Mathematical notation throughout this work is listed below.

## Coordinate systems

Label	Description
$(P_r, x, y, z)$	Mobile triad with the origin in the rear contact point $P_r$ , according to SAE J670
$x$	Forward and parallel to the longitudinal plane of symmetry
$y$	Lateral on the right side of the motorcycle
$z$	Downward with respect to the horizontal plane
$(A_r, X_r, Y_r, Z_r)$	Triad attached to rear frame
$a_1$	Parallel to $x$ axis
$a_2$	Parallel to $y$ axis
$a_3$	Parallel to $z$ axis

## Kinematics and dynamics parameters

Label	Description
$V$	Forward velocity
$\xi$	Steering ratio
$\delta$	Steering angle
$\Delta$	Kinematic steering angle
$\Delta^*$	Effective steering angle
$\mu$	Pitch angle of the main frame
$\Psi$	Yaw angle of the main frame

---

$\Omega$	Yaw angular velocity about the $z$ axis
$f$	Frequency
$f_p$	Natural frequency of pitch vibration
$f_b$	Natural frequency of bounce vibration
$V_{\text{slide}}$	Slippage velocity
$\omega_f$	Front wheel rolling angular velocity
$M$	Matrix of mass and inertia terms
$q$	Generalized coordinate
$f$	Applied forces
$\phi$	Constraint vector
$\lambda$	Lagrange multiplier

---

## Motorcycle parameters

---

Label	Description
$a$	Mechanical trail (trail)
$a_n$	Normal trail
$b$	Longitudinal distance from rear axis to the motorcycle mass center
$b_n$	Normal rear trail
$c$	Viscous damping coefficient of suspension
$d$	Fork offset: distance from the center of the front wheel to the steering axis
$h$	Height of motorcycle mass center
$I_{yG}$	Moment of inertia of motorcycle about the $y$ axis through its center of mass (pitch inertia)
$k$	Suspension stiffness
$L$	Swinging arm length
$m$	Motorcycle mass
$p$	Wheelbase
$P$	Tire contact point with the ground
$G$	Motorcycle center of mass
$\Delta_h$	Lowering of the steering head
$\varepsilon$	Caster angle
$\varphi$	Roll angle of the rear frame (camber angle of the rear wheel)

---

$\beta$	Roll angle of the front frame (camber angle of the front wheel)
$\eta$	Chain angle respect to the ground plane

---

## Front frame parameters

---

Label	Description
$b_f$	Distance of the mass center of front frame from steering axis
$h_f$	Distance of the mass center of front frame from the line passing through the rear wheel center and perpendicular to the steering axis
$G_f$	Mass center of front frame
$k_f$	Effective (reduced) front suspension stiffness
$m_f$	Front unsprung mass
$M_f$	Front frame mass
$y$	Travel distance of front wheel along front suspension sliders
$\Delta y$	Deformation of front suspension springs due to preload

---

## Forces and Moments

---

Label	Description
$N_s$	Static load on the wheel
$N$	Dynamic load on the wheel
$N_a$	Normalized dynamic load on the wheel: ratio of the dynamic load to the motorcycle weight
$N_{tr}$	dynamic load transfer
$F$	Braking force
$F$	Lateral force on the tire
$M_X$	Overturning moment
$M_Y$	Rolling resistance moment
$M_Z$	Yawing moment
$M_t$	Twisting moment
$\mu$	braking/driving force coefficient (normalized longitudinal force): ratio of the braking/driving force to the vertical load

---

## Tires and wheels

Label	Description
$a_t$	Tire trail
$d$	Rolling friction parameter
$f_w$	Rolling resistance coefficient
$R$	Outside radius of the tire
$\rho$	Radius of torus revolution of the tire
$t$	Radius of cross section of the tire
$L$	Relaxation length of the tire
$k_p$	Radial stiffness of the tire
$k_s$	Lateral stiffness of the tire
$K_k$	Longitudinal slip stiffness of the tire
$K_\varphi$	Camber (roll) stiffness of the tire
$R_o$	Effective rolling radius
$\lambda$	Sideslip angle of the tire

## Random road parameters

Label	Description
$L$	Length of road profile
$x$	Abscissa variable from 0 to $L$
$\Delta_n$	Frequency band
$B$	Sampling interval
$n_{\max}$	Maximum theoretical sampling spatial frequency
$k$	A constant value depending from ISO road profile classification
$\varphi_i$	Random phase angle following an uniform probabilistic distribution within the $0-2\pi$ range

# Chapter 1

## Introduction

The development of the motorcycle has been ongoing for over a century since the Hildebrand & Wolfmüller, the world's first production motorcycle, came off the assembly line in 1894. Nowadays, to suit lots of different purposes, there is a variety of models of motorcycle available, such as cruisers, sport bikes, tourers, and so on. Joining a motorcycle club or attending motorcycle rallies also has become part of daily life for some people. At the same time, the rider not only needs a comfortable riding experience, but also pursues the sense of freewheeling handling. Thus, scholars have never stopped the pace of innovation and research on motorcycles. The most common style of motorcycle is made up of four parts. They are the rear assembly, the front assembly, the front wheel and the rear wheel. The steering axis and the two wheel axles connect these assemblies by three revolute joints as shown in Figure 1.1.

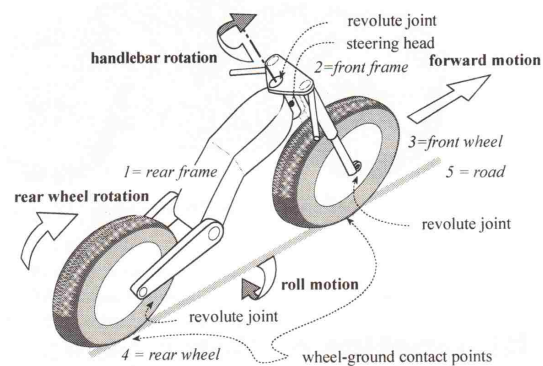


Figure 1.1: Kinematic structure of a motorcycle (reproduced from Cossalter[1])

In this thesis, the research focuses on the front assembly, especially the fork. Differing from the traditional motorcycle model, there are eleven rigid bodies, and a rigid rider assumption in this model. The rigid rider means the rider is assumed to be a rigid body, which is completely fixed on the frame. The parameters are based largely on those given by Sharp et. al.[2]. The front wheel, rear wheel and rear assembly are

unchanged from Sharp's model. A schematic diagram of the proposed suspension configuration is shown in Figure 1.2. In this concept, the steering and suspension kinematics are separated. The mechanism is described by Minaker and Durfy[3] as follows:

The suspension mechanism consists of four locating arms, two on each side of the cycle. The arms are mounted such that they lie in the horizontal plane, one above the other, and are symmetric across the cycle. Each arm is attached to the frame at the rear end, and to the lower fork, or front wheel carrier, at the front end. In practice, the arms would be attached by Heim joints at both ends, but in the model, one spherical joint and one universal joint are used on each arm, to prevent the rotation of the arm around its own axis. The geometry of the arms is such that if the centreline was extended, it would intersect the axis of its opposite side counterpart at a point directly on the steer axis of the front wheel. In fact, it is the geometry of the two intersection points that defines the steer axis. In order to produce the desired geometry, the rear of the arms are spaced wider apart than the front. The upper arms are angled more than the lower, such that their intersection is further back, giving a steer axis that is inclined rearward as in a typical fork arrangement. In the model, the geometry of the arms is chosen such that the values of the effective rake and trail are identical to the conventional fork suspension. The mass and inertia values of the lower fork body are maintained to represent the wheel carrier. The upper fork body is also maintained in the model to represent the handlebars and steering mechanism, but the translational joint representing the telescopic connection to the lower fork is removed. A telescopic steering shaft with universal joints on both ends is used to transmit the steering torque from the upper fork body to the lower fork body. In the multibody model, this shaft is represented by a constraint equation that enforces matching rotation of the upper and lower fork around the steering axis. The front suspension springs are mounted between the upper and lower fork bodies, but are modelled as using spherical joints on both ends.

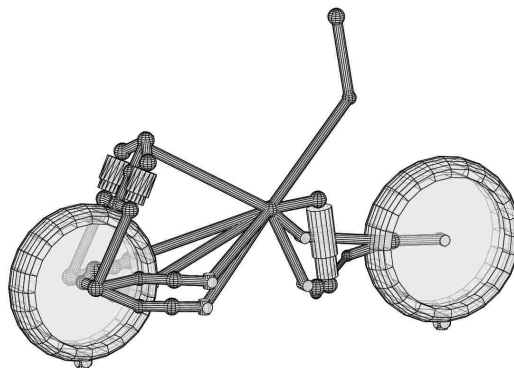


Figure 1.2: Schematic diagram of multibody model of the bike fitted with multi-link front suspension (reproduced from Minaker and Durfy[3])

## 1.1 Background

### 1.1.1 Development of the Bicycle

Dating back to over 300 years ago, human beings had already realized the potential of their own powered transportation[4]. Compared to wind power and horse power, humans using their own strength were free of restrictions posed by environmental limitations and influence. There are two types of mechanism, cranks and levers respectively, which have been used to allow the rider to drive a vehicle. This mechanism can be defined only as a vehicle but not a bicycle, because these early vehicular contraptions[5] were too huge and heavy to be well used. Also, except for using two wheels, they were absolutely different than the next generation of machines.

In 1817, the German inventor Baron Karl von Drais got inspiration from the ice sledge[6]. This vehicle still cannot be described as a bicycle, because it seems just like the ice sledge with two wheels. Thus, it should be called a running machine or draisine[6]. Figure 1.3 shows the draisine from the side perspective. The seat is a long bar that looks like a saddle. During driving, the rider is able to lay his or her arm on a small stuffed rest, which is between the front handle and seat. The power of this draisine comes from the rider's leg movement. The front wheel is steerable. To popularize his machine, von Drais traveled to many European countries. In France, his running machine had a demonstration to show its speed and obstacle performance. After that, the draisine experienced a short period of European popularity. An English designer, Denis Johnson, upgraded the draisine and began to manufacture his product, named the hobby horse, after the draisine spread to England in late 1818[7]. Its boom did not last long. The absence of drive and braking capabilities made this draisine uncomfortable to ride. Furthermore, there is almost no difference between going on foot and riding the draisine.



Figure 1.3: The draisine, or running machine  
(reproduced from Smithsonian National Museum[8])

The most obvious difference between the draisine and bicycle is the pedal mechanism. There is some controversy about the history of the pedal-drive mechanism invention[5]. There are two mainstream opinions



on the inventor responsible. One of them is Kirkpatrick Macmillan, a Scotsman who introduced the first two wheeled pedal-drive mechanism in 1840[4]. Another viewpoint is that in approximately 1861, Pierre Michaux, a French coach builder added pedals on when a rider brought him a broken draisine for repairs. This improvement resulted in a milestone machine in bicycle development, called the Michaux machine. The appearance of the Michaux machine in Figure 1.4 seems very close to a modern bicycle. The total weight of this vehicle is about 60 pounds. This velocipede is very famous, because it was essentially the first time the pedal mechanism had been used on a human-propelled vehicle. This innovation greatly promoted the development of the mobility tool, although this machine was only popular for about three years. Its elimination was due to the extremely uncomfortable ride. One of the most common problems was that the rider's legs were caught by the front wheel when cornering. To overcome this flaw, central hinged frames and rear-steering were tried, but they did not work well[9].



Figure 1.4: Velocipede by Pierre Michaux et Cie of Paris, France circa 1869.  
(reproduced from The Online Bicycle Museum[10])

The popularity of the Michaux machine not only made the public accept this means of transportation, but also awakened their desire for speed. This trend also had ended the velocipede development due to its bulk, its harsh ride, and a poor gear ratio to the driven wheel[7]. At the same, a new type of human-propelled vehicle had been designed (see Figure 1.5). This vehicle was the first to be called a bicycle, and had a very large front wheel and relatively much smaller rear wheel. This different wheel size made the bicycle faster than the velocipede. Most importantly, this whole bicycle is made of metal materials, and was lighter than its predecessor. This bicycle was also the first single-track vehicle in the world with the center-steering head, which is still used today[7]. The huge front wheel with solid rubber tire and long spokes gave a smoother ride and higher speed to the bicycle, which made it very popular among young people. However, this structure also brought some dangerous problems. It is difficult for the rider to mount and dismount, due to the position of the seat. As can be seen from Figure 1.5, the high and forward position of the center of mass puts the entire machine at high risk to rotate forward around its front axle. In the event of a crash, it means that the rider's head can easily contact the ground first.



Figure 1.5: Penny farthing, or ordinary.  
(reproduced from UDC Penny Farthings[11])

Based on the design of the original bicycle, there were many attempts to improve its performance, which made the bicycle what it is today. Some of them had a significant role to play during the development of the bicycle. For example, the pneumatic tire was invented by John Boyd Dunlop in 1899[7]. This new tire increased the speed of the bicycle, especially after the upgrade of the Pneumatic Tyre Company, which developed a stout canvas lining for the inner surface of the tire[5]. The chain and sprocket drive system, another key innovation, improved the efficiency of the actuating unit and has continued to do so[4]. Furthermore, other inventions such as equal size wheels, lightweight stiff steel frames, caliper brakes, sprung seats, front and rear suspension systems, free-running drive hubs, and multispeed Deraileur gear trains made up the current bicycle, and also produced multiple branches, like mountain bikes and road bikes[12].

With the continuous development of bicycles, the theory and technology has also progressed during the same period. It is obvious that the mathematical model of a bicycle is a multibody system. In 1869, there were five consecutive short articles that discussed the dynamics of bicycles. A heuristic inverted-pendulum-type model was built to analyze balancing, steering and propulsion performance of the bicycle[13]. These papers had a little technical value. In fact, they only proved that rear-wheel steering was not suitable for ordinary use in a bicycle.

In 1899, Francis John Welsh Whipple published a seminal paper, which is the first substantial contribution to the theoretical bicycle literature[14]. His achievement became the basis of the following researchers' theory. In this paper, the non-linear differential equations were first set to describe the general motion of a bicycle and rider. Moreover, a torsional steering spring was used to simulate the rider steering torque. However, the solution to Whipple's general non-linear equations could not be computed, as the mathematical capabilities at that time were not enough. As a result, a linear equation was used to analyze small motions around straight running trim conditions at a given constant speed[7].

The basic bicycle model is made up of four parts. Two of them are the front and rear wheels that are free to rotate around their axles, which are rigidly attached to the front and rear frames respectively. Each wheel is assumed to be thin and touch with the ground only at a single contact point. Also, the wheels, which are also assumed to be non-slipping, are modeled by holonomic constraints in the normal (vertical) direction and by nonholonomic constraints in the longitudinal and lateral directions[15]. The rear frame can translate in three axial directions and also has roll motion around the longitudinal axis. Nowadays, the analysis of bicycle motion usually needs to consider the aerodynamics, frame flexibility and suspension system, but it is impossible to do these analyses at the time when the original bicycle dynamics theory was born. Under the constant speed assumption, the Routh criteria was used to deduce the stability implications associated with the equation of motion[7]. The quartic equation calculation is relatively much simpler today. The dynamic properties of a forward- and reverse-running bicycle as a function of speed can be seen in Figure 1.6. This graph was produced using MATLAB<sup>®</sup> software.

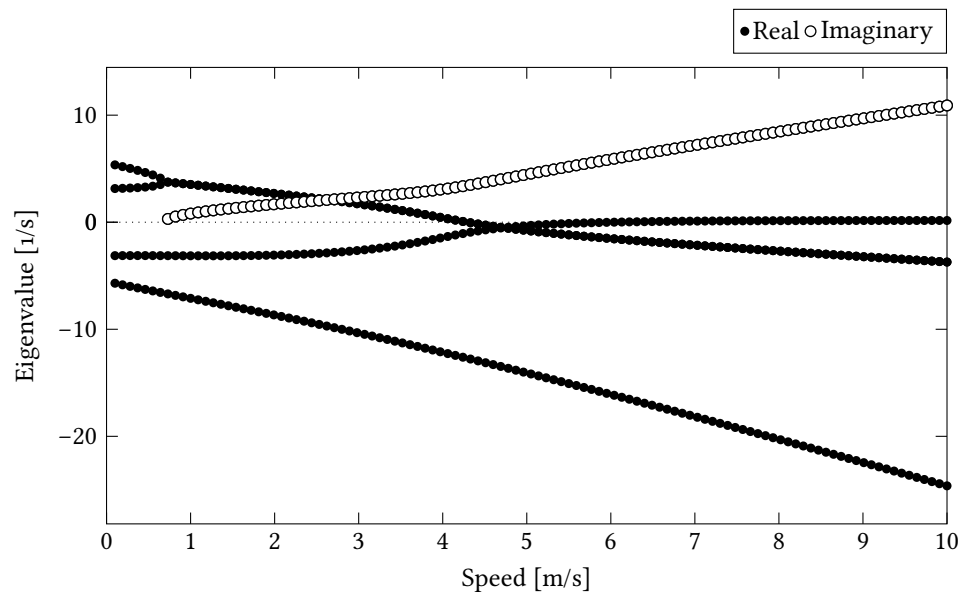


Figure 1.6: Real and imaginary parts of the eigenvalues of the straight-running Whipple bicycle model as functions of speed.

At the same time as Whipple's discovery, there were some surveys related to the motion between the front frame and wheel. To be more precise, the effect of the gyroscopic moment resulting from the front wheel on the free-steering stability was studied. Carvallo[16] built a free-steering bicycle linearized model and derived its equations of motion. Also, Klein and Sommerfeld[17] built a straight-running bicycle model, which integrated all the front wheel assembly parts into the front wheel. However, from a practical point of view, this survey did not have much value, because the instability of the front wheel can easily be replaced by low-bandwidth rider control action[18].

Another important element of the bicycle dynamics research is the tire. The concept of the bicycle with side-slipping and force-generating tires first appeared in an article from Roland[19]. Neimark and Fufaev[20] added the pneumatic tires to the straight-running bicycle model, which was used to analyze the stability. After that, some different tire models have been proposed by Hand[21] and Schwab[22]. On the other hand, some interesting bicycle-related experiments, utilizing control theory knowledge have been developed by Astrom[23].

There is also a novel experiment worth some attention. The ‘Unridable Bicycle’ model was developed in the context of bicycle dynamics[18]. The most obvious feature of this model is the cancellation of the front wheel gyroscopic moment using a very slightly smaller counter-rotating wheel mounted alongside the front wheel. However, a series of experiments proved that this bicycle is still very rideable and the cancellation of the gyroscopic moment did not have a significant impact. Meanwhile, this model has also been proved unstable and tested many times with three kinds of changes[18], resulting from the modification of the front-wheel radius and the magnitude and sign of the fork offset.

### 1.1.2 Development of the Motorcycle

The invention of motorcycles began after the development of bicycles and engines. In fact, the first motorcycles were merely bicycles with small engines thrust into the frame[24]. Nowadays, as one of the world’s most popular means of transport, the motorcycle is not the early period monster that was made of metal and solid wood; it is rich in variety, advanced technology and well-made. Comparing with other modes of transport, it has unparalleled advantages. For the businessman, it is a small investment that can deliver goods to earn money. For tourists, it is an economical, convenient and fast way to travel far away. For athletes, it is the most thrilling competition item on the sports field, the ‘nice ride’ with high-speed mechanical power. During nearly 130 years of development, pioneering builders have exhausted their own intelligence and created numerous milestone achievements, leaving their name in the history books.

In 1770, a French man, Nicolas Joseph Cugnot, developed and manufactured the world’s first steam-powered tricycle, which used steam generated from a boiler in front of the vehicle to push a piston in a cylinder to drive the front wheel. This 3.5 km/h speed vehicle, accompanied with loud rumbling and rolling smoke of the steam engine, indicated that human force has gradually replaced natural force to drive the beginning of the vehicle era. In 1868, an American, Sylvester H. Roper, first designed and mounted a boiler on a bike (see Figure 1.7). This steam-powered bike was also equipped with a cylinder, connecting rod, crank arm, exhaust pipe, front brake, and other devices. However, the structure of the vehicle was rough and insecure.

In 1869, the French engineer Pierre Michaux and Louis Guillaume Perreaux also installed a small steam engine that was designed and manufactured on an ‘outdated bike’ for a motorized test. This motorcycle that combined the small steam engine and bicycle actually ran about 16 km from Paris to Saint-Germain. This vehicle made a great deal of progress in decreasing the structural size, and improving ease-of-use. In 1884,

the Copeland brothers in the United States also produced a steam bike prototype called a 'penny-farthing' and then made a commercial motor tricycle. In 1885, Rover designed a diamond-shaped frame and chain drive safety bike, which built a reliable foundation for the subsequent motorcycle frame and transmission system design.



Figure 1.7: Sylvester Roper steam motorcycle.  
(reproduced from The Smithsonian Museum[25])

Although the world's technology pioneers designed and manufactured a variety of steam-type motor vehicles that could also run a short distance, the brake, transmission, ignition, clutch, controls, and other elements of the design of the vehicle were not reliable and safe, and did not even have modern motorcycle basic structural features. Thus, these vehicles could not be successfully mass produced. Over the years, various methods to use the steam engine to power motor vehicles were tried. However, the steam engine power was too small, and most importantly, the engine was too large and very unsafe, and could easily cause injury to the driver.

In 1876, the German Dr. Nikolaus Otto made a great breakthrough in the gasoline engine structural design, and received related patents. In 1883, Dr. Otto's student Gottlieb Daimler re-designed and created a small gasoline engine, capable of running at 700 rev/min. This gasoline engine was installed between the two wheels (see Figure 1.8). The power was transferred from the belt to the intermediate shaft and then from the gear to the rear wheel. The frame and fork were made of wood and iron pipes. The seat was made of wood and its surface was covered by several layers of leather cushions. In addition to the front and rear wheel, two small wooden wheels could also be installed on both sides of the body to enhance the stability of the vehicle. Therefore, this vehicle actually had four wheels on the ground. There were some genius designs that were used in the prototype. For example, a rotating handle with a ratchet decoupling structure was used to control the brake of the rear wheel and the clutch. On November 10, 1885, Daimler's son Paul drove the vehicle from Cannstatt to Untertürkheim, around 9.5 km. He also became the world's first motorcycle driver. Although the original motorcycle was very simple and crude, after 100 years of development, hundreds of millions of modern motorcycles have resulted from continuous change and improvement.



Figure 1.8: Daimler petrol-powered motorcycle.  
(reproduced from The American Society of Mechanical Engineers[26])

In 1893, the Italian engineer Enrico Bernardi designed the world's first motorcycle equipped with four-stroke single-cylinder gasoline engine. In 1894, the water-cooled, two cylinder horizontal parallel and four-stroke gasoline engine with 1488 ml engine displacement was developed by Hildebrand and Wolfmüller. The power of this motorcycle (see Figure 1.9) was 1.84 kW and it was soon put into mass production, becoming the first series production motorcycle.



Figure 1.9: The Hildebrand and Wolfmüller, the world's first mass produced motorcycle  
(reproduced from Hemmings[27])

From the end of the 19<sup>th</sup> century to the early 20<sup>th</sup> century was the heyday of motorcycle innovation development, which also laid the basis for motorcycle products. There have been many famous motorcycle factories, such as the British Invincible<sup>®</sup> and Triumph<sup>®</sup>, the Italian Biaggio<sup>®</sup> and Ducati<sup>®</sup>, the German BMW<sup>®</sup> and Boer<sup>®</sup>, the American Harley<sup>®</sup> and the French Peugeot<sup>®</sup>. A motorcycle is a product of the times, reflecting the level of science and technology at that time. During the two World Wars, a large number of motorcycles were used by the belligerents on the battlefield, which also directly promoted the development of motorcycle production technology. In 1901, the Werner brothers split the front frame of the motorcycle

pedal to fix the engine in the gap. This design changed the weight distribution and reduced the height of the centre of mass. It also used an electronic ignition and jet carburetor. In the next century, most modern motorcycles imitated and evolved from the Werner brothers' design. At the beginning of the 20<sup>th</sup> century, due to the lessons learned from the bicycle, the motorcycle began to enter mass production in the factory and showed its actual value. In fact, from the twenties of the 20<sup>th</sup> century to the present, improvements have become the main theme of the development of motorcycles.



Figure 1.10: Suzuki<sup>®</sup> GSX-R1000. This motorcycle has a maximum output power of approximately 117 kW at 13200 rev/min. The corresponding top speed is in excess of 80 m/s [288 km/h].  
(reproduced from [contramanillar.com](http://contramanillar.com) [tr. [countermeasures.com](http://countermeasures.com)][28])

The modeling and control of a motorcycle are different from the process for a bicycle. There are three main reasons. First of all, the weight of a motorcycle is much larger than that of a bicycle; the difference is about ten times. Secondly, due to the disparate weight, the rider has a different role to play during the model building process between a motorcycle and a bicycle. Thirdly, the speed is also hugely different. Usually, the speed of a bicycle can be around 20 km/h. A modern motorcycle can achieve a top speed of about 180 km/h. For some sport motorcycles, the speed is able to reach even 220 km/h. Under this speed, the modeling process should not only consider the normal dynamics of the bicycle, but should also consider the aerodynamic force analysis.

As mentioned before, Francis John Welsh Whipple[14] provided the main theoretical basis for bicycle dynamics research. In the Whipple study, there is a method named the nondimensional approach[14], which is helpful for the motorcycle to describe its behavior. The foundation of the method is still to establish the quartic characteristic equation. However, the speed and weight of the model change a lot. The nondimensional approach works for this difference, which allows those changes of variable to become independent of the mass and speed units used. It also means that in this restricted sense, an adult riding a motorcycle is dynamically similar to a child riding a bicycle. According to a Limebeer and Sharp paper[7], four rules of a viable motorcycle model have been posed by combining Whipple's theory and their observations. These four rules[7] are as follows:

- Must be consistent with bicycle-like behavior at low speed
- Must reproduce the autostability properties predicted by Whipple[14]
- Must reproduce the motorcycle's inclination to wobble at intermediate and high speeds
- Must reproduce the observed high-speed weave characteristics of high-performance motorcycles

Based on the ideas above, the theory of motorcycle dynamics has been perfected gradually, and some scholars have even done experimental research based on their own experience. Tommy Smith is one of them. He made several high-speed runs at the Bonneville Salt Flats in Utah. To change the load on the front wheel, he had to try some unusual riding position, e.g. as shown in Figure 1.11. In the end, he ran his motorcycle at a very high speed. The front wheel began to wobble for about three to five seconds. At 224 km/h, he finally could not maintain his hold on the handlebars, to prevent himself from falling off. His injuries proved the theory that light riders might be more likely to suffer from the wobble instability.

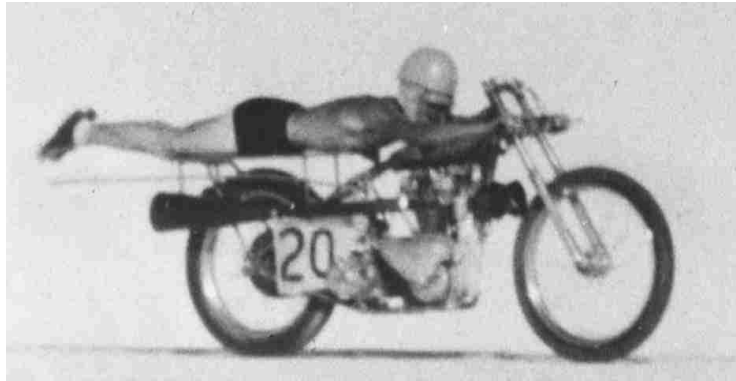


Figure 1.11: Tommy Smith riding a modified 650-cc Triumph Thunderbird at the Bonneville Salt Flats in Utah.  
(reproduced from D.J.N. Limebeer and R.S. Sharp[7])

After that, Limebeer, Sharp and Evangelou[29] confirmed this result by computer simulation studies. Especially in Sharp's 1971 paper[30], which stated that the frequency of wobble motion is typically from 7 Hz to 9 Hz, and acts on the steering system. It also predicted that during low speeds, the wobble mode is well damped, but gradually tends to be lighter damped at high speeds. After Smith's experiments, Spierings[31], and Sharp and Alstead[32] also studied the wobble motion and found that the motorcycle has a tendency to wobble at high speed. With the increasing amount of literature on motorcycle dynamics, the capsize, wobble and weave modes gradually moved up to the central role for describing motorcycle handling qualities. Most importantly, these modes relate to safety, and are connected to several high-profile accidents in the literature[29].

There are two kinds of motions that are usually analyzed for the dynamics of a motorcycle, the in-plane and out-of-plane motions, respectively. In Cossalter and Lot[33], the cornering models and the straight-running models have been built to analyze the two motions above. It is obvious that the former model is more



complex than the latter. In this thesis, based on the research results of the former, the models focused mainly on the straight running case and partly on the cornering case. Some specific theories about motorcycle dynamics will be mentioned and explained in Chapter 3.

### 1.1.3 Motorcycle Front Suspension

When comparing with the motorcycle's rapid technological progress, the improvement of the front suspension is not so obvious. There are mainly two basic functions of a motorcycle suspension system. One is to isolate the bumps in the road, to ensure the comfort of riders and protect passengers' safety. The second is to provide the steering and control motions of the rider with support. The typical configuration of a modern motorcycle front suspension system is the front fork, which is laid on both sides of the front wheel. However, the real needs are much more than the 'typical configuration' can provide. The front suspension system not only needs to adapt to the increases in speed and weight, but also has to satisfy the demands of control quality and stability. Therefore, during the history of the motorcycle development, there have been some attempts to improve the front suspension system.



Figure 1.12: Hub-center steering mechanism.  
(reproduced from ISR Brakes-Sweden[34])

Inherited from the structure of the bicycle, the telescopic front fork has been used for a long time. Even now, it is still the top choice for most motorcycle makers. However, it is undeniable that the defects of this mechanism have gradually been identified by the industry. In 1910, the British James Cycle Company firstly developed the hub-center steering concept. In this structure, the entire steering mechanism is installed inside the wheel hub (see Figure 1.12). Each side of the front wheel has a connecting rod that is used to transfer the handlebar force. To be more precise, the cooperation between the two rods pushing and pulling can produce steering motion of the motorcycle.

Following the 'hardtail' (no rear suspension used at all) choppers popular in the 1960s and 1970s, Harley-Davidson<sup>®</sup> began to equip its traditional motorcycle with a 'springer' style front suspension system[36], as shown in Figure 1.13. Two parallel sets of legs on each side of the front wheel is the characteristic part of this

mechanism. Furthermore, the four-spring shock absorber system is also very interesting. These two pairs of springs are arranged along the front fork separately. During the wheel movement, the upper pair of springs and the lower pair of springs will have opposite motion, compression or stretch respectively.



Figure 1.13: Springer fork suspension.

(reproduced from ZERO Engineering original Springer fork[38])

In the late 1980s, many motorcycle racing teams turned their forks 'upside-down', as seen Figure 1.14, which improved their motorcycles' handling. Upside-down forks are now the standard on many current motorcycles. Comparing to the traditional telescopic front fork, the upside-down fork structure is exactly the opposite. The inner tube is mounted on the lower front axle and the outer tube is mounted in the upper triangular clamp. There are two advantages of this arrangement. One is to reduce the unsprung mass in the suspension system, which is supposed to be light and sensitive for better handling control. The second is the increase of bending rigidity (the larger diameter outer fork tubes are used where the bending moments are highest) that also helps to improve the handling quality. This fork is used mainly for sports type motorcycles, because the cost of the upside-down fork is much more than the traditional fork.



Figure 1.14: Upside-down forks.

(reproduced from Speed Moto Blog[35])

In the early 1980s, the Telelever front suspension system (Figure 1.15) was developed by Saxon-Motodd<sup>®</sup> in Britain. After that, the Telelever is one of the signs for BMW<sup>®</sup> motorcycles. At first glance, the Telelever and telescopic fork appear very similar. In fact, these two structures are quite different.

The telescopic fork is supported by upper and lower triangular clamps, which are in turn attached to the frame by the steering head bearing. The Telelever has only one upper triangular clamp fixed to the frame by a spherical bearing. Instead of the lower triangular clamp, it uses an A-arm hinged to the frame, and fixed to the lower fork by second spherical joint. It is mechanically similar in operation to a MacPherson strut style automotive suspension, except that the A-arm is located above the wheel rather than inside as on a car. This design also allows the slide tube to be longer, that is, the overlap area between the sliding and fixed tube is increased, which helps to improve the front fork rigidity and enhance the stability.



Figure 1.15: Telelever suspension.  
(reproduced from BMW<sup>®</sup> Motorrad[37])

Another advantage of the Telelever is the significant reduction in diving during emergency braking, which makes the anti-lock braking system work smoother. Although the anti-lock braking system will produce a pulsating braking force, the Telelever will not let the rider feel the sense of forward decline, which also enhances stability and the rider's ability to control the steering.

In 2004, based on a design of Norman Hossack[39], BMW<sup>®</sup> developed its new front suspension named the Duolever, seen in Figure 1.16. This new system was first mounted on the K1200S model. This suspension is different from the telescopic or Telelever fork, and is mechanically similar to an automotive double A-arm type suspension. In high-speed emergency braking, the Duolever's characteristics offer significant improvement in the suspension performance of the K1200S[40]. In addition, comparing with the traditional BMW<sup>®</sup> Telelever front suspension, the Duolever weight is reduced by 10%; the net weight is only 13.7 kg.



Figure 1.16: Doulever front forks.  
(reproduced from Inter Cars[41])

In 2012, the new Honda<sup>®</sup> CBR1000RR model was launched, featuring Big Piston suspension technology. The Big Piston suspension system, shown in Figure 1.17 has a built-in large-capacity damping chamber that significantly reduces the resulting hydraulic pressure during the extension of the fork. The manufacturer claims that this makes the whole damping process smoother, while at the same time, providing the rider with rich and delicate feedback. Also, under emergency braking, the rider feels more stability at the front end.



Figure 1.17: Big piston suspension system.  
(reproduced from Sport Rider[42])

During the same year, Ducati<sup>®</sup> developed a semi-active suspension system called Ducati<sup>®</sup> Skyhook Suspension, which assumes that there is a fixed control point over the vehicle. The sensor that is installed in the 'elastic' and 'inelastic' parts of the frame provides dynamic information to the suspension system. Based on the rider set driving mode, through the Skyhook algorithm, the compression and rebound damping of the suspension system will be adjusted rapidly. The corresponding increase or decrease of the damping force effectively offsets the impact from a bumpy road, braking, acceleration, and deceleration.

In 2016, the Kawasaki<sup>®</sup> ZX-10R model was launched. Its front wheel is equipped with the Free Balanced Front fork, which is directly imported from the World SuperBike racing series and is the first use on a production motorcycle. In a conventional fork, cavitation is often caused by rapid pressure fluctuations during the hydraulic balance, which also results in poor performance of the suspension. The Free Balanced Front suspension can help suppress fluctuations in pressure balance. It can also improve the riding comfort by providing independent adjustment of compression and rebound damping.

Throughout the development of the motorcycle front suspension, there were a variety of attempts for modifying the structure that show the designers' wisdom and innovation. Mavroudakis and Eberhard[43] provide a sample of some of the different suspension configurations that have been attempted. They also note that advanced material coatings, such as TiN or carbon matrix composites, have also been applied in an attempt to reduce sliding friction.

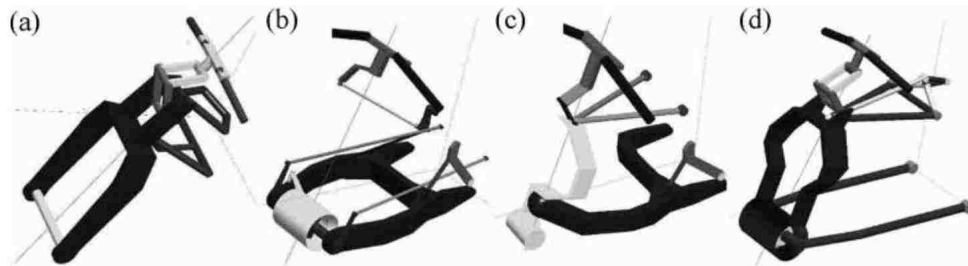


Figure 1.18: Alternate front suspensions  
(reproduced from Mavroudakis and Eberhard[43])

However, looking at the motorcycles on the market right now, the telescopic front suspension still holds the majority of the market, although customers already know it has some drawbacks. This also means that these series of studies and innovations have not fundamentally solved all the problems of the front suspension. Therefore, in this thesis, a novel multi-link suspension will be studied for the front assembly of the motorcycle. Meanwhile, there are already many related patents (Figure 1.18) describing improvements that aim to resolve these defects, some which will be mentioned below.

#### 1.1.4 Patent Search

It should be noted that the multi-link suspension system analyzed in this project is currently the subject of a patent application by the author's supervisor, Dr B. Minaker. The legal team has returned the results of the initial patent search. They have identified fourteen patents that relate to the design of motorcycle front suspensions. A variety of concepts are mentioned in these patents. Some of them are impressive and innovative ideas. In this section, three patents will be introduced.

First of all, the patent named ‘Motorcycle with air suspensions’ was invented by Calzavara[44] and authorized by the European Patent office. The purpose of this invention is to make the suspension easier to be adjusted to achieve the best riding position, and which, at the same time, is cheap and easy to produce. As can be seen in Figure 1.19, this mechanism is actually a whole motorcycle structural design. This section mainly describes the peripheral mechanism around the front wheel, because this thesis is working for the improvement of the motorcycle front suspension. There are in total three connecting rods on one side of the front wheel. Two of them play a connection and support role between the motorcycle body frame and front wheel. The other one works for the motorcycle steering motion. This mechanism separates the steering and damping functions of the front suspension[44]. For the front wheel connecting structure, it looks very similar with the novel multi-link suspension in this thesis. However, at the connection point of the mechanism, they are totally different. In this patent, all of the connection joints are revolute joints (i.e. hinges). But in the novel multi-link suspension, they are spherical joints (i.e., ball joints). Most importantly, the steering motion is realized by the push and pull forces, which act on the steering linkage rod. This is also different with the design in this thesis. In general, the idea of this patent is very novel, especially the way it connects the front and rear wheel suspension mechanisms using the linkage adjustment of the suspension system.

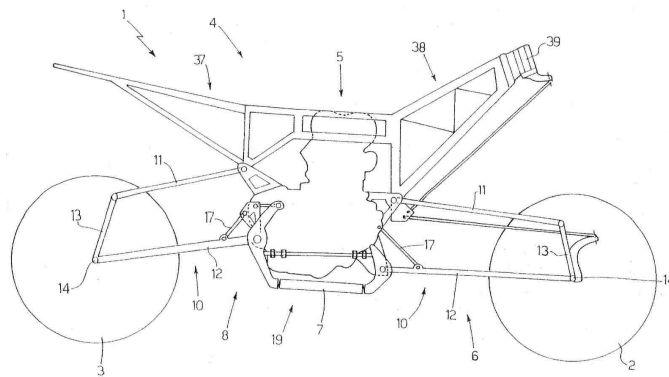


Figure 1.19: Motorcycle with air suspensions.

(reproduced from Calzavara[44])

The second patent, named ‘Motorcycle provided with a steering hub’, describes an invention by Van der Heide[45] and authorized by the United States Patent office. The purpose of this invention is to improve the stability of the hub-center steering mechanism during both curving and straight running. As mentioned previously in Section 1.1.3, one of the hub-center steering characteristics is that it shrinks the steering mechanism and brings it inside the front wheel hub. To carry the steering mechanism, a single pair of support arms connect the frame and the steering mechanism. However, the problem usually comes from the support arms due to the influence of transverse forces, which can easily twist the arms and change the position of the front wheel[45]. Thus, this patent aims to resolve this problem by installing an additional stabilization mechanism.

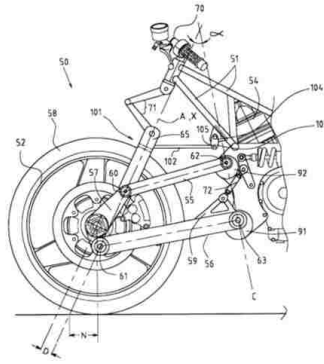


Figure 1.20: Motorcycle provided with a steering hub.  
(reproduced from Van der Heide[45])

As can be seen from Figure 1.20, similar to the previous patent, it also uses a linkage mechanism to eliminate the above drawbacks. This mechanism is able to fix the position of the front wheel. Moreover, it is supposed to reduce vibration of the suspension. Notably, a revolute joint is specified as the connector for these rods, which limits the rod to rotate around a fixed axis. Comparing with the novel multi-link suspension studied in this thesis, there are two main differences. First, the steering mechanism is fundamentally different. Another distinction is that the linkage mechanism of this patent is only set on one side of the front wheel. In general, this patent takes interesting improvements for the hub-center steering mechanism. It also implies that the link mechanism can play an effective role in maintaining the front wheel stability.

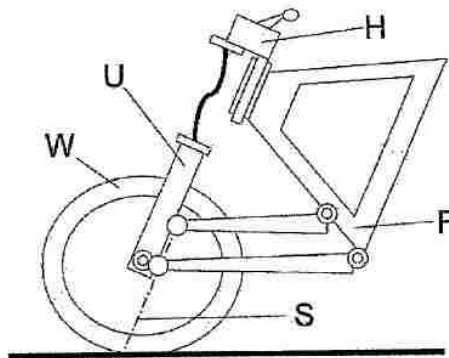


Figure 1.21: MOTORCYCLE. One of the fifteen different possible topologies  
(reproduced from Glover[46])

The third patent, directly named ‘MOTORCYCLE’, describes an invention by Glover and authorized by the United States Patent office. This is a particularly notable example, because in this patent, Glover[46] identified fifteen different possible topologies of the front suspension. Despite the large number of claims and patents, and even though some of them are similar to the mechanism used in this project at first glance,

it appears that the concept developed here is novel and unique, and has the strong possibility of receiving a patent.

For example, Figure 1.21 shows the most similar of all topologies identified by Glover. It has two swing arms supporting the front wheel. Nevertheless, there are still some obvious differences with the novel multi-link front suspension. In this patent, the joint between the swing arm and the body frame is again a revolute joint. As a result, the steering axis is determined by the location of the forward spherical joints. In the design described in this thesis, the support arms are mounted via spherical joints, and the steering axis is located at a 'virtual' point, as will be described in more detail in Chapter 3. Furthermore, the position of the suspension sliders and the steering mechanism is also different.



## Chapter 2

# Motivation, Objectives, and Thesis

## Structure

### 2.1 Motivation

Imagine a rider on a motorcycle, finding a turn up ahead. To decrease the speed of the motorcycle, the rider needs to apply the brake on the front wheel. At the same time, the front forks compress and motorcycle pitches forward, which results in the rider feeling like they are being thrown slightly forward. As the rider reaches the turn, and releases the brake, the bike wobbles gradually. If there is some emergency situation during the turn, the rider will immediately grab the brakes in order to do an emergency stop. The motion of the motorcycle and the feeling of rider will become more intense than the usual braking, which will make the steering heavy and the wheel start to shudder[24]. The rider finally stops the motorcycle and has a bad experience. In reality, many of these problems come from the usage of telescopic front forks on modern motorcycles.

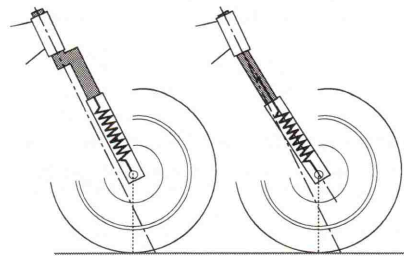


Figure 2.1: Schemes of telescopic forks  
(reproduced from Cossalter[1])

The main functions of a motorcycle's front suspension are: to guide the front wheel, to steer, to spring, to dampen, and to provide support under braking[50]. It is well known that the telescopic front fork (Figure 2.1) is the most widely used front suspension for motorcycles, because the first motorcycle was a bicycle with a small engine mounted into the frame. However, there are a number of shortcomings inherent in this design. First of all, between the sliding parts of this suspension, the static friction cannot be eliminated. Because telescopic forks are mechanically prismatic joints, there is significant sliding contact, and the sliding friction is increased when the prismatic joint flexes under bending loads. This friction results in low work efficiency of the front suspension when the motorcycle is running with small road excitations. To resolve this problem, one significant advancement to the state-of-the-art was introduction of the 'upside-down' forks, where the outer tube of the telescopic joint was placed above the inner tube, to better resist the bending moments. Also, advanced material coatings, such as TiN or carbon matrix composites, were applied in an attempt to reduce friction, but the intrinsic disadvantage is still present[43].

Most importantly, as the fork structure was inherited from the bicycle, it did not adapt to the gradually increasing speed, mass, and tire width of the motorcycle. Fundamentally, the telescopic fork cannot separate steering and braking forces. As a result, the long and thin fork tubes need to carry forces through the steering head bearings to transfer them to the frame. The whole fork and wheel assembly must be steered in and out of turns. Thus, the increased loads present in a motorcycle requires that fork legs must be strengthened, bearing areas widened and frame structures enlarged in an ever-downward spiral towards heavier and bulkier systems[24].

## 2.2 Research Objectives

After searching the related literature and understanding the current situation regarding motorcycle dynamics, the objectives for this thesis are set as follows:

- Building linear and non-linear dynamic models for both conventional and multi-link front fork motorcycles.
- Building open loop simulations of the out-of-plane modes (both conventional and multi-link models)
- Building open loop simulations of the in-plane modes (both conventional and multi-link models)
- Collecting and preparing the data from the simulation above
- Finalizing an appropriate method of comparison between conventional and multi-link models
- Determine the advantages and disadvantages of each model

There are some points that should be mentioned for these objectives. Firstly, the EoM open-source software developed by the University of Windsor Vehicle Dynamics and Control Research Group will be used for the linear model analysis. MotionView<sup>®</sup>, a commercial code developed by Altair Engineering, Inc. and released as part of their HyperWorks suite of CAE tools, will be used for the non-linear model analysis. This means that four models will be built in this project (both linear and non-linear variations of the both the fork and multi-link models). Secondly, in an open loop vehicle simulation, both the rectilinear and steady turning motions are mainly explored by adding predetermined applied forces or torques to appropriate bodies. In a closed loop simulation, a driver model needs to be built, which is based on a series of driver's correction parameters and algorithms. Finally, the appearance of capsize, weave, and wobble modes will be one of the means used to assess the performance of these models.

### 2.2.1 Comparisons of Simulations and Experiment

In this thesis, there are two software tools used for the linear and non-linear analysis, respectively. To conduct the linear analysis, the equations of motion are first generated using the EoM software. The EoM software is a programming package based on the MATLAB<sup>®</sup> language. It is able to generate the equations of motion for a three dimensional mechanism composed of rigid bodies, and coupled by either rigid or flexible connectors. The EoM software returns a series of matrices, which constitute the main body of the equations of motion. The EoM software also uses these resulting equations to do some typical linear analysis, including eigenvalues and frequency response. In this project, the EoM software will be used to build models of both styles of motorcycles, first using the conventional fork suspension, followed by the multi-link style.

For the non-linear analysis, Altair MotionView<sup>®</sup>, a commercial software for multibody dynamics, is available for this project. The modeling task will be conducted in MotionView<sup>®</sup>, and then the simulation conducted using the MotionSolve<sup>®</sup> engine. To be more precise, to predict forces, kinematics and dynamics of motion, MotionSolve<sup>®</sup> can accurately simulate any mechanical system. The mechanical system may consist of rigid or structurally flexible bodies connected by various kinds of kinematic constraints and flexible connectors. Environmental forces and motion excitations drive the motion of the entire system[47]. MotionSolve<sup>®</sup> provides new and advanced options for calculating mechanical system behavior. A choice of six solvers is available to tackle a large variety of dynamics problems. The solvers include implicit/explicit, stiff/non-stiff, and differential algebraic equation/ ordinary differential equation (DAE/ODE) based algorithms[47]. More detailed software and modeling content will be described in Chapter 3.

Based on the study of this thesis, a prototype motorcycle will be manufactured. However, unfortunately, it is not complete at the time of writing of this thesis, and so no experimental results are included. Therefore, in this section, a comparison of simulation and experiment should to be discussed. Simulation results can sometimes be doubted by researchers due to lack of actual experimental data as a comparison, especially for the non-linear analysis. The linear analysis is usually based on a reliable formula and its results are more biased towards theoretical or ideal values, but for the non-linear analysis, the non-linear algorithm is built

to simulate system performance and is more likely to assess the actual situation, as was the MotionView<sup>®</sup> software that was used in this thesis.

There are already many studies about comparisons of multibody dynamics simulations and experiments, e.g., the results published by Ardiri et al[48] attest to the validity of the simulation for vehicle dynamics modelling. In this article, the MotionView<sup>®</sup> software was used to build a scooter model. The scooter is a motorcycle with step through frame and a platform for the rider's feet. The reference vehicle modeled in this paper is similar to the models in this thesis. The model structure of the scooter is based on the Roller Bench Test (RBT) experiment. The RBT experiment is a common test widely used inside motorcycle companies[48].

A standard implementation of this experiment has not been defined. Therefore, this article mainly refers to the RBT experiment used by the well known Italian scooter manufacturer Piaggio<sup>®</sup> & C. SpA, where the vehicle is positioned above two rolling drums and provided with suitable obstacles[49]. A model of the scooter comprised of three parts is described. First, a multibody model representing the frame and suspension components is used; secondly, a spring and hydraulic damper model is developed; finally, a pneumatic tire model is added. The construction of the entire model pursues reality as closely as possible. A numerical analysis is conducted using MotionView<sup>®</sup>, and compared with experimental results based on the roller bench test.

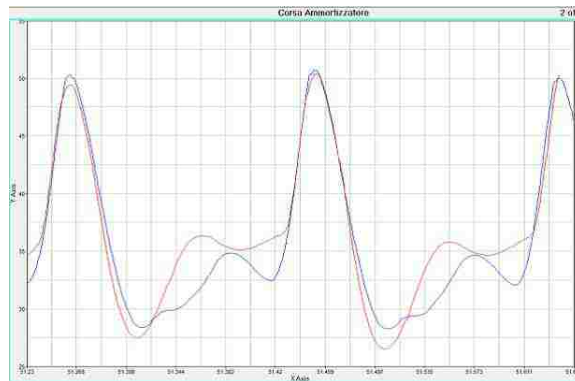


Figure 2.2: Model validation.

The suspension stroke time histories in the numerical analysis and experimental results  
 The red line presents the numerical results. The blue line presents the experimental results.  
 (reproduced from Ardiri[48])

As can be seen in Figure 2.2, the suspension stroke time histories in the numerical analysis result is very similar to the experimental result, especially for the extreme values of the maximum compression and the maximum extension of the suspension. During the simulation process, the 'jacking down' phenomenon of the suspension that results from asymmetric damping behaviour has been identified. It is typical that less damping is used in compression than in rebound as experience has shown that doing so improves ride quality, as different responses are sought when driving over a bump versus over a hole. The result is that the

suspension does not oscillate around the static equilibrium point. Furthermore, the reported discrepancy between experimental and simulation results is less than 5% [48], meaning that the agreement of the results concerning this effect are fairly good too. Overall, this paper provides some evidence that the simulation tools are capable of accurately predicting the trends and relative merit of various motorcycle suspension configurations. As a result, the simulation results developed in this thesis will be taken as acceptably close to reality such that no experimental results are strictly necessary.

## 2.3 Thesis Structure

This thesis studies the performance of a proposed innovative multi-link front suspension design to potentially improve ride quality and handling performance. In this section, brief description of each chapter will be given, to help in understanding structure of this thesis.

Chapter 1 introduces the history of development from bicycle to motorcycle. The relevant theories are also explained. After that, in order to cater to the main topic of this thesis, several common motorcycle front suspension systems are introduced. Most importantly, the innovation structure of multi-link front suspension motorcycle is demonstrated. Furthermore, due to a related patent application, a variety of concepts are mentioned in these patents are described.

Chapter 3 expounds on the theoretical basis of this thesis. The kinematics of motorcycles is first explained and then some parameters related to the front suspension assembly of the motorcycle are described. In the next part, the out-of-plane modes, three typical motorcycle dynamics motions are introduced. In-plane modes are explained and their relevance to the front suspension system is also mentioned. The structure and characteristics of a typical motorcycle front suspension are demonstrated. Moreover, some changes of front assembly caused by the new design are explained. The 'Magic Formula' tire model is described. Afterwards, this section describes the theory of multibody dynamics that are relevant for the modelling. The two software tools used for the modelling are described, and some model parameters are also given in this chapter.

Chapter 4 shows the simulation results of both telescopic and multi-link front suspension motorcycle models. The first result is the verification of multi-link front suspension structure and tire model. The second result is the comparison of the linear and non-linear models, through the out-of-plane motions. Also, the results of unforced and forced straight running performance for these two kinds of motorcycles are displayed. After that, the results of in-plane simulation can be seen in this section, which shows the performance of both telescopic and multi-link front suspension systems.

Chapter 5 analyzes and also discusses the results presented in the previous chapter. Following the order of Chapter 4, the rationality and effectiveness of multi-link front suspension structure is discussed. Then, the result of out-of-plane simulation is analyzed to confirm whether the linear and non-linear models for both telescopic and multi-link motorcycles are reasonable or not. Furthermore, the unforced and forced straight

running performance of these two kinds of motorcycles are compared. For the in-plane simulation results, all analysis and discussion focus on the performance of front suspension system. This is also the main topic of this thesis. Its conclusion determines whether the new front suspension design meets the expectations for ride quality and handling performance.

Chapter 6 summarizes simulation and analysis that has been done in this research. The conclusion section covers the effectiveness of multi-link front suspension and the method of comparison between conventional and multi-link models. Recommendations and suggested future work are also included.

## Chapter 3

# Motorcycle Dynamics and Modeling

In this chapter, the theory of motorcycle dynamics will be described. First of all, it is important for this thesis to introduce the kinematic study of motorcycles, because it relates to the dynamic behavior. It is the basic knowledge of this thesis. Secondly, based on the kinematic structure of the motorcycle, the dynamic motion of motorcycles need to be analyzed. According to Dr. V. Cossalter, a widely recognized researcher on motorcycle behavior and performance, as described in his text *Motorcycle Dynamics*[1], there are two basic categories of motorcycle motion: rectilinear, and steady turning. The study of rectilinear motion relates to braking and acceleration behavior under different road conditions. It is possible for the motorcycle to have some unsafe situations, such as forward overturning or wheeling, during rectilinear motion. In steady turning motion, a zero, positive or negative value of torque may be applied to the handlebars, with the aim of maintaining equilibrium of the motorcycle. To better control the motorcycle in a turn, the rider usually moves their leg and body towards the interior in the saddle to reduce the roll angle of the motorcycle. On the other hand, based on the two motions, the free-modes of the motorcycle can be grouped as in-plane modes and out-of-plane modes[51]. The former includes the pitch, bounce, and front and rear wheel hops, with motion fully in the motorcycle symmetric plane. The other modes are capsizel, weave, and wobble. Usually, information regarding riding safety, handling capabilities, and riding comfort can be obtained from the modal and stability analysis. After that, due to the difference between the automotive and motorcycle tires, the characteristics of the motorcycle tire will be introduced. In the next section, it is also necessary to explain the theory of multibody dynamics; the simulation process in this thesis directly uses multibody dynamic analysis tools. Finally, the multibody modeling process for both the linear and non-linear analysis will be described, relating to the two software tools that were mentioned in Chapter 1.

### 3.1 Kinematics of Motorcycles

The motorcycle has a complex set of mechanical and control mechanisms. However, all of these mechanisms can be simplified as four rigid parts. They are the rear assembly, the front assembly, the front wheel, and the

rear wheel. As can be seen from Figure 1.1, three revolute joints connect these four rigid bodies. Each body has six degrees of freedom and every revolute joint imposes five constraints. Moreover, in this structure, the lowest point on each wheel must remain in contact with the ground. As a result, the total number of degrees of freedom is three. Table 3.1 shows the details of this value.

Rigid Bodies	Constraints	
	Revolute joints	Wheel-ground constraints
Rear frame	Steering	Front
Front frame	Front wheel	Rear
Front wheel	Rear wheel	
Rear wheel		
$4 \times 6 = 24$	$3 \times 5 = 15$	$2 \times 3 = 6$

Table 3.1: Degrees of freedom of the basic motorcycle model

These three degrees of freedom represent three most important movements of motorcycle. The first movement is that each wheel rotates around its axle, which creates the motorcycle forward motion. The second movement is the roll motion around the straight line that passes through the ground contact points of both front and rear wheels. The third movement is the steering rotation, which is the front wheel rotates around the axis passing through the steering head bearing. All three major movements combine with in various combinations to produce an infinite number of possible time history trajectories. The rider uses these to create their own riding style. However, it is worth noting that in this original kinematic structure of the motorcycle, the tire slippage movement is ignored, but in reality, this slippage movement has a crucial role to play in the motorcycle dynamic analysis. Also, due to the topic of this thesis, the suspension movement needs to be considered. Therefore, in this thesis, the number of degrees of freedom of the motorcycle model should be eleven, similar to the example given by Sharp[2]. Table 3.2 shows the details of this value.

Chassis free motion	6
Steering	1
Front and rear suspensions	2
Front and rear wheels	2
Total degrees of freedom	11

Table 3.2: Degrees of freedom of the advanced motorcycle model

The data in Table 3.2 is from another point of view to analyze the degrees of freedom of motorcycles. The chassis has free motion, which allows it to have six degrees of freedom. As with the original kinematic structure of the motorcycle, the basic three degrees of freedom are still there. Furthermore, the front and rear suspensions add two degrees of freedom. In this advanced motorcycle model, both longitudinal and lateral



tire force models have been considered, which incorporate tire slippage in both directions, i.e., the wheel-ground constraints are removed. This advanced motorcycle model will be used to analyze the performance of both telescopic and multi-link front suspension motorcycles.

### 3.1.1 The Geometry of Motorcycles

Figure 3.1 shows the geometry of a motorcycle. There are many parameters to define the motorcycle geometry; they are presented in the Nomenclature. In this section, three major parameters will be described.

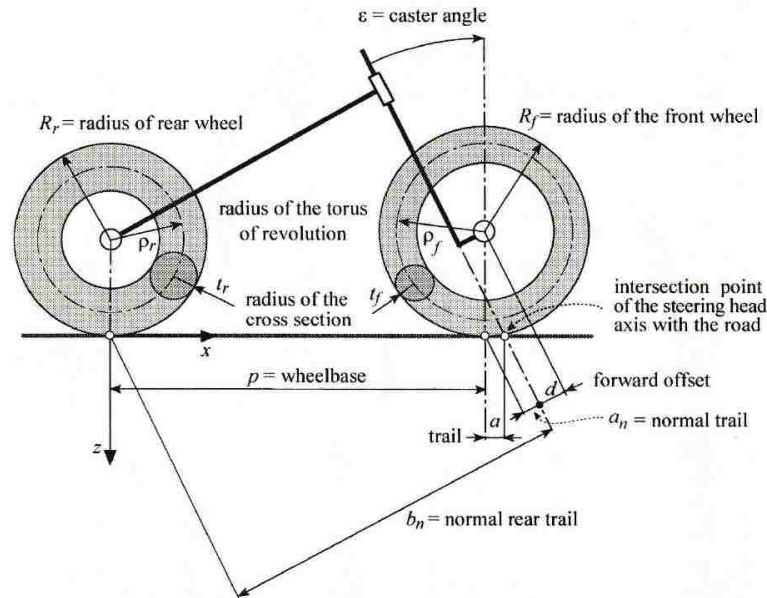


Figure 3.1: Geometry of a motorcycle. (reproduced from Cossalter[1])

Firstly, the *wheelbase*  $p$  is the distance from the ground contact point of the front wheel to the rear wheel contact point. This value ranges from 1200 mm (small scooters) to 1600 mm (touring motorcycles) according to the type of motorcycle. Usually, a larger wheelbase results in increased flexional and torsional deformation of the frame. This flexibility is not good for maneuverability[1]. Additionally, the increase in wheelbase also has a negative role to play for the steering motion, because the minimum curvature radius is increased, which leads to more torque applied to the handlebars. The impact of a larger wheelbase is not all bad; a larger wheelbase means a longer frame that can carry more load, and reduces the load that transfers from front wheel to rear wheel under acceleration. Thus, during acceleration and braking, the pitching movement is reduced. Moreover, a larger wheelbase is also helpful for directional stability.

The second important parameter is the caster angle  $\epsilon$ . This angle can be measured between the vertical axis and the axis of the steering head. For sport motorcycles, the caster angle is relatively small, usually from  $19^\circ$  to  $24^\circ$ . A smaller caster angle provides the rider with a more sensitive steering manipulation, which is supposed to improve the performance in competition. Nevertheless, this small angle heavily influences the

performance of the front fork, and even the whole motorcycle. Dangerous vibrations can occur around the axis of the steering head. It also means that better steering performance results in higher design requirements for the front fork. For touring motorcycles, the caster angle may be as high as  $34^\circ$ , allowing the rider to have a very relaxed riding experience.

The value of *trail*  $a$  is significant for the front suspension system. The trail is the distance between the contact point of the front wheel and the intersection point of the steering head axis with the road, measured in the ground plane[1]. The value of the trail can be found from Equation 3.1 below:

$$a = a_n / \cos \varepsilon \quad (3.1)$$

The *normal trail*  $a_n$  is the perpendicular distance between the contact point and the axis of the steering head. This value can be found from three other parameters: the *caster angle*  $\varepsilon$ , the *fork offset*  $d$  and the radius of the front tire  $R_f$ . The value of trail is also important for the steering system; it influences the ability to change direction or to assure equilibrium. When the road plane contact point of the front wheel is behind the axis intersection point of the steering head with the road, the sign of the normal trail value is positive, otherwise it is negative. In rectilinear motion, the stability of the motorcycle is influenced by the value of the trail. Usually, positive trail has an advantage in straight running. Figure 3.2 below shows the reason.

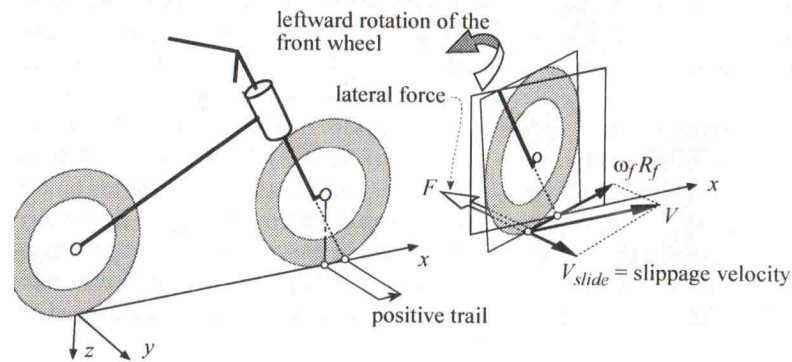


Figure 3.2: The stabilizing effect of positive trail during forward movement.

(reproduced from Cossalter[1])

As can be seen from Figure 3.2, the left graphic shows the meaning of positive trail more directly. To prove the advantage of the positive trail, a slight lateral disturbance, like an irregularity in the road surface, is assumed during straight ahead running. The speed  $V$  of the motorcycle is constant. The  $\omega_f R_f$  is the velocity that is produced from rolling motion, and its direction depends on the steering angle. The  $V_{slide}$  is the sliding velocity of the contact point with respect to the road plane. The advantage of the positive trail is described more succinctly by Cossalter[1] as below:

A frictional force,  $F$ , therefore acts on the front tire.  $F$  is parallel to the velocity of slippage but has the opposite sense, as illustrated in Figure 3.2. Since the trail is positive, the friction

force  $F$  generates a moment that tends to align the front wheel. The straightening moment is proportional to the value of the normal trail.

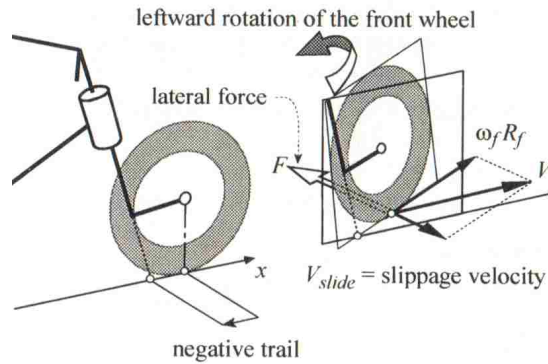


Figure 3.3: The destabilizing effect of negative trail during forward movement.  
(reproduced from Cossalter[1])

Also, in [1], the disadvantage of negative trail is demonstrated as below, further proving the importance of trail to the front fork system and even the whole motorcycle.

If the value of the trail were negative (the contact point in the front of the intersection point of the steering head axis with the road plane) and considering that friction force  $F$  is always in the opposite direction of the velocity of slippage, a moment around the steering head axis that would tend to increase the rotation to the left would be generated. In Figure 3.3 one can observe how friction force  $F$  would amplify the disturbing effect, seriously compromising the motorcycle's equilibrium.

### 3.1.2 Kinematics of the Steering Mechanism

There are two variations of the steering mechanism: no fork offset, and non-zero fork offset. To realize a perfect steady turning, the motorcycle should maintain its vertical body position while steering. This requires that the front and rear wheel center can neither rise nor fall with steer input. According to the literature, the non-zero fork offset style produces less lowering of the front wheel center than no fork offset. This is one reason that almost all modern motorcycles use the non-zero offset fork design. In Cossalter[1], there are very detailed calculations and analysis processes that will be summarized concisely in this section. First, in the left graph of Figure 3.4, a simple front wheel steering model with no fork offset is established.

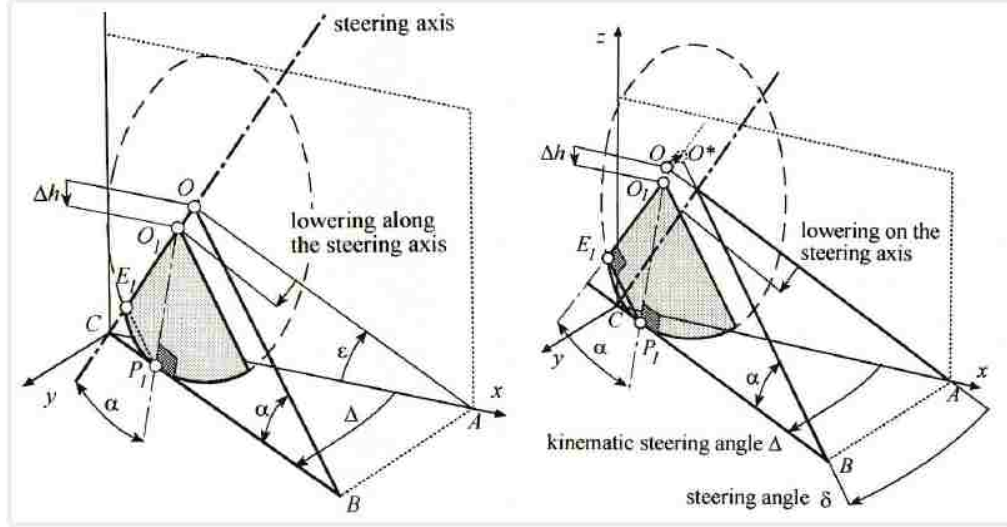


Figure 3.4: Geometry of the steering mechanism. Lowering wheel center with the motorcycle in vertical position.  
(reproduced from Cossalter[1])

There are two assumptions for this model. One is that the roll angle of the motorcycle is zero. Another is the wheels have zero thickness. The variables shown in Figure 3.4 are the radius of the front tire  $R_f$ , the caster angle  $\epsilon$ , the steering angle  $\delta$  and the camber angle of the front wheel  $\beta$ . The formula of the vertical displacement of the wheel center can be seen as below:

$$\Delta_h = (1 - \sqrt{1 - \sin^2 \delta \sin^2 \epsilon}) R_f \quad (3.2)$$

The right graphic of Figure 3.4 is the model of non-zero fork offset, which is similar to the former. After the same assumption and calculation, the formula for the vertical displacement of the wheel center can be found:

$$\Delta_h = R_f(1 - \sqrt{1 - \sin^2 \delta \sin^2 \epsilon}) - d \cdot \sin \epsilon \cdot (1 - \cos \delta) \quad (3.3)$$

It is obvious that the first term in the two formulas is the same. Therefore, the values of these two vertical displacements of the wheel center are comparable. According to the results, under the same input of the steering angle, the non-zero fork offset wheel center vertical displacement is smaller than the other type, which means that the non-zero fork offset makes the motorcycle steering geometry closer to ideal. Also, this clear difference can be seen from Figure 3.4. Thus, in this thesis, the motorcycle that is used to build the simulation model is equipped with the non-zero fork offset steering mechanism.

### 3.1.3 Roll Motion and Steering

During the steering motion of a two-wheeled vehicle, its kinematics analysis is more complicated than the four-wheeled vehicle. Suppose a motorcycle is entering a corner, with a speed  $V$ . With an increasing steering angle  $\delta$ , the position of the motorcycle body gradually changes from vertical to tilted with the roll angle  $\varphi$ . Figure 3.5 shows the motorcycle in this state.

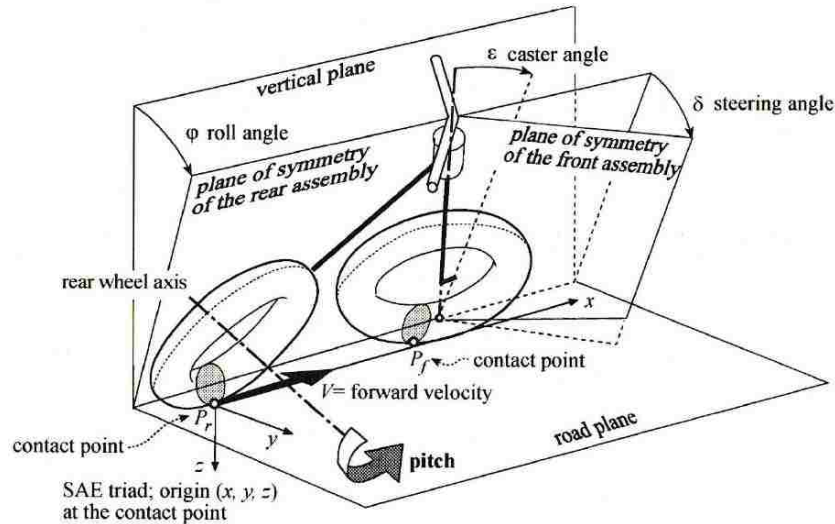


Figure 3.5: Motorcycle in a curve. (reproduced from Cossalter[1])

As can be seen from Figure 3.5, there is a small lowering of the steering head due to the roll motion. As a result, the rear frame will have a slight pitch motion, around the axis of the rear wheel. The pitch motion will be described more specifically in the following section. In this section, front and rear wheel movement is the main research subject. According to the model in Figure 3.5, to analyze the motion of rear wheel, there are two triads that need to be built, described by Cossalter[1] as follows:

a mobile triad  $(P_r, x, y, z)$ , defined as specified by the Society of Automotive Engineers (SAE). The origin is established at the contact point  $P_r$  of the rear wheel with the road plane. The axis  $x$  is horizontal and parallel to the rear wheel plane. The  $z$  axis is vertical and directed downward while the  $y$  axis lies on the road plane. The road surface is therefore represented by the plane  $z = 0$ ; a triad fixed to the rear frame  $(A_r, X_r, Y_r, Z_r)$  which is superimposed on the SAE triad when the motorcycle is perfectly vertical and the steering angle  $\delta$  zero.

Through a series of experiments and discussions, it has been proved that the contact point of the rear wheel with the road plane is displaced. It seems that there are some movements along the  $y$  direction between the mobile triad and the triad fixed to the rear frame. The front wheel behavior is more complicated than the rear wheel. Firstly, it suffers the same roll and pitch motion during the steering motion of the motorcycle. Then the rider applies a force on the handlebar for the turning, which is also transferred along the fork

and finally to the front wheel. Therefore, the lateral slippage has a crucial role to play for the front wheel analysis. Furthermore, this lateral slippage is more dependent on the tire properties analysis, which will be presented in the following sections. While a small lateral slippage of the front and rear tires will always occur when cornering, of course if the slippage becomes too large, it usually results in a crash. A crash is casually referred to as 'low side' when either the front or rear wheel slides out, usually as a result of either too much braking into the corner, which means that the motorcycle falls down to the same side as the way the rider is cornering. On the other hand, if the rear wheel loses lateral grip and then regains it violently after a large slide has been initiated, a 'high side' crash will happen. It also can be caused when the engine is seized (engine failure that locks the crankshaft) or when the chain comes off, both of which frequently lead to the rear wheel locking. The high side crash is much more dangerous, because the rider can be thrown over a metre into the air in front of the bike.

In this thesis, the first simulation is to check the kinematic properties for both the telescopic and multi-link front suspension motorcycles models. There are two parameters, caster angle and trail respectively, that are the most important values that need to be assessed. Moreover, the occurrence of low side or high side crashes will be used to assess the performance in some motion simulations for these two motorcycle models.

## 3.2 Out-of-plane Modes

During straight running or gentle turning motion, a two-wheeled vehicle can experience oscillation around the steering axis, which is caused by the motion of the front and rear wheels, even when they are well balanced. This oscillation heavily influences the stability of the motorcycle. It also becomes one of the most significant standards to assess the handling performance of the motorcycle. Through a lot of experiments and observation, three major modes of motion are identified: the *capsize*, *wobble*, and *weave* modes, which have a crucial role to play in the analysis of motorcycle performance. Also, they are grouped as the out-of-plane modes. They are identified using an eigenvalue analysis, using a linear approach to identify the oscillation characteristics, and the motion of each part of the motorcycle.

Figure 3.6 gives information about the capsize mode. Roll motion, lateral displacement, plus some steering and yaw movements constitute the capsize mode. The rider action on the handlebar heavily influences this mode. Normally, it is stable at low speeds because of the steering modal component of its eigenvector, whereas at higher speeds it may become very slightly unstable[1].

There are some oscillations around the steering axis at the front assembly, shown in Figure 3.8. This phenomenon, called wobble, will happen on the motorcycle from fairly low to middle range speeds. Typical frequency values of the wobble oscillations range from 4 Hz for heavy motorcycles to 10 Hz for lightweight motorcycles[1].

The weave mode is generally stable in the middle speed range. In the low and high speed ranges, from a practical standpoint, it may be unstable or even uncontrolled. This oscillation is mainly concentrated

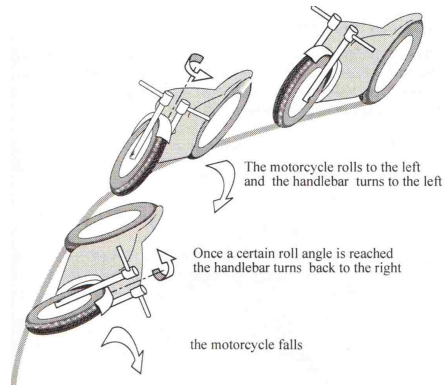


Figure 3.6: Capsize mode. Roll motion combined with a lateral displacement plus some less important steering and yaw movements  
(reproduced from Cossalter[1])

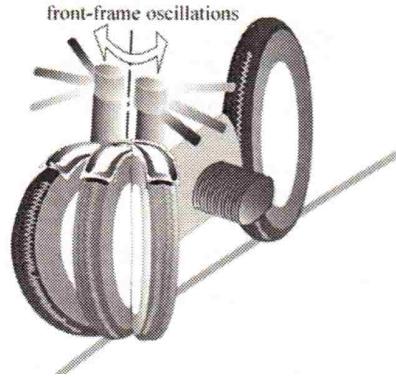


Figure 3.7: Wobble mode. An oscillation of the front assembly around the steering axis  
(reproduced from Cossalter[1])

on the rear end and gradually spreads to the entire motorcycle (Figure 3.7). The natural frequency of this side-to-side motion is zero when the forward speed is also zero, and ranges from 0 to 4 Hz at high speed[1]. Based on the knowledge of these inherent motions, many researchers strive to make new discoveries to meet the expectations of continuous improvement in motorcycle handling behavior.

In this thesis, these three major out-of-plane modes will be used to analyze the performance of a motorcycle during straight running and turning motion. This analysis is mainly done through the eigenvalues, data comparison, and simulation animation to identify the mode occurrence time, duration, and motion amplitude. Through this analysis, the running performance of the telescopic and multi-link front suspension motorcycles can be conveniently compared.



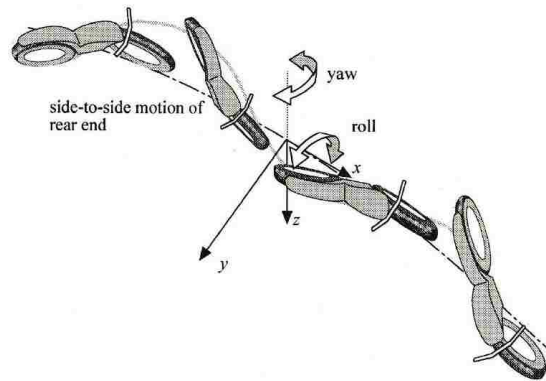


Figure 3.8: Weave mode. An oscillation of the entire motorcycle  
(reproduced from Cossalter[1])

### 3.3 In-plane Modes

The in-plane modes are the most important part of this thesis, because this analysis includes the suspension performance. As mentioned before, this thesis mainly focused on a multibody dynamics model of a motorcycle with a multi-link front suspension. The front and rear suspension is very important for the in-plane modes analysis. There are three main functions of the suspension system. First of all, the tire is usually supposed to absorb small bumps on the ground. Thus, during the irregular road conditions, the rider's driving comfort needs to be maintained by the suspension system, which will reduce most vibrations. The second function is to maintain the grip of the tire. It is difficult for the rider to steer under uneven ground conditions, because of the loss of tire grip. The front suspension can support the front wheel and keep it in contact with the ground. Thirdly, compared to a four-wheeled vehicle, a motorcycle has more obvious load transfer during acceleration, braking, and entering and exiting turns. The desired control of both longitudinal and lateral directions of the motorcycle need to be ensured by the suspension system.

Different types of motorcycles also have different suspension demands, which is expected to serve other purposes. For example, a racing motorcycle needs more contact with the ground and support of the desired rider control. Therefore, its suspension design is more focused on these two aspects and relatively ignores ride comfort. Other motorcycles, like a touring motorcycle, are designed to provide the rider with the best riding comfort. Its suspension system mainly works for shock and vibration absorption. In this thesis, the in-plane modes analysis includes a bounce and pitch response analysis, and a bumpy road analysis, which give strong evidence to prove the performance of the novel front suspension system.

#### 3.3.1 In-plane Dynamics Model

As mentioned before, the in-plane modes affect the riding comfort. Actual road unevenness[52] provides the motorcycle front and rear wheels with a random fluctuation of surface elevation. The vibrations, which are



generated by the vertical displacements of both wheels due to road unevenness forces, are transmitted through the suspensions to the frame and rider. Usually, because of human sensitivities, whole-body vibrations range from 1 Hz to 8 Hz[53] and the arm-hand vibrations range from 12 Hz to 16 Hz[54]. These ride frequency bands are important for the full dynamic model of the motorcycle to have an evaluation of the suspension system.

The most basic model of the motorcycle in-plane modes is similar to the *quarter car* model used in vehicle dynamics studies of automobiles. This two degrees of freedom model is not only the most basic but also the most significant one in the motorcycle ride model. It is composed by two parts, namely the sprung mass and unsprung mass. The chassis, engine and rider all belong to the sprung mass. The unsprung mass contains the wheel, hub, and suspension components, which can be divided into two parts, the front unsprung mass and rear unsprung mass, respectively. Figure 3.9 shows the schematic diagram of this model.

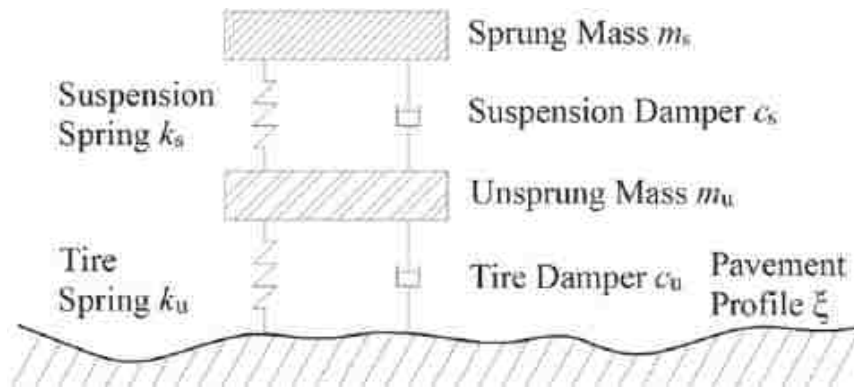


Figure 3.9: The most basic model of the motorcycle in-plane modes.

(reproduced from Zhang, Zhiming, et al.[55])

From this model, it is reasonable to derive the equations of motion. The coordinate  $Z_s$  is the distance of the movement of the sprung mass  $m_s$ . The spring stiffness and damping coefficient between the sprung mass and unsprung mass are  $K_s$  and  $C_s$  respectively. The coordinate  $Z_u$  is the distance of movement of the unsprung mass  $m_u$ . The tire stiffness and tire damping coefficient are  $K_u$  and  $C_u$  respectively. The ground input motion is represented by  $Z_r$ . For the in-plane dynamics of the motorcycle, it is not enough for the analysis to use this two degrees of freedom model, because this model can only provide bounce motion analysis. Therefore, in order to analyze the in-plane dynamics of the motorcycle more comprehensively, another two degrees of freedom model has been developed. Initially, the model appears to be composed of two basic models, and to have four degrees of freedom, but the original two degrees of freedom model indicates that the sprung and unsprung mass motions are at relatively different frequencies. Thus, an idea has been raised to ignore unsprung mass motions, consider the chassis as a rigid body, and extend the chassis motions to include both bounce and pitch, which results in a new two degrees of freedom system. The model appears as below:

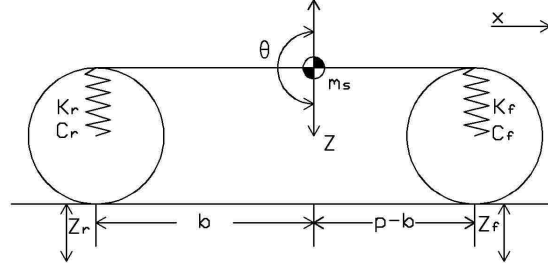


Figure 3.10: The bounce and pitch model of the motorcycle in-plane modes.

In this model, the vertical motion (bounce) and the rotating motion (pitch) are combined, which both contribute to the vibration modes of the motorcycle in the symmetric plane. In the analysis, these two motions need to be discussed separately. The bounce motion can be found from the frame mass center height displacement and the pitch motion can be found from the change of the frame rotation angle. The motion equations of the vertical bounce mode and the pitching mode can be seen as below:

$$m\ddot{z} + (K_r + K_f)z = 0 \quad (3.4)$$

$$I_{yG}\ddot{\theta} + [K_r b^2 + K_f (p-b)^2] \theta = 0 \quad (3.5)$$

In these equations,  $m$  is the mass of the sprung mass. The stiffnesses of the front and rear suspension are  $K_f$  and  $K_r$ , respectively. The value  $p$  is the length of the wheelbase. The value  $b$  is the distance from the sprung mass center to the rear wheel center. The rotation angle of the sprung mass is  $\theta$ , and  $I_{yG}$  is the polar moment of inertia around the  $y$  axis.

$$f_b = \frac{1}{2\pi} \sqrt{\frac{K_f + K_r}{m}} \quad (3.6)$$

$$f_p = \frac{1}{2\pi} \sqrt{\frac{K_f \frac{(p-b)^2}{p^2} + K_r \frac{b^2}{p^2}}{m}} \quad (3.7)$$

According to these two equations, the vertical bounce motion natural frequency  $f_b$  and the pitching motion natural frequency  $f_p$  can be found. Normally, both pitch rotational movement and bounce vertical hop oscillate with a low frequency (from 2 Hz to 3 Hz) because of the substantial inertia of the sprung mass; the pitch is generally more damped than the bounce[51].

The two degrees of freedom model above gives a relatively comprehensive analysis. However, it is reasonable for the in-plane dynamics analysis in this thesis to add the unsprung mass when building both linear and non-linear models. Adding the sprung mass, such as tires, should give simulation results closer to reality. After adding the sprung mass to the model, it becomes four degrees of freedom. Figure 3.11 shows this model.

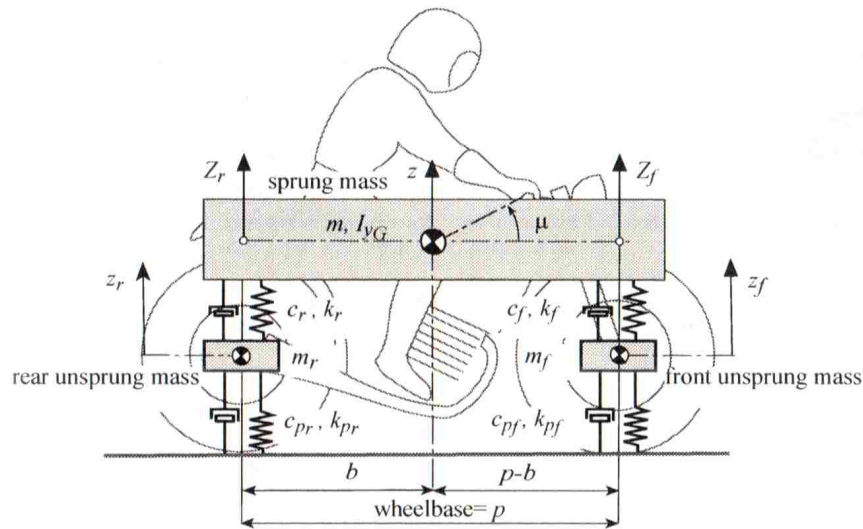


Figure 3.11: The four degrees of freedom model. (reproduced from Cossalter[1])

In this model, the front and rear wheel hop modes of the motorcycle have common characteristics, which are large displacements of the unsprung mass and insignificant movements of the sprung mass. The setup of the suspensions and the tires radial characteristics heavily influences the frequencies of these modes; they usually range from 10 Hz to 14 Hz. The damping ratios depend on the tire and suspension properties and also moderately on speed. In particular, the damping of the rear hop decreases as the velocity increases, whereas the damping of the front hop has an opposite evolution[51].

In this thesis, during the straight running simulation, out-of-plane and in-plane modes are uncoupled and will be examined separately. The out-of-plane modes relate mainly to the stability and control properties of the motorcycle. The in-plane modes are mainly responsible for analyzing the riding comfort and the front suspension performance.

### 3.4 Front Suspension Structure and Characteristics

A motorcycle suspension's main function is to absorb the impact and vibration of the wheels that result from the uneven fluctuation of the road surface. It is used to transmit the force and torque from the handlebar to the wheels. It also plays an important role on the motorcycle ride comfort and safety. The front suspension is provided between the front wheel and the motorcycle body, and the rear suspension device is arranged between the rear wheel and the motorcycle body for transmitting the driving force to the road surface. The initial structure of the front suspension is only used as the strength component that acts the same function as the steering mechanism of the bicycle, and then adds the buffer function and gradually develop to the present front suspension. At present, the main type of front suspension is the telescopic front suspension

that can be seen from Figure 3.12.

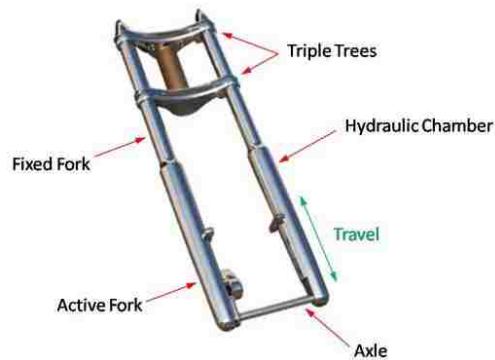


Figure 3.12: The structure of the telescopic front suspension system. (reproduced from Motorcycle MD[56])

A telescopic fork style front suspension generally uses upper and lower clamps or ‘triple trees’ to support the shock absorber assembly as a front fork. The steering head connects the frame and the triple trees with a bearing. The handlebar is generally mounted on the upper triple tree. While turning the handlebar, the upper and lower triple trees drive the front fork to rotate around the steering head, which leads to the steering motion of the motorcycle. This kind of suspension is of course named for the telescope, with which it has obvious similarities in the style of motion. The relative parallel movement between the internal and external tubes allows the distance change required for suspension travel. The assembly is collectively referred to as a telescopic front suspension system. Nowadays, almost all of the currently used front suspensions are this type.

There are three main characteristics values of the suspension system that need to be defined. They are stiffness, damping, and preload. There are also lots of elements that can influence the choice of the front and rear suspension. These parameters include the weight of the rider and the motorcycle, the weight distribution, the properties of the tires, the acceleration and braking performance, the type of the motorcycle, the road condition and so on. During this section, the parameter choice of the front suspension is the main topic. According to the in-plane dynamics model above, the front suspension is usually analyzed at the vertical position, which is used to connect the unsprung masses and the sprung mass. However, in fact, the front suspension is always installed in a tilted position as in the left graphic of Figure 3.13. Therefore, the concept of the reduced front suspension stiffness should be mentioned.

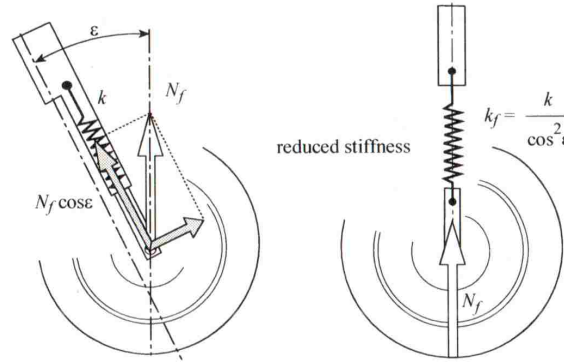


Figure 3.13: Reduced front suspension stiffness. (reproduced from Cossalter[1])

As can be seen from Figure 3.13, the stiffness of the equivalent vertical suspension can be found from the equation below. Here,  $k$  is the real stiffness and the  $k_f$  is the reduced stiffness.

$$k_f = \frac{k}{\cos^2 \varepsilon} \quad (3.8)$$

Under the same vertical load, similar with the stiffness, the damping devices also have an equivalent vertical suspension that can be found from the equation below. The  $c$  is the real damping and the  $c_f$  is the reduced damping.

$$c_f = \frac{c}{\cos^2 \varepsilon} \quad (3.9)$$

It should be mentioned that both the stiffness  $k$  and the damping  $c$  are equal to the sum of the stiffness and damping of the two springs and dampers from the two fork tubes. According to these two equations, it is obvious that the increase in the caster angle causes a reduction in the stiffness and damping cosine coefficients of the reduced stiffness model of suspension.

Another important parameter is the preload of the front suspension system. The reduced stiffness that has been mentioned above is determined on the basis of simple static loads. However, the preload value is not only used to find the compression caused by the static load of the sprung mass weight, but must also be considered when finding the variation of the load on the springs. The force exerted by the spring with preload can be seen in the equation below. In this equation, the  $y$  is the value of the front wheel travel along the suspension sliders. The  $\Delta_y$  stands for the deformation of the springs due to the preload, which is also a significant parameter in the suspension system settings. The values of the suspension preload and stiffness determine the largest and smallest travel distance capability of the suspension.

$$F = k\Delta_y + ky \quad (3.10)$$

Reviewing Figure 3.13 above, during straight running, the force on the tire is generated from an irregular road surface. This direction of the force is perpendicular to the road surface. However, due to the front

suspension's tilted installation, the vertical road force cannot be transferred to the fork directly. It will produce a component force along another direction, which is normal to the force along the fork. This force heavily influences the performance of the telescopic front suspension system, especially under braking. On the other hand, as mentioned before, increasing of the caster angle and trail improve the stability during rectilinear motion, which also means the tilted attitude of the front fork should be increased. Therefore, in the new suspension design proposed in this thesis, the goal is to minimize the impact of component strength requirements, while maintaining the stability properties.

The multi-link front suspension system is expected to alleviate many of these existing design challenges inherent in telescopic front suspension system. Firstly, the steering and damping functions are separated, because in the telescopic mechanism, the combination of steering and road bump forces applied on the suspension will result in twisting, or bending, back and forth or to the side of the fork tubes. This flexibility is very undesirable, especially at extreme occasions when one needs rigidity most[24].

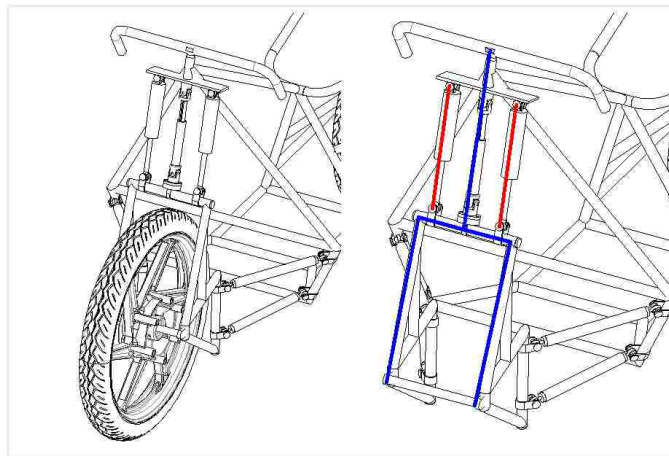


Figure 3.14: The multi-link front suspension system.

The red lines represent the springs. The blue lines represent the steering mechanism.

Figure courtesy Zechariah Van Steenberg.

As can be seen from Figure 3.14, two springs are marked as red lines, which are connected by two universal joints to the handlebar assembly, and the wheel carrier. The blue lines present the steering mechanism of the multi-link front suspension system. It is obvious that the multi-link front suspension system achieves the separation of steering and shock absorption functions, which means the damping function is largely unaffected during the steering motion.

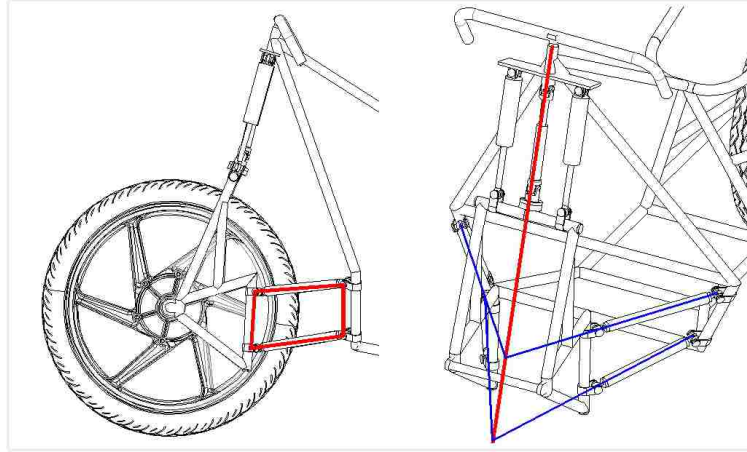


Figure 3.15: The side view of the multi-link front suspension system.

The red lines in left figure represent the four locating arms. In the right graphic, the red lines represent the steering mechanism. The blue lines present the extension lines of four locating arms. Figure courtesy Zechariah Van Steenberg.

Another very obvious difference is the four-bar linkage mechanism, which is symmetrically mounted on both sides of the front tire (Figure 3.15). As can be seen from the right graphic of Figure 3.15, the intersection points of the extension lines of the two upper arms and also the two lower arms can define the steering axis of the multi-link front suspension system. For the telescopic front suspension system, the steering axis is along the steering head bearing connecting the front assembly and the the chassis. This mechanism is inherently flexible, as it relies on bending stiffness of the fork tubes.

The four-bar linkage mechanism on each side helps the unsprung mass to become more rigidly mounted. The disturbing forces will not only transfer along the tubes of the suspension, but also by the four-bar linkage mechanism. The braking performance is noteworthy, when sudden braking leads to a huge inertia force transmitted from the motorcycle body to the front wheel, which will pass through the fork tubes of the telescopic front suspension system. It means these thin tubes needs to bear a very large force that may cause them to bend destructively. The four-bar linkage mechanism can provide strong support as the component arms are only loaded in tension or compression. Additionally, due to their geometry, they can generate an effect called ‘anti-dive’, where forces generated during braking motion tend to counteract the natural tendency to pitch forward.

Looking at the multi-link front suspension mechanism from both top and bottom view (Figure 3.16), the upper arms and wheel carrier form a four-bar linkage mechanism, and the lower arms form another one. These two four-bar linkage mechanisms allow the steering mechanism to realize the steady turning motion. The combined four bar linkages of the system allow the shock absorption motion and the steering requirement at the same time.

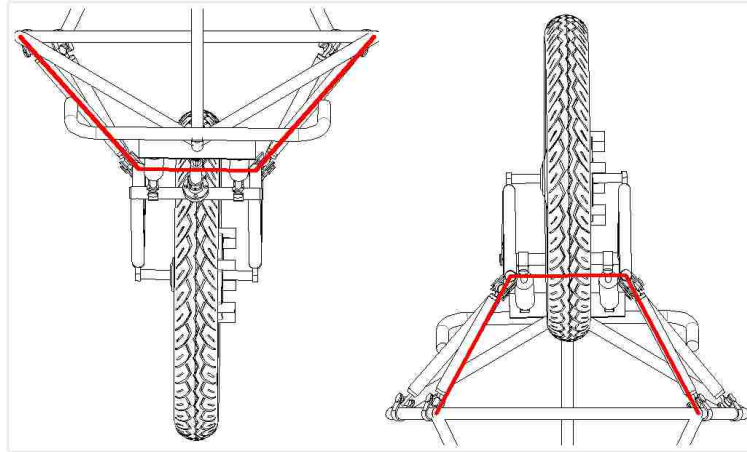


Figure 3.16: The top and bottom view of the multi-link front suspension system.

### 3.5 Motorcycle Tires

Since the advent of the first pneumatic tire, the tire has gradually become one of the motorcycle's most important components. The characteristics of the tire have a crucial role to play in deciding the performance of the motorcycle. The fundamental characteristic of the tire is its deformability. The simulation of the tire is very complicated, even on its own. This complex system can be roughly modeled as three forces and three moments, which are described by Cossalter[1] through Figure 3.17 and the corresponding statement as below.

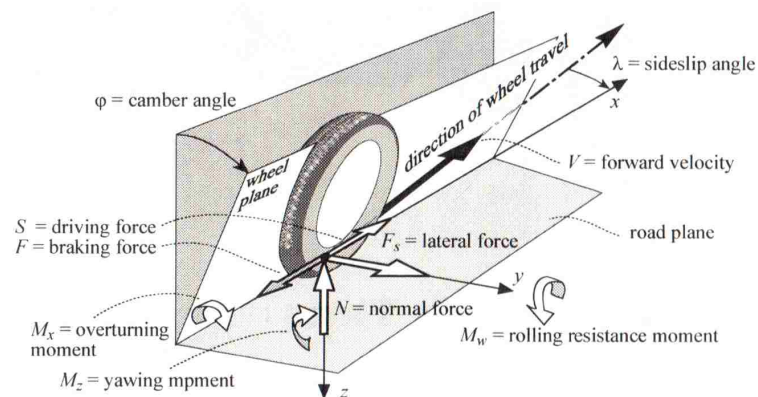


Figure 3.17: Forces and torques of contact between the tire and the road plane. (reproduced from Cossalter[1])

a longitudinal force acting along the axis parallel to the intersection of the wheel plane with the road plane, and passing through the contact point (assumed positive if driving and negative if braking), in the  $x$  direction;

a vertical force orthogonal to the road plane (a vertical load that acts on the wheel, assumed positive in an upward direction), along the  $z$  axis;



- a lateral force, in the road plane, orthogonal to the longitudinal force, in the  $y$  direction;
- an overturning moment around the  $x$  axis,
- a rolling resistance moment around the  $y$  axis,
- a yawing moment around the  $z$  axis.

Based on the above model, there are many theories relating to the tire force and moment generating properties. In this thesis, the Magic Formula, a widely used tire model, is used to calculate steady-state tire force and moment characteristics for the application in the motorcycle dynamics analysis. The Magic Formula model, first proposed by Pacejka in 1993, is widely used in both automotive and motorcycle tire modelling. The functions were developed from a purely empirical approach, and are used to describe the tire horizontal force generation when experiencing combined lateral and longitudinal slip. Through continuous exploration and evolution, the Magic Formula has developed into a single expression that can present the force and moment along and around the three axes. The formula can be seen as below:

$$y = D \sin(C \arctan(Bx - E(Bx - \arctan Bx))) \quad (3.11)$$

with

$$\begin{aligned} Y(X) &= y(x) + S_V \\ x &= X + S_H \end{aligned} \quad (3.12)$$

In this formula, parameters  $B$ ,  $C$ ,  $D$  and  $E$  represent the values of four significant coefficients. The  $S_H$  signifies the horizontal shift of the curve along the  $x$  axis. The  $S_V$  expresses the vertical shift of the curve along the  $y$  axis. The independent variable  $x$  will be either the tire slip angle  $\alpha$  or the tire longitudinal slip  $k$ . The dependent variable is the output for the longitudinal thrust  $F_x$  or the lateral force  $F_y$ , or possibly the aligning torque  $M_z$  around the  $z$  axis. The effects of load  $F_z$  and camber angle  $\gamma$  are included in the parameters  $B$ ,  $C$ ,  $D$  and  $E$  [57].

The typical form of this curve passes through the origin of the coordinates and is anti-symmetrical with respect to the origin. After passing through the origin point, this curve will reach its maximum value and then gradually become flat until it reaches a near constant level. Figure 3.18 displays the curve produced from the formulas above and also demonstrates the parameters that determine the shape of the curve. The parameter  $B$  controls the slope of the curve that passes through the origin. The value of  $C$  determines the shape of the resulting curve, which limits the range of the sine function in Equation 3.11. The peak value that relates to the vertical load can be presented by the  $D$ . The parameter  $E$  indicates the curvature near the peak and also determines the peak position. Moreover, Figure 3.18 shows how the result of the product  $BCD$  characterizes the slope at the origin.

As mentioned before, the Magic Formula has been used widely in the analysis of motorcycle tires. Unlike an automotive tire, a motorcycle tire is heavily influenced by the camber angle. During high speed cornering of a motorcycle, the camber angle is much larger than the corresponding angle in a car or truck, and can

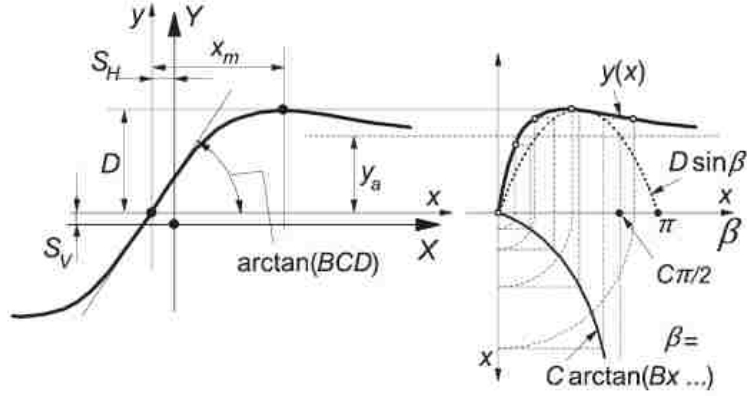


Figure 3.18: Curve produced by the original sine version of the Magic Formula. (reproduced from Pacejka[57])

reach maximums of up to 55 degrees in extreme conditions. This difference leads to the special analysis of the lateral forces when modeling motorcycle tires. In this thesis, a series of formulas evolved from the Magic Formula for predicting the lateral forces in pure side-slip and camber will be applied for the tire force analysis. These formulas can be seen below.

$$\begin{aligned}
 F_{y0} &= D_y \sin \left( C_y \arctan \left( B_y \beta - E_y \left( B_y \beta - \arctan \left( B_y \beta \right) \right) \right) + C_y \arctan \left( B_y \gamma - E_y \left( B_y \gamma - \arctan \left( B_y \gamma \right) \right) \right) \right) \\
 C_y &= p_{c_{y1}} \\
 D_y &= \mu_y F_z \\
 \mu_y &= p_{D_{y1}} \exp \left( p_{D_{y2}} df_z \right) / \left( 1 + p_{D_{y3}} \gamma^2 \right) \\
 E_y &= p_{E_{y1}} + p_{E_{y2}} \gamma^2 + p_{E_{y4}} \gamma \operatorname{sgn}(\beta) \\
 K_{y\alpha o} &= p_{k_{y1}} F_{z0} \sin \left( p_{k_{y2}} \arctan \left( F_z / \left( \left( p_{k_{y3}} + p_{k_{y4}} \gamma^2 \right) F_{z0} \right) \right) \right) \\
 K_{y\alpha} &= K_{y\alpha o} / \left( 1 + p_{k_{y5}} \gamma^2 \right) \\
 B_y &= K_{y\alpha} / \left( C_y D_y \right) \\
 C_y &= p_{c_{y2}} \\
 K_{y\gamma} &= \left( p_{k_{y6}} + p_{k_{y7}} df_z \right) F_z \\
 E_y &= p_{E_{y5}} \\
 B_y &= K_{y\gamma} / \left( C_y D_y \right)
 \end{aligned} \tag{3.13}$$

In these formulas,  $\beta$  and  $\gamma$  represent the side-slip and camber angle, respectively. The  $F_z$  is the normal load of the tire and the  $F_{z0}$  is the nominal normal load. The coefficient of friction  $\mu_y$  should be smaller than 1.3, which was adhered to by the solver for camber angles up to 70 degrees. There is a practical experimental result produced by de Vries and Pacejka in 1997, and reported by Evangelou[58] that can show the entire

analysis process using these formulas. In this example, the tire is a size 180/55 ZR17. The parameters in Table 3.3 are produced from experimental data. Unfortunately, data sets for the front and rear tires of different size were unavailable at the time of preparation of this thesis, so the same tire model was used for both the front and rear tire. While this is undoubtedly a shortcoming of the work, the same conditions were used for the analysis of both the fork and multi-link models, so the results should still be comparable. Furthermore, in this thesis, certain parameters of the tire model, such as the radius and stiffness, were modified to match the properties of the tire model of used by Sharp[2].

Tire type	$p_{Cy1}$	$p_{Dy1}$	$p_{Dy2}$	$p_{Dy3}$	$p_{Ey1}$	$p_{Ey2}$	$p_{Ey4}$	$p_{ky1}$
180/55								
Data	0.9	1.3	0	0	-2.2227	-1.669	-4.288	15.791
Tire type	$p_{ky2}$	$p_{ky3}$	$p_{ky4}$	$p_{ky5}$	$p_{Cy2}$	$p_{ky6}$	$p_{ky7}$	$p_{Ey5}$
180/55								
Data	1.6935	1.4604	0.669	0.18708	0.61397	0.45512	0.013293	-19.99

Table 3.3: Best-fit parameter values for lateral force from 180/55 tire

According to these parameters, the lateral forces will be calculated and the line graph can be seen in Figure 3.19. This line graph is based on the side slip as the abscissa and with the lateral force as the ordinate.

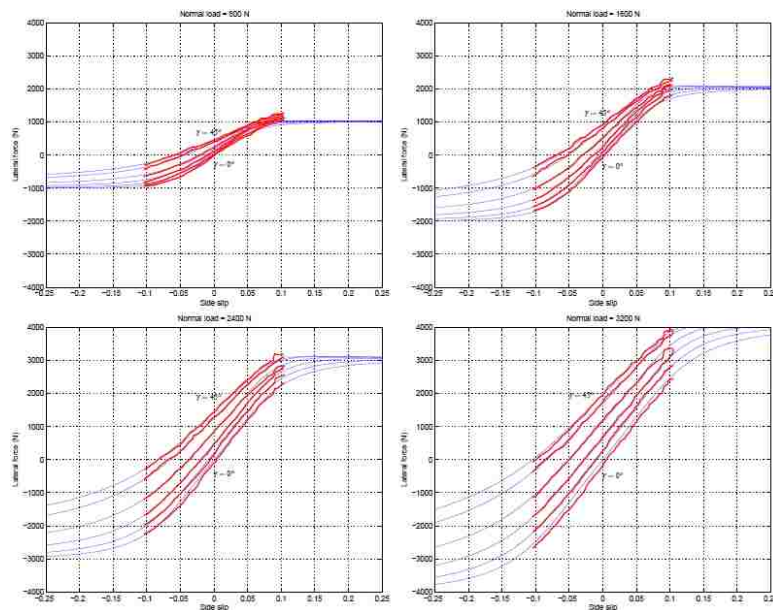


Figure 3.19: 180/55 tyre lateral force results from (de Vries and Pacejka, 1997) (thick lines) with best-fit reconstructions (thin lines) for 0°, 10°, 20°, 30°, 40°, 45° camber angles and 800 N, 1600 N, 2400 N, 3200 N normal loads. (reproduced from Evangelou[58])

The graph above shows curves that indicate the relationship between the side slip and the lateral force. This curve can be reproduced under different camber angles and normal loads. Through these reliable analyses, the properties of the motorcycle tires are able to be used directly into the motorcycle dynamics analysis. During the simulation part of this thesis, there are two types of the tire model, linear and non-linear respectively. For the linear tire model, the stiffness and damping of the tire are the most important parameters that need to be defined, which constitute a relatively simple tire model. For the non-linear tire model, the data for a tire model named ‘MF-Tyre’ will be directly provided by the Altair MotionView® software. The model was developed by TASS International. It has a huge amount of parameters, based on the Magic Formula. In order to prove the validity of this tire model, a special model will be built in the MotionView® software that can be seen from the following chapter.

### 3.6 Multibody Dynamics

In this work, two 11-DOF motorcycle models are employed to simulate and analyze both telescopic and multi-link front suspension systems. The model was constructed by using the theoretical knowledge that relates to multibody dynamics. Therefore, in this section, part of the theory for multibody dynamics will be introduced. Meanwhile, based on this theory, two multibody modeling software tools, EoM and MotionView®, are used to build the linear and non-linear models, respectively. The process will also be described in this section.

Multibody dynamics is the branch of physics that deals with the analysis of systems of interconnected rigid and deformable components. Usually, a multibody system consists mainly of three subsystems; they are bodies, components and substructures. Different types of joints kinematically constrain the motion of every subsystem, which should have six degrees of freedom (translation along  $x$ ,  $y$  and  $z$  axes and rotation around  $x$ ,  $y$  and  $z$  axes) in the absence of restraint. Bushings, springs and dampers have no effect on degrees of freedom, meaning they do not kinematically constrain motion. They are available to connect bodies together, using forces that are dependent upon motions such as displacement and velocity. In this thesis, all of bodies in the simulation models are rigid bodies, which indicates two arbitrary points on the body cannot change position with respect to each other. Meanwhile, in order to describe the motion of each rigid body, there are two coordinate systems needed. One of them is the global system and another is a system that fixed to the body itself. For each degree of freedom, one equation is needed to describe the motion. Based on Newton’s laws of motion, the corresponding equation is shown as below, expressed in terms of acceleration and forces acting on the body and can be employed to describe an arbitrary rigid body motion.

$$\mathbf{M}\ddot{\mathbf{q}} = \mathbf{f}(\mathbf{q}, \dot{\mathbf{q}}, t) + \frac{\partial \phi'}{\partial \mathbf{q}} \boldsymbol{\lambda} \quad (3.14)$$

In Equation 3.14, the matrix  $\mathbf{M}$  represents mass and inertia terms. The  $\mathbf{q}$  stands for generalized coordinate, which consists of six global position coordinates for each body. The  $\mathbf{f}$  represents applied forces. The  $\boldsymbol{\phi}$  and  $\boldsymbol{\lambda}$  stand for the constraint vector and Lagrange multiplier respectively.

$$\boldsymbol{\phi}(\mathbf{q}, t) = 0 \quad (3.15)$$

The constraint equations  $\boldsymbol{\phi}$  can vary depending on the type of constraints in the system, and is written in the form of a holonomic constraint equation above. This form is widely used in this research and usually results from restrictions on the configuration of the system.

As in the description above, both kinematic and kinetic differential equations need to be built, which should also satisfy the algebraic constraint equations. These differential algebraic equations make up the equations of motion. Motions and forces in the system are determined by these equations, which must be integrated with respect to time. Multibody dynamics softwares use a variety of solvers for calculating the equations of motion. For example, based on the mathematical computing language MATLAB<sup>®</sup>, the EoM software has the capability to conveniently reduce the differential algebraic equations to a lower dimensional ordinary differential equations system in standard state space form, while maintaining an equivalent input/output relationship[3].

### 3.6.1 Model in EoM Software

There are two linear models built in the EoM software, the telescopic and multi-link front suspension motorcycles. It should be mentioned that these models in the EoM software had been previously presented in Minaker and Durfy[3]. Original models from this paper were made available to continue this research. As mentioned before, the telescopic front suspension has been used over a century, which means its linear simulation and conclusions are relatively mature and widely reported. The theoretical eigenvalue results can be used as a valid reference for verifying whether the EoM model is correct. Therefore, in the EoM software, the linear model of telescopic motorcycle can be established reasonably and reliably. After that, based on the telescopic linear model, the linear model of multi-link motorcycle can be created directly by replacing the front assembly. These two linear models will be used in both unforced and forced straight running simulations.

#### Telescopic Model

The parameters are based largely on those given by Sharp et. al.[2]. The geometry of the multibody model is given in Table 3.4. The inertia properties are listed in Table 3.5. There are eight rigid bodies in the model. It should be mentioned that the rider is treated as rigidly fixed to the frame, so the rider is included in the frame body. The rear suspension consists of a swing arm and ‘monoshock’ mechanism; the latter is used to increase the motion ratio by amplifying the spring motion. In the ‘monoshock’ mechanism, the bell crank

is set as a massless body and the pull rod that connects the trailing arm to the bell crank is set as a fixed length constraint. In reality, the mass of these components is very small, and so their influence is only on the kinematics of the spring mechanism[3]. The front fork is modelled as two parts, an upper fork and a lower fork. A translational joint connects these two components and allows them to slide in parallel with each other. Two identical springs are used as the suspension mechanism, one on each side of the front wheel, and its springs and dampers are taken as linear. The stiffness and damping of the two springs are 12500 N/m and 1067 Ns/m, respectively.

Table 3.4: Body CG locations and mass

No.	Body Name	Location [m]	Mass [kg]
1	Frame	0.678, 0.000, 0.472	165.130
2	Upper body	0.415, 0.000, 1.140	33.680
3	Upper fork	1.164, 0.000, 0.770	9.990
4	Lower fork	1.365, 0.000, 0.324	7.250
5	Swing arm	0.196, 0.000, 0.311	8.000
6	Bell crank	0.493, 0.000, 0.173	0.000
7	Front wheel, bike	1.410, 0.000, 0.282	11.900
8	Rear wheel, bike	0.000, 0.000, 0.297	14.700

Table 3.5: Body inertia properties

No.	Body Name	Inertia <sup>†</sup> [kg m <sup>2</sup> ] ( $I_{xx}$ , $I_{yy}$ , $I_{zz}$ ; $I_{xy}$ , $I_{yz}$ , $I_{zx}$ )		
1	Frame	11.085, 22.013, 14.982	0.000, 0.000, 3.691	
2	Upper body	1.428, 1.347, 0.916	0.000, 0.000, -0.443	
3	Upper fork	1.341, 1.548, 0.413	0.000, 0.000, 0.000	
4	Lower fork	0.000, 0.000, 0.000	0.000, 0.000, 0.000	
5	Swing arm	0.020, 0.259, 0.259	0.000, 0.000, 0.000	
6	Bell crank	0.000, 0.000, 0.000	0.000, 0.000, 0.000	
7	Front wheel, bike	0.270, 0.484, 0.270	0.000, 0.000, 0.000	
8	Rear wheel, bike	0.383, 0.638, 0.383	0.000, 0.000, 0.000	

<sup>†</sup>Inertias are defined as the positive integral over the body.

For example,  $I_{xy} = +\int r_x r_y dm$ .

In this model, both front and rear tires are treated as narrow disks (i.e., the finite radius of the tire cross section is ignored). The tire is modelled as two linear dampers applied in the horizontal direction, and a linear spring in the vertical direction. Furthermore, the tire damping coefficients decrease as the inverse of speed, effectively treating the longitudinal and lateral tire force as proportional to the slip ratio and slip angle, respectively[3].

There are eleven degrees of freedom in this model. However, the eigenvalues analysis mainly focuses on possible unstable modes such as weave, wobble and capsize.

### Multi-link Model

The linear model of multi-link motorcycle is produced through a transformation of the telescopic suspension linear model. This model still has eleven degrees of freedom. The geometry of the multibody model is given in Table 3.6. The inertia properties are listed in Table 3.7. There are twelve rigid bodies in the model. The frame, the rear suspension, and the tires remain unchanged. The only change is in the front suspension section, which is replaced by the multi-link front suspension.

Table 3.6: Body CG locations and mass

No.	Body Name	Location [m]	Mass [kg]
1	Frame	0.678, 0.000, 0.472	165.130
2	Upper body	0.415, 0.000, 1.140	33.680
3	Upper fork	1.164, 0.000, 0.770	9.990
4	Lower fork	1.365, 0.000, 0.324	7.250
5	Swing arm	0.196, 0.000, 0.311	8.000
6	Bell crank	0.493, 0.000, 0.173	0.000
7	Front wheel, bike	1.410, 0.000, 0.282	11.900
8	Rear wheel, bike	0.000, 0.000, 0.297	14.700
9	Lower left arm	1.140, 0.156, 0.200	2.000
10	Upper left arm	1.140, 0.175, 0.300	2.000
11	Lower right arm	1.140, -0.156, 0.200	2.000
12	Upper right arm	1.140, -0.175, 0.300	2.000

Table 3.7: Body inertia properties

No.	Body Name	Inertia ( $I_{xx}, I_{yy}, I_{zz}; I_{xy}, I_{yz}, I_{zx}$ ) [kg m <sup>2</sup> ]
1	Frame	11.085, 22.013, 14.982    0.000, 0.000, 3.691
2	Upper body	1.428, 1.347, 0.916    0.000, 0.000, -0.443
3	Upper fork	1.341, 1.548, 0.413    0.000, 0.000, 0.000
4	Lower fork	0.000, 0.000, 0.000    0.000, 0.000, 0.000
5	Swing arm	0.020, 0.259, 0.259    0.000, 0.000, 0.000
6	Bell crank	0.000, 0.000, 0.000    0.000, 0.000, 0.000
7	Front wheel, bike	0.270, 0.484, 0.270    0.000, 0.000, 0.000
8	Rear wheel, bike	0.383, 0.638, 0.383    0.000, 0.000, 0.000
9	Lower left arm	0.002, 0.007, 0.009    -0.004, 0.000, 0.000
10	Upper left arm	0.004, 0.007, 0.010    -0.005, 0.000, 0.000
11	Lower right arm	0.002, 0.007, 0.009    0.004, 0.000, 0.000
12	Upper right arm	0.004, 0.007, 0.010    0.005, 0.000, 0.000

Note: inertias are defined as the positive integral over the body, e.g.,  $I_{xy} = \int r_x r_y dm$ .

For the multi-link mechanism, the content related to its structure and design concept is already mentioned above. As the most characteristic part of this front suspension, the four locating arms are installed with two on each side of the front wheel. Also, they are symmetric across the front wheel. Each of the four arms is attached to the frame by one universal joint, and one spherical joint is used to connect the lower

fork. As mentioned before, the steering axis is defined by the geometry of two intersection points of the four locating arms. Therefore, in order to produce the reasonable steering axis, each arm has a designated location that has been detailed in Chapter 1. Another difference is that a telescopic steering shaft is used to connect the handlebar and the wheel carrier with universal joints on both ends. Furthermore, the position of front suspension springs is also different; they are mounted between the wheel carrier and handlebar assembly bodies, and spherical joints are used on both ends.

Unlike the telescopic suspension model, the motion of front wheel for the multi-link motorcycle is initially directly vertical when the suspension mechanism actuates. Therefore, due to this difference, the properties of multi-link front suspension springs need to be adjusted. The stiffness of front spring is increased from 12500 N/m to 14970 N/m to compensate for the newly reduced motion ratio. Meanwhile, the front damping is increased in the same proportion from 1067 Ns/m to 1278 Ns/m[3].

### 3.6.2 Model in Altair MotionView®

In this thesis, the Altair MotionView® software is used to do the non-linear simulation. There are two non-linear models built in the MotionView® software, the telescopic and multi-link model. Moreover, these two non-linear models are used in both in-plane and out-of-plane simulations. Figure 3.20 and Figure 3.21 below show the non-linear models of the telescopic and multi-link front suspension motorcycle respectively.

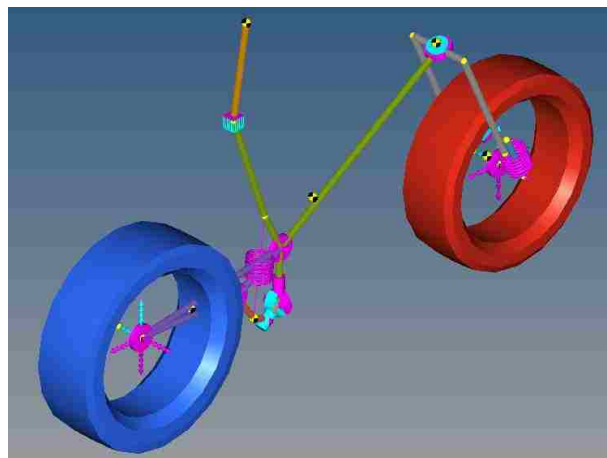


Figure 3.20: The non-linear model of telescopic front suspension motorcycle.

There are nine bodies in the telescopic suspension non-linear model. However, as can be seen from Figure 3.20, the rider is connected with the frame through a fixed joint, which means the rider and frame can be treated as one body, as in the linear model. Similarly, for the multi-link motorcycle (Figure 3.21), the number of bodies for the non-linear model is one more than the linear model, which is also due to the rider and frame connection. Furthermore, the connection joints and suspension spring properties of non-linear model are the same as the linear model for both the telescopic and multi-link front suspension motorcycles.



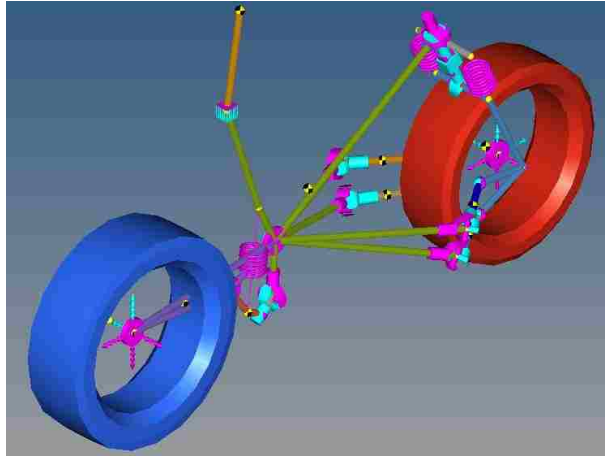


Figure 3.21: The non-linear model of multi-link front suspension motorcycle.

There are two important differences between the linear and non-linear models. Firstly, in linear model, the tires are modelled as linear dampers and springs. In the non-linear model, the tire model is based on the theory of the Magic Formula, which has been mentioned above. In the MotionView<sup>®</sup> software, the tire model is defined by a series of formulas that relate to the theory of the Magic Formula. The parameters in these formulas are entered through a ‘tir’ file, which is provided by Delft-Tyre<sup>®</sup>.

The second difference is the solution produced by the simulation. For linear simulation, the EoM software is based on the mathematical computing language MATLAB<sup>®</sup>, which is well known and has notable advantages in linear analysis. The outputs from EoM are also very detailed, including eigenvalue analysis, frequency response, and steady state sensitivity. The matrices and algorithms that are used in the software are open and easy to access, which also means the EoM software provides both the equations of motion and their solution. In the default case, EoM does not produce a time history solution, as for linear ODE’s the form of the solution is known to be exactly a linear combination of sinusoids and exponentials. Instead, the properties of these sinusoids and exponentials are given by the eigenvalue analysis. However, inherent in the linear solution produced by EoM is that certain effects are ignored. For example, the changes in the geometry of the mechanism as it moves away from the equilibrium condition are ignored, as are fully nonlinear expressions for gyroscopic and centripetal terms.

For non-linear simulation, the MotionView<sup>®</sup> software is a commercial code whose integrators include implicit/explicit, stiff/non-stiff and DAE/ODE based algorithms. Also, in this software, because the nonlinear differential equations of motion are used, the only solution available is a numerical time history of the locations, orientations, and forces etc. While the solution is more precisely correct, it cannot be represented conveniently as a compact data set, like the eigenvalues. In addition, each time history solution depends on the initial conditions chosen, and the result can sometimes vary widely and unpredictably with even small changes to these initial conditions.

### 3.7 Generation of a Random Road

The random road simulation has a crucial role to play for the evaluation of motorcycle front suspension performance. The motorcycle speed and the elevation of road surface unevenness influence the dynamic properties of motorcycle front suspension system especially the vibration levels[61]. In this thesis, based on the International Standards Organization (ISO) 8608 standard, different road roughness profiles characterized by different damage levels are generated by the EoM software.

The spatial frequency, road profile, and Power Spectral Density (PSD) form the fundamental concepts in ISO 8608. The unit of spatial frequency is cycles/meter, which is contrary to the ordinary time frequency unit of Hertz. The road profile is the result of a road height change measured in longitudinal and lateral directions along the road. As Agostinacchio et. al. described[62], in order to use the ISO 8608, the given road needs to be assumed to have equal statistical properties everywhere along the section to be classified. It also means there are lots of larger and smaller bump amplitudes coupled with different periods in the geometry of road surface. The combination is the same wherever one looks along the road section. The ISO 8608 describes a method for generating two different programs by using data from field measurements for generating the road surface profile; its calculation details can be found in [63].

In this thesis, using the EoM software, the artificial random road profile from ISO classification can be generated by the following equation[64]:

$$h(x) = \sum_{i=0}^N \sqrt{\Delta_n} 2^k 10^{-3} \left( \frac{n_0}{i \cdot \Delta_n} \right) \cos(2\pi i \Delta_n x + \varphi_i) \quad (3.16)$$

In this equation, the meaning of each parameter is as follows:

- $L$ , the length of road profile
- $x$ , the abscissa variable from 0 to  $L$
- $\Delta_n = 1/L$ , the frequency band
- $B$ , the sampling interval
- $n_{max} = 1/B$ , the maximum theoretical sampling spatial frequency
- $N = n_{max}/\Delta_n = L/B$
- $k$ , a constant value depending from ISO road profile classification, it assumes integers increasing from 3 to 9, corresponding to the profiles from class A to class H (Table 3.8)
- $n_0 = 0.1$  cycles/m
- $\varphi_i$ , random phase angle following an uniform probabilistic distribution within the  $0-2\pi$  range

The  $k$  values for ISO road roughness classification can be seen as below.

Road class		k
Upper limit	Lower limit	
A	B	3
B	C	4
C	D	5
D	E	6
E	F	7
F	G	8
G	H	9

Table 3.8: ISO road roughness  $k$  values classification

According to Equation 3.16 and Table 3.8 above, it is obvious that the road profile is classified by an integer from 3-9, which corresponds to the transitions between ISO classes A-H. In this thesis, based on the ISO 8606 standard and calculation in the EoM software, the road profile can be graded from class 3 that is very good (ISO A-B class, with  $h_{\max} = \pm 15$  mm), to class 4, which is good (ISO B-C class, with  $h_{\max} = \pm 25$  mm), class 5 that is average (ISO C-D class, with  $h_{\max} = \pm 50$  mm), and class 6, which is poor (ISO D-E class, with  $h_{\max} = \pm 100$  mm). The MATLAB<sup>®</sup> code for random road generation is attached in Appendix A.

## Chapter 4

# Simulation Results

In this chapter, the results of the simulation will be displayed. Based on the model established in the previous chapter, a series of simulations will be carried out, which are used to detect and compare the performance and properties between the conventional and multi-link front suspension system. First of all, the caster angle and trail need to be verified to assess whether they meet the expectations regarding the kinematics of the motorcycle. Secondly, a tire test model was built as a modified version of the basic model to confirm the effectiveness of the tire model, because the properties of the non-linear tire model in the MotionView<sup>®</sup> software is very complex. After these detection steps, the out-of-plane modes simulation of both the conventional and multi-link front suspension motorcycles will be conducted, in two steps. The first step is the unforced straight running simulation that is also used to determine whether the results of the EoM and the MotionView<sup>®</sup> are similar. The second step is the forced straight running, where a torque is applied on the motorcycle handlebar. The last simulation, the most important part of this section, is the in-plane modes simulation of both the conventional and multi-link front suspension systems. There are three types of simulations: braking, plank road, and bumpy road. All of these three simulations relate to the performance of the front suspension system, which is the main topic of this thesis. Finally, note that many simulation results will be presented in this chapter, but the discussion regarding the results will not be presented until Chapter 5.

### 4.1 Kinematics Simulation

The kinematic study of the motorcycle in this thesis is very important, because it decides whether the new front suspension system can be used under standard operating conditions. The caster angle and trail are treated together because the change of the caster angle is coupled with the corresponding change of the trail. In order to verify the feasibility of the multi-link front suspension system, a simple 3D model (Figure 4.1) was created in the SolidWorks<sup>®</sup> CAD software. Through setting two different heights of the front wheel position, the SolidWorks<sup>®</sup> software can produce two corresponding two-dimensional drawings.

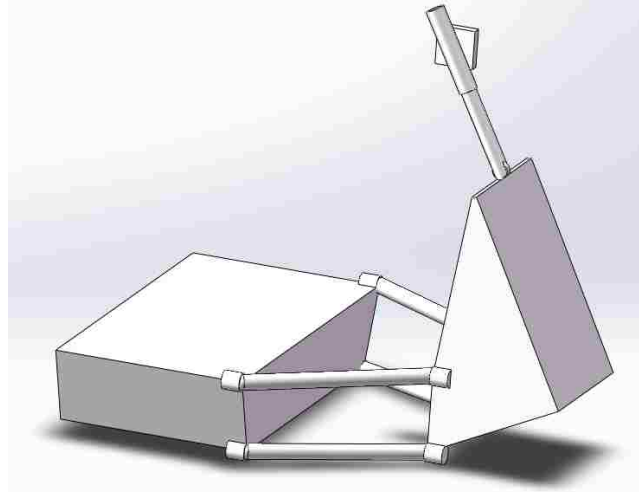


Figure 4.1: The simple 3D model of the multi-link front suspension system.

These two 2D drawings will be processed using AutoCAD® software. The measurement function of this software is able to provide values of the caster angle and trail. The results can be seen from Figure 4.2.

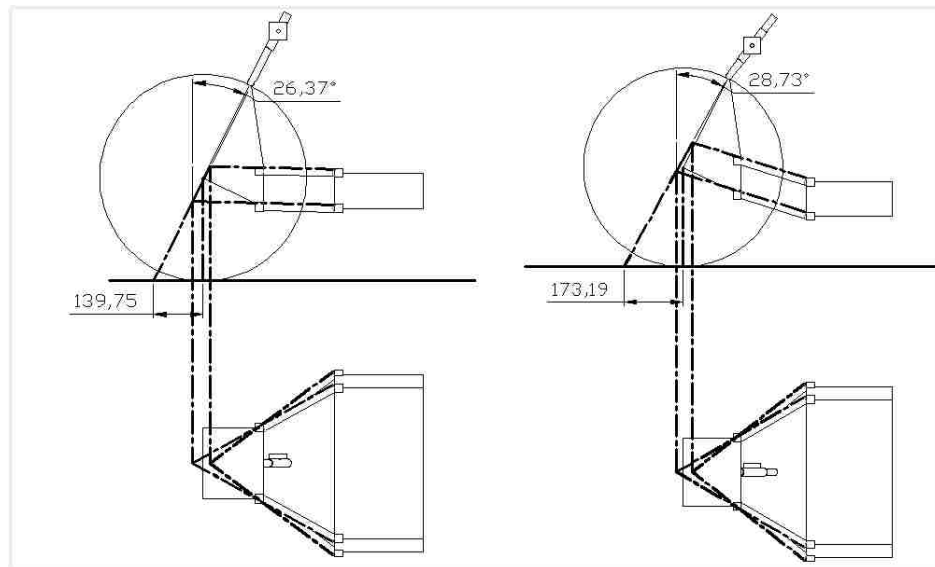


Figure 4.2: The 2D drawings of the multi-link front suspension system in two different front wheel height positions. The figure shows the side view and bottom view.

As can be seen from Figure 4.2, the ground in the right graph is higher than the ground in the left. The values of the caster angle and trail are marked out. For the lower ground, the caster angle is  $26.37^\circ$  and the trail is 139.75 mm. For the higher ground, the caster angle is  $28.73^\circ$  and the trail is 173.19 mm. The kinematic steering characteristics of the multi-link front suspension system can be judged by comparing the data from the two graphs. Clearly, the caster angle and trail are increasing as the suspension moves into compression,

unlike the telescopic fork, where they remain fixed.

## 4.2 Tire Test

In Chapter 3, the Magic Formula tire theory that is used in this thesis model has been presented. In order to confirm the effectiveness of the tire model, a test model was built. In this model, a simple single tire modeled with the Magic Formula parameters and equations is allowed to move only along the longitudinal and lateral direction. The forward velocity is set to a fixed  $u = 10$  m/s. During the straight running of the tire, a lateral speed is applied on the tire body. This speed results in the displacement along lateral direction of the tire model, which also leads to the slippage motion of tire body. As a result, a known slip angle is produced, which is the most significant input for the tire model analysis. According to Figure 3.18, the curve in the left graph is the expected result of this tire test simulation. It means that in the final graph, the magnitude y should represent the lateral force, while x represents the corresponding slip angle quantity. The lateral force is available directly from the MotionView<sup>®</sup> simulation results. For example, Figure 4.3 is line graph of the lateral force change when the lateral speed is  $v = 1$  m/s. The stable value of the rear half of the curve is the required result of simulation.

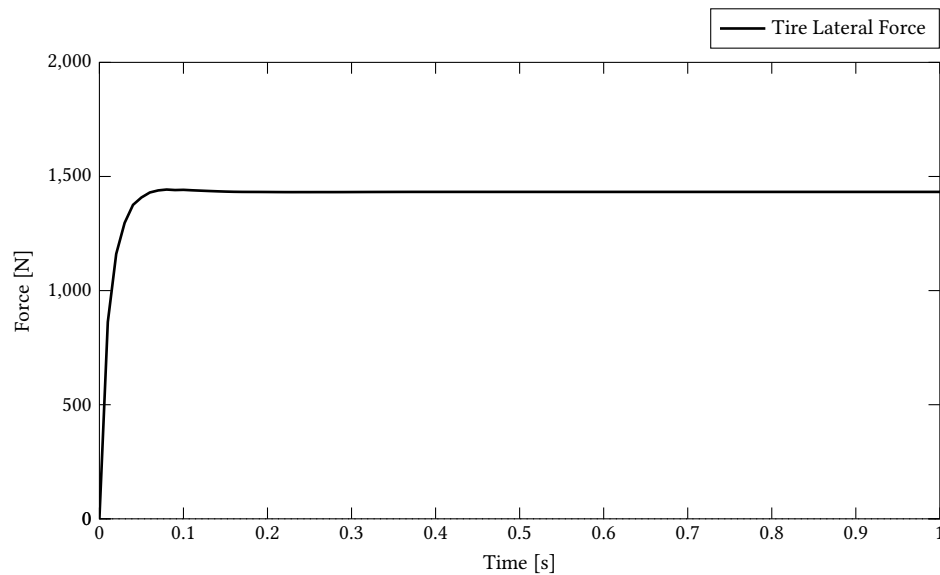


Figure 4.3: The lateral force change in the tire test simulation result when the lateral speed is 1 m/s.

The definition of tire slip angle is the angle between the direction the tire points and the direction it travels. In this simulation, the slip angle can be calculated by the division between the forward speed and the lateral speed. Equation 4.1 below shows the method.

$$\alpha = \arctan\left(\frac{v}{u}\right) \quad (4.1)$$

According to the method above, the two required elements in the tire test result can be obtained. In this thesis, there are 28 speed values involved in the simulation. The simulation result can be seen from Table 4.1. It should be mentioned that at the lateral speed of 0 m/s, the corresponding slip angle and lateral force are all equal to zero.

Lateral speed	Slip angle [deg]	Lateral force [N]	Lateral speed	Slip angle [deg]	Lateral force [N]
0.1 m/s	0.57	188.28	10 m/s	45.00	1495.80
0.3 m/s	1.72	549.77	20 m/s	63.43	1355.13
0.5 m/s	2.86	870.87	30 m/s	71.57	1309.49
0.7 m/s	4.00	1137.53	40 m/s	75.96	1287.84
1.0 m/s	5.71	1432.45	50 m/s	78.69	1275.34
1.5 m/s	8.53	1703.55	60 m/s	80.54	1267.25
2.0 m/s	11.31	1810.84	70 m/s	81.87	1261.58
3.0 m/s	16.70	1831.36	80 m/s	82.87	1257.40
4.0 m/s	21.80	1776.48	90 m/s	83.66	1254.19
5.0 m/s	26.57	1711.88	100 m/s	84.29	1251.65
6.0 m/s	30.96	1652.98	130 m/s	85.60	1246.45
7.0 m/s	34.99	1602.68	150 m/s	86.19	1245.11
8.0 m/s	38.66	1560.53	170 m/s	86.63	1245.11
9.0 m/s	41.99	1525.31	200 m/s	87.14	1245.11

Table 4.1: The various values of tire lateral speed results to the corresponding tire lateral force and tire slip angle.

The data in Table 4.1 is enough to draw the graph that is needed for the result. Figure 4.4 that is produced from Table 4.1 shows the result for tire lateral force versus the tire slip angle for various values of tire lateral speed. This graph can be used to analyze and discuss the rationality and effectiveness of the tire model in this thesis.

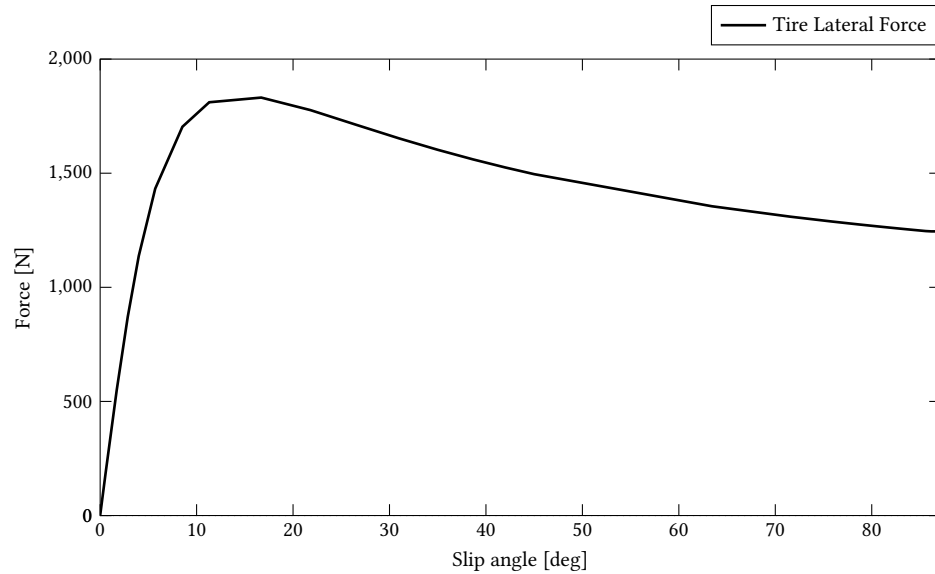


Figure 4.4: The tire lateral force versus the tire slip angle for various values of tire lateral speed.

### 4.3 Out-of-plane Simulation

According to the previous simulation, there are three modes that have a crucial role to play in the out-of-plane simulation: capsize, weave and wobble. There are two types of simulation in this section. One of them is the unforced straight running simulation. This model only needs to add a constant velocity in the longitudinal direction to the base model. Both of the EoM and MotionView<sup>®</sup> software are used to analyze this mode, which will provide linear and non-linear results, respectively. As mentioned before, these two results will be compared to determine the reliability of non-linear models. Also, the unforced straight running performance of the telescopic and multi-link front suspension system will be demonstrated by these results. Another simulation is the forced straight running. There will be a torque applied on the steering head of the motorcycle and the response of the motorcycle will be studied.

#### 4.3.1 Unforced Straight Running Simulation

In this simulation, the results of both EoM and MotionView<sup>®</sup> software will be displayed. The capsize, weave and wobble modes will appear in these results, which give a reliable basis for the analysis. First of all, the results of the EoM software are presented in subsequent articles. Figure 4.5 and Figure 4.6 show the eigenvalues at different speeds. As mentioned before, positive eigenvalues means an instability is present. Therefore, the part of the curve in the figure that is greater than zero will be particularly concerning.



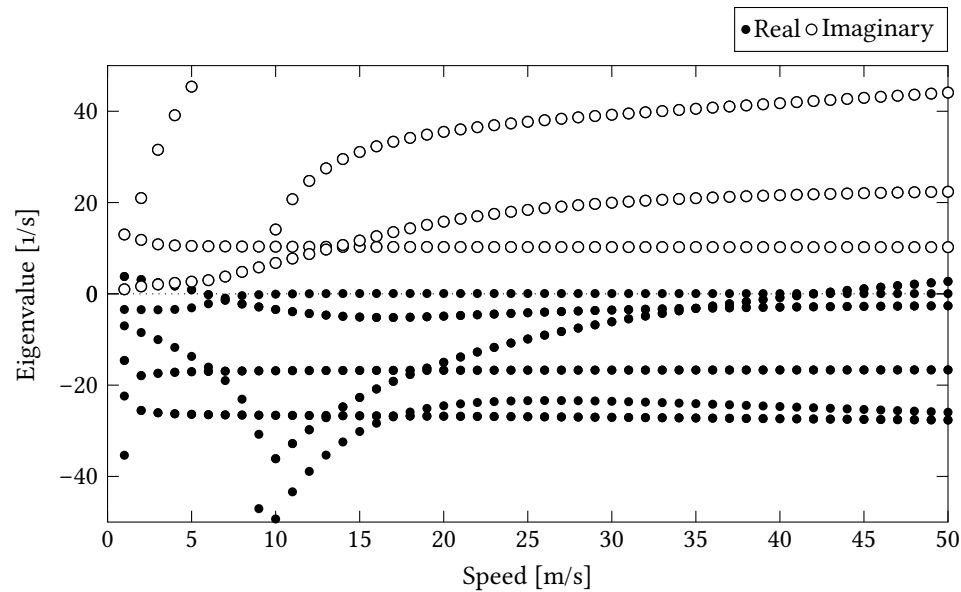


Figure 4.5: Eigenvalues vs speed of telescopic front suspension motorcycle.  
Note that only the positive values of the imaginary roots are plotted for clarity.

Figure 4.5 gives information about the frequencies and damping properties of the telescopic front suspension motorcycle out-of-plane modes as a function of the forward velocity from 1 m/s to 50 m/s. In these curves, each line represents a different meaning, such as weave, capsize, wobble, and rear wobble. It is difficult to distinguish the meaning of each line. However, as can be seen from Figure 4.5, each speed corresponds to multiple eigenvalues and they are not the same. Therefore, it is possible to determine the meaning of each line in the graph by discriminating and analyzing the eigenvalues of a velocity point. For example, at a speed 25 m/s, the eigenvalues and frequencies can be seen in Table 4.2 as below.

There are 9 degrees of freedom. There are 4 oscillatory modes, 3 damped modes, 1 unstable modes, and 6 rigid body modes. Through the comparison of the size between these eigenvalues, it is very direct to find each eigenvalue in the corresponding position in Figure 4.5 and then further deduce the frequency corresponding to each eigenvalue. The frequencies and damping ratios are seen in Table 4.3. It should be mentioned that some of the frequencies are not exact; very small values of frequency or very large time constants can result from numerical round-off error, and actually indicate rigid body modes. Furthermore, the eigenvalues and frequencies with the speed of 5 m/s, 10 m/s and 40 m/s are attached in Appendix B.

Table 4.2: Eigenvalues of telescopic front suspension at 25 m/s

No.	Real [rad/s]	Imaginary [rad/s]	Real [Hz]	Imaginary [Hz]
1	$-4.2692 \times 10^2$	$0.0000 \times 10^0$	$-6.7947 \times 10^1$	$0.0000 \times 10^0$
2	$-3.4011 \times 10^2$	$0.0000 \times 10^0$	$-5.4131 \times 10^1$	$0.0000 \times 10^0$
3	$-2.6921 \times 10^1$	$1.1202 \times 10^2$	$-4.2846 \times 10^0$	$1.7829 \times 10^1$
4	$-2.6921 \times 10^1$	$-1.1202 \times 10^2$	$-4.2846 \times 10^0$	$-1.7829 \times 10^1$
5	$-9.8898 \times 10^0$	$3.7698 \times 10^1$	$-1.5740 \times 10^0$	$5.9999 \times 10^0$
6	$-9.8898 \times 10^0$	$-3.7698 \times 10^1$	$-1.5740 \times 10^0$	$-5.9999 \times 10^0$
7	$-2.3402 \times 10^1$	$0.0000 \times 10^0$	$-3.7245 \times 10^0$	$0.0000 \times 10^0$
8	$-1.6723 \times 10^1$	$1.0255 \times 10^1$	$-2.6615 \times 10^0$	$1.6321 \times 10^0$
9	$-1.6723 \times 10^1$	$-1.0255 \times 10^1$	$-2.6615 \times 10^0$	$-1.6321 \times 10^0$
10	$-4.1387 \times 10^0$	$1.8394 \times 10^1$	$-6.5870 \times 10^{-1}$	$2.9275 \times 10^0$
11	$-4.1387 \times 10^0$	$-1.8394 \times 10^1$	$-6.5870 \times 10^{-1}$	$-2.9275 \times 10^0$
12	$-1.7504 \times 10^{-6}$	$0.0000 \times 10^0$	$-2.7858 \times 10^{-7}$	$0.0000 \times 10^0$
13	$1.7505 \times 10^{-6}$	$0.0000 \times 10^0$	$2.7860 \times 10^{-7}$	$0.0000 \times 10^0$
14	$7.4557 \times 10^{-2}$	$0.0000 \times 10^0$	$1.1866 \times 10^{-2}$	$0.0000 \times 10^0$
15	$1.2961 \times 10^{-11}$	$2.3971 \times 10^{-6}$	$2.0628 \times 10^{-12}$	$3.8151 \times 10^{-7}$
16	$1.2961 \times 10^{-11}$	$-2.3971 \times 10^{-6}$	$2.0628 \times 10^{-12}$	$-3.8151 \times 10^{-7}$
17	$-1.5775 \times 10^{-12}$	$0.0000 \times 10^0$	$-2.5106 \times 10^{-13}$	$0.0000 \times 10^0$
18	$-3.6254 \times 10^{-13}$	$0.0000 \times 10^0$	$-5.7699 \times 10^{-14}$	$0.0000 \times 10^0$

Note: oscillatory roots appear as complex conjugates.

Table 4.3: Natural frequency, damping ratio at 25 m/s

No.	Frequency [Hz]	Damping Ratio	Time Constant [s]	Wavelength [s]
1	–	–	$2.3423 \times 10^{-3}$	–
2	–	–	$2.9402 \times 10^{-3}$	–
3	$1.8336 \times 10^1$	$2.3367 \times 10^{-1}$	$3.7146 \times 10^{-2}$	$5.6089 \times 10^{-2}$
4	$1.8336 \times 10^1$	$2.3367 \times 10^{-1}$	$3.7146 \times 10^{-2}$	$5.6089 \times 10^{-2}$
5	$6.2029 \times 10^0$	$2.5375 \times 10^{-1}$	$1.0111 \times 10^{-1}$	$1.6667 \times 10^{-1}$
6	$6.2029 \times 10^0$	$2.5375 \times 10^{-1}$	$1.0111 \times 10^{-1}$	$1.6667 \times 10^{-1}$
7	–	–	$4.2732 \times 10^{-2}$	–
8	$3.1221 \times 10^0$	$8.5248 \times 10^{-1}$	$5.9799 \times 10^{-2}$	$6.1270 \times 10^{-1}$
9	$3.1221 \times 10^0$	$8.5248 \times 10^{-1}$	$5.9799 \times 10^{-2}$	$6.1270 \times 10^{-1}$
10	$3.0006 \times 10^0$	$2.1952 \times 10^{-1}$	$2.4162 \times 10^{-1}$	$3.4159 \times 10^{-1}$
11	$3.0006 \times 10^0$	$2.1952 \times 10^{-1}$	$2.4162 \times 10^{-1}$	$3.4159 \times 10^{-1}$
12	–	–	$5.7131 \times 10^5$	–
13	–	–	$-5.7127 \times 10^5$	–
14	–	–	$-1.3412 \times 10^1$	–
15	$3.8151 \times 10^{-7}$	$-5.4068 \times 10^{-6}$	$-7.7156 \times 10^{10}$	$2.6211 \times 10^6$
16	$3.8151 \times 10^{-7}$	$-5.4068 \times 10^{-6}$	$-7.7156 \times 10^{10}$	$2.6211 \times 10^6$
17	–	–	$6.3393 \times 10^{11}$	–
18	–	–	$2.7583 \times 10^{12}$	–

Notes: a) oscillatory roots are listed twice, b) negative time constants denote unstable roots.

As seen in Table 4.2 and Table 4.3, it is obvious that there are four frequencies that are valuable to be analyzed. In order to identify these frequencies more intuitively, the EoM software also provides the three-dimensional animations as an auxiliary function. After discovering the eigenvalues at 25 m/s, these eigenvalues can be identified from top to bottom as the capsize, weave, wobble and rear wobble modes. Thus, the curves of these eigenvalue points also have their own meaning. Furthermore, each mode can be described in detail according to the identity of each curve. The capsize mode is in an unstable state almost throughout the speed range and also it is not a vibration mode. The weave mode frequency increases with speed after the early instability, but its eigenvalues are always below the zero line, which means that this mode is always in a stable state. The wobble mode becomes unstable when the velocity reaches a certain value. For the telescopic front suspension motorcycle, the velocity where instability appears is around 42 m/s. It is worth mentioning that the unstable wobble mode results from the absence of a steering damper in the model.

The figures and tables above are the results of the telescopic front suspension motorcycle. Of course, in order to compare the unforced straight running performance between the telescopic and multi-link front suspension motorcycles, the simulation of the latter will also be run and studied. Figure 4.6 shows the information about the eigenvalues properties of the multi-link front suspension motorcycle out-of-plane modes as a function of the forward velocity, which is also from 1 m/s to 50 m/s. A similar method will be used to analyze the modes during the simulation.

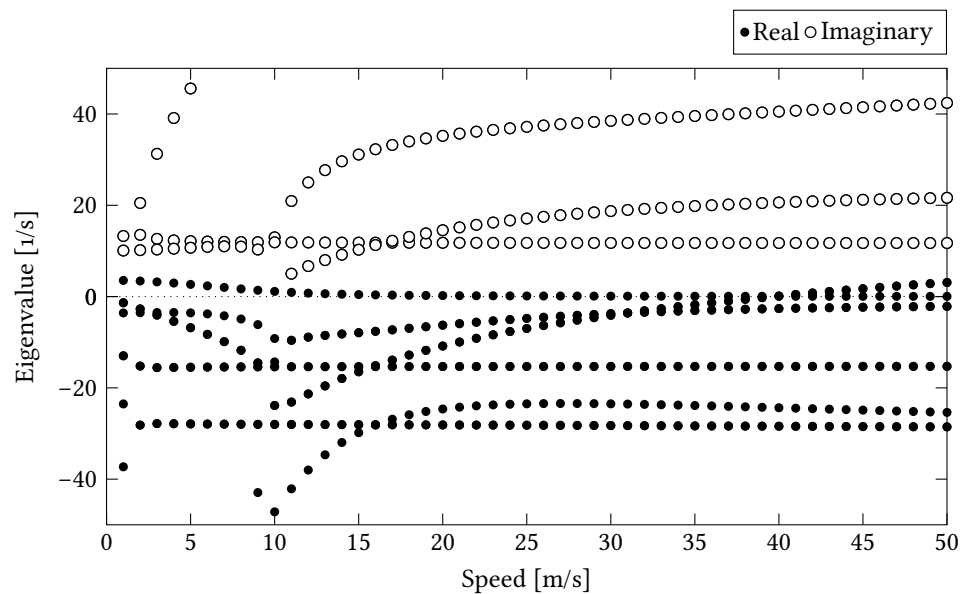


Figure 4.6: Eigenvalues vs speed of multi-link front suspension motorcycle.  
Note that only the positive values of the imaginary roots are plotted for clarity.

Table 4.4: Eigenvalues of multi-link front suspension at 25 m/s

No.	Real [rad/s]	Imaginary [rad/s]	Real [Hz]	Imaginary [Hz]
1	$-4.0961 \times 10^2$	$0.0000 \times 10^0$	$-6.5192 \times 10^1$	$0.0000 \times 10^0$
2	$-3.4081 \times 10^2$	$0.0000 \times 10^0$	$-5.4242 \times 10^1$	$0.0000 \times 10^0$
3	$-2.8184 \times 10^1$	$1.1373 \times 10^2$	$-4.4856 \times 10^0$	$1.8100 \times 10^1$
4	$-2.8184 \times 10^1$	$-1.1373 \times 10^2$	$-4.4856 \times 10^0$	$-1.8100 \times 10^1$
5	$-6.9861 \times 10^0$	$3.7185 \times 10^1$	$-1.1119 \times 10^0$	$5.9182 \times 10^0$
6	$-6.9861 \times 10^0$	$-3.7185 \times 10^1$	$-1.1119 \times 10^0$	$-5.9182 \times 10^0$
7	$-4.7847 \times 10^0$	$1.7097 \times 10^1$	$-7.6151 \times 10^{-1}$	$2.7211 \times 10^0$
8	$-4.7847 \times 10^0$	$-1.7097 \times 10^1$	$-7.6151 \times 10^{-1}$	$-2.7211 \times 10^0$
9	$-1.5314 \times 10^1$	$1.1764 \times 10^1$	$-2.4373 \times 10^0$	$1.8723 \times 10^0$
10	$-1.5314 \times 10^1$	$-1.1764 \times 10^1$	$-2.4373 \times 10^0$	$-1.8723 \times 10^0$
11	$-2.3497 \times 10^1$	$0.0000 \times 10^0$	$-3.7396 \times 10^0$	$0.0000 \times 10^0$
12	$1.3724 \times 10^{-1}$	$0.0000 \times 10^0$	$2.1842 \times 10^{-2}$	$0.0000 \times 10^0$
13	$-4.2604 \times 10^{-11}$	$3.0354 \times 10^{-6}$	$-6.7806 \times 10^{-12}$	$4.8310 \times 10^{-7}$
14	$-4.2604 \times 10^{-11}$	$-3.0354 \times 10^{-6}$	$-6.7806 \times 10^{-12}$	$-4.8310 \times 10^{-7}$
15	$-2.7306 \times 10^{-6}$	$0.0000 \times 10^0$	$-4.3459 \times 10^{-7}$	$0.0000 \times 10^0$
16	$2.7307 \times 10^{-6}$	$0.0000 \times 10^0$	$4.3460 \times 10^{-7}$	$0.0000 \times 10^0$
17	$1.8700 \times 10^{-13}$	$0.0000 \times 10^0$	$2.9762 \times 10^{-14}$	$0.0000 \times 10^0$
18	$1.8526 \times 10^{-14}$	$0.0000 \times 10^0$	$2.9486 \times 10^{-15}$	$0.0000 \times 10^0$

Note: oscillatory roots appear as complex conjugates.

Table 4.5: Natural frequency, damping ratio at 25 m/s

No.	Frequency [Hz]	Damping Ratio	Time Constant [s]	Wavelength [s]
1	-	-	$2.4413 \times 10^{-3}$	-
2	-	-	$2.9342 \times 10^{-3}$	-
3	$1.8648 \times 10^1$	$2.4054 \times 10^{-1}$	$3.5482 \times 10^{-2}$	$5.5247 \times 10^{-2}$
4	$1.8648 \times 10^1$	$2.4054 \times 10^{-1}$	$3.5482 \times 10^{-2}$	$5.5247 \times 10^{-2}$
5	$6.0217 \times 10^0$	$1.8464 \times 10^{-1}$	$1.4314 \times 10^{-1}$	$1.6897 \times 10^{-1}$
6	$6.0217 \times 10^0$	$1.8464 \times 10^{-1}$	$1.4314 \times 10^{-1}$	$1.6897 \times 10^{-1}$
7	$2.8257 \times 10^0$	$2.6950 \times 10^{-1}$	$2.0900 \times 10^{-1}$	$3.6750 \times 10^{-1}$
8	$2.8257 \times 10^0$	$2.6950 \times 10^{-1}$	$2.0900 \times 10^{-1}$	$3.6750 \times 10^{-1}$
9	$3.0735 \times 10^0$	$7.9302 \times 10^{-1}$	$6.5299 \times 10^{-2}$	$5.3409 \times 10^{-1}$
10	$3.0735 \times 10^0$	$7.9302 \times 10^{-1}$	$6.5299 \times 10^{-2}$	$5.3409 \times 10^{-1}$
11	-	-	$4.2559 \times 10^{-2}$	-
12	-	-	$-7.2865 \times 10^0$	-
13	$4.8310 \times 10^{-7}$	$1.4036 \times 10^{-5}$	$2.3472 \times 10^{10}$	$2.0700 \times 10^6$
14	$4.8310 \times 10^{-7}$	$1.4036 \times 10^{-5}$	$2.3472 \times 10^{10}$	$2.0700 \times 10^6$
15	-	-	$3.6622 \times 10^5$	-
16	-	-	$-3.6621 \times 10^5$	-
17	-	-	$-5.3475 \times 10^{12}$	-
18	-	-	$-5.3977 \times 10^{13}$	-

Notes: a) oscillatory roots are listed twice, b) negative time constants denote unstable roots.

Comparing with Figure 4.5, in Figure 4.6, each eigenvalue curve of its corresponding mode is similar. The main difference is distributed among the low speed range; to be more precise, it is from 0 m/s to 10 m/s. In order to further verify the meaning of these curves, the speed 25 m/s is still chosen to be used for the analysis. Table 4.4 and Table 4.5 shows the eigenvalues and frequency properties of the forced straight running simulation of the multi-link front suspension motorcycle when the speed is 25 m/s.

Once again, by comparing the size of the eigenvalue in Table 4.4 and analyzing the corresponding frequency in Table 4.5, the meaning of each curve in Figure 4.6 can be confirmed again. As mentioned above, there are some differences in the capsize and weave eigenvalues in the low speed range. For example, in the simulation of the telescopic front suspension motorcycle, the eigenvalues gradually become positive after the negative value at low speed. However, in the simulation of the multi-link front suspension motorcycle, the eigenvalues are always in the positive part of the ordinate. Although there are slight distinctions, in general, the unforced straight running simulation performance of these two motorcycle models that are equipped with different front suspension systems is similar, although the multilink model is slightly more unstable at low speeds. The wobble mode will still become unstable as the speed increases. The critical value of the velocity between stability and instability is about 40 m/s. The EoM results of the unforced straight running simulation above are based on linear analysis. In order to get data closer to reality, the non-linear model will also be used to do the unforced straight running simulation in the MotionView<sup>®</sup> software.

During the non-linear analysis of the unforced straight running simulation, the telescopic and multi-link front suspension motorcycles will have their own models. Unlike the previous linear analysis, the results of the non-linear simulation are mainly obtained from the observation of the animation and the analysis of the time history graphs. For instance, according to Figure 4.5 and Figure 4.6, it is notable that the speed range around 40 m/s is a very sensitive area, which may produce unstable wobble modes. After running the unforced straight running simulation with a speed of 40 m/s, the corresponding animation and line graph results can be generated. First of all, for the telescopic front suspension motorcycle, its animation shows that the unstable wobble modes directly start from the beginning of the animation and rollover occurs after about 2.05 s. The appearance of the other modes is not obvious due to the intense wobble motion. Figure 4.7 shows the change of angular velocity around the z-axis of the steering head with respect to time.

As can be seen from Figure 4.7, the nonlinear simulation results agree with the previous description of the performance of the motorcycle at the speed of 40 m/s. The fluctuation range of the yaw rate curve in the graph increases with time, and the wobble amplitude of the front handlebar of the motorcycle gradually increases until the loss of control. For the multi-link front suspension motorcycle, the change of angular velocity around z-axis of the steering head with respect to time at the speed of 40 m/s is seen in Figure 4.8. It is obvious that the wobble amplitude of its front handlebar also has the upward trend. The only difference is the time range from the beginning to overturn. The running time of the multi-link front suspension motorcycle is even less than the telescopic suspension motorcycle.

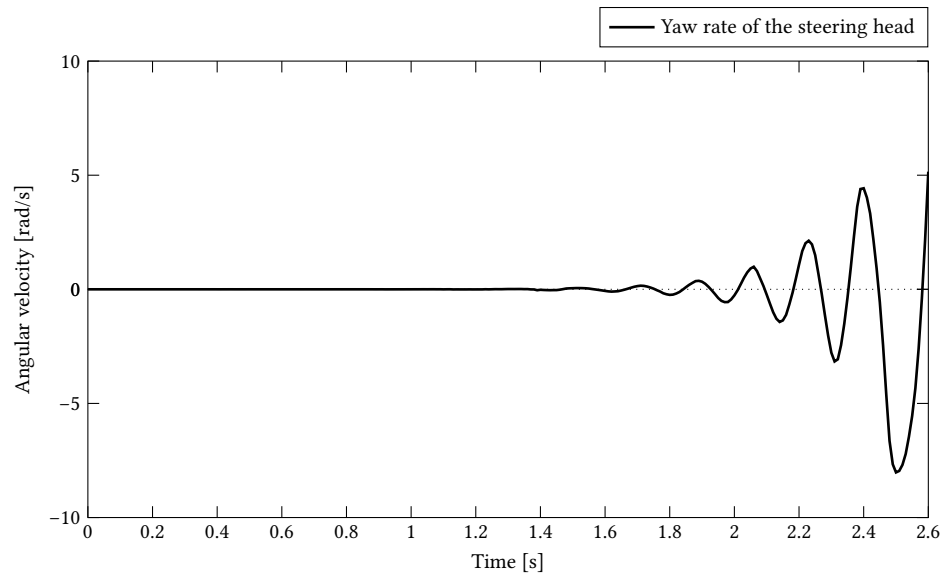


Figure 4.7: Angular velocity around z-axis of the steering head of the telescopic front suspension motorcycle as a function of time

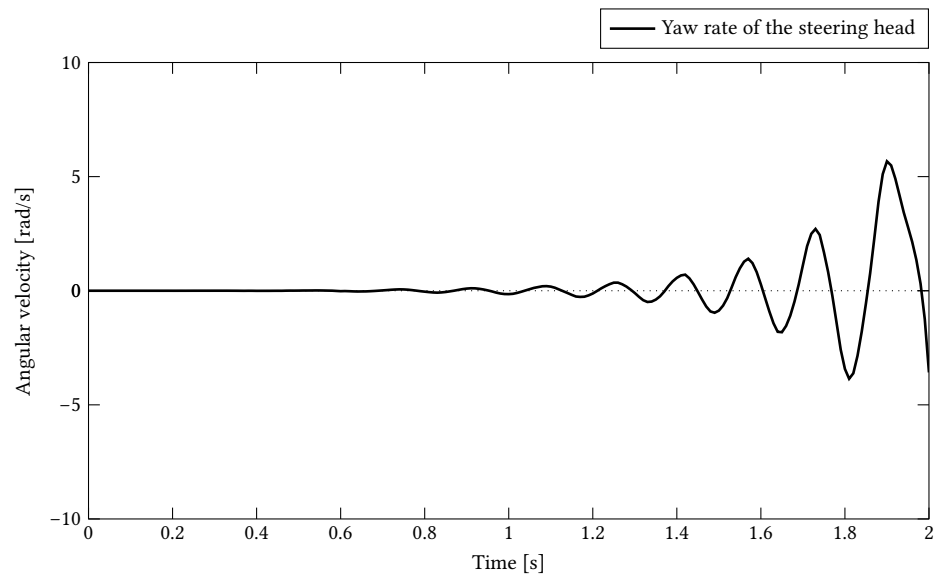


Figure 4.8: Angular velocity around z-axis of the steering head of the multi-link front suspension motorcycle as a function of time

Through the above animation description and line graph of the example, the performance of the motorcycle will be displayed intuitively. Table 4.6 summarizes the performance of both telescopic and multi-link front suspension motorcycles within a certain speed range, which starts from 5 m/s and gradually increases to 50 m/s with the rate of 5 m/s.

Speed	Telescopic front suspension motorcycle	Multi-link front suspension motorcycle
5 m/s	Unstable (weave)	Unstable (capsize)
10 m/s	Barely stable (mild weave)	Unstable (capsize)
15 m/s	Stable	Stable
20 m/s	Stable	Stable
25 m/s	Barely stable (mild wobble)	Barely stable (combined mild wobble and weave)
30 m/s	Unstable (wobble)	Unstable (combined wobble and weave)
35 m/s	Unstable (wobble)	Unstable (wobble)
40 m/s	Unstable (wobble)	Unstable (wobble)
45 m/s	Very unstable (wobble)	Very unstable (wobble)
50 m/s	Very unstable (wobble)	Very unstable (wobble)

Table 4.6: The performance of both telescopic and multi-link front suspension motorcycles within a certain speed range.

### 4.3.2 Forced Straight Running Simulation

After the simulation of the unforced straight running, a torque was applied on the front handlebar of the motorcycle to realize the forced straight running simulation. The magnitude of the torque follows a sinusoidal function. There are five values of the torque function amplitude  $A$ : 1 Nm, 5 Nm, 10 Nm, 30 Nm and 50 Nm. The frequency  $f$  of the applied torque also has six values: 0.5 Hz, 1 Hz, 2 Hz, 4 Hz, 6 Hz and 8 Hz. These values of the amplitude and frequency result in 30 combinations. The sinusoidal function of the torque is:

$$y(t) = A \sin(2\pi ft) \quad (4.2)$$

After applying a torque with Equation 4.2 on the front handlebar, and the reaction torque on the frame, the motion of the frame was evaluated. Figure 4.9 gives the result of the magnitude of the angular velocity around z-axis of the frame with respect to the time. Figure 4.9 is the simulation result of the telescopic front suspension motorcycle. These 30 torque expressions will be applied on each of the telescopic and multi-link front suspension models, which means there are 60 sets of data in total. The forced response was processed using the MotionView<sup>®</sup> software.

Figure 4.9 is the graph that results from the simulation. However, it cannot be used directly to determine the motorcycle frame reaction yaw rate, because this result is heavily influenced by the other response modes of the whole motorcycle. This is the reason that the curve in Figure 4.9 appears non-smooth. Therefore, a filter was used in this section, which is designed and carried out in the MATLAB<sup>®</sup> software. The frequency of the frame yaw rate should be equal to the frequency of the torque applied on the handlebar, because the frame is directly connected with the handlebar. A bandpass Butterworth filter is able to remove the interference frequencies and leave the required frequency. In this example, the torque frequency is 0.5 Hz. Thus, the frequency of the result should also be 0.5 Hz, which can be seen from Figure 4.10 below.

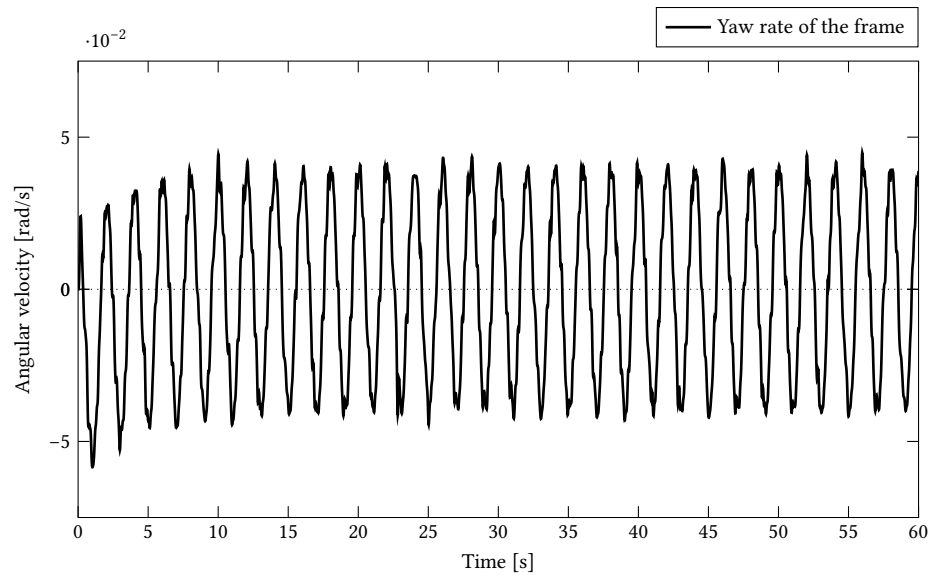


Figure 4.9: Angular velocity around z-axis of the frame of the telescopic front suspension motorcycle in response to an applied steer torque

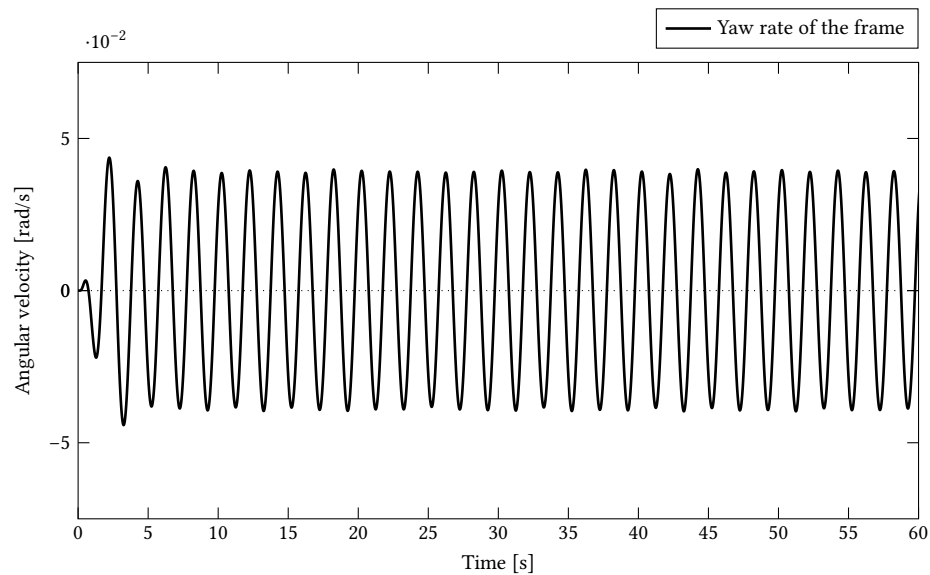


Figure 4.10: Angular velocity around z-axis of the frame of the telescopic front suspension motorcycle in response to an applied steer torque, after filtering

In Figure 4.10, after processing by the filter, the real yaw rate of the frame is obtained. As can be seen from Figure 4.10, the waveform has stabilized after 5 seconds. The amplitude of this stable waveform represents the maximum value that frame yaw achieves during the stabilization period. The similar approach is applied to the telescopic and multi-link front suspension motorcycle models, which produces 60 line graph results.



These data are summarized in Table 4.8 and Table 4.9. It is necessary to mention that one of the amplitudes of the torque, 50 Nm, does not appear in the result tables, because under this torque, both telescopic and multi-link front suspension motorcycles are not stable. For instance, Figure 4.11 shows the results of the torque with 50 Nm and 1 Hz parameters for the multi-link front suspension motorcycle. It is obvious that the frame motion is continuously irregular until overturning. The value of the amplitude of the stable waveform cannot be found in this case. Moreover, according to observation of the animations, all of the overturning results belong to the ‘low side’ type crash.

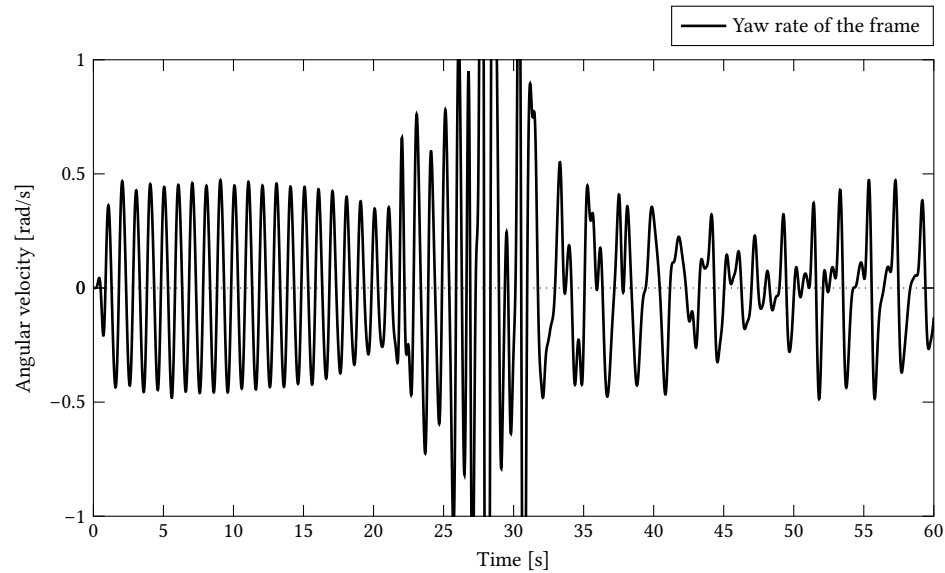


Figure 4.11: Angular velocity around z-axis of the frame of the multi-link front suspension motorcycle as a function of time. Produced after the filter.

The results of the linear and non-linear analysis are shown in the three tables below. In each table, every value has its corresponding frequency and torque. First of all, for the linear analysis, the forced straight running simulation of both telescopic and multi-link front suspension motorcycles are processed by the EoM software. The frame yaw rate (rad/s) result in Table 4.7 of the linear simulation with the torque 1 Nm is used as a reference for the non-linear analysis. It should be mentioned that for the linear simulation, the amplitude of motorcycle frame yaw rate grows at the same multiple as the increase of torque. Therefore, it is enough for the linear model to be simulated only with 1 Nm torque.

Torque frequency	0.5 Hz	1 Hz	2 Hz	4 Hz	6 Hz	8 Hz
Telescopic yaw rate	0.00814	0.01034	0.02551	0.02288	0.01285	0.00593
Multi-link yaw rate	0.00797	0.01003	0.02161	0.02059	0.01374	0.00533

Table 4.7: The result of the forced response linear simulation with a 1 Nm torque applied

Table 4.8 gives the information of the non-linear forced straight running simulation result of the telescopic

front suspension motorcycle. This frame yaw rate (rad/s) result is produced from the simulation by the MotionView<sup>®</sup> software. The animation and line graphs provide a strong basis for these results.

Frequency	0.5 Hz	1.0 Hz	2.0 Hz	4.0 Hz	6.0 Hz	8.0 Hz
1 Nm	0.00816	0.01039	0.02468	0.02424	0.01298	0.00564
5 Nm	0.03941	0.05725	0.11790	0.11711	0.06133	0.02695
10 Nm	0.09427	0.10229	0.24761	0.22153	0.12840	0.08614
30 Nm	0.37197	0.26312	0.72862	0.53921	0.36593	0.24209

Table 4.8: The frame yaw rate (rad/s) of the non-linear forced straight running simulation of the telescopic front suspension motorcycle

Table 4.9 gives the information of the non-linear forced straight running simulation result of the multi-link front suspension motorcycle. This frame yaw rate (rad/s) result is also produced from the simulation by the MotionView<sup>®</sup> software. The animation and line graphs provide a strong basis for these results. The plots of both Table 4.8 and Table 4.9 are shown in Chapter 5, which are used for more intuitive analysis of the forced straight running simulation results.

Frequency	0.5 Hz	1.0 Hz	2.0 Hz	4.0 Hz	6.0 Hz	8.0 Hz
1 Nm	0.00767	0.00960	0.01864	0.02051	0.01475	0.00564
5 Nm	0.03782	0.05035	0.09232	0.10843	0.07257	0.03552
10 Nm	0.07193	0.10186	0.18164	0.20909	0.17121	0.08184
30 Nm	0.23575	0.28779	0.55842	0.61858	0.45907	0.21967

Table 4.9: The frame yaw rate (rad/s) of the non-linear forced straight running simulation of the multi-link front suspension motorcycle

## 4.4 In-plane Simulation

The in-plane simulation is the most important part of the thesis, because it directly relates to the front suspension performance, which is the main topic of this thesis. There are three parts of this simulation: braking, plank road, and random road. There are some changes to both the telescopic and multi-link front suspension models for the in-plane simulation. The whole motorcycle is constrained on its own symmetric plane, which means it can only run along the longitudinal direction, with no roll or steering motion; a parallel axes joint is applied between the frame and global axes. A fixed joint is used to confine the steering motion of the handlebar. Through the simulation of this motorcycle model, the data required to evaluate the front suspension performance is obtained.

#### 4.4.1 Braking Simulation

In this part, the performance of the motorcycle model equipped with different front suspension system at the time of braking will be evaluated. In the MotionView<sup>®</sup> software, the entire simulation process was designed to use the following steps. First, the motorcycle is ridden at a constant speed. As shown in Table 4.6, 25 m/s is selected as the best simulation speed, because this speed is the maximum that was achieved under stable conditions during the unforced straight running simulation. After 5 s of straight running, there is a torque directly applied on the front wheel, in a direction opposite to the direction of rotation. The reaction torque acts on the lower fork or the wheel carrier. This torque imitates the braking motion, which continuously acts on the front wheel until the motorcycle stops moving forward. There are some properties that can be used as the assessment reference of the braking performance. As mentioned before, the pitch motion of the motorcycle during the braking heavily influences the riding quality and it has a close relationship with the structure of the front suspension system. Therefore, the pitch angle is one of the most significant properties that need to be evaluated. The time history line plot of the change in angle is found from the MotionView<sup>®</sup> software, but the theory of Euler parameters is used in this software to represent the angle change. A detailed explanation of this theory is given by Baruh[59]. In this section, the use of Euler parameters can be seen from Figure 4.12 as below.

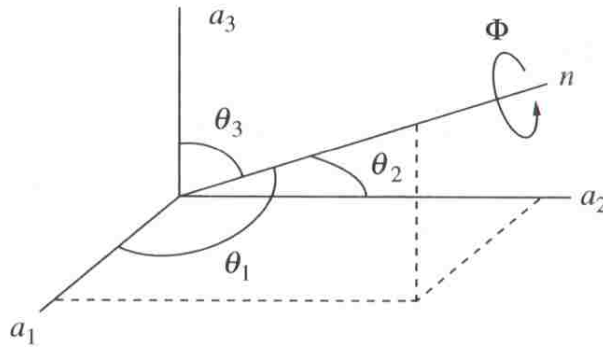


Figure 4.12: Euler parameters principle line (reproduced from Baruh[59])

In Figure 4.12, the direction cosines ( $C_1$   $C_2$   $C_3$ ) of the principal line can be denoted by the angles ( $\theta_1$   $\theta_2$   $\theta_3$ ) of the principal line with respect to the coordinate axis as below.

$$C_1 = \cos \theta_1 \quad C_2 = \cos \theta_2 \quad C_3 = \cos \theta_3 \quad (4.3)$$

The four parameters ( $E_0$   $E_1$   $E_2$   $E_3$ ) define the Euler parameters as below:

$$E_0 = \cos \left( \frac{\Phi}{2} \right) \quad E_1 = C_1 \sin \left( \frac{\Phi}{2} \right) \quad E_2 = C_2 \sin \left( \frac{\Phi}{2} \right) \quad E_3 = C_3 \sin \left( \frac{\Phi}{2} \right) \quad (4.4)$$

The MotionView® software provides a plot of the four parameters ( $E_0$   $E_1$   $E_2$   $E_3$ ) as a function of time. For the in-plane braking simulation, the motorcycle can only travel along the plane defined by the  $a_1$  and  $a_3$  coordinates ( $x$ - $z$  plane). It means  $\theta_2$  will remain at zero and  $\Phi$  is the pitch angle that is needed for the result. Therefore, according to the four parameters in Equation 4.4, the plot of the  $E_2$  is the best choice to show the change of the pitch angle. Note that the  $C_2$  is equal to one when  $\theta_2$  is zero.

The braking performance of both the telescopic and multi-link front suspension motorcycles will be evaluated within a certain braking torque range, which starts from 100 Nm and gradually increases to 800 Nm in steps of 100 Nm. The reason for the choice of the torque range is that forward overturning occurs when the braking torque is larger than 800 Nm. After the simulation of the in-plane braking, the first result should be the graph of the forward speed. For example, when the torque is 500 Nm, the change of the velocity for both telescopic and multi-link front suspension motorcycles can be seen from Figure 4.13 as below.

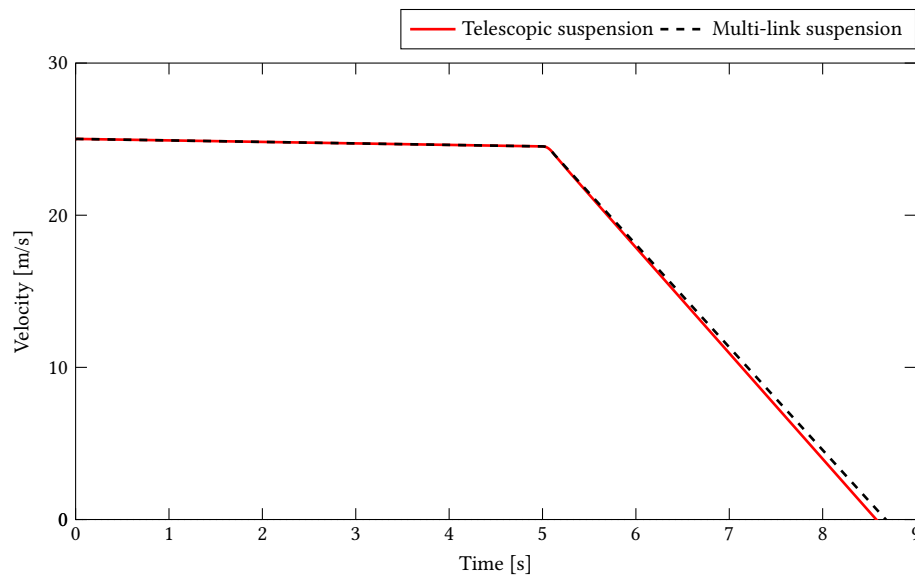


Figure 4.13: Forward velocity of both telescopic and multi-link front suspension motorcycles as functions of time, in response to the 500 Nm braking torque, starting from 5 s

It is obvious that the speed of telescopic model gradually declines starting from 5 s and reaches zero at around 8.6 s. It suggests that the design of the in-plane braking simulation of the telescopic front suspension motorcycle is reasonable. Also, with the same braking torque 500 Nm, a reasonable change in the velocity of the multi-link front suspension motorcycle can also be seen.

After demonstrating the feasibility of the model, the graph of the Euler parameter  $E_2$  is available. Figure 4.14 shows the curve of Euler parameter  $E_2$  as a function of time for both telescopic and multi-link front suspension motorcycles.

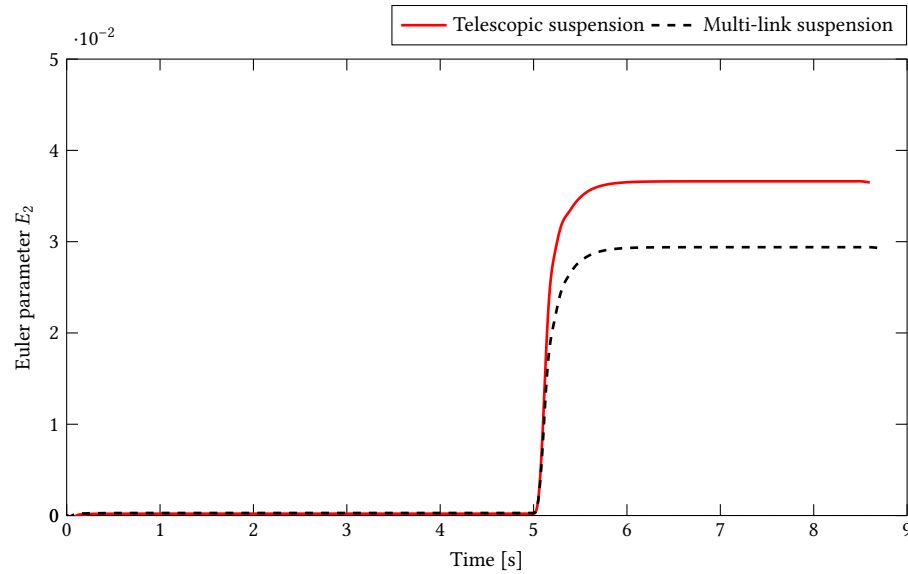


Figure 4.14: Euler parameter  $E_2$  of both telescopic and multi-link front suspension motorcycles as functions of time, in response to the 500 Nm braking torque, starting from 5 s

With the application of the braking torque, the Euler parameter value  $E_2$  grows rapidly until a stable value is reached. This stable value was recorded and used to calculate the pitch angle according to Equation 4.4. This pitch angle was compared with the pitch angle from the simulation result of the multi-link front suspension motorcycle. The value  $E_2$  of the multi-link front suspension motorcycle also can be seen in Figure 4.14.

Another important parameter that can be used to evaluate the braking performance is the height change of the motorcycle frame. As mentioned before, during the braking motion, the forks compress and the rider is thrown slightly forward, which also results in the movement of the frame. Thus, the amount of change in the height of the frame can be used as a reference for evaluating the performance of the motorcycle brake. For example, continuing to use a 500 Nm braking torque, the curves of both telescopic and multi-link front suspension motorcycles frame height can be seen in Figure 4.15 below. For the telescopic suspension, in the first 5 s, the height of frame is maintained at a stable level. With the application of braking torque, the height suddenly decreases to around 460 mm and then rises to about 470 mm, which is maintained until the end. The final height is the value that is recorded, and will be used to compare with the height value in the simulation result of the multi-link front suspension motorcycle.

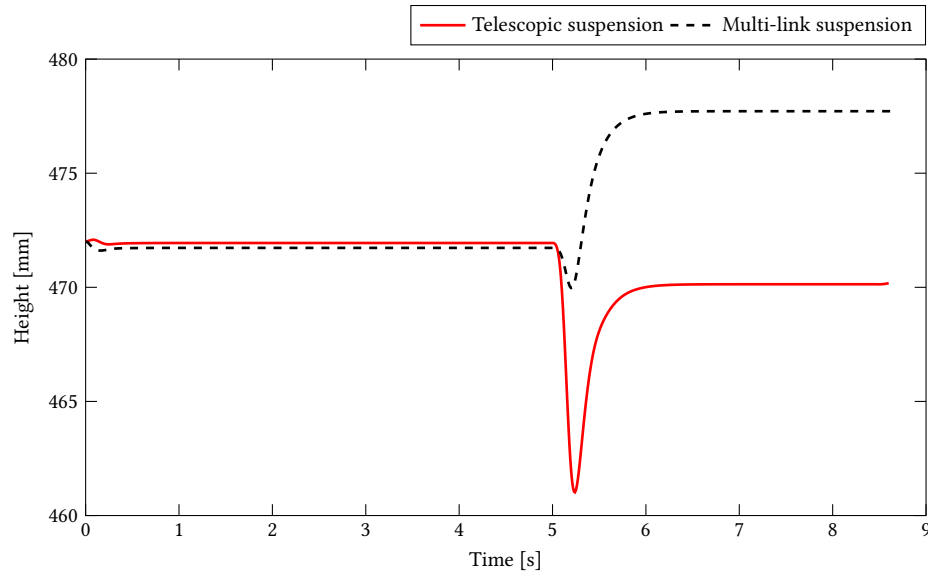


Figure 4.15: The height change of both telescopic and multi-link front suspension motorcycles as functions of time, in response to the 500 Nm braking torque, starting from 5 s

Figure 4.15 also gives the information about the height change of multi-link front suspension motorcycle under 500 Nm braking torque, which starts from 5 s. Similar to the telescopic front suspension motorcycle, during the first 5 s, the height of the frame is maintained at a stable level. With the application of the torque, the height suddenly decreases to around 470 mm and then rises to about 478 mm, which was maintained until the end.

According to the simulation above, the pitch angle, stop time and frame height can be found under different braking torques. These results are used to evaluate the braking performance and are summarized in Table 4.10 and Table 4.11 below. Table 4.10 shows the results of the telescopic front suspension motorcycle.

Torque	Stop time [s]	Pitch angle [deg]	Frame Height [mm]
100 Nm	17.00	0.82197	471.181
200 Nm	8.79	1.63665	470.586
300 Nm	5.92	2.46901	470.187
400 Nm	4.46	3.32117	470.020
500 Nm	3.58	4.19624	470.134
600 Nm	2.99	5.09879	470.592
700 Nm	2.56	6.03592	471.491
800 Nm	2.24	7.01824	472.980

Table 4.10: The braking simulation results of the telescopic front suspension motorcycle

Table 4.11 shows the results of the multi-link front suspension motorcycle.

Torque	Stop time [s]	Pitch angle [deg]	Frame Height [mm]
100 Nm	17.46	0.62829	472.968
200 Nm	9.03	1.25642	474.186
300 Nm	6.09	1.91973	475.378
400 Nm	4.59	2.62226	476.550
500 Nm	3.68	3.36897	477.716
600 Nm	3.07	4.16615	478.897
700 Nm	2.64	5.02209	480.138
800 Nm	2.31	5.94859	481.523

Table 4.11: The braking simulation results of the multi-link front suspension motorcycle

The tables above display the results of braking simulation. From these data, the basis to assess the performance of motorcycles with telescopic or multi-link front suspension system is available. In addition to these values, there are also two important parameters, caster angle and trail, that need to be considered. As mentioned before, the value of caster angle and trail have a crucial role to play for the geometry of motorcycle front assembly. Usually, the change of these two values heavily influences the stability of the motorcycle, which is especially important during the braking process. Therefore, in this part, the test model of caster angle and trail will be established and simulated in the MotionView<sup>®</sup> software.

Firstly, for the caster angle, there are some parts added into the basic model, especially for the multi-link front suspension motorcycle. The structure of the telescopic front suspension motorcycle allows one to get the caster angle directly, which can be calculated from the Euler parameter  $E_2$  of the upper fork, because the upper and lower fork are connected by the translational joint. However, for the multi-link front suspension motorcycle, its structure makes the establishment of the test model complicated, because the steering axis is defined by the four arms that are symmetrically distributed on both sides of the front wheel. As a result, a massless cylinder body needs to be built to represent the steering axis. Figure 4.16 shows the caster angle test model of the multi-link front suspension motorcycle. There is a cylinder body next to the center of front wheel that is used to simulate the steering axis. The upper end point of the cylinder is constrained on extension lines of the two upper arms, which means this point is also the intersection point of the upper arms extension lines. The lower end point of the cylinder also has the same position on the extension lines of the lower arms. The joints that are used to achieve this cylinder position are ‘in-line’ joints, which constrains one body to translate along the axis of a reference coordinate on another body. The caster angle can be calculated by the Euler parameter  $E_2$  of the cylinder. The initial speed of this simulation was 25 m/s, the same as the braking simulation before. The caster angle values under different braking torques will be recorded.

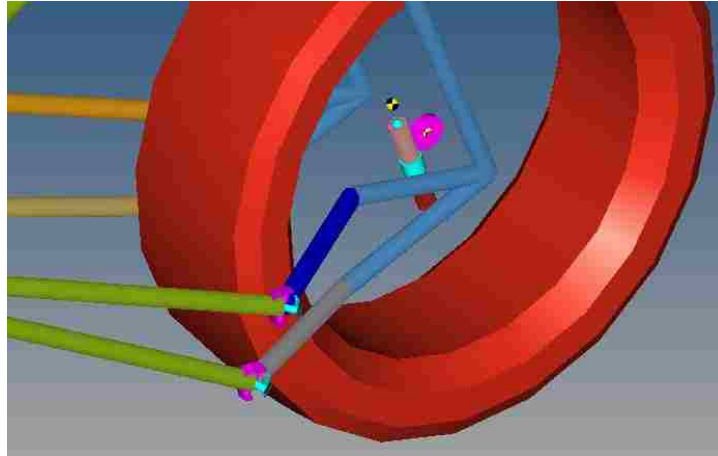


Figure 4.16: The caster angle test model of multi-link front suspension motorcycle

For the trail, there are also some changes that need to be added on both the telescopic and multi-link front suspension motorcycle models. The intersection point of the steering axis extension line and the ground needs to be marked. Taking this point as the center, a massless body is built. This body is only allowed to move in the ground plane. Figure 4.17 shows the front assembly part of the trail test model, especially the massless body on the ground. It is worth mentioning that the front assembly part of the telescopic motorcycle also has exactly the same changes. It can be imagined that this body will follow the rotation of steering axis. The distance between this massless body and front wheel contact point is the value of trail. The trail should increase with the rise of caster angle and vice versa. Therefore, the relationship between the numerical results of caster angle and trail can be used as a basis for proving the correctness of the test model.

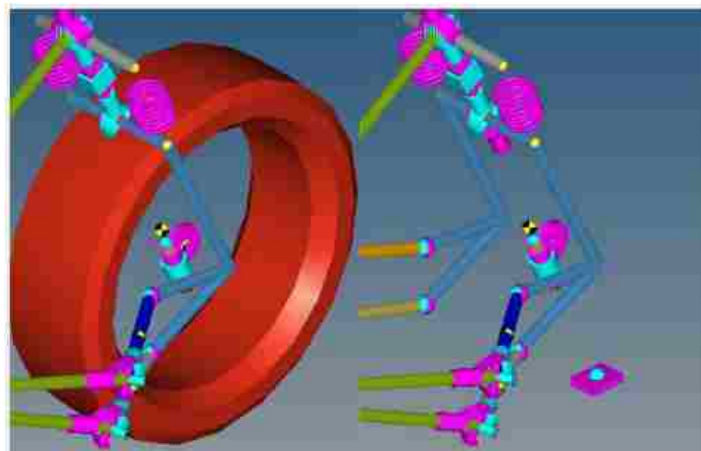


Figure 4.17: The trail test model of multi-link front suspension motorcycle;  
the massless body is on the ground in the right figure



In order to more intuitively describe the simulation results, there is an example result of the caster angle and trail test simulation. The braking torque is 500 Nm. For the telescopic front suspension motorcycle, the plot of Euler parameter  $E_2$  can be seen from Figure 4.18. On the whole, it has a very similar trend with the braking simulation plot of height and Euler parameter  $E_2$  before. Also, the steady value of the latter half of the curve is needed for the result. This Euler parameter  $E_2$  needs to be converted to the value of the angle  $\Phi$  according to Equation 4.4. After that, this angle should be reduced by the initial caster angle to get the new angle during the braking motion. For the multi-link front suspension motorcycle, the plot of Euler parameter  $E_2$  also can be seen from Figure 4.18. Again, the steady value of the rear half of the curve is needed for the result.

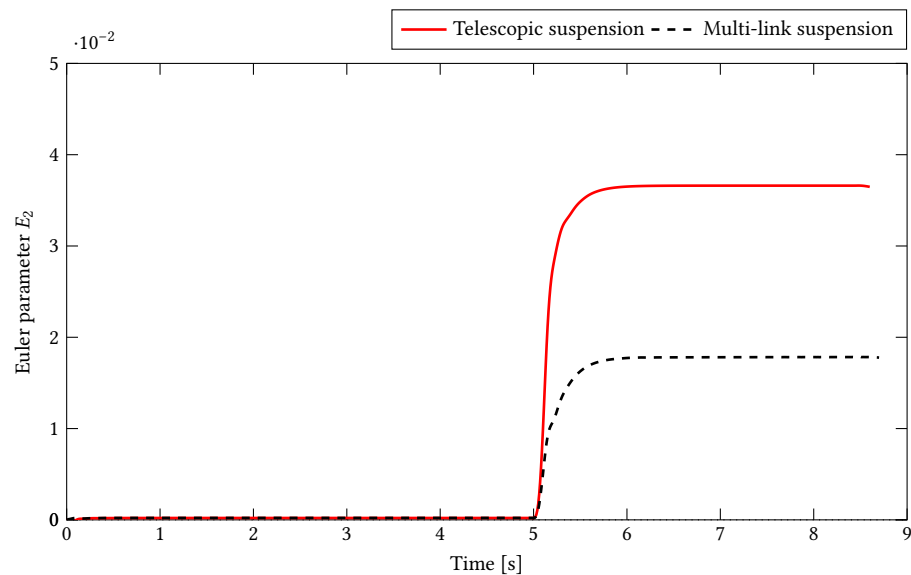


Figure 4.18: The Euler parameter  $E_2$  change of steering axis for both telescopic and multi-link front suspension motorcycles as a function of time under 500 Nm braking torque starting from 5 s.

Under the same braking torque, the graph of trail for both telescopic and multi-link front suspension motorcycles is seen in Figure 4.19.

Different from the caster angle, the trail does not require any extra calculation. The steady length of rear half of the curve is the trail result that needs to be recorded. For the multi-link front suspension motorcycle, the plot of trail can be seen from Figure 4.19, too.

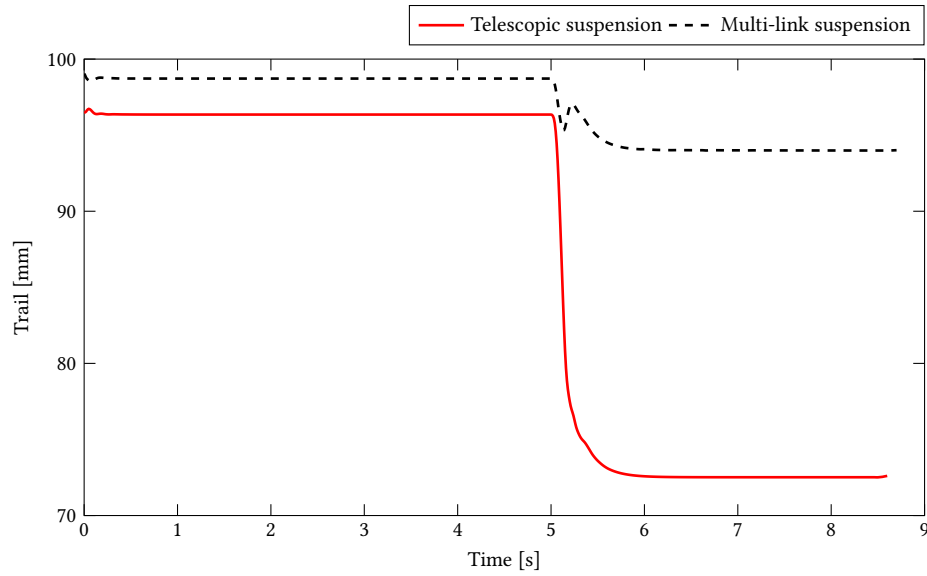


Figure 4.19: The trail change of steering axis for both telescopic and multi-link front suspension motorcycles as a function of time, in response to the 500 Nm braking torque, starting from 5 s

Results of both caster angle and trail are summarized in two tables as below. Moreover, the pitch angle will serve as an important reference. For the telescopic front suspension motorcycle, Table 4.12 gives information of the simulation results for both caster angle and trail.

Torque	Pitch angle [deg]	Caster angle [deg]	Trail [mm]
0 Nm	0	24.00127	96.4966
100 Nm	0.82197	23.17803	91.6413
200 Nm	1.63665	22.36335	86.9100
300 Nm	2.46901	21.53099	82.1532
400 Nm	3.32117	20.67883	77.3605
500 Nm	4.19624	19.80376	72.5167
600 Nm	5.09879	18.90121	67.5996
700 Nm	6.03592	17.96408	62.5750
800 Nm	7.01824	16.98176	57.3950

Table 4.12: The simulation results of the telescopic front suspension motorcycle for caster angle and trail in response to torque and pitch angle

For the multi-link front suspension motorcycle, Table 4.13 gives information of the simulation results for both caster angle and trail. Furthermore, it should be mentioned that a series of results for both 100 Nm and 800 Nm braking torque are attached in Appendix C.

Torque	Pitch angle [deg]	Caster angle [deg]	Trail [mm]
0 Nm	0	24.34109	99.04761
100 Nm	0.62829	23.97250	98.02070
200 Nm	1.25642	23.60523	97.23900
300 Nm	1.91973	23.20851	96.34020
400 Nm	2.62226	22.77475	95.27790
500 Nm	3.36897	22.29836	93.99000
600 Nm	4.16615	21.76491	92.39650
700 Nm	5.02209	21.16426	90.38210
800 Nm	5.94859	20.47375	87.79430

Table 4.13: The simulation results of the multi-link front suspension motorcycle for caster angle and trail in response to torque and pitch angle

#### 4.4.2 Plank Road Simulation

The purpose of the plank road simulation is to evaluate the performance of front suspension when the motorcycle crosses a barrier. In the MotionView<sup>®</sup> software, the shape of the barrier is available to be set directly in the road file. As can be seen from Figure 4.20, there are five parameters that need to be used for the road barrier design. These parameters include the height of the cleat, which is 0.05 m in this model. The distance along longitudinal direction of the road to the start of the cleat is 10 m. The length of the cleat along the longitudinal direction of the road is 0.4 m. The length of the 45° bevel edge of the cleat is 0.01 m. The rotation angle of the cleat about the vertical axis with respect to the lateral axis of the road is 45°. Moreover, the speed of the motorcycle is set to 10 m/s, which can be used to cross the barrier safely.

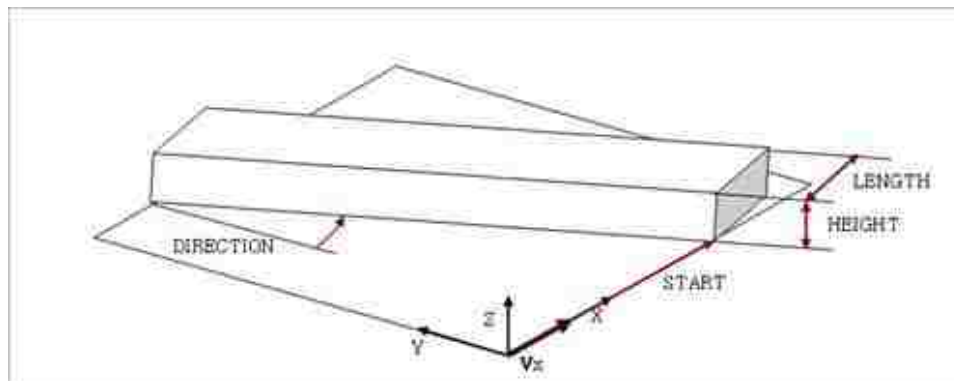


Figure 4.20: The geometry definition of the plank road (reproduced from RecurDyn[60])

There are three sets of data involved in the evaluation. They are the pitch angle, frame height and suspension travel distance. To measure the suspension travel, there is a point defined on the front wheel center whose relative position with the frame is fixed. If there is some vertical motion of the wheel, the distance between this point and front wheel center will not be zero. Furthermore, this distance change

represents the suspension travel.

Figure 4.21 shows graphs of the pitch angle of both the telescopic and multi-link front suspension motorcycles.

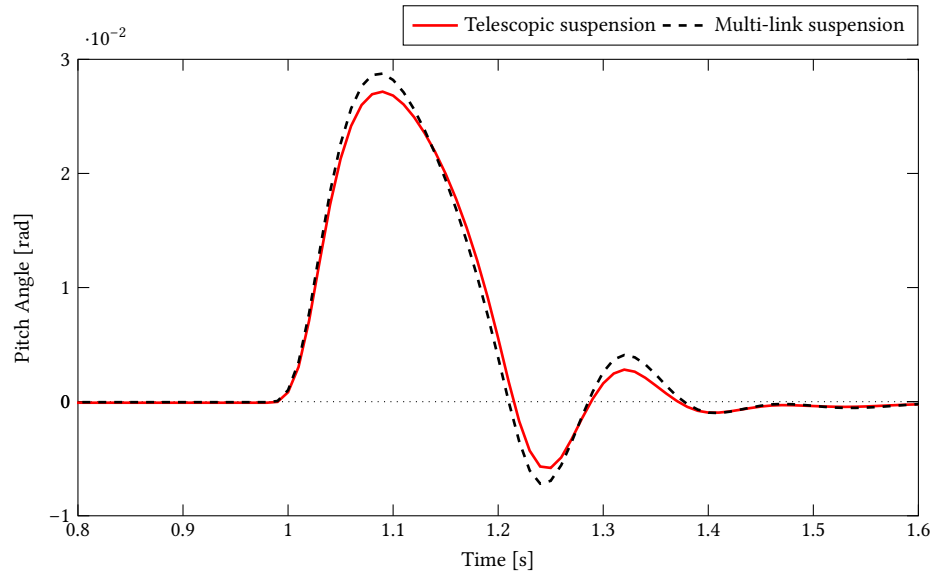


Figure 4.21: The pitch angle during the telescopic and multi-link front suspension motorcycle crosses the plank road respectively.

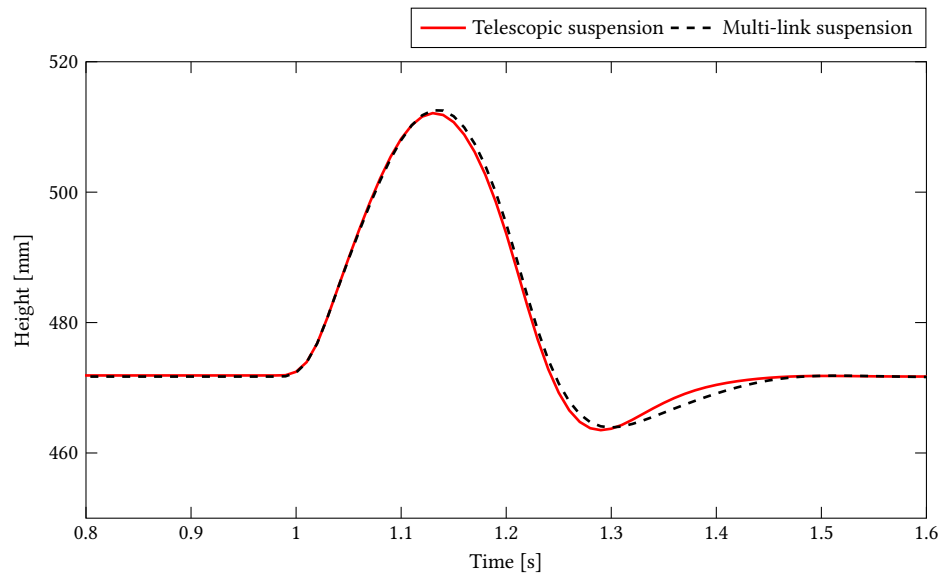


Figure 4.22: The frame height during the plank road crossing for the telescopic and multi-link suspension motorcycle

It is worth mentioning that the simulation time is only 3 s. However, in Figure 4.21, it is obvious that the valuable results are mainly limited around a short time period. Therefore, the time range of the graph is from 0.8 s to 1.6 s. Similarly, the following plots use the same interval to make the results clearer.

Figure 4.22 shows a graphs of the frame height of both the telescopic and multi-link front suspension motorcycles. Figure 4.23 shows graphs of the suspension travel distance of both the telescopic and multi-link front suspension motorcycles.

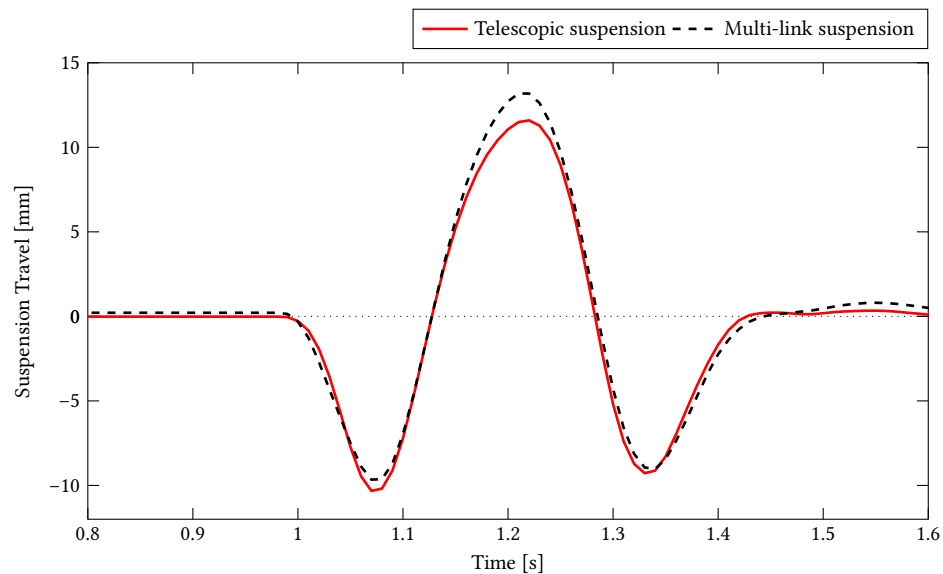


Figure 4.23: The suspension travel distance during the plank road crossing for the telescopic and multi-link front suspension motorcycle

#### 4.4.3 Random Road Simulation

The random road simulation explores the performance and makes a more clear comparison between the telescopic and multi-link front suspension motorcycle models. As mentioned in Chapter 3, random road profiles are used to conduct the simulations. The MotionView<sup>®</sup> software is again used to run the entire simulation. Firstly, the random road coordinate file is generated from the EoM software. Then, this file is directly input into the tire model, which has a dedicated part responsible for the pavement definition.

During the simulation, the length of the road profile is set to 100 m and two velocities, 10 m/s and 30 m/s, are given to the motorcycle model. The sampling frequency of the road profile is 512 Hz. An integer from 3-9 classifies the road profile, corresponding to the transition between ISO classes A-H. For instance, class 4 is equal to the transition between B and C class, which is smooth ( $h_{\max} \approx \pm 25$  mm) and class 9 refers to the G-H transition, which is very rough ( $h_{\max} \approx \pm 100$  mm). Figure 4.24 shows the output of this random road vertical displacement as a function of longitudinal distance.

The first step of this simulation is to confirm the road level range that the model can run normally with

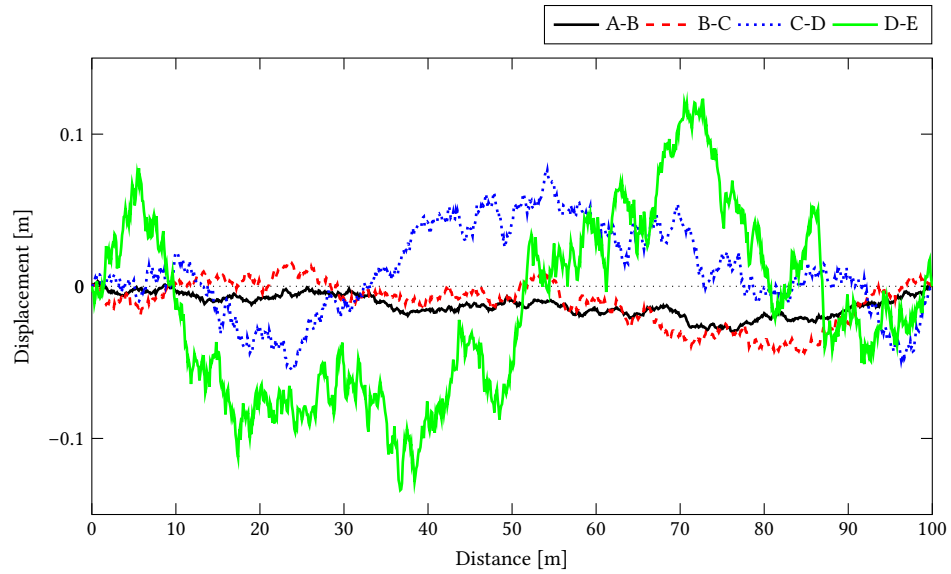


Figure 4.24: Random road vertical displacement as a function of longitudinal distance

a 10 m/s forward speed. The definition of the normal condition is that there should not be any instances of zero contact force between the tire and the road, because this means the tire has left the ground, and the suspension performance can not be evaluated in this case. The verification process starts from the level 3 random road and the zero contact force first appears in the result of the level 6 random road, for both telescopic and multi-link front suspension motorcycles. Figure 4.25 shows the contact force change between the telescopic suspension motorcycle front tire and the road.

It is obvious that the contact force in Figure 4.25 has values that equal to zero, which means the level 6 is not available to be used in the analysis. Figure 4.26 below shows the contact force change between the multi-link suspension motorcycle front wheel and the road.

Figure 4.26 once again shows that the level 6 random road should not be used for analysis. Therefore, level 3, 4 and 5 random roads are considered in the analysis. Furthermore, similar to the braking simulation, three characteristics, pitch angle, frame height, and suspension travel distance, are needed for the performance comparison between the telescopic and multi-link front suspension motorcycles.

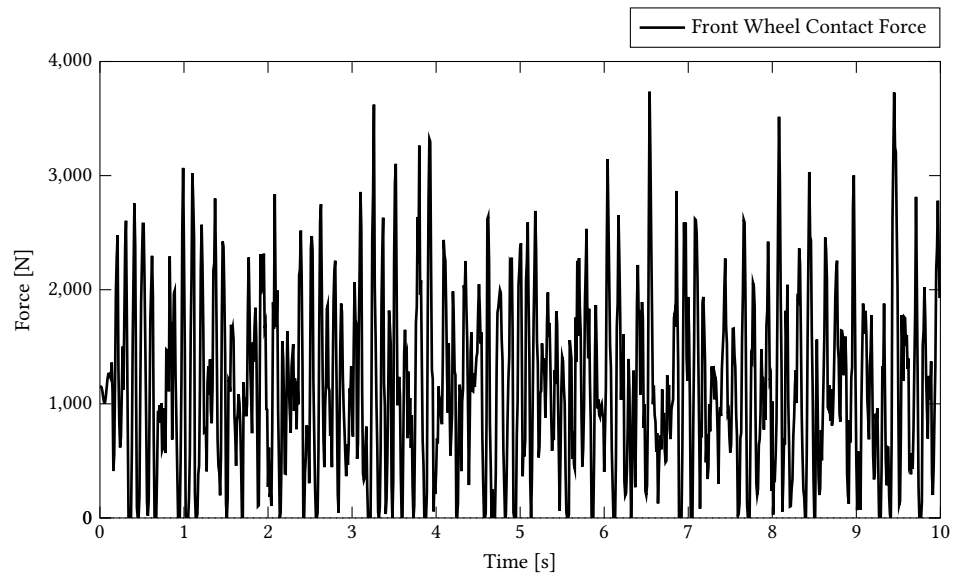


Figure 4.25: Vertical contact force between the telescopic suspension motorcycle front tire and the level 6 random road as a function of time

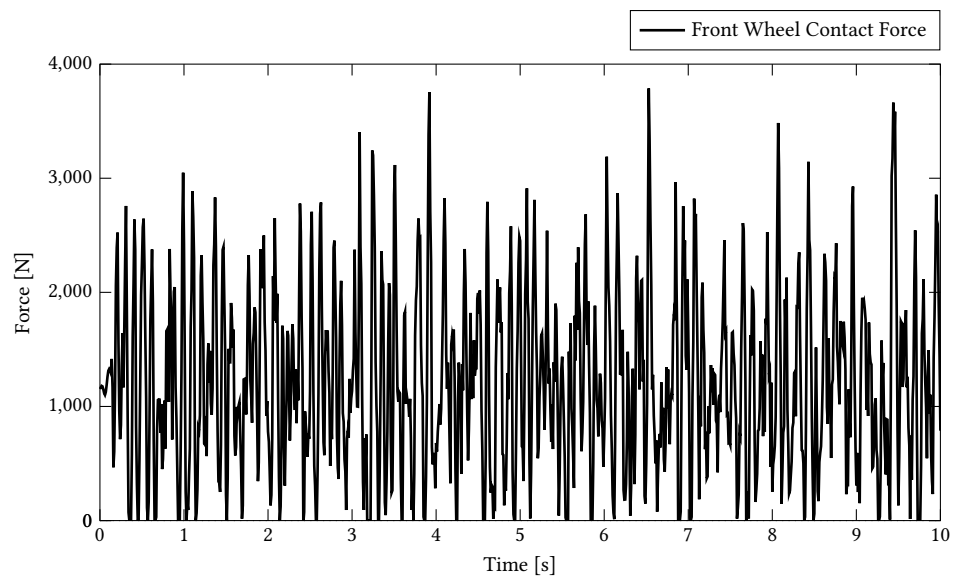


Figure 4.26: Vertical contact force between the multi-link suspension motorcycle front tire and the level 6 random road as a function of time

### Level 3 Random Road (10 m/s)

The result of the level 3 random road simulation is shown in this section. First of all, the level 3 random road condition can be seen from Figure 4.27. Comparing with the other random roads, the level 3 is the mildest one; the total distance of the simulation road is 100 m. When these three levels of roads are displayed, the scale of the ordinate is set to be invariant to more clearly show the road conditions of each level.

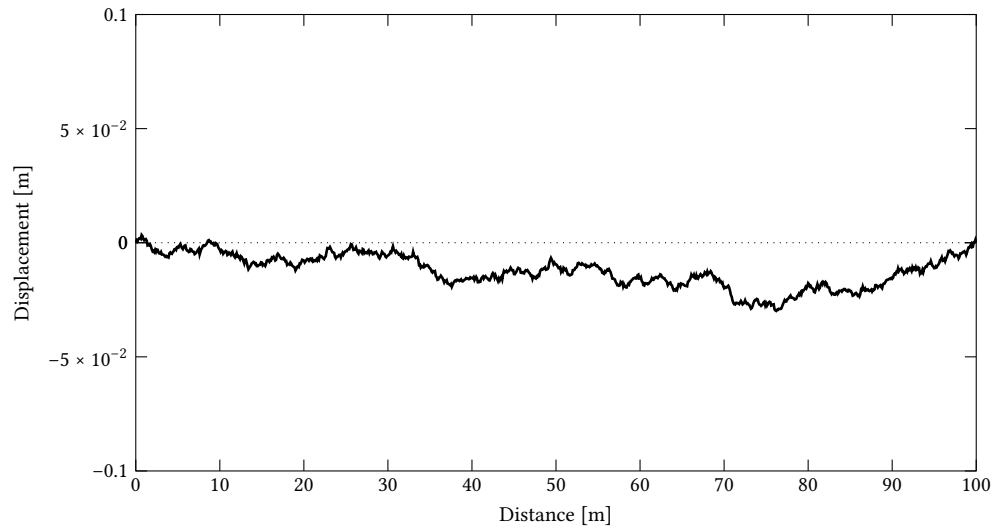


Figure 4.27: Level 3 random road

Figure 4.28 below gives the information about frame height change of the telescopic and multi-link front suspension motorcycles as a function of time running on the level 3 random road. These two curves are similar to the curve in Figure 4.27. Also, the curves in Figure 4.28 appear smoother due to the installation of the suspension system. The performance of frame height change for the telescopic and multi-link front suspension motorcycles is almost the same.

Figure 4.29 below shows the pitch angle change of the telescopic and multi-link front suspension motorcycles as a function of time running on the level 3 random road. It should be mentioned that results in the figure have been converted from Euler parameter  $E_2$  to the actual angle values.



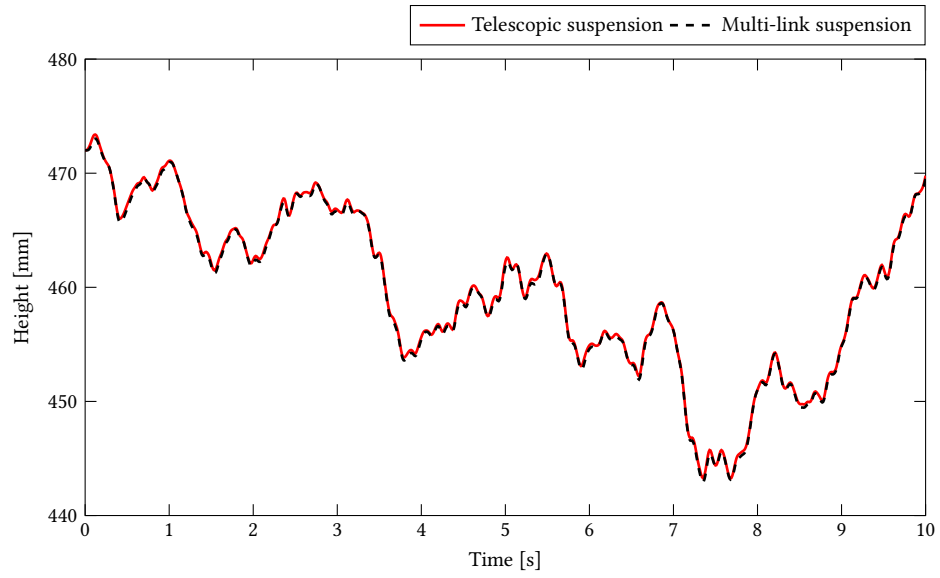


Figure 4.28: The frame height of both telescopic and multi-link front suspension motorcycles as a function of time running on the level 3 random road

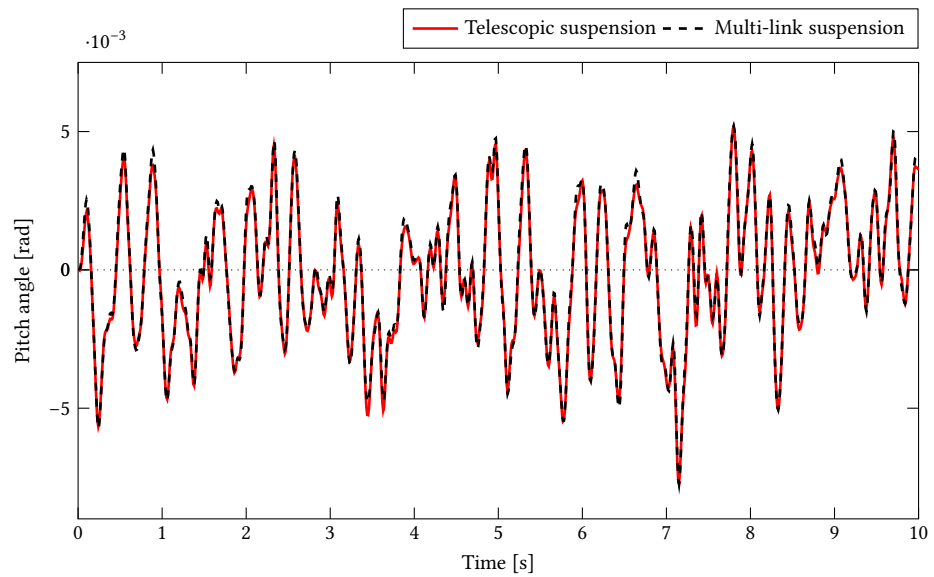


Figure 4.29: The pitch angle of both telescopic and multi-link front suspension motorcycles as a function of time running on the level 3 random road

The suspension travel distance of the telescopic and multi-link front suspension motorcycles as a function of time running on the level 3 random road can be seen in Figure 4.30. The positive value means the suspension is rebounding and negative means compressing.

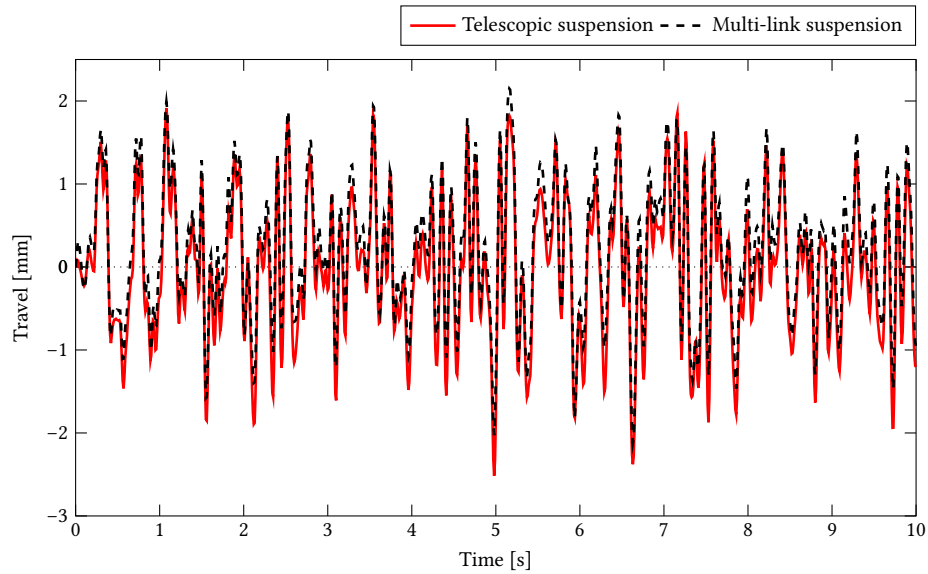


Figure 4.30: The suspension travel distance of both telescopic and multi-link front suspension motorcycles as a function of time running on the level 3 random road

#### Level 4 Random Road (10 m/s)

The result of the level 4 random road simulation is shown in this section. First of all, the level 4 random road condition can be seen from Figure 4.31. Comparing with the level 3 random roads, the level 4 is more intense and total distance of the simulation road is also 100 m.

Figure 4.32 shows the result of the frame height for both telescopic and multi-link front suspension motorcycles as a function of time running on the level 4 random road. It seems that these two curves are again very similar; it is hard to find any difference. It should be mentioned that the result of frame height directly reflects the rider's comfort and also provides a very important basis for the analysis of suspension travel distance.

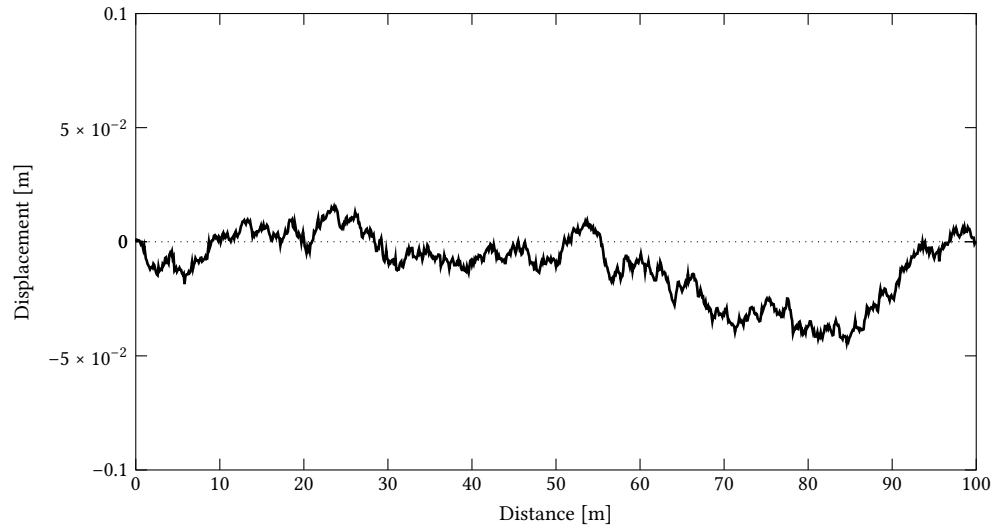


Figure 4.31: Level 4 random road

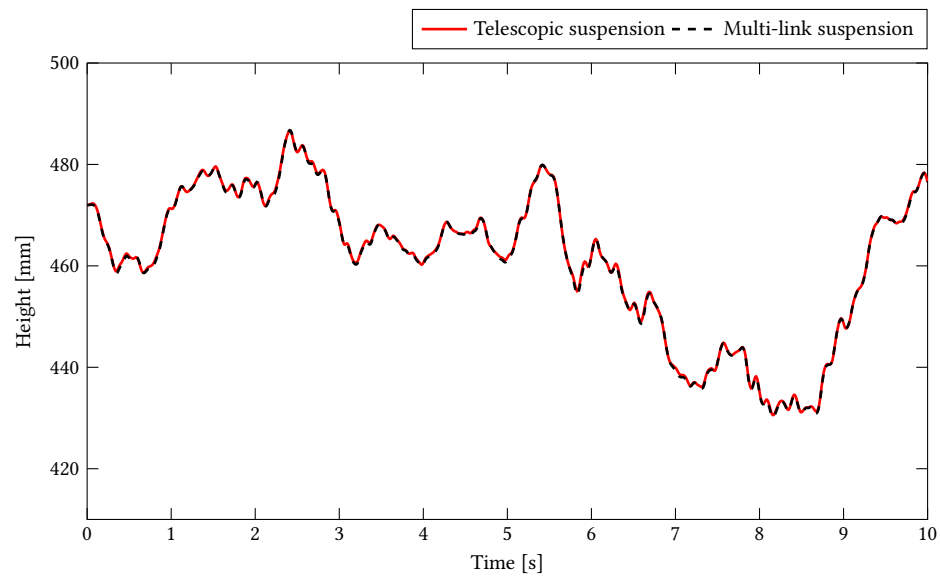


Figure 4.32: The frame height of both telescopic and multi-link front suspension motorcycles as a function of time running on the level 4 random road

Figure 4.33 and Figure 4.34 give the information about pitch angle and suspension travel distance respectively for both the telescopic and multi-link front suspension motorcycles as a function of time running on the level 4 random road.

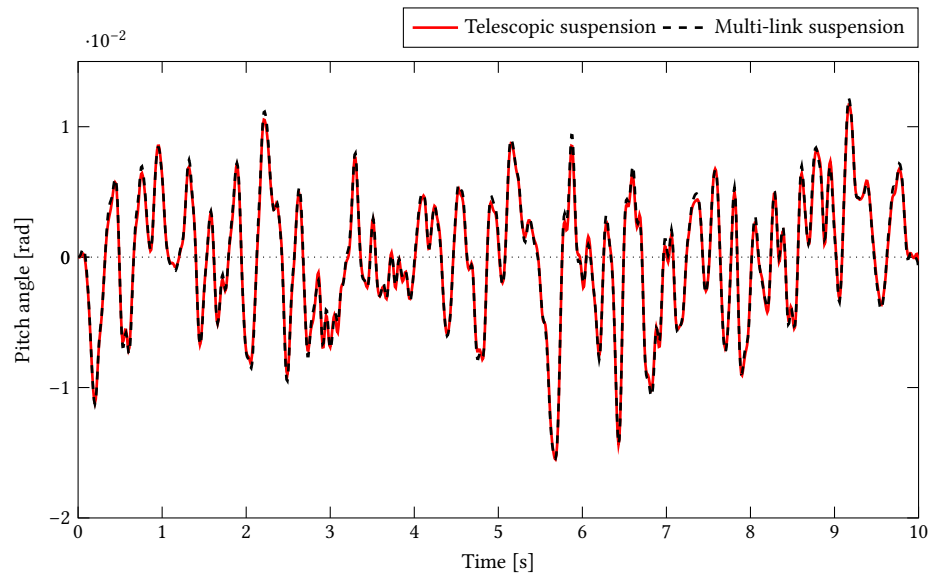


Figure 4.33: The pitch angle of both telescopic and multi-link front suspension motorcycles as a function of time running on the level 4 random road

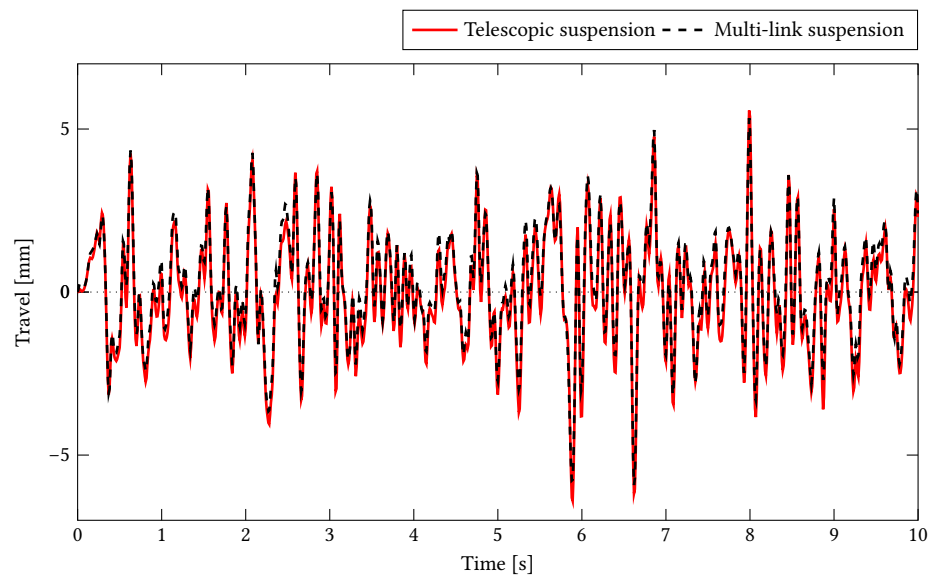


Figure 4.34: The suspension travel distance of both telescopic and multi-link front suspension motorcycles as a function of time running on the level 4 random road

### Level 5 Random Road (10 m/s)

In this section, the simulation result of the level 5 random road is displayed. The road condition of level 5 is shown in Figure 4.35. Comparing with the other two random roads, level 5 has the most intense road condition; the total distance of the simulation road is still 100 m.

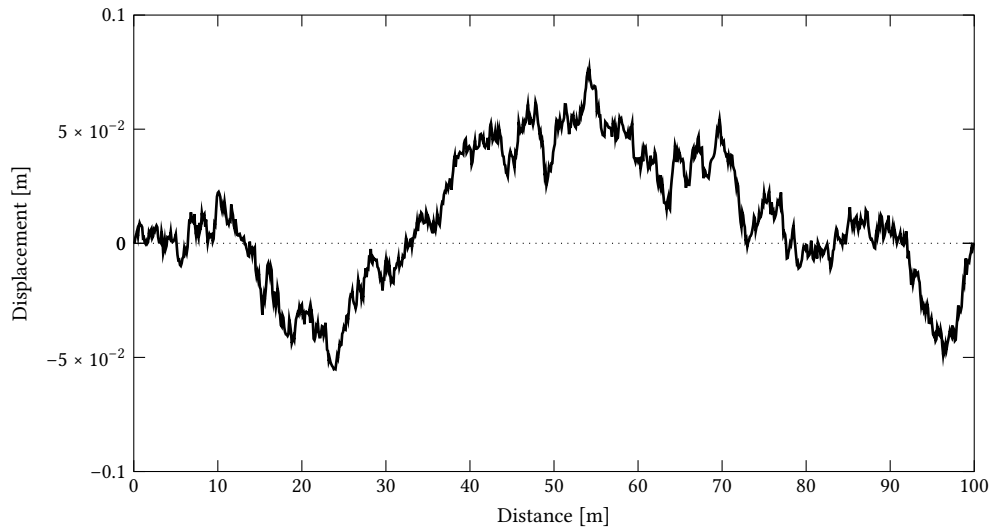


Figure 4.35: Level 5 random road

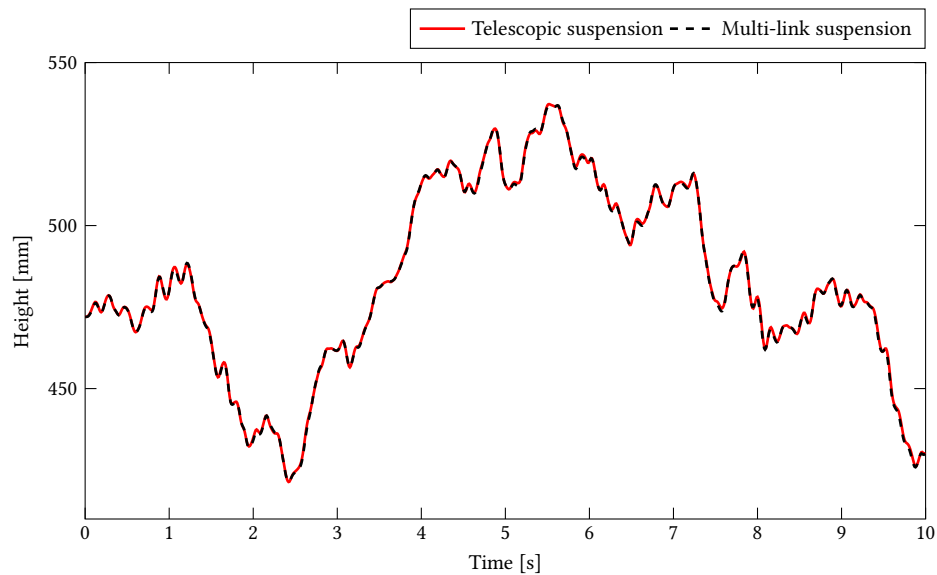


Figure 4.36: The frame height of both telescopic and multi-link front suspension motorcycles as a function of time running on the level 5 random road

Following the same order as before, Figure 4.36 above shows frame height change of both the telescopic and multi-link front suspension motorcycles as a function of time running on the level 5 random road. After that, Figure 4.37 is the result of the pitch angle and then the plot of suspension travel distance can be seen in Figure 4.38.

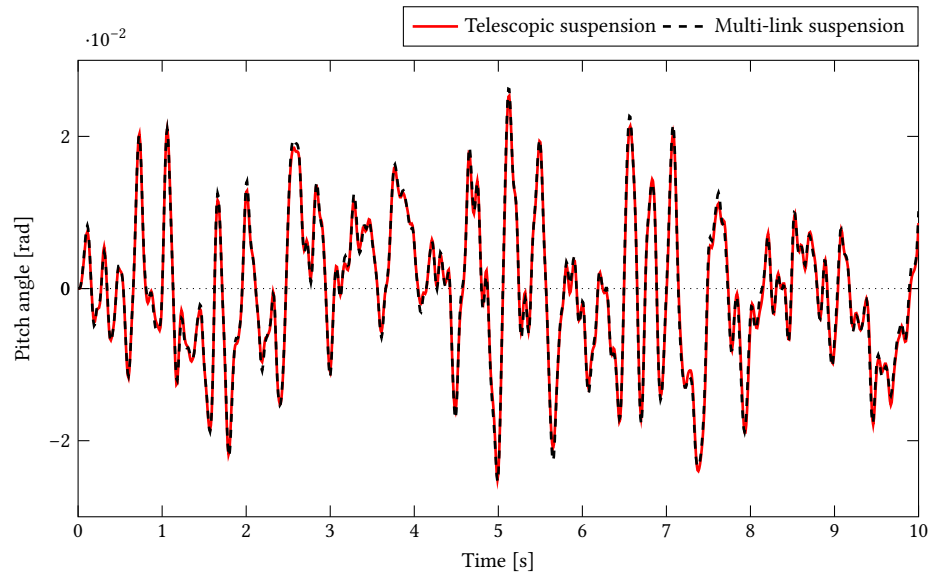


Figure 4.37: The pitch angle of both telescopic and multi-link front suspension motorcycles as a function of time running on the level 5 random road

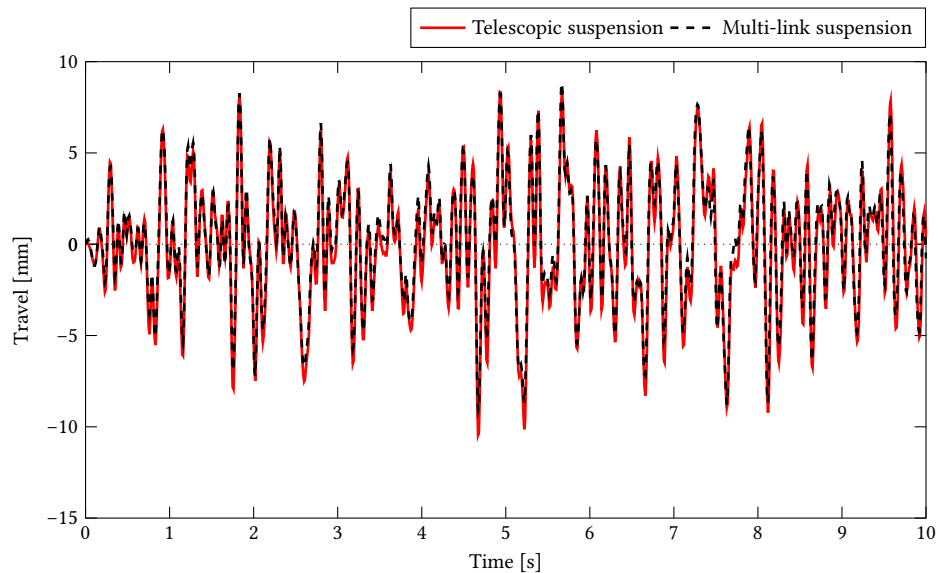


Figure 4.38: The suspension travel distance of both telescopic and multi-link front suspension motorcycles as a function of time running on the level 5 random road

The second part in this section shows the results of the random road simulation for both the telescopic and multi-link front suspension motorcycles with a speed of 30 m/s. Similar to the simulation at 10 m/s, the first step is also to confirm the road level range of motorcycles that can run normally with a 30 m/s forward speed. As mentioned before, if there is any zero contact force between tire and road in the simulation result, the road level corresponding to it will not be analyzed. The verification process also starts from the level 3 random road and the zero contact force appears in the result of the level 5 random road for both telescopic and multi-link front suspension motorcycles. Figure 4.39 shows the contact force between the telescopic motorcycle front wheel and the road.

As can be seen from Figure 4.39, some values of the contact force are equal to zero, which means the level 5 is not available to be used in the analysis. Figure 4.40 below shows the contact force change between the multi-link motorcycle front wheel and the road, which once again suggests that the level 5 random road could not be used for analysis. Therefore, level 3 and 4 random roads only are considered in the analysis.

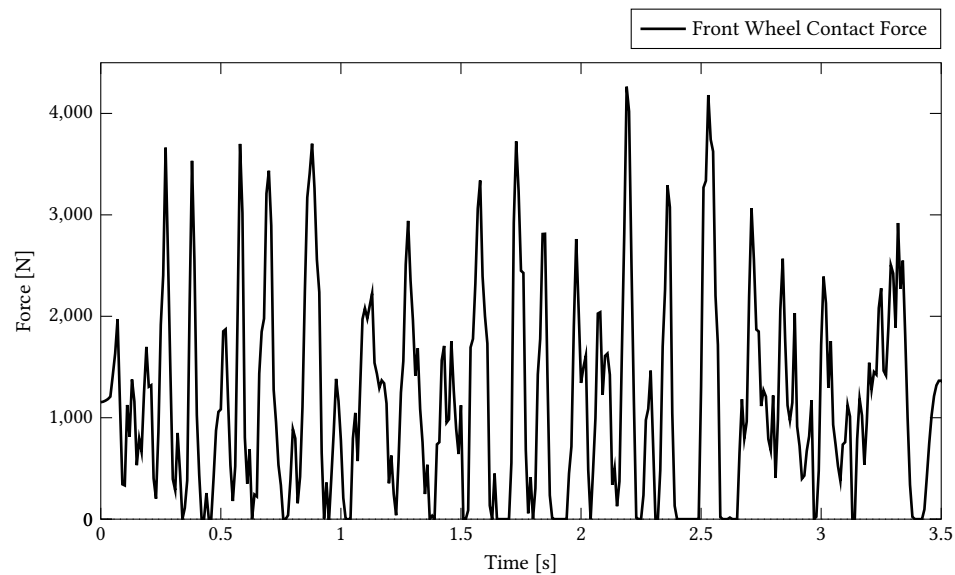


Figure 4.39: Vertical contact force between the telescopic suspension motorcycle front tire and the level 5 random road as a function of time

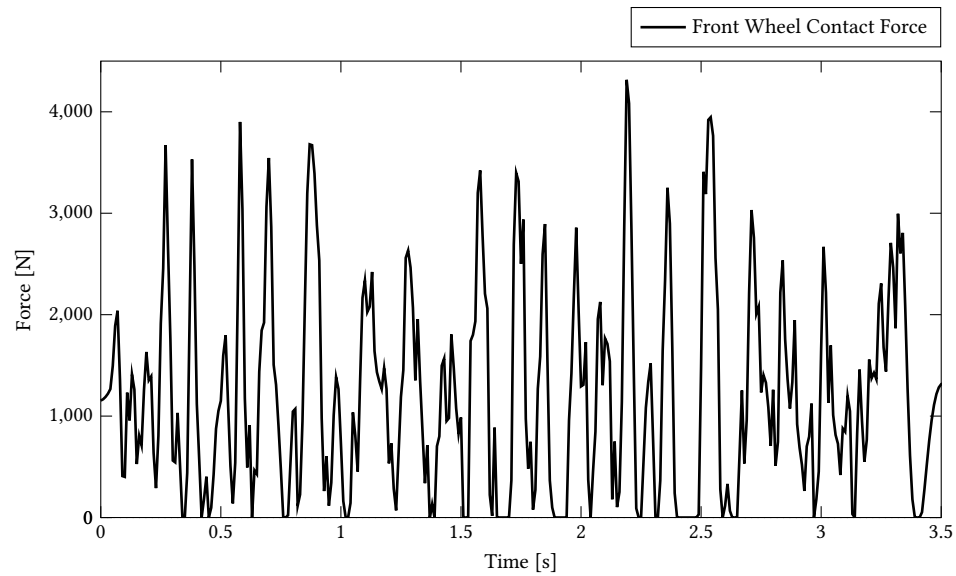


Figure 4.40: Vertical contact force between the multi-link motorcycle front tire and the level 5 random road as a function of time

### Level 3 Random Road (30 m/s)

In the case of 30 m/s forward speed, Figure 4.41 below gives the information about frame height change of the telescopic and multi-link front suspension motorcycles as a function of time running on the level 3 random road. Comparing with the corresponding road level result with the speed of 10 m/s, the difference between these two curves seems larger, especially around some peaks and valleys.

Figure 4.42 below shows pitch angle change of the telescopic and multi-link front suspension motorcycles as a function of time running on the level 3 random road. Also, these data in the figure have been converted from Euler parameter  $E_2$  to the actual angle values. On the whole, the amplitude of the pitch angle change for the multi-link suspension looks greater than the telescopic suspension, and its difference is also larger than the corresponding road level result with the speed of 10 m/s.



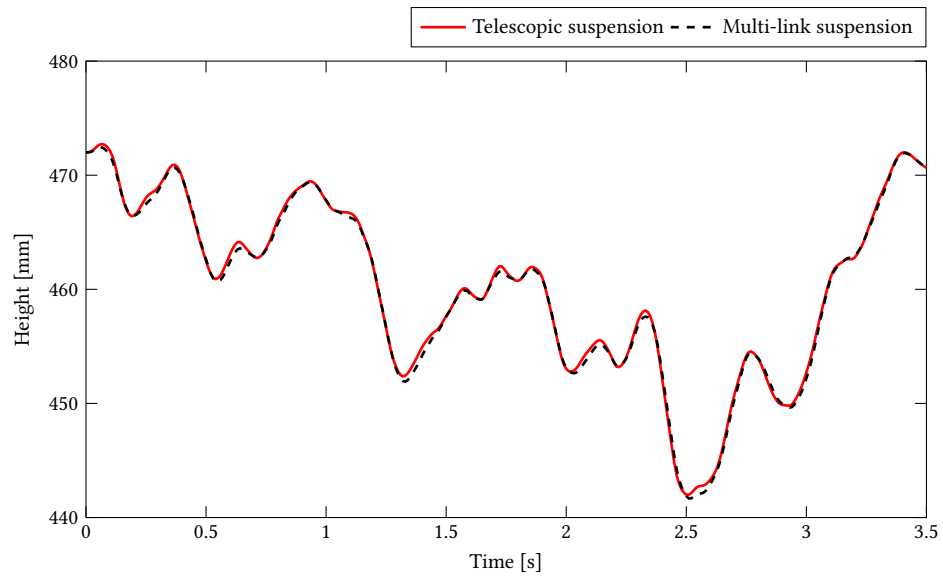


Figure 4.41: The frame height of both telescopic and multi-link front suspension motorcycles as a function of time running on the level 3 random road

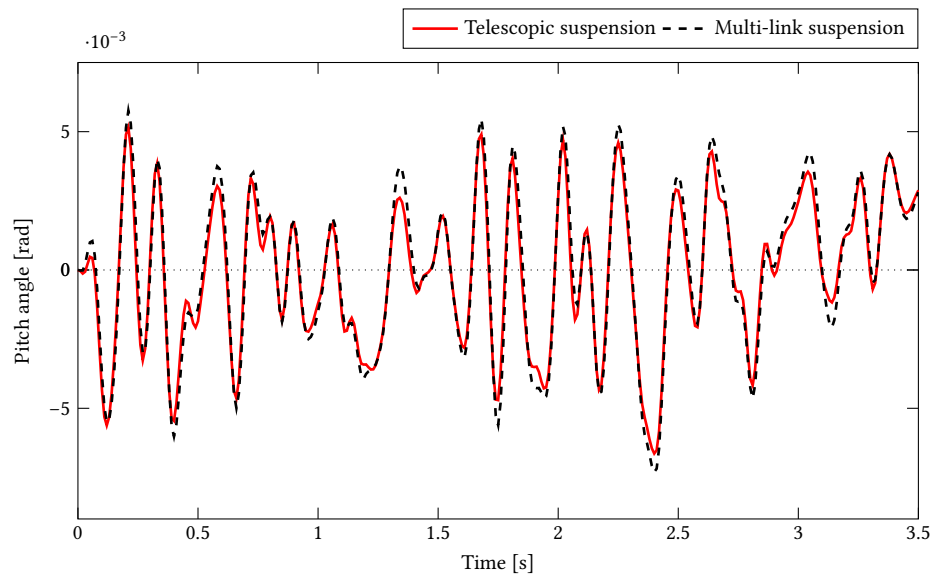


Figure 4.42: The pitch angle of both telescopic and multi-link front suspension motorcycles as a function of time running on the level 3 random road

With the speed of 30 m/s, the suspension travel distance of the telescopic and multi-link front suspension motorcycles as a function of time running on the level 3 random road can be seen from Figure 4.43. It once again suggests that with increasing speed, the difference between the results of the telescopic and multi-link suspensions is also increased.

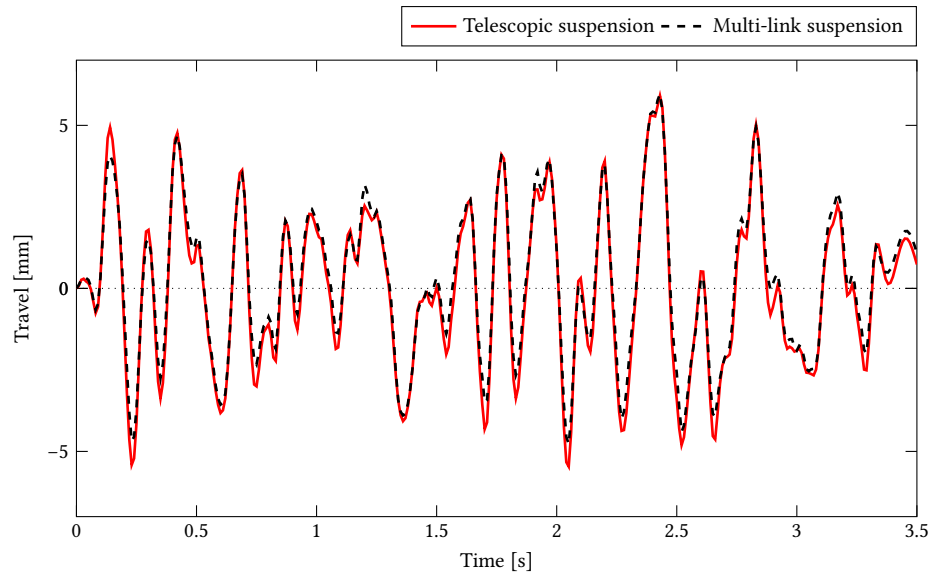


Figure 4.43: The suspension travel distance of both telescopic and multi-link front suspension motorcycles as a function of time running on the level 3 random road

#### Level 4 Random Road (30 m/s)

In this section, the simulation results of level 4 random road with the forward speed of 30 m/s are displayed. As usual, Figure 4.44 firstly shows frame height change of both the telescopic and multi-link front suspension motorcycles as a function of time running on the level 4 random road.

After that, Figure 4.45 below is the result of the pitch angle, while the plot of suspension travel distance can be seen in Figure 4.46. As seen in the figure, when comparing with the result of 10 m/s, the suspension travel distance in this section has been significantly increased, by approximately 10 mm.

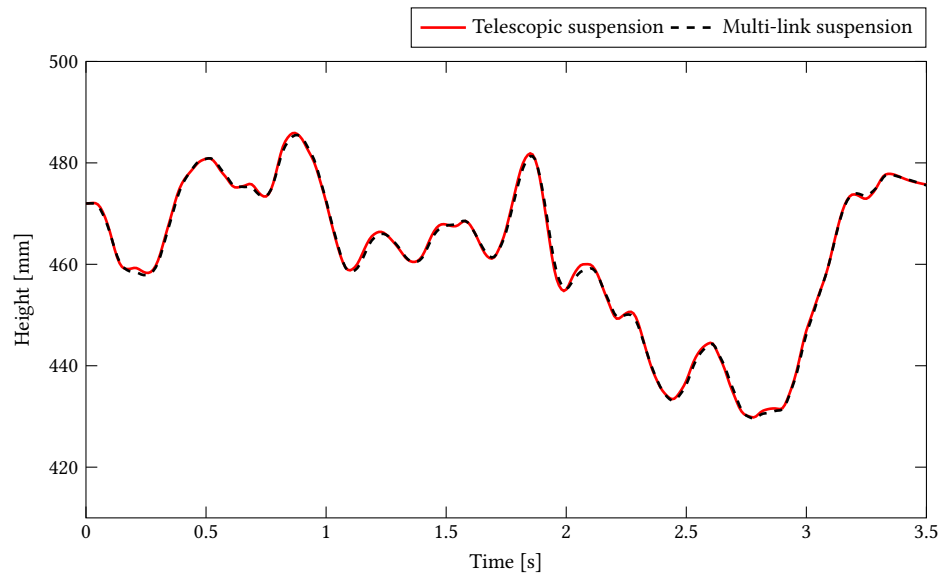


Figure 4.44: The frame height of both telescopic and multi-link front suspension motorcycles as a function of time running on the level 4 random road

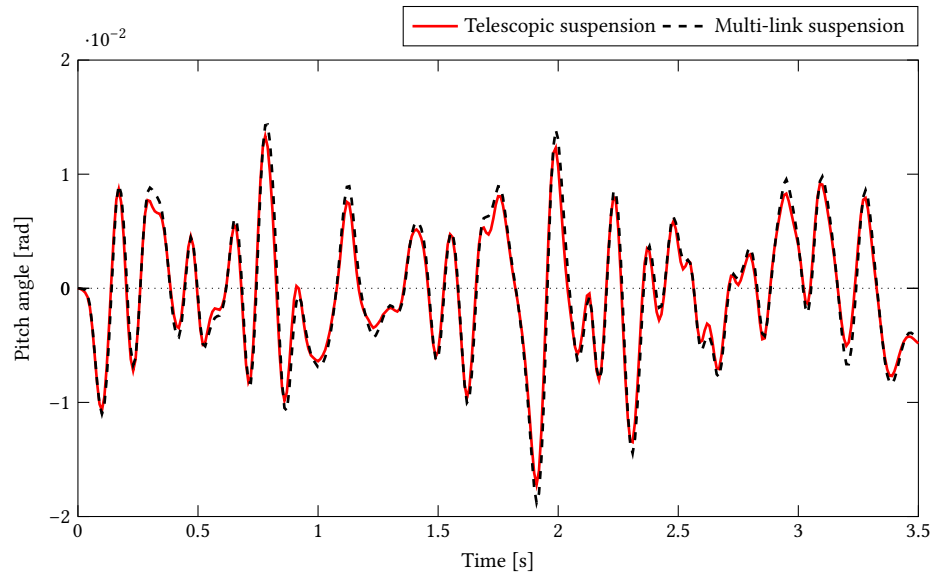


Figure 4.45: The pitch angle of both telescopic and multi-link front suspension motorcycles as a function of time running on the level 4 random road

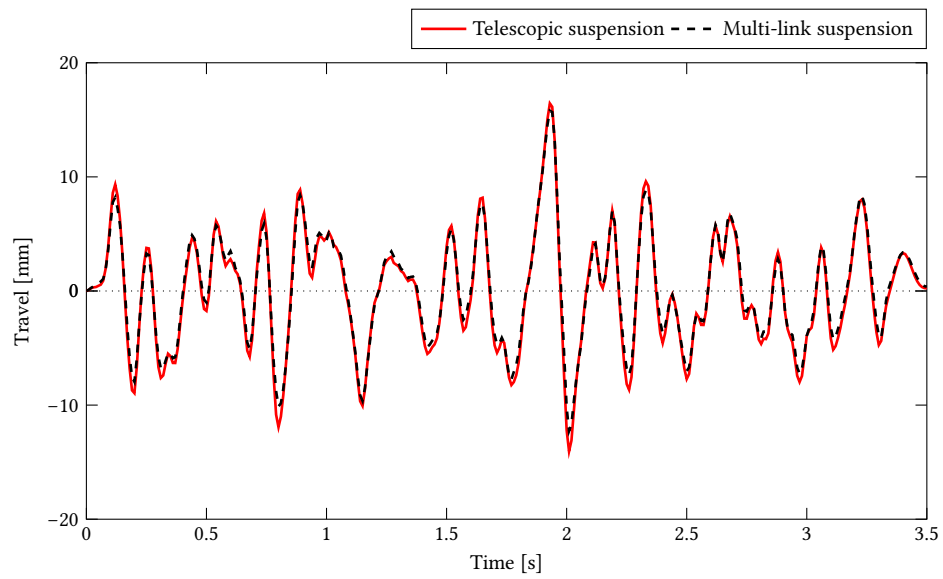


Figure 4.46: The suspension travel distance of both telescopic and multi-link front suspension motorcycles as a function of time running on the level 4 random road

## Chapter 5

# Discussion of Results

The simulation results presented in Chapter 4 will now be discussed and analyzed. The structure of this chapter follows a series of logical sequences. On the whole, there are three main steps. The first step is to verify the rationality of the multi-link front suspension motorcycle with the kinematic structure definition mentioned in Chapter 3. On the basis of proving that the new design is reasonable, the second step can be processed, which aims to suggest the rationality of both the linear and non-linear models. The assessment method of the linear model is to compare its result with the known theory. If the linear model is reasonable, it will be a reference for the non-linear model result to suggest its model feasibility. After confirming the non-linear model is acceptable, a set of simulations of the performance of the telescopic and multi-link front suspension motorcycles will be run. Through these simulations, the advantages and disadvantages of the two kinds of front suspension systems will be summarized. In fact, during the simulations of the second step, there have been some performance evaluations of the front suspension system. However, they are more biased towards the overall movement of motorcycles.

Following the above order and combining with the results in Chapter 4, the performance and properties of the telescopic and multi-link front suspension system will be shown more convincingly. Although the structure of Chapter 5 is similar to the previous chapter, it analyzes and discusses the simulation results from another perspective, to make the findings more logical and reliable. At the same time, the comparison of the performance of the telescopic and multi-link front suspension systems is consistent throughout this chapter, which is also the main topic of this thesis.

### 5.1 Model Assessment

The analysis of the motorcycle kinematic structure is the process to suggest that the multi-link front suspension system is reasonable. To be more precise, it uses known rules of motorcycle geometry to confirm whether this new design is acceptable. Thus, during the entire research of this thesis, the test of the kinematic structure is the most basic part, which dictated whether to do the following steps. There are two components

in this section; the first one is the caster angle and trail. Another is the tire model.

### 5.1.1 Caster Angle and Trail

The caster angle and trail are the most important parameters for the front assembly part of the motorcycle. According to the theory of motorcycle dynamics, caster angle and trail have a very close and direct relationship. These two parameters have a crucial role to play for the stability of the motorcycle during straight running, steering and braking motion. Especially when the motorcycle crosses a barrier, the front wheel will travel along the vertical direction. Under this circumstance, the value of caster angle and trail should maintain a stable value or even larger, because the contact point between the tire and ground will move forward when crossing the obstacle, which results in the decrease of caster angle and trail. This reduction may lead to instability of the motorcycle front assembly. In Figure 4.2, the front wheel position in the right graphic is higher than the wheel in the left one. It is obvious that both values of caster angle and trail of the higher wheel position are larger than the values of lower one, which means the kinematics structure of multi-link front suspension system is reasonable. This conclusion allowed the subsequent modeling and analysis steps.

### 5.1.2 Motorcycle Tire

The simulation of the tire is one of the most complex components of the motorcycle. However, in this simulation, the telescopic and multi-link front suspension motorcycle use the same tire model, which means the tire is not a variable. Therefore, the purpose of the tire test simulation is to suggest that the tire model can be used reasonably and effectively. As mentioned in Chapter 4, the assessment process of the tire model is very straightforward. This method is mainly through the comparison between the numerical result curve (Figure 4.4) and the theoretical curve (Figure 3.18) to confirm whether the tire meets the expectation of the Magic Formula theory. It is obvious that the simulation result curve looks similar to the expected result. This is a very straightforward confirmation that the tire model used in this thesis is reasonable and practical.

## 5.2 Out-of-plane Simulation Analysis

There are two simulations in this section, unforced and forced straight running. As mentioned before, there are three main functions of the out-of-plane simulation. The first function is to verify the linear model that is built and simulated with the EoM software. The second function is to verify the non-linear model that is built and simulated by the MotionView<sup>®</sup> software. The last function is to compare the performance between the telescopic and multi-link front suspension systems. The unforced straight running simulation can act on all three functions, while the forced straight running simulation mainly works for the last two functions.

### 5.2.1 Unforced Straight Running Simulation Analysis

According to the results presented in Chapter 4, the analysis and discussion can be separated into three parts. They are linear model justification, non-linear model justification, and performance comparison of telescopic and multi-link front suspension motorcycles.

#### Linear Model Confirmation

For the unforced straight running linear simulation, the book 'Motorcycle Dynamics'[1] by Dr. V. Cossalter provides a strong reference. Figure 5.1 shows the frequencies and the damping properties of the main out-of-plane modes as a function of the forward speed, which is coming from this book. The results of unforced straight running linear simulation for both telescopic and multi-link front suspension motorcycles in this thesis will be compared with the reference plot to decide whether the linear model is reasonable.

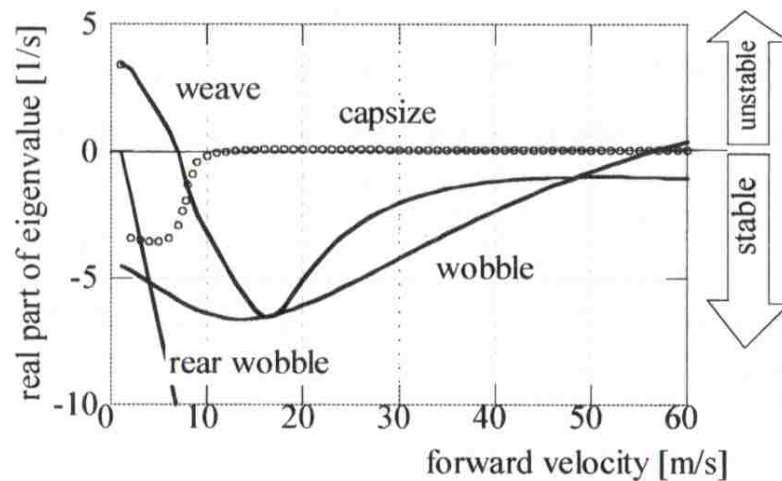


Figure 5.1: Theoretical unforced straight running result. Real parts of vibration modes as a function of speed.  
(reproduced from Cossalter[1])

As mentioned in Chapter 4, Figure 4.5 gives information about the frequencies and damping properties of the telescopic front suspension motorcycle out-of-plane modes as a function of the forward velocity from 1 m/s to 50 m/s. Comparing this plot with the theoretical reference graph, most of the curves corresponding to different modes are very similar. It is reasonable that there are some differences between the theoretical and simulation results, because the models are using different mass and geometry parameters, which also means there is no expectation of an exact match. The main difference is in the starting speed of the unstable wobble modes. In the theoretical graph, the value of unstable starting speed is around 55 m/s. In Figure 4.5, the value of unstable starting speed is around 43 m/s. This main difference is acceptable, because also from the theory of the book[1], wobble mode gradually becomes unstable with increasing speed, which also means the initial unstable speed is in the high speed range. Usually, the highway speed is limited at around 28 m/s. Therefore,

43 m/s is a reasonable value for the initial unstable speed. It can be concluded that the linear model of the telescopic front suspension motorcycle is reasonable and it also can be used to simulate and analyze directly.

Figure 4.6 gives information about the frequencies and damping properties of the multi-link front suspension motorcycle out-of-plane modes as a function of the forward velocity from 1 m/s to 50 m/s. Similarly, it also needs to compare with the theoretical reference graph from Dr. V. Cossalter. Although there is a little difference during the low speed range, the trend of each curve is still very similar. The starting unstable speed of wobble mode is around 40 m/s, which is acceptable. The difference mainly focuses on the weave and capsize mode in the speed range from 0 m/s to 5 m/s, but it is unlikely to affect the overall performance of the motorcycle. Furthermore, this difference may also result from the new design of the multi-link front suspension system, which will be elaborated and discussed below. It can be concluded that the linear model of the multi-link front suspension motorcycle is reasonable and it also can be used to simulate and analyze directly.

According to the verification process above, both telescopic and multi-link front suspension motorcycle models are available to be used in the following simulation and analysis. It also means that the linear model is a reliable reference for the non-linear model.

### **Non-linear Model Justification**

The non-linear model of both telescopic and multi-link motorcycle are built and simulated by the MotionView<sup>®</sup> software. In order to confirm whether the non-linear model is correct and reasonable, the unforced straight running non-linear simulation result needs to be compared with the linear simulation result, which has been considered reasonable and effective. In Chapter 4, Table 4.6 shows results of both the telescopic and multi-link suspension motorcycles according to the corresponding animations and line graphs.

Firstly, for the telescopic front suspension motorcycle, the result of its non-linear model can be seen from Table 4.6. Contrasting with the linear results in Figure 4.5, it is obvious that the state of most velocity points in the table is consistent with the meaning of the corresponding point in the figure. For instance, at the speed of 5 m/s, Figure 4.5 shows that the weave mode is the main destabilizing factor. This result can also be obtained from Table 4.6, which indicates the motorcycle is firstly in a steady state and then gradually does a weave motion until overturning. Especially for the wobble mode, the unstable starting speed range in Table 4.6 basically conforms to the corresponding unstable area in Figure 4.5. It can be concluded that the non-linear model of the telescopic front suspension motorcycle is reasonable and it also can be used to simulate and analyze directly.

Secondly, for the multi-link front suspension motorcycle, the result of its non-linear model simulation can be seen from Table 4.6. Correspondingly, Figure 4.6 shows the information about the eigenvalue properties of the multi-link front suspension motorcycle out-of-plane modes as a function of the forward velocity. Through the analysis of different modes during each speed, it can be confirmed that the state of most velocity points in the table is consistent with the meaning of the corresponding speed in the figure. For example, still



at the speed of 5 m/s, Figure 4.6 shows that the capsize mode is supposed to be the only unstable motion. In Table 4.6, at the same speed, its description is that the motorcycle is firstly in a steady state and then experiences the capsize motion, which starts from about 5 s. This means the result of the non-linear model is consistent with the result of the linear model. Also, the unstable speed range of the wobble mode of the non-linear model is similar to the speed range of linear model. After these verifications, it can be concluded that the non-linear model of the multi-link front suspension motorcycle is reasonable and it also can be used to simulate and analyze directly.

Based on the above comparison with reliable linear results, it can be confirmed that the non-linear models of both telescopic and multi-link front suspension motorcycles are reasonable and can be used in the following simulation and analyses.

### **Performance of Telescopic and Multi-link Motorcycles**

After proving the rationality and effectiveness of both linear and non-linear models, the unforced straight running performance of telescopic and multi-link front suspension motorcycles needs to be discussed. It should be mentioned that the main purpose of this contrast is to find out if there is any differences in the performance for the motorcycle that is equipped with the multi-link front suspension system.

For the linear simulation of unforced straight running, Figure 4.5 and Figure 4.6 give the most intuitive contrast. The main difference focuses on the low speed range from 0 m/s to 10 m/s. The telescopic front suspension motorcycle mainly experiences an unstable wobble mode during this speed period. The multi-link front suspension motorcycle mainly experiences the unstable capsize mode during this speed period. Another difference is the starting speed of the unstable wobble mode in the high speed range. For the telescopic and multi-link suspension motorcycles, they are 43 m/s and 40 m/s respectively. For a more detailed and reliable observation of these differences, the simulation of each speed needs to be conducted to get the data of the eigenvalues and frequencies at these speeds. As mentioned in Chapter 4, there are four modal frequency results. They are bounce, pitch, wobble and weave. Table 5.1 and Table 5.2 is the list of each mode's frequencies in the speed range from 0 m/s to 40 m/s.

First of all, Table 5.1 shows the frequency result of the bounce and pitch for both telescopic and multi-link front suspension motorcycles. It is obvious that the frequency of these two kinds of front suspension motorcycles are very similar. There is only a very small difference between them. The bounce frequency of the telescopic motorcycle is larger than the multi-link, but for the pitch frequency, the opposite is true.

Speed [m/s]	Bounce frequency [Hz]		Pitch frequency [Hz]	
	Telescopic	Multi-link	Telescopic	Multi-link
1	3.1108	2.9538		
2	3.4165	3.2414	5.2611	5.5431
3	3.2643	3.1904	6.5136	6.6620
4	3.2135	3.1529	7.5009	7.6428
5	3.1881	3.1317	8.3571	8.5057
10	3.1455	3.0937	11.6952	11.8924
20	3.1262	3.0768	16.4245	16.7028
30	3.1190	3.0712	20.0695	20.4100
40	3.1145	3.0683	23.1629	23.5493

Table 5.1: The frequency result of the bounce and pitch for both telescopic and multi-link front suspension motorcycles. The blank part of the table means the mode at this speed is non-oscillatory

Speed [m/s]	Wobble frequency [Hz]		Weave frequency [Hz]	
	Telescopic	Multi-link	Telescopic	Multi-link
1		1.6188	0.6259	
2		1.6747	0.5621	
3		1.7639	0.5093	
4		1.8807	0.4693	
5		2.0196	0.4482	
10	6.1702	4.3222	1.2070	
20	6.1325	5.8632	2.6345	2.5189
30	6.3203	6.1606	3.2272	3.0389
40	6.6481	6.4500	3.4705	3.3083

Table 5.2: The frequency result of the wobble and weave modes for both telescopic and multi-link front suspension motorcycles. The blank part of the table means the mode at this speed is non-oscillatory

Secondly, Table 5.2 above shows the frequency result of the wobble and weave modes for both telescopic and multi-link front suspension motorcycles. In order to identify the weave and wobble modes clearly, there is a process that is established in the EoM software to compare the frequency between frame yaw rate and the oscillation around steering axis. As can be seen from Table 5.2, there are some differences between the frequency result of the telescopic and multi-link front suspension motorcycles. Especially during the low speed range, the multi-link front suspension motorcycle suffers from the unstable wobble mode and the telescopic front suspension motorcycle suffers from the unstable weave mode. It should be mentioned that the wobble mode is usually more unfavorable than the weave mode. However, as can be seen from Table 5.2, the wobble frequency of the multi-link motorcycle is very low, which means it will be more easily controlled. Furthermore, in reality, there could be some dampers on the handlebar to prevent a dangerous wobble mode. This damper is not included in any of the models of this thesis.

Overall, the discussion of unforced straight running linear simulation results can conclude that during the low speed range (0 m/s-10 m/s), there are some differences mainly due to the oscillation of wobble and weave modes. After this low speed period, the performance of the telescopic and multi-link motorcycles are

almost the same. The non-linear simulation results can be seen from Table 4.6. The main function of this simulation is to find the same stable period of the speed between these two motorcycles with different front suspension systems. It can be easily seen that the stable state of both telescopic and multi-link motorcycles is from 15 m/s to 25 m/s. This stable speed range plays an important role in the speed selection of the following in-plane simulation. On the other hand, the results in Table 4.6 again confirms the result of the previous linear simulations.

### 5.2.2 Forced Straight Running Simulation Analysis

In this section, there are two main procedures. The first one is the justification of the non-linear model, which is to further suggest the rationality and effectiveness of the non-linear model during the forced straight running condition. The second is the comparison between the performance of the telescopic and multi-link front suspension motorcycles for the forced straight running simulation. The linear model of both the telescopic and multi-link front suspension motorcycles needs to be simulated under forced straight running condition. The results can be seen in Table 4.7 in Chapter 4. This result is supposed to be the reference for non-linear simulation of the forced straight running model.

#### Non-linear Model Justification

The results of the forced straight running non-linear simulation can be seen in Table 4.8 and Table 4.9. It should be mentioned that the reference linear result is the values of the frame yaw rate at different torque frequencies, but only under 1 Nm torque. For the telescopic front suspension motorcycle, in Table 4.8, the frame yaw rate values with 1 Nm torque at different frequencies are similar to the corresponding reference linear result in Table 4.7. Figure 5.2 shows the plot of linear and non-linear results of the frame yaw rate with 1 Nm torque in response to different frequencies. Although there are some differences that can be seen between these two curves in Figure 5.2, the overall trend of the two curves is the same, which once again is evidence for the correctness of non-linear model for the telescopic front suspension motorcycle.

For the multi-link front suspension motorcycle, the graph of the linear and non-linear results of the frame yaw rate under 1 Nm torque in response to different frequencies can be seen in Figure 5.3. These two curves also have the same trend, albeit with a slightly larger discrepancy, which again justifies the multi-link motorcycle non-linear model.

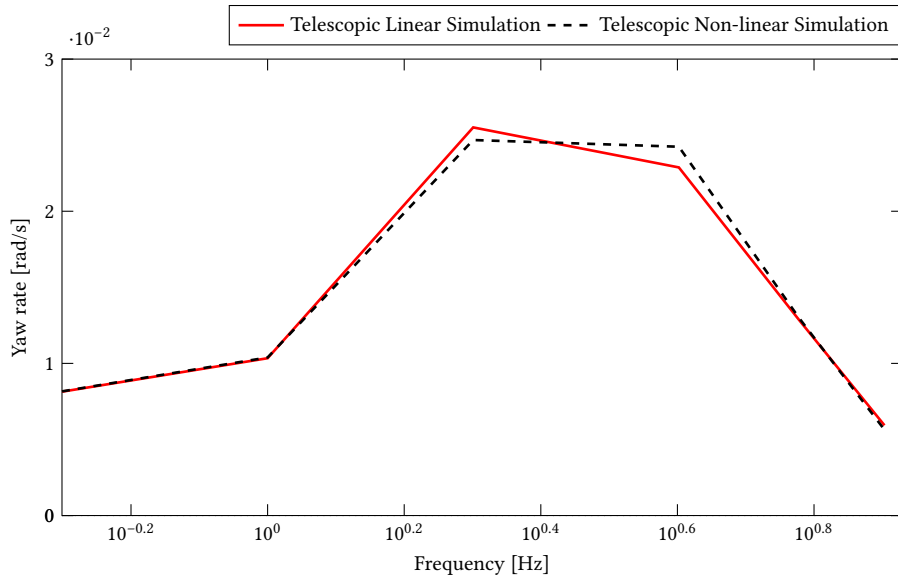


Figure 5.2: The telescopic front suspension motorcycle linear and non-linear simulation result of frame yaw rate under 1 Nm torque in response to frequencies 0.5 Hz, 1 Hz, 2 Hz, 4 Hz, 6 Hz, 8 Hz

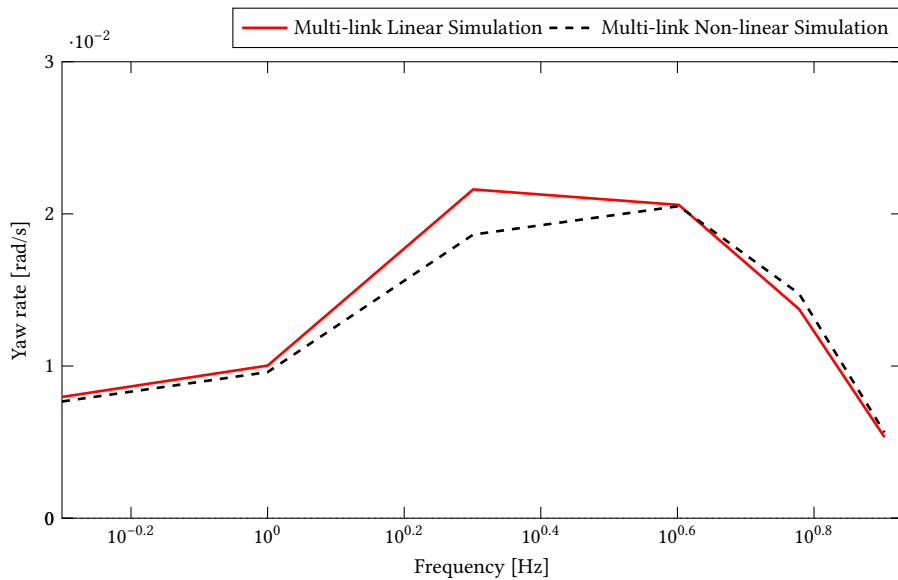


Figure 5.3: The multi-link front suspension motorcycle linear and non-linear simulation result of frame yaw rate under 1 Nm torque in response to frequencies 0.5 Hz, 1 Hz, 2 Hz, 4 Hz, 6 Hz, 8 Hz

For the non-linear simulation, the result is plotted and used to suggest the rationality and validity for both telescopic and multi-link front suspension motorcycle non-linear models, which are built using the MotionView<sup>®</sup> software. Figure 5.4 shows the plots of the frame yaw rate sensitivity under different amplitude and frequency of the torque for the telescopic front suspension motorcycle.

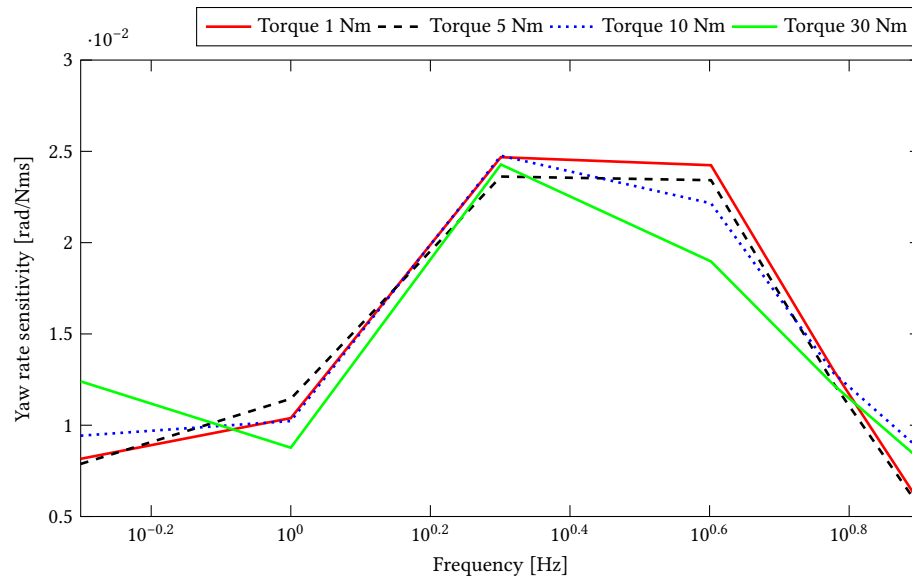


Figure 5.4: The telescopic front suspension motorcycle non-linear simulation result of frame yaw rate sensitivity under 1 Nm, 5 Nm, 10 Nm, 30 Nm torque in response to frequencies 0.5 Hz, 1 Hz, 2 Hz, 4 Hz, 6 Hz, 8 Hz

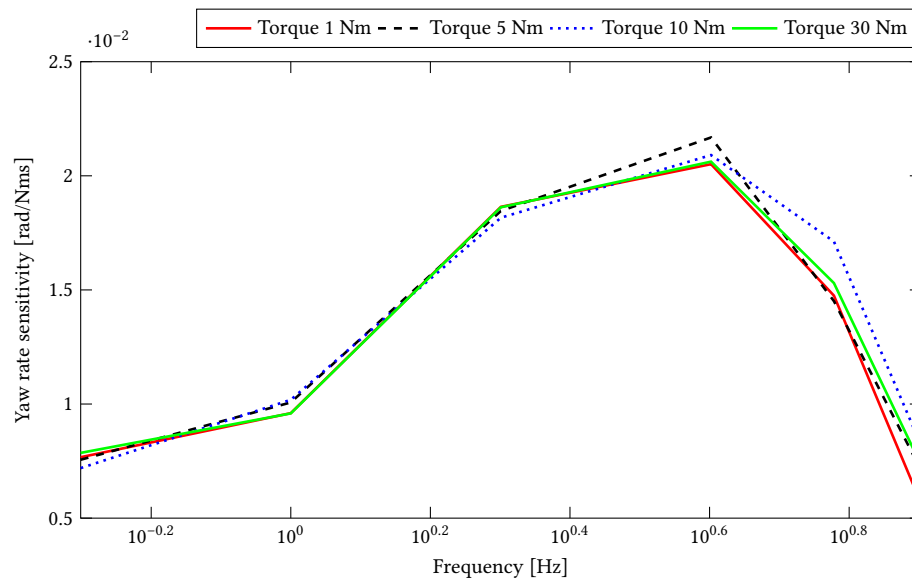


Figure 5.5: The multi-link front suspension motorcycle non-linear simulation result of frame yaw rate sensitivity under 1 Nm, 5 Nm, 10 Nm, 30 Nm torque in response to frequencies 0.5 Hz, 1 Hz, 2 Hz, 4 Hz, 6 Hz, 8 Hz

As can be seen from Figure 5.4, on the whole, the rising and falling trends of these four curves are similar. From 0.5 Hz to 1 Hz, the frame yaw rate sensitivity has a slight increase and then rapidly rises to a peak at around 2 Hz. After that, the yaw rate sensitivity gradually declines back to the starting level. This graph indicates that the most sensitive frequency range for the telescopic front suspension motorcycle is around 2

Hz. The curves show a relatively small sensitivity to changes in steering moment, suggesting again that the non-linear model of the telescopic front suspension motorcycle is reasonable and can be used in the following simulation.

In Figure 5.5 above, there are four curves that represent the frame yaw rate sensitivity under different amplitudes and frequencies of steering torque for the multi-link front suspension motorcycle. It is obvious that these four curves have similar rising and falling trends as well. The maximum frame yaw rate sensitivity happens at a frequency around 4 Hz. After that, the yaw rate sensitivity experiences a rapid decrease. There is almost no sensitivity to the steering torque amplitude. Besides, the similarity of the overall trends of these four curves also suggests that the non-linear model of the multi-link front suspension motorcycle is reasonable and can be used in the following simulation.

### **Performance of Telescopic and Multi-link Motorcycles**

After proving rationality and practicality of non-linear model for both telescopic and multi-link front suspension motorcycles, the comparison of forced straight running performance between these two motorcycle models also need to be discussed.

First of all, at the six frequencies and the speed of 20 m/s, according to Figure 5.4 and Figure 5.5, the curves of these two kinds of models with the corresponding same torque frequency and amplitude looks roughly similar to each other. The difference of performance is that for the telescopic front suspension motorcycle the peak value of yaw rate sensitivity happens at 2 Hz and for the multi-link, it is 4 Hz. Referencing the data in Table 5.2 above, it can be found that at the speed of 20 m/s, the frequency of the weave mode for the telescopic motorcycle is closer to 2 Hz, which means the telescopic suspension motorcycle is mainly engaged in weave motion. Using the same method, it can be confirmed that the multi-link suspension motorcycle is mainly engaged in wobble motion at the speed of 20 m/s.

It can be concluded that there are some differences between the performance of the telescopic and multi-link suspension motorcycle forced straight running simulations. For example, at a speed of 20 m/s, the most easily excited mode of the telescopic suspension motorcycle is the weave mode, while for the multi-link suspension motorcycle, it is the wobble mode. After the comparison of the out-of-plane simulation results, whether from a linear and non-linear perspective or from the different types of the front suspension system, it can be confirmed that the non-linear model is available to be used in the in-plane simulation and also the multi-link front suspension system is valuable to be compared with the telescopic front suspension system in the following simulation.

### 5.3 In-plane Simulation Analysis

In this section, the in-plane simulation results of both the telescopic and multi-link front suspension motorcycles will be compared and discussed. There are three parts of these simulation results: braking, plank road, and random road. The front suspension system has a crucial role to play in the in-plane simulation analysis, which also indicates the importance of this section.

#### 5.3.1 Braking Simulation Analysis

As mentioned in Chapter 4, the simulation results of braking are divided into two main components. The first one is the change of three characteristic values during the braking motion. They are stop time, pitch angle, and frame height.

First of all, Figure 5.6 shows the stop time of the telescopic and multi-link front suspension motorcycles in response to various values of braking torque starting from 5 s. According to this graph and corresponding tables, it can be concluded that the stop time of multi-link front suspension motorcycle is larger than the telescopic, which seems like a disadvantage of the new design.

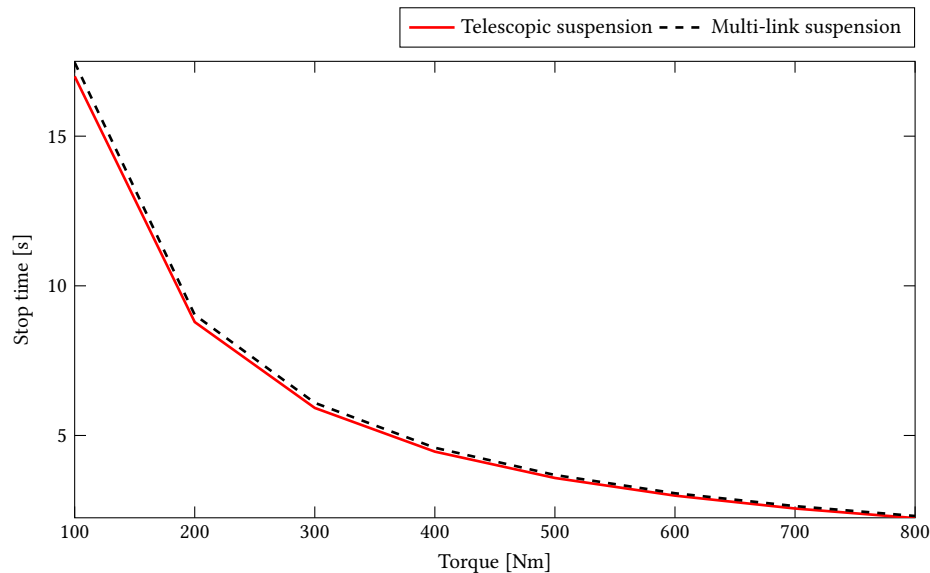


Figure 5.6: Stop time of the telescopic and multi-link front suspension motorcycles in response to various values of braking torque starting from 5 s.

However, it also can be seen from Figure 5.6 that difference between the stop times is very small and the two curves are almost coincident. Thus, this unfavorable gap is very small, and does not have any significant influence on the performance of multi-link front suspension motorcycle during the braking motion. Secondly, Figure 5.7 shows the pitch angle of the telescopic and multi-link front suspension motorcycles in response to various values of braking torque. As seen in Figure 5.7, it is obvious that the pitch angle of multi-link front

suspension motorcycle is smaller than the telescopic. In particular, with the increasing amounts of braking torque, the gap between the pitch angles is also gradually increasing. It means that under braking, the pitch motion amplitude of the multi-link front suspension motorcycle is less than the telescopic, especially for emergency braking. This result reflects an advantage of the new design. It suggests that the multi-link front suspension system is able to reduce the discomfort of the rider when braking.

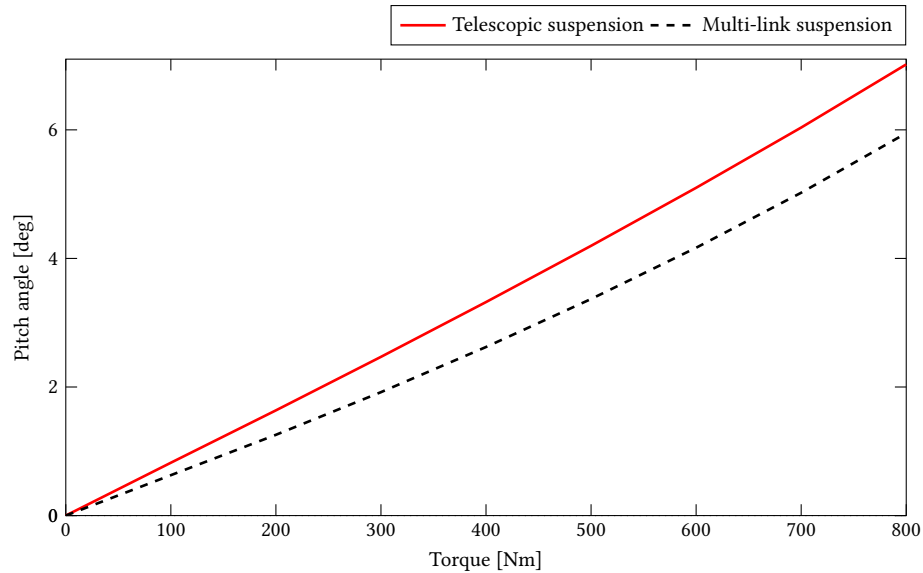


Figure 5.7: Pitch angle of the telescopic and multi-link front suspension motorcycles in response to various values of braking torque starting from 5 s

In addition to the two results above, the last characteristic value is the frame height. Figure 5.8 shows frame height of the telescopic and multi-link front suspension motorcycles in response to various values of braking torque. It should be mentioned that the original frame height is 472 mm when no brake torque is applied to the front wheel. As can be seen from Figure 5.8, for the telescopic front suspension motorcycle, the change of frame height experiences a decline under gentle braking, but returns to the original position at higher brake torques. The line of the multi-link front suspension motorcycle is in the rising state until the value around 480 mm. This continual rise may be caused by the reaction force of the four locating arms when the inertial braking force is applied on them.



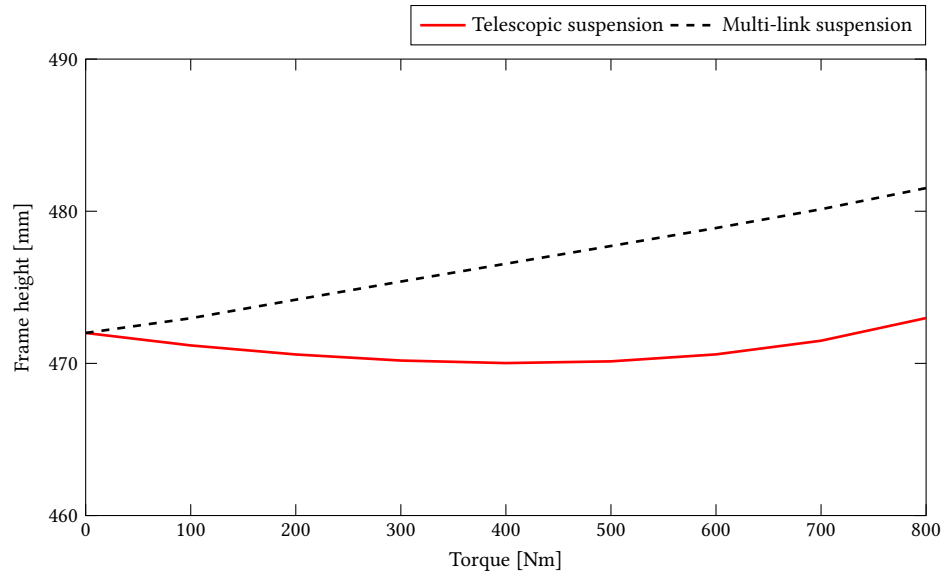


Figure 5.8: Frame height of the telescopic and multi-link front suspension motorcycles in response to various values of braking torque starting from 5 s

The completely different chart trend of the frame height for these two kinds of front suspension motorcycles has brought doubts about the correctness of its results. Therefore, it is necessary to verify the reliability of this simulation result. The method is to generate and analyze the normal force of the motorcycle on the front and rear wheels during the braking motion.

Figures 5.9 and 5.10 show the normal forces on the front and rear wheels of the telescopic and multi-link front suspension motorcycles as a function of time under a 500 Nm braking torque starting from 5 s. As can be seen from Figure 5.9, during the first 5 s constant speed running, the normal forces of both the front and rear wheels maintain at stable values. After that, with the beginning of the 500 Nm braking torque, the normal force graphs of the front and rear wheels go in opposite directions. As mentioned in Chapter 2, the weight of the rider and motorcycle is thrown forward onto the front wheel during the braking motion, especially for an emergency stop. Therefore, in Figure 5.9, the normal force of the telescopic suspension motorcycle front wheel experiences a fast upward trend and then once again keeps on a stable value. Meanwhile, the normal force of the rear wheel goes through a reverse process, which firstly experiences a fast downward trend and then also keeps on a stable value. The normal force graph of the multi-link suspension motorcycle in Figure 5.10 is almost the same as the graph of the telescopic suspension.

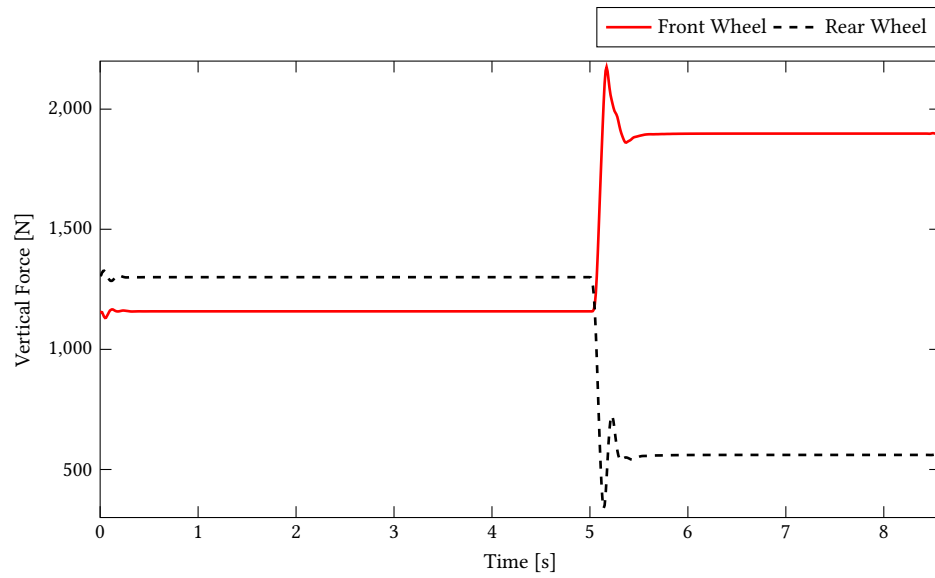


Figure 5.9: Front and rear wheels normal forces of the telescopic front suspension motorcycle in response to the time under 500 Nm braking torque starting from 5 s

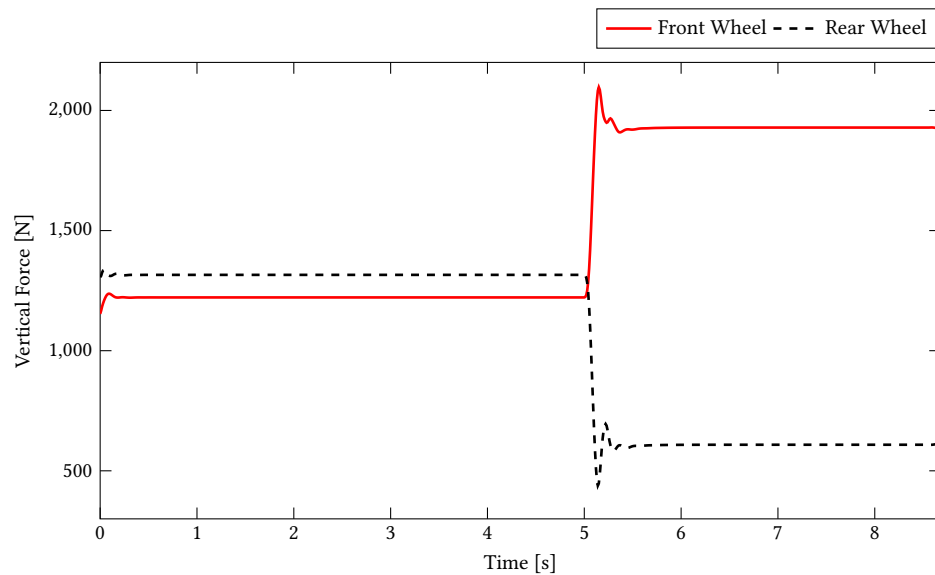


Figure 5.10: Front and rear wheels normal forces of the multi-link front suspension motorcycle in response to the time under 500 Nm braking torque starting from 5 s

After the description of these two graphs, the results need to be analyzed and discussed. The value required for this analysis is the stable value in the later part of each curve. All the data is summarized in Table 5.3 below.

Telescopic front suspension		Multi-link front suspension	
Front wheel	Rear wheel	Front wheel	Rear wheel
1898.220 N	560.652 N	1928.810 N	608.545 N
Total	2458.872 N	Total	2537.355 N

Table 5.3: Vertical forces of front and rear wheels for the telescopic and multi-link front suspension motorcycles under 500 Nm braking torque starting from 5 s

The normal forces of the front and rear wheels can be compared and analyzed directly. During the braking motion, total normal force of the telescopic front suspension motorcycle is 2458.872 N and the multi-link is 2537.355 N. The difference between these two normal forces is 78.483 N. This is reasonable, because according to Chapter 1, the weight difference between the telescopic and multi-link front suspension structures is the four locating arms on both sides of the front wheel. The total weight of these four arms is 8 kg or 78.4 N. It is obvious that the difference between these two normal forces is almost exactly equal to the weight of four locating arms. Thus, it can be suggested that the results of the simulation is reasonable. Besides, there is an interesting result about normal force distribution of the multi-link front suspension motorcycle. As mentioned, the four locating arms are added near to the front wheel, which means that the front wheel should be more affected. However, as can be seen from Table 5.3, the amount of increase for front wheel normal force is smaller than the rise of rear wheel. They are 30.59 N and 47.893 N respectively. This is an ideal result because it means that although the increased weight of 8 kg is added near to the front wheel, during the braking motion, this weight does not influence the front assembly much. The rear part of motorcycle takes on the most weight of the four locating arms.

It should be mentioned that similar to the comparison of stop times before, the difference of frame height for the telescopic and multi-link motorcycles is very small, which is usually in the range of 10 mm or less. This height change is unlikely to have much of an impact on the rider. Therefore, for the frame height, the telescopic and multi-link front suspension motorcycles do not have much difference.

After analyzing three characteristic values, the caster angle and trail results need to be analyzed and discussed. Above all, according to Table 4.12 and Table 4.13, the caster angle in response to various values of braking torque is available to be plotted as below.

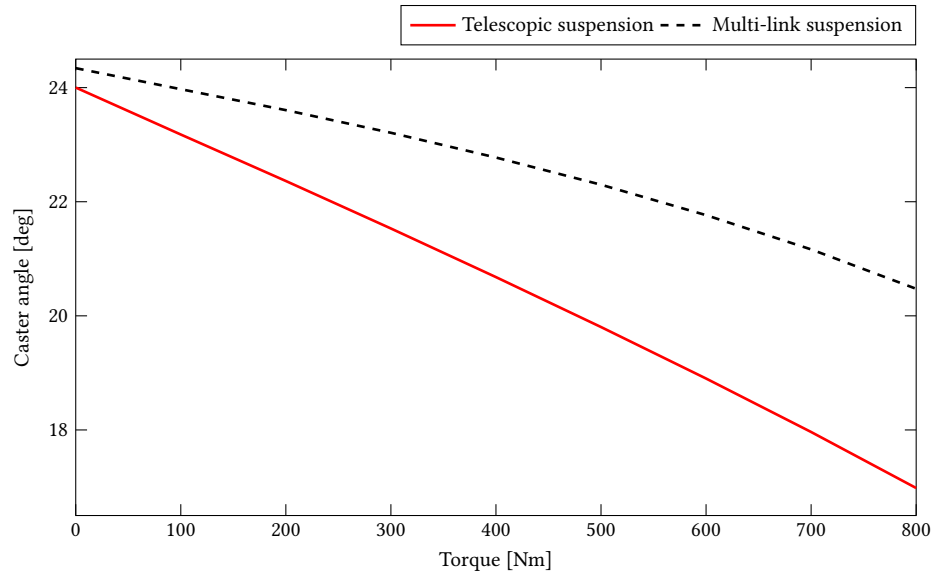


Figure 5.11: Caster angle of the telescopic and multi-link front suspension motorcycles in response to various values of braking torque

As can be seen from Figure 5.11, in response to various values of braking torque, the caster angle of the telescopic suspension motorcycle is smaller than the multi-link suspension motorcycle. The difference value between the caster angles of these two types of motorcycles increases with the increasing number of the braking torque, at 800 Nm, the difference reaches to about  $3.5^\circ$ .

It also illustrates that the caster angle of multi-link front suspension motorcycle is larger than the caster angle of telescopic during the braking motion. Furthermore, it suggests that the multi-link front suspension motorcycle is more stable when braking than the telescopic front suspension motorcycle. This is also an important improvement that is brought by this new design. In order to further confirm this advantage, the trail of multi-link front suspension motorcycle in response to various values of braking torque needs to be plotted as below.

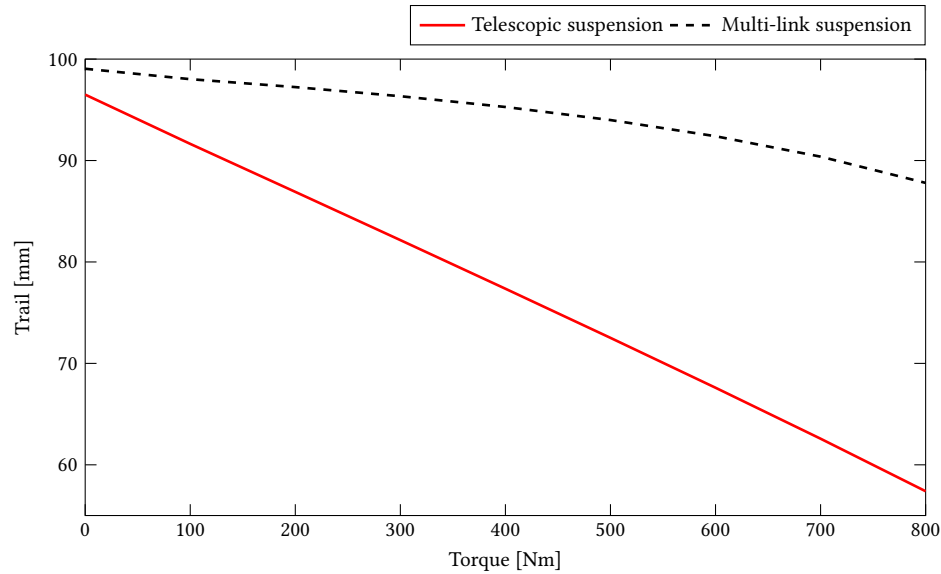


Figure 5.12: Trail of the telescopic and multi-link front suspension motorcycles in response to various values of braking torque

Figure 5.12 above shows the telescopic and multi-link front suspension motorcycles trail change in response to the increase of braking torque. In Chapter 3, the definition of caster angle and trail has been described. It is worth mentioning that in theory, an increase in the caster angle is usually coupled with a corresponding increase in the trail. Simultaneously, similar to Figure 5.11, the slope of multi-link front suspension motorcycle trail line is significantly smaller than the slope of telescopic suspension motorcycle. Thus, the two lines in Figure 5.12 are reasonable, which once again suggests the advantages of the multi-link front suspension motorcycle.

### 5.3.2 Plank Road Simulation Analysis

The plank road simulation simulated the process of a motorcycle crossing an obstacle. There are three components of the plank road simulation results. They are pitch angle, frame height and suspension travel. The results of both telescopic and multi-link front suspension motorcycles will be analyzed and discussed in this section.

The first result can be seen from Figure 4.21, which shows curves of pitch angle for both telescopic and multi-link front suspension motorcycles. The two curves in the graph are all subject to two fluctuations. This is reasonable because the pitch motion of motorcycle usually happens at the beginning of climb up and down. In Figure 4.21, different parts of the two curves are mainly concentrated in the peak position. Around this position, the pitch angle of the multi-link suspension motorcycle is generally greater than the telescopic. The specific difference is about  $0.003^\circ$ , which is too small to have any effect on the rider's driving experience. Therefore, the pitch angle of telescopic and multi-link front suspension motorcycles are almost same when

they cross a barrier.

The second result is the graph of frame height for both telescopic and multi-link front suspension motorcycles. It is obvious that in Figure 4.22, two curves almost coincide with each other. The main difference occurs when the motorcycle is out of the barrier. The frame height of the multi-link motorcycle is a little bit smaller than the telescopic. Overall, similar to the pitch angle, the frame height of the telescopic and multi-link front suspension motorcycles are almost the same when they cross a barrier.

The last result can be seen from Figure 4.23, which shows curves of suspension travel distance for both telescopic and multi-link front suspension motorcycles. Similar to the pitch angle, the curve of suspension travel distance also experiences two fluctuations. In the peak positions, the distance value of multi-link front suspension motorcycle is about 2 mm larger than the telescopic. According to the angle plot in Figure 4.21, the pitch angle of the multi-link motorcycle is also larger than the telescopic at peak positions. The greater pitch angle can result in a higher load on the front suspension, which leads to larger travel distance.

Overall, it can be concluded that in the plank road simulation, the performance of both telescopic and multi-link front suspension motorcycles are almost the same. The main difference is the pitch angle, which also results in the difference of front suspension travel distance. However, the value of this difference is very small such that does not influence the ride quality of motorcycle.

### 5.3.3 Random Road Simulation Analysis

The results of the random road simulation can be seen in Chapter 4. There are two methods to analyze these results in this thesis. The first approach is to directly observe the graphs to analyze the performance of two motorcycle models running on different levels of road. The second approach is to use the statistical methods to analyze the result data more rationally. To be more precise, there are two statistical parameters, the mean value and the standard deviation, that can be applied to the result analysis.

The mean value is a widely used evaluation parameter. The frame height, pitch angle and suspension travel distance can be analyzed by the mean value method. In statistics, the amount of variation or dispersion for an array of data values can be quantified by the standard deviation. In this section, all of these three characteristics in the random road simulation results can be considered as a set of discrete data values. For example, the standard deviation of frame height can be expressed as:

$$\sigma = \sqrt{\frac{1}{N}[(H_1 - H_0)^2 + (H_2 - H_0)^2 + \dots + (H_N - H_0)^2]} \quad (5.1)$$

$$H_0 = \frac{1}{N}(H_1 + H_2 + \dots + H_N) \quad (5.2)$$

In Equation 5.1,  $\sigma$  is the standard deviation,  $N$  is the number of data samples, and  $H_N$  is the  $N$ th data point of the frame height. The mean value  $H_0$  of all the samples can be found from Equation 5.2. The following section will analyze the three parameters separately.

### Frame Height Analysis

According to the order in Chapter 4, the first item to be analyzed is frame height. Tables 5.4 and 5.5 give the information for the standard deviations and mean values of frame height for both telescopic and multi-link front suspension motorcycles in response to the level 3, 4 and 5 random roads with the speeds of 10 m/s and 30 m/s respectively.

Statistics	Random road	Telescopic	Multi-link	Difference value
Standard deviation [mm]	Level 3	7.2282	7.2417	0.0135
	Level 4	14.4048	14.4323	0.0275
	Level 5	28.6027	28.6786	0.0759
Mean value [mm]	Level 3	459.6212	459.4495	0.1717
	Level 4	461.0659	460.9057	0.1602
	Level 5	482.8454	482.6617	0.1837

Table 5.4: The standard deviations and mean values of frame height for both telescopic and multi-link front suspension motorcycles in response to the level 3, 4 and 5 random road with the speed of 10 m/s.

As can be seen from Table 5.4, with the speed of 10 m/s, the standard deviation of frame height for the telescopic motorcycle is smaller than the multi-link at all of these three levels random road. It also means that the fluctuations of variation for the telescopic frame height change is more moderate than the multi-link. For the mean values, results are the opposite, the telescopic motorcycle is larger than the multi-link at all of these three levels random road. Furthermore, according to the difference values, the gap of both standard deviation and mean values between telescopic and multi-link motorcycles is too small to have any influence on the ride quality, especially the largest value is still less than 0.2 mm.

After the speed increases to 30 m/s, comparing with the result in Table 5.4, the values of standard deviations and mean are also increased. Similar with the previous results, the standard deviation of frame height for the telescopic motorcycle is also smaller than the multi-link, while the mean values are still the opposite. The difference value in Table 5.5 demonstrates that with the increasing speed, the gap of both standard deviation and mean values between telescopic and multi-link motorcycles is still small.

Statistics	Random road	Telescopic	Multi-link	Difference value
Standard deviation (mm)	Level 3	7.7839	7.8011	0.0172
	Level 4	15.1384	15.1862	0.0478
Mean value (mm)	Level 3	460.1319	459.9675	0.1644
	Level 4	461.8210	461.6727	0.1483

Table 5.5: The standard deviations and mean values of frame height for both telescopic and multi-link front suspension motorcycles in response to the level 3, 4 and 5 random road with the speed of 30 m/s.

According to these results, through using standard deviations and mean values, it can be concluded that the frame height change of random road simulation for both telescopic and multi-link front suspension motorcycles are almost the same. For more intuitive analysis, the difference values between these two kinds of motorcycles need to be plotted. Through the observation and analysis of the frame height change results in the previous chapter, the difference value that produced by level 3 random road simulation with the speed of 30 m/s is the most obvious one, which means this result can be used to plot the difference value graph.

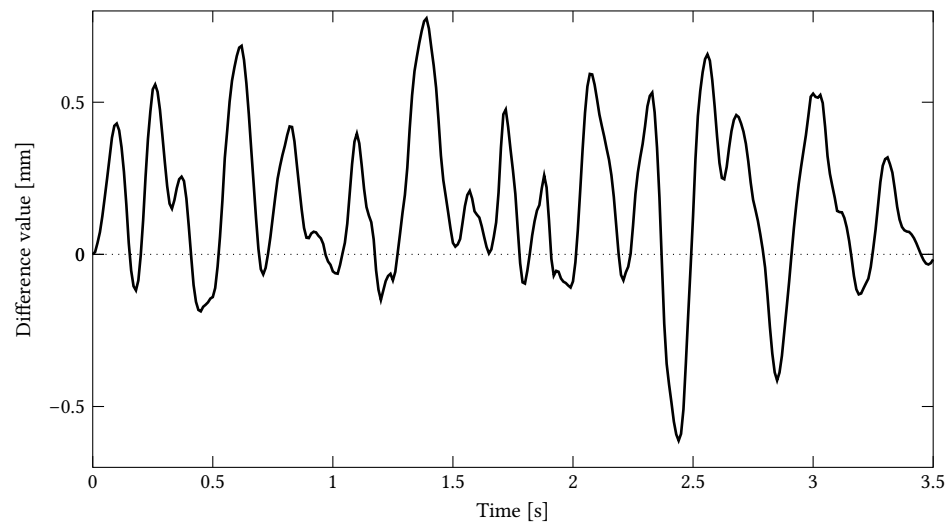


Figure 5.13: The difference values of frame height change between telescopic and multi-link front suspension motorcycles in response to the time running on the level 3 random road with the speed of 30 m/s.

As can be seen from Figure 5.13, the maximum value in the graph is still less than 0.8 mm, which once again suggests that there is almost no difference between these two frame height change results. It should be mentioned that each difference value in the figure is equal to the frame height value of telescopic motorcycle minus the corresponding value of the multi-link. According to the level 3 random road condition in Figure 4.27, it can be found that during peaks and valleys area of the road, the difference value of frame height change between these two kinds of motorcycles is relatively larger. Also, positive and negative parts of the figure demonstrate that in most of the run time, the frame height of multi-link motorcycle is less than the telescopic in a very small range.



### Pitch angle analysis

As mentioned in Chapter 3, too large or drastic changes of the pitch angle value may cause the riders to be uncomfortable. Therefore, both mean value and standard deviation of the pitch angle should be as small as possible. First of all, with the speed of 10 m/s, the mean value and standard deviation of pitch angle for both telescopic and multi-link front suspension motorcycles in response to the level 3, 4 and 5 random road can be seen from Table 5.6.

Statistics	Random road	Telescopic	Multi-link	Difference value
Standard deviation [rad]	Level 3	0.0024	0.0025	0.0001
	Level 4	0.0048	0.0049	0.0001
	Level 5	0.0094	0.0096	0.0002
Mean value [rad]	Level 3	$1.9807 \times 10^{-4}$	$1.0407 \times 10^{-4}$	$9.4000 \times 10^{-5}$
	Level 4	$9.3572 \times 10^{-5}$	$1.6996 \times 10^{-5}$	$7.6576 \times 10^{-5}$
	Level 5	$4.3359 \times 10^{-4}$	$3.7983 \times 10^{-4}$	$5.3760 \times 10^{-5}$

Table 5.6: The standard deviations and mean values of pitch angle for both telescopic and multi-link front suspension motorcycles in response to the level 3, 4 and 5 random road with the speed of 10 m/s.

As can be seen from Table 5.6, similar to the results of frame height in the previous section, the standard deviation of frame height for the multi-link motorcycle is larger than the telescopic at all of these three levels of random road. Meanwhile, the mean values of multi-link motorcycle is smaller than the telescopic. According to the results of each random road level in Chapter 4, the difference between these two pitch angle curves is too small to be identified from the graph. This is also reflected in the results from the table above, which shows the difference values of both standard deviation and mean value are very small. Therefore, the overall level and change range for multi-link suspension motorcycle pitch angle are similar to the telescopic.

Table 5.7 below shows mean values and standard deviation of pitch angle for both telescopic and multi-link front suspension motorcycles in response to the level 3 and 4 random road with the speed of 30 m/s. The size comparison of these two statistical values between telescopic and multi-link motorcycles is the same as 10 m/s results. In this form, although difference values are larger than the values in Table 5.6, they are still a very small order of magnitude, which is hard to be perceived by riders.

Statistics	Random road	Telescopic	Multi-link	Difference value
Standard deviation [rad]	Level 3	0.0026	0.0029	0.0003
	Level 4	0.0055	0.0060	0.0005
Mean value [rad]	Level 3	$7.8605 \times 10^{-5}$	$-5.3740 \times 10^{-6}$	$8.3979 \times 10^{-5}$
	Level 4	$3.3704 \times 10^{-4}$	$2.9377 \times 10^{-4}$	$4.3270 \times 10^{-5}$

Table 5.7: The standard deviations and mean values of pitch angle for both telescopic and multi-link front suspension motorcycles in response to the level 3, 4 and 5 random road with the speed of 30 m/s.

It should be mentioned that the positive value of pitch angle means angular displacement in a ‘nose down’ direction. Therefore, in Table 5.7, there is a negative value, which states this angle displacement leads to a ‘nose up’ movement. After observing the results of line graph and analyzing the data in above two tables, the results of level 4 random road with the speed of 30 m/s are selected for plotting the difference value graph.

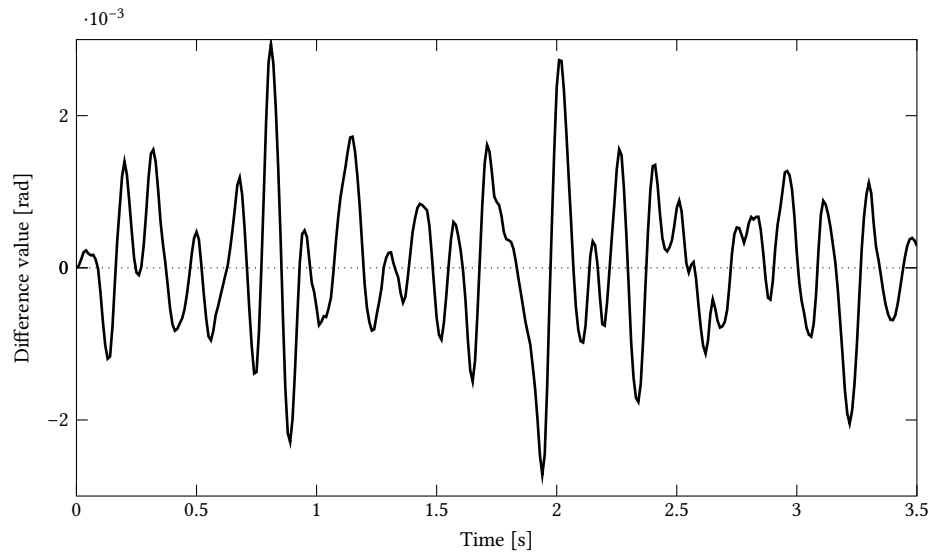


Figure 5.14: The difference values of pitch angle change between telescopic and multi-link front suspension motorcycles in response to the time running on the level 4 random road with the speed of 30 m/s.

In Figure 5.14, the maximum angle in the graph is less than 0.003 rad, which is so small that it cannot be perceived by riders. The large difference values are mainly concentrated in the peaks and valleys area. According to the curves shape in both positive and negative parts in Figure 5.14, it can be concluded that the performance of pitch angle for both telescopic and multi-link front suspension motorcycles are very similar. Differences exist only in a small range, which can almost be ignored.

### Suspension Travel Analysis

As mentioned before, the suspension travel result has a crucial role to play for the performance assessment of front suspension system. According to the description of the most basic in-plane mode in Chapter 3, there is a close relationship between the frame height change, suspension travel distance, and tire compression. Usually, an efficient suspension system means that it is capable to absorb more vibrations that are produced by the road irregularities. Therefore, a larger standard deviation of the suspension travel distance is generally better. Table 5.8 and Table 5.9 give the information of standard deviations and mean values of suspension travel distance for both telescopic and multi-link front suspension motorcycles in response to the level 3, 4 and 5 random road with the speed of 10 m/s and 30 m/s respectively.

Statistics	Random road	Telescopic	Multi-link	Difference value
Standard deviation [mm]	Level 3	0.8301	0.7953	0.0348
	Level 4	1.6969	1.6254	0.0715
	Level 5	3.3362	3.1705	0.1657
Mean value [mm]	Level 3	-0.0219	0.2085	0.2304
	Level 4	-0.0447	0.2009	0.2456
	Level 5	-0.0817	0.2015	0.2832

Table 5.8: The standard deviations and mean values of suspension travel for both telescopic and multi-link front suspension motorcycles in response to the level 3, 4 and 5 random road with the speed of 10 m/s.

As can be seen from Table 5.8, with the speed of 10 m/s, the standard deviation of suspension travel distance for the telescopic suspension motorcycle is larger than the multi-link at all three levels of random road. For the mean values, the negative result of the telescopic suspension motorcycle explains that the average value is in compression, while the positive result of the multi-link motorcycle illustrates that the average value is in rebound. This result means that the compression of the telescopic front suspension is greater than the amount of elongation, and the multi-link is the opposite. This distinction may be caused by the different mounting position of the front suspension. However, it is difficult to judge which performance is better according to these results, because the difference values compared with the available sliding distance of the suspension are too small to be identified. On the other hand, it also suggests that with the speed of 10 m/s, the performance of both telescopic and multi-link front suspensions is almost identical.

Statistics	Random road	Telescopic	Multi-link	Difference value
Standard deviation [mm]	Level 3	2.4267	2.2998	0.1269
	Level 4	5.0509	4.7443	0.3066
Mean value [mm]	Level 3	-0.0158	0.2141	0.2299
	Level 4	-0.0653	0.2053	0.2706

Table 5.9: The standard deviations and mean values of suspension travel for both telescopic and multi-link front suspension motorcycles in response to the level 3, 4 and 5 random road with the speed of 30 m/s.

Table 5.9 shows standard deviations and mean values of suspension travel for both telescopic and multi-link front suspension motorcycles in response to the level 3 and 4 random road with a speed of 30 m/s. On the whole, comparing with the results in Table 5.8, except for the increase of both standard deviation and mean value, the relationship between the size of data corresponding to each random road level is exactly the same as that of 10 m/s results. Furthermore, the small difference value once again shows that the performance of the telescopic and multi-link front suspension motorcycles is almost identical.

Figure 5.15 below shows the difference values of suspension travel distance between telescopic and multi-link front suspension motorcycles in response to the time running on the level 4 random road with the speed of 30 m/s.

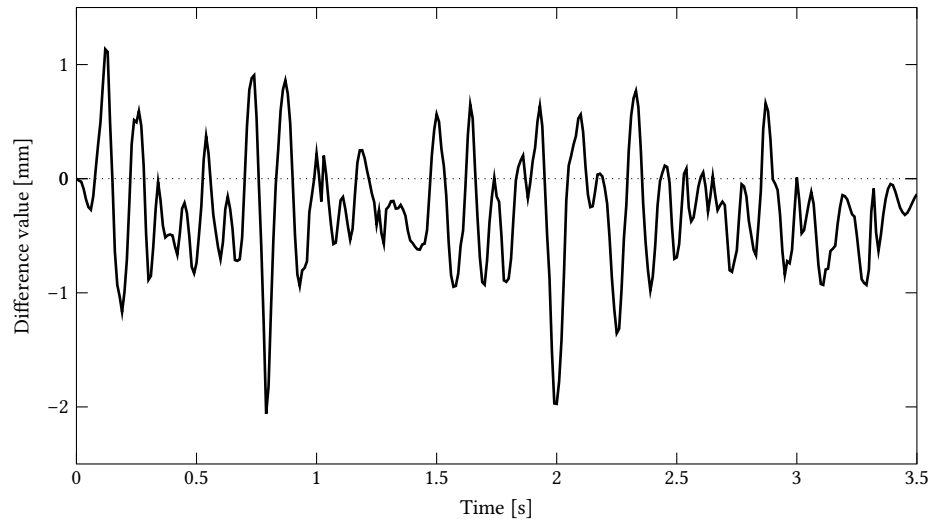


Figure 5.15: The difference values of suspension travel distance between telescopic and multi-link front suspension motorcycles in response to the time running on the level 4 random road with the speed of 30 m/s.

As mentioned before, each difference value is equal to the suspension travel distance value of the telescopic suspension motorcycle minus the corresponding value of the multi-link. As can be seen from Figure 5.15, most of curves in the graph are in the negative area, which means the suspension travel distance of the multi-link suspension motorcycle is bigger than the telescopic in most of the run time. Meanwhile, Figure 5.15 shows that the range of difference is from 0 mm to 2.5 mm. Furthermore, it also states the multi-link suspension absorbs more vibrations than the telescopic does.

More pavement bumps absorbed by the suspension means that the pressure on the tire is supposed to be reduced accordingly, which also means the tire compression should be less. This is a favorable result, as less variation in tire compression should equate to less likelihood of loss of tire grip. In order to verify this result, the graph of tire compression needs to be plotted and the result of the level 4 random road with a speed of 30 m/s is still chosen as the object of analysis. According to Hooke's law, the tire compression can be found from the equation between vertical contact force and tire stiffness. Figure 5.16 below shows the front tire compression of both telescopic and multi-link front suspension motorcycles in response to the level 4 random road with the speed of 30 m/s.

As can be seen from Figure 5.16, the two lines are staggered together. It is difficult to compare the size of the two sets of data and the obvious difference can only be found in the peak and valley regions. Therefore, the difference value graph needs to be plotted and used for analysis. Figure 5.17 shows the difference values of tire compression between telescopic and multi-link front suspension motorcycles in response to the time running on the level 4 random road with the speed of 30 m/s.

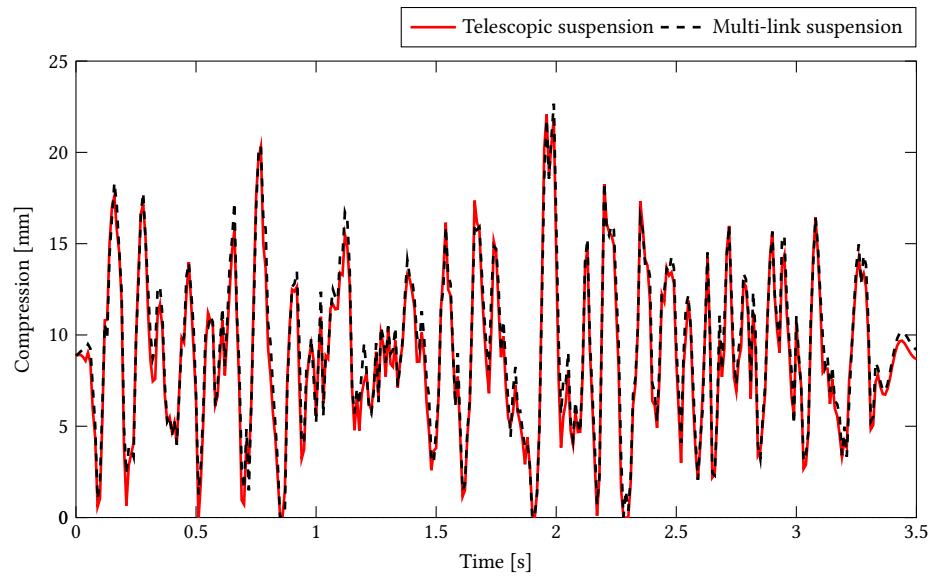


Figure 5.16: The front tire compression of both telescopic and multi-link front suspension motorcycles in response to the level 4 random road with the speed of 30 m/s

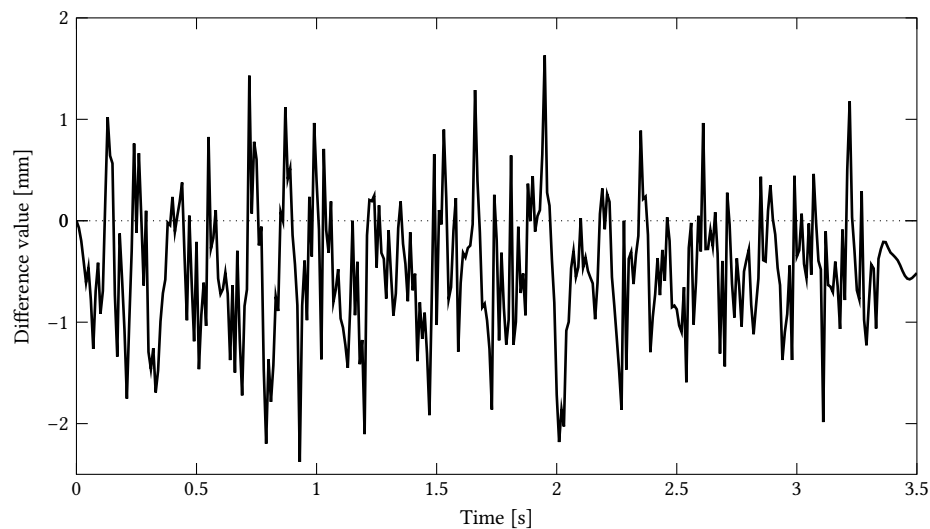


Figure 5.17: The difference values of tire compression between telescopic and multi-link front suspension motorcycles in response to the time running on the level 4 random road with the speed of 30 m/s.

In Figure 5.17, most of the result values are negative, which means the tire compression of the multi-link front suspension motorcycle is larger than the telescopic. This result is different from the prediction based on the suspension travel results. Moreover, the mean value of tire compression for the multi-link motorcycle is 9.2959 mm, which is 0.4709 mm larger than the telescopic. According to the description of motorcycles' specifications, this different result may be caused by the distinct weight and mass distribution between

telescopic and multi-link motorcycles. To verify this assumption, the state for the two types of motorcycles on a flat road needs to be separately analyzed.

First of all, with a speed of 30 m/s, the vertical contact force of the front tire for the telescopic suspension motorcycle is 1148.16 N, which also means the tire compression should be 8.8320 mm. For the multi-link motorcycle, the vertical force is 1211.52 N and the tire compression is 9.3194 mm; that is 0.4874 mm larger than the telescopic. Comparing with the results of the random road simulation, it can be confirmed that larger tire compression of the multi-link motorcycle is mainly due to its heavier weight, which also results in the larger vertical contact force on the front tire. Even though the amount of suspension travel distance of the multi-link motorcycle is greater than the telescopic, it still cannot completely offset the tire deformation caused by its heavier weight.

Overall, according to the results of frame height, pitch angle, and suspension travel, it can be concluded that the performance of the random road simulation for the telescopic and multi-link front suspension motorcycles are almost the same. Although different weights can cause distinct tire deformation, on the whole, the similar frame height and pitch angle still suggest that the ride quality of telescopic and multi-link motorcycles are almost identical.

## Chapter 6

# Conclusions, Recommendations, and Contributions

### 6.1 Conclusions

This thesis describes a novel multi-link motorcycle front suspension concept and explores its dynamic behaviour to determine its potential performance improvement over a conventional telescopic fork suspension. The expectation was that the separation of steering and suspension kinematics combined with the four locating arms can offer the multi-link front suspension with a number of advantages over the telescopic fork in both out-of-plane and in-plane simulations. According to the analysis, some of the results reach the expectation.

Based on the results of the out-of-plane simulation, during the unforced straight running, the multi-link front suspension motorcycle mainly experiences an unstable capsize mode in the low speed range from 0 m/s to around 10 m/s. In the same speed range, the telescopic suspension motorcycle mainly experiences an unstable weave mode. According to the description of the three out-of-plane modes, the capsize mode is deeply influenced by rider action on the handlebar, which means this mode should be shifted from the unstable zone to the stable zone by the rider, where the weave mode is relatively more difficult to control. The characteristics of these two modes suggest that the multi-link suspension motorcycle may be easier to control than the telescopic at low speed range. However, it is still hard to determine which type of front suspension performs better, because the simulation results also indicate that the unstable weave mode of telescopic suspension motorcycle reaches a stable condition at a lower speed than the unstable capsize mode of the multi-link suspension motorcycle. In the medium to high speed range, the performance of telescopic and multi-link front suspension motorcycles is almost the same. After that, based on the results of the forced straight running simulations with a speed of 20 m/s and the analysis of the eigenvalues at multiple velocities, it can be found that in the low to medium speed range (0–20 m/s), the wobble mode is more likely to be

excited for the multi-link suspension motorcycle, and for the telescopic suspension motorcycle, the weave mode is more active. Based on the concept of the three basic modes, usually, for the wobble mode, adding a steering damper can increase the damping effect on the front assembly and, consequently, the stability of the motorcycle[1]. Compared with the wobble mode, it is more difficult to find a method to adjust the weave mode, which also means that the telescopic suspension motorcycle may be slightly harder to stabilize than the multi-link suspension during straight running. For the multi-link front suspension motorcycle, the wobble mode may be mainly caused by the effect of the added mass of the locating arms. Therefore, the question of how the weave and wobble modes might change with the lightweight locating arms is worth exploring.

The analysis of the in-plane simulation results is directly related to the front suspension properties. In the results of the braking simulation, the smaller pitch angle, larger caster angle and larger trail suggest that the multi-link front suspension performs better than the telescopic, especially during an emergency stop. In the plank road and random road simulations, due to the very small difference values, the results of frame height, pitch angle and suspension travel distance predict that the performance of both telescopic and multi-link front suspension motorcycles is almost the same.

Overall, it can be concluded that in the straight running, the multi-link front suspension motorcycle may be easier to stabilize than the telescopic, especially in the low to medium speed range. At high speed, there is no difference between the performance. The better performance of the multi-link front suspension motorcycle in braking meets the design expectations. Finally, the different road conditions do not make any visible difference in the ride performance.

## 6.2 Recommendations

Numerous uncertainties still exist and are avenues for future study.

- The performance of steady turning motion for both telescopic and multi-link front suspension motorcycles may need to be evaluated and compared by appropriate simulation. The turning motion of a motorcycle is more complicated than an automobile, because the motorcycle needs a larger roll angle to pass through a corner. Especially, the torque required on the handlebar for these two types of front suspension during the steady turning motion with different speeds is worthwhile to analyze.
- The performance of the brakes during steady turning for both telescopic and multi-link front suspension motorcycles may need to be evaluated and compared by appropriate simulation. In this thesis, the multi-link front suspension motorcycle has been shown to have better braking performance during straight running. Therefore, it is worthwhile to explore whether it also has better braking performance during steady turning.
- According to the analysis of out-of-plane simulation results, the steering damper is considered to help



maintain the stability of multi-link front suspension motorcycles during straight running. Therefore, the performance of rectilinear motion for both telescopic and multi-link front suspension motorcycles that are equipped with the same steering damper may need to be evaluated and compared by appropriate simulation.

- In order to suit lots of different purposes, there is a variety of models of motorcycle available, such as the cruiser, sport bike, tourer, and so on. Different purposes also means different requirements of the front assembly properties. As mentioned in this thesis, the change of position of the four locating arms adjust the geometry of the steering axis and may influence the weave and wobble modes of a multi-link suspension motorcycle in the low speed range. Therefore, it is valuable to simulate and analyze the effects of different locating arm positions, and weights, on the performance of a multi-link front suspension motorcycle.
- After simulating and analyzing the performance of all possible situations for the multi-link front suspension motorcycle, the prototype motorcycle needs to be made and used to verify the simulation results. Most importantly, the experimental results in reality can better prove whether the new design can enter the market.

In summary, this thesis has presented a novel multi-link motorcycle front suspension concept and explored its dynamic behaviour by modeling and simulating a series of experiments. For the results, a complete set of analysis and comparison processes has been conducted. The novel front suspension has been proposed and, to some extent, can increase the stability during the rectilinear motion of motorcycle. In braking, the motorcycle that is equipped with the novel multi-link front suspension should show a significant improvement in stability. However, there are several issues that remain and further investigation is needed before the recommendation can be made to implement this design.

### 6.3 Contributions

In this thesis, there are three main contributions as follows.

- A model of a novel multi-link front suspension system has been developed. The suspension mechanism described in this thesis is, to the best of the author's knowledge, novel and unused, and presents a number of design advantages. The novel multi-link motorcycle front suspension, to some extent, makes up for the shortcomings of the conventional telescopic front fork, and especially in braking, the performance has potential to be greatly improved. It also means that the telescopic fork could be replaced by the multi-link front suspension in the future.
- An appropriate method of performance assessment for both telescopic and multi-link front suspension motorcycles has been developed in this thesis. Figure 6.1 gives the information about the performance

assessment method for both telescopic and multi-link suspension motorcycles. There are two components of this method, namely out-of-plane and in-plane simulation. The out-of-plane simulation is mainly used to compare the two motorcycles' performance of stability and handling during rectilinear motion. The in-plane simulation is mainly used to compare the performance of the two motorcycles in braking and riding under different road conditions. The out-of-plane simulation is more focused on the whole motorcycle's riding performance. For the in-plane simulation, its results are directly related to the performance of the suspension system. Combining the results and analysis of these two components, the performance assessment of motorcycle can be obtained reasonably and reliably.

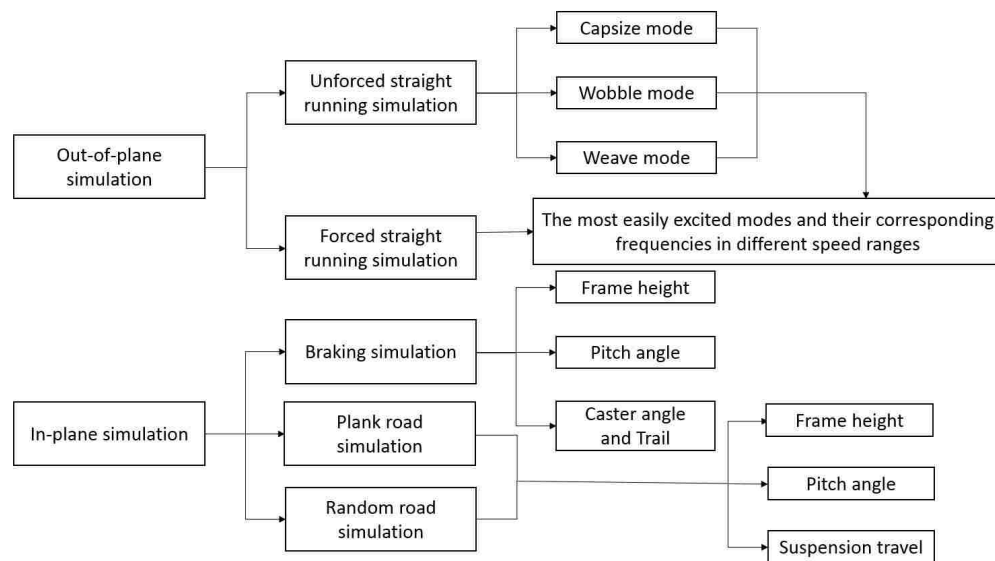


Figure 6.1: The processes of performance assessment method for both telescopic and multi-link front suspension motorcycles

- An appropriate method of comparison between telescopic and multi-link front suspension motorcycles has been developed in this thesis. Figure 6.2 shows the comparison method between the telescopic and multi-link suspension motorcycles. In the figure, the letter C means comparison and the arrow that marks the letter C points to the object being compared. Two-way arrows mean that two objects need to be compared with each other. As can be seen from Figure 6.2, after confirming that the linear result of unforced straight running simulation for telescopic motorcycle is similar to the theoretical result, there are two ways to simultaneously verify the rationality of linear and non-linear models for both telescopic and multi-link motorcycles. After that, the reliable non-linear models can be used for in-plane simulations. As mentioned before, in this thesis, linear simulation is mainly handled by the EoM software and the MotionView<sup>®</sup> software deals with non-linear simulation, because the motorcycle model with the non-linear tire model can not be used for linear simulations in the MotionView<sup>®</sup>

software. Therefore, the processes of comparison method are completed by the cooperation between these two softwares. It also means that this method can be used for similar comparative studies.

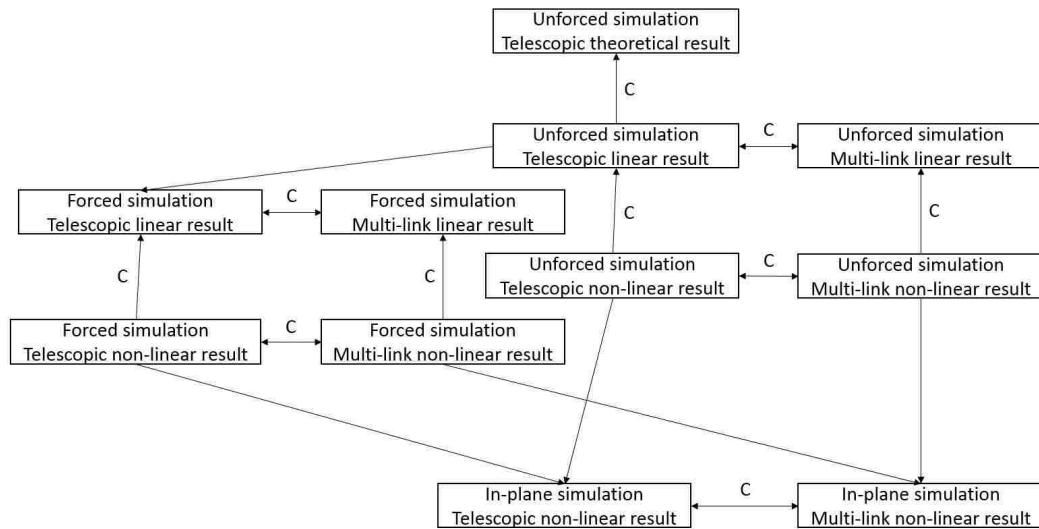


Figure 6.2: The processes of comparison method between telescopic and multi-link front suspension motorcycles

# References

- [1] V. Cossalter, *Motorcycle dynamics*, Lexington, KY: Lulu, 2010. Print.
- [2] R.S. Sharp, S. Evangelou, and D.J.N. Limebeer, “Advances in the modelling of motorcycle dynamics,” *Multibody Systems Dynamics* **12** (2004), pp. 251–283.
- [3] B.P. Minaker, B. Durfy, “A Multibody Dynamic Analysis of a Motorcycle with a Multilink Front Suspension,” *Proceeding of Bicycle and Motorcycle Dynamics, Milwaukee, Wisconsin, USA*, 2016.
- [4] A. Sharp, *Bicycles and Tricycles: An Elementary Treatise on Their Design and Construction* White Plains, NY: Longman, 1896. (Reprinted as: *Bicycles and Tricycles: A Classic Treatise on Their Design and Construction* Mineola, NY: Dover, 1977)
- [5] D.V. Herlihy, *Bicycle: The History*, New Haven, CT: Yale Univ.Press, 2004.
- [6] M. Hamer, “Brimstone and bicycles,” *New Scientist*, issue 2428, pp. 48-49, Jan. 2005.
- [7] D.J.N. Limebeer, R.S. Sharp, “Bicycles, motorcycles, and models,” *IEEE control systems*, **26.5** (2006): 34-61.
- [8] “Smithsonian National Museum”[Online]. Available: <http://www.newsdesk.si.edu/>
- [9] N. Clayton, *Early Bicycles*, Princes Risborough, Bucks, UK: Shire Publications, 1986.
- [10] “The Online Bicycle Museum”[Online]. Available: <http://www.oldbike.eu/>
- [11] “UDC Penny Farthings”[Online]. Available: <https://www.udcpennyfarthing.com/>
- [12] F.J. Berto, *The Dancing Chain: History and Development of the Derailleur Bicycle*, San Francisco, CA: Van der Plas Publications, 2005.
- [13] W.J.M. Rankine, “On the dynamical principles of the motion of velocipedes,” *The Engineer*, pp. 2, 79, 129, 153, 175, 1869/1870.
- [14] F.J.W. Whipple, “The stability of the motion of a bicycle,” *Q. J. Pure Appl. Math.*, vol. 30, pp. 312-348, 1899.
- [15] H. Goldstein, *Classical Mechanics*, 2nd ed. Reading, MA: Addison-Wesley, 1980.
- [16] M.F. Carvalho, “Theorie du mouvement du monocycle, part 2: Theorie de la bicyclette,” *J. LfiEcole Polytechnique*, vol. 6, pp. 1-118, 1901.

- [17] F. Klein, A. Sommerfeld, *Über die Theorie des Kreisels*, Teubner, Leipzig, 1910, Chap. IX, Sec. 8, "Stabilität des Fahrrads," Leipzig, Germany: B.G. Teubner, pp. 863-884.
- [18] D.E.H. Jones, "The stability of the bicycle," *Phys. Today*, vol. 23, no. 4, pp. 34-40, 1970.
- [19] R.D. Roland, "Computer simulation of bicycle dynamics," in *Proc. ASME Symp. Mechanics Sport*, 1973, pp. 35-83.
- [20] J.I. Neimark, N.A. Fufaev, "Dynamics of nonholonomic systems," (Amer. Math. Soc. Translations Math. Monographs, vol. 33), 1972.
- [21] R.S. Hand, "Comparisons and stability analysis of linearized equations of motion for a basic bicycle model," M.Sc. Thesis, Cornell Univ., 1988.
- [22] A.L. Schwab, J.P. Meijaard, and J.M. Papadopoulos, "Benchmark results on the linearized equations of motion of an uncontrolled bicycle," in *Proc. 2nd Asian Conf. Multibody Dynamics*, Aug. 2004, pp. 1-9.
- [23] K.J. Astrom, R.E. Klein, and A. Lennartsson, "Bicycle dynamics and control," *IEEE Control Syst. Mag.*, vol. 25, no. 4, pp. 26-47, 2005.
- [24] G.M. Kanai, "Motorcycle front suspension systems: Traditional problems and alternative solutions," *Sheldon's EMU*, September 1996.
- [25] "The Smithsonian Museum"[Online]. Available: <https://www.si.edu/>
- [26] "The American Society of Mechanical Engineers"[Online]. Available: <https://www.asme.org/>
- [27] "The Hemmings"[Online]. Available: <https://www.hemmings.com/>
- [28] "The Contramanillar"[Online]. Available: <http://www.contramanillar.com/>
- [29] D.J.N. Limebeer, R.S. Sharp, and S. Evangelou, "Motorcycle steering oscillations due to road profiling," *J. Appl. Mech.*, vol. 69, no. 6, pp. 724-739, 2002.
- [30] R.S. Sharp, "The stability and control of motorcycles," *J. Mech. Eng. Sci.*, vol. 13, no. 5, pp. 316-329, 1971.
- [31] P.T.J. Spierings, "The effects of lateral front fork flexibility on the vibrational modes of straight-running single-track vehicles," *Vehicle Syst. Dyn.*, vol. 10, no. 1, pp. 21-35, 1981.
- [32] R.S. Sharp, C.J. Alstead, "The influence of structural flexibilities on the straight running stability of motorcycles," *Vehicle Syst. Dyn.*, vol. 9, no. 6, pp. 327-357, 1980.
- [33] V. Cossalter, R. Lot, "A motorcycle multi-body model for real time simulations based on the natural coordinates approach," *Vehicle Syst. Dyn.*, vol. 37, no. 6, pp. 423-447, 2002.
- [34] "ISR Brakes-Sweden"[Online]. Available: <http://www.isrbrakes.se/>
- [35] "Speed Moto Blog"[Online]. Available: <https://speedmotoblog.wordpress.com/>
- [36] *Choppers Magazine*, Roth, Spring 1968, pp.57-63, Roth Productions, Los Angeles.

- [37] "BMW<sup>®</sup> Motorrad"[Online]. Available: <https://www.bmw-motorrad.com/>
- [38] "ZERO Engineering original Springer fork"[Online]. Available: <https://www.alibaba.com/>
- [39] T. Foale, *Motorcycle Chassis Design*, Osprey Publishing Ltd., pp. 91-93, 1984.
- [40] "2005 BMW<sup>®</sup> K1200S Specifications," *Sport Rider*. Accessed June 26, 2017.  
<http://www.sportrider.com/2005-bmw-k1200s-specifications>.
- [41] "Inter Cars"[Online]. Available: <http://intercars.grupasiedlce.pl/>
- [42] "Sport Rider"[Online]. Available: <http://www.sportrider.com/>
- [43] B. Mavrouidakis, P. Eberhard, "Analysis of alternative front suspension systems for motorcycles," *Vehicle Systems Dynamics* 44, Supp. (2006), pp. 679-689.
- [44] *EU Patent No. 07122393.7*
- [45] *US Patent No. 6,349,784*
- [46] *US Patent No. 8,851,221*
- [47] "Altair", *Multibody Simulation, Kinematics and Dynamics*, Altair MotionSolve. N.p., n.d. 2017.
- [48] D. Ardiri, A. Cammarata, and R. Sinatra, "Simulation of roller test bench for fatigue validation of a scooter frame," *Italy: Piaggio Brand Unit Vehicle Mechanical System & CAE*, 2014.
- [49] N. Riservata, 7299/LT, *Two wheel vehicles-Roller bench fatigue test*.
- [50] B. Lindsay, 'BMW springs ahead.', *Chilton's Automotive Industries*, June 1993, pp. 71-2.
- [51] V. Cossalter, R. Lot, and F. Maggio, "The Modal Analysis of a Motorcycle in Straight Running and on a Curv", *Meccanica* 39 (2004) pp. 1-16.
- [52] V. Cossalter, et al., "Frequency-domain method for evaluating the ride comfort of a motorcycle," *Vehicle System Dynamics* 44.4 (2006): 339-355.
- [53] ISO 2631, 2003, *Evaluation of Human Exposure to Wholebody Vibration*.
- [54] ISO 5349, 2001, *Guidelines for the Measurement and Assessment of Human Exposure to Hand Transmitted Vibration*.
- [55] Z. Zhang, et al., "Road roughness evaluation using in-pavement strain sensors" *Smart Materials and Structures* 24.11 (2015): 115029.
- [56] "Motorcycle MD"[Online]. Available: <http://motorcyclemd.com/>
- [57] H. Pacejka, *Tire and vehicle dynamics*. Elsevier, 2005.
- [58] S. Evangelou, *Control and stability analysis of two-wheeled road vehicles*. Diss. University of London, 2004.

- [59] H. Baruh, *Analytical dynamics*. Boston: WCB/McGraw-Hill, 1999.
- [60] "RecurDyn"[Online]. Available: <http://www.functionbay.co.kr/>
- [61] G.R. Watts, "Traffic-induced ground-borne vibrations in dwellings," *TRRL RESEARCH REPORT 102* (1987).
- [62] J. Lundstrm, "Road roughness estimation using available vehicle sensors," (2009).
- [63] C.J. Dodds, J.D. Robson, "The description of road surface roughness," *Journal of sound and vibration* **31.2** (1973): 175-183.
- [64] M. Agostinacchio, D. Ciampa, and S. Olita, "The vibrations induced by surface irregularities in road pavements-a MATLAB<sup>®</sup> approach," *European Transport Research Review* **6.3** (2014): 267-275.

# Appendix A

## A.1 MATLAB<sup>®</sup> Codes of Random Road

```

function z=road(varargin)
% class is an integer from 3 - 9, where class=3 is an A-B road (smooth), class=9 is G-H
% road (rough)
if (nargin==1)
    class=varargin{1};
else
    class=3;
end

if (class<3)
    class=3;
end

if (class>9)
    class=9;
end

global h;
global x;
global v;
v=5; % forward speed [m/s], assume constant;
L=100; % max wavelength [m], also equals road length
B=v/512; % sampling distance, capture at 512 Hz
deltan=1/L % frequency interval
N=L/B % number of samples
x=0:B:L; % road coordinate
n=(deltan:deltan:N*deltan); % frequency span
n(1) % max spatial frequency
n(N)

phi=rand(1,N)*2*pi; % random phase lag for each frequency
a=sqrt(deltan)*(2^class)*1e-3*(0.1./n); % amplitude of each frequency, based on psd
content

```



```
a(1)
a(N)

h=zeros(size(x)); % road vertical

for i=1:length(n) % sum for each frequency included
    h=h+a(i)*cos(2*pi*n(i)*x+phi(i));
end

figure(1)
plot(x,h);
xlabel('Road Vertical Location [m]');
ylabel('Location [m]');

% compute the psd of the random road
% should be a straight line in log space, down to wl_min
% looks ok
sf=1/B; % sampling frequency
N=length(x); % number of samples
xdft=fft(h); % fast Fourier transform
xdft=xdft(1:N/2+1); % take only half results (symmetric)
psdx=(1/(sf*N))*abs(xdft).^2; % compute power
psdx(2:end-1)=2*psdx(2:end-1); % other half
freq=0:sf/N:sf/2; % compute frequencies
wl=1./freq; % compute wavelengths
figure(2) %semilogx(wl,10*log10(psd))
loglog(freq,psdx)
xlabel('Freq [cycles/m]') %ylabel('Power/Frequency [dB m/cycle]')
```

## A.2 MATLAB<sup>®</sup> Codes of Power Spectral Density

```
load tireforce.dat
fs=100
T=1/fs
time=tireforce(:,1)
chassis=tireforce(:,2)
plot(time, chassis)
title('time history response');
xlabel('Time (s)');
ylabel('force')
nfft=501
X=fft(chassis)
p2=abs(X/nfft)
p1=p2(1:nfft/2+1)
p1(2:end-1)=2*p1(2:end-1)
f=(0:nfft/2)*fs/nfft;
figure
semilogx(f, p1)
title('frequency history response');
xlabel('frequency(Hz)');
ylabel('power')
X=X(1:nfft/2+1)
psd=(1/(fs*nfft))*abs(X).^2
psd(2:end-1)=2*psd(2:end-1)
freq=0:fs/nfft:fs/2
figure
loglog(freq, psd)
title('Power spectral density');
xlabel('frequency(Hz)');
ylabel('power/frequency (dB/Hz)')
q=trapz(freq, psd)
hold on
```

# Appendix B

## B.1 Eigenvalues, Natural Frequency, Damping Ratio of Telescopic Front Suspension at 5 m/s

Table B.1: Eigenvalues of telescopic front suspension at 5 m/s

No.	Real [rad/s]	Imaginary [rad/s]	Real [Hz]	Imaginary [Hz]
1	$-2.1264 \times 10^3$	$0.0000 \times 10^0$	$-3.3843 \times 10^2$	$0.0000 \times 10^0$
2	$-1.7005 \times 10^3$	$0.0000 \times 10^0$	$-2.7065 \times 10^2$	$0.0000 \times 10^0$
3	$-1.4164 \times 10^2$	$0.0000 \times 10^0$	$-2.2543 \times 10^1$	$0.0000 \times 10^0$
4	$-1.0031 \times 10^2$	$0.0000 \times 10^0$	$-1.5964 \times 10^1$	$0.0000 \times 10^0$
5	$-2.6393 \times 10^1$	$4.5394 \times 10^1$	$-4.2005 \times 10^0$	$7.2247 \times 10^0$
6	$-2.6393 \times 10^1$	$-4.5394 \times 10^1$	$-4.2005 \times 10^0$	$-7.2247 \times 10^0$
7	$-1.7060 \times 10^1$	$1.0498 \times 10^1$	$-2.7152 \times 10^0$	$1.6708 \times 10^0$
8	$-1.7060 \times 10^1$	$-1.0498 \times 10^1$	$-2.7152 \times 10^0$	$-1.6708 \times 10^0$
9	$-1.3702 \times 10^1$	$0.0000 \times 10^0$	$-2.1807 \times 10^0$	$0.0000 \times 10^0$
10	$-3.0628 \times 10^0$	$0.0000 \times 10^0$	$-4.8746 \times 10^{-1}$	$0.0000 \times 10^0$
11	$8.9535 \times 10^{-1}$	$2.6700 \times 10^0$	$1.4250 \times 10^{-1}$	$4.2495 \times 10^{-1}$
12	$8.9535 \times 10^{-1}$	$-2.6700 \times 10^0$	$1.4250 \times 10^{-1}$	$-4.2495 \times 10^{-1}$
13	$4.1457 \times 10^{-13}$	$2.9667 \times 10^{-6}$	$6.5982 \times 10^{-14}$	$4.7216 \times 10^{-7}$
14	$4.1457 \times 10^{-13}$	$-2.9667 \times 10^{-6}$	$6.5982 \times 10^{-14}$	$-4.7216 \times 10^{-7}$
15	$5.5913 \times 10^{-13}$	$9.5291 \times 10^{-7}$	$8.8989 \times 10^{-14}$	$1.5166 \times 10^{-7}$
16	$5.5913 \times 10^{-13}$	$-9.5291 \times 10^{-7}$	$8.8989 \times 10^{-14}$	$-1.5166 \times 10^{-7}$
17	$-1.7429 \times 10^{-13}$	$0.0000 \times 10^0$	$-2.7739 \times 10^{-14}$	$0.0000 \times 10^0$
18	$4.4843 \times 10^{-13}$	$0.0000 \times 10^0$	$7.1370 \times 10^{-14}$	$0.0000 \times 10^0$

Note: oscillatory roots appear as complex conjugates.

Table B.2: Natural frequency, damping ratio at 5 m/s

No.	Frequency [Hz]	Damping Ratio	Time Constant [s]	Wavelength [s]
1	–	–	$4.7027 \times 10^{-4}$	–
2	–	–	$5.8805 \times 10^{-4}$	–
3	–	–	$7.0602 \times 10^{-3}$	–
4	–	–	$9.9694 \times 10^{-3}$	–
5	$8.3571 \times 10^0$	$5.0263 \times 10^{-1}$	$3.7889 \times 10^{-2}$	$1.3841 \times 10^{-1}$
6	$8.3571 \times 10^0$	$5.0263 \times 10^{-1}$	$3.7889 \times 10^{-2}$	$1.3841 \times 10^{-1}$
7	$3.1881 \times 10^0$	$8.5167 \times 10^{-1}$	$5.8616 \times 10^{-2}$	$5.9850 \times 10^{-1}$
8	$3.1881 \times 10^0$	$8.5167 \times 10^{-1}$	$5.8616 \times 10^{-2}$	$5.9850 \times 10^{-1}$
9	–	–	$7.2984 \times 10^{-2}$	–
10	–	–	$3.2650 \times 10^{-1}$	–
11	$4.4820 \times 10^{-1}$	$-3.1793 \times 10^{-1}$	$-1.1169 \times 10^0$	$2.3532 \times 10^0$
12	$4.4820 \times 10^{-1}$	$-3.1793 \times 10^{-1}$	$-1.1169 \times 10^0$	$2.3532 \times 10^0$
13	$4.7216 \times 10^{-7}$	$-1.3974 \times 10^{-7}$	$-2.4121 \times 10^{12}$	$2.1179 \times 10^6$
14	$4.7216 \times 10^{-7}$	$-1.3974 \times 10^{-7}$	$-2.4121 \times 10^{12}$	$2.1179 \times 10^6$
15	$1.5166 \times 10^{-7}$	$-5.8677 \times 10^{-7}$	$-1.7885 \times 10^{12}$	$6.5937 \times 10^6$
16	$1.5166 \times 10^{-7}$	$-5.8677 \times 10^{-7}$	$-1.7885 \times 10^{12}$	$6.5937 \times 10^6$
17	–	–	$5.7375 \times 10^{12}$	–
18	–	–	$-2.2300 \times 10^{12}$	–

Notes: a) oscillatory roots are listed twice, b) negative time constants denote unstable roots.

## B.2 Eigenvalues, Natural Frequency, Damping Ratio of Telescopic Front Suspension at 10 m/s

Table B.3: Eigenvalues of telescopic front suspension at 10 m/s

No.	Real [rad/s]	Imaginary [rad/s]	Real [Hz]	Imaginary [Hz]
1	$-1.0645 \times 10^3$	$0.0000 \times 10^0$	$-1.6942 \times 10^2$	$0.0000 \times 10^0$
2	$-8.5027 \times 10^2$	$0.0000 \times 10^0$	$-1.3532 \times 10^2$	$0.0000 \times 10^0$
3	$-2.6611 \times 10^1$	$6.8495 \times 10^1$	$-4.2353 \times 10^0$	$1.0901 \times 10^1$
4	$-2.6611 \times 10^1$	$-6.8495 \times 10^1$	$-4.2353 \times 10^0$	$-1.0901 \times 10^1$
5	$-4.9324 \times 10^1$	$0.0000 \times 10^0$	$-7.8502 \times 10^0$	$0.0000 \times 10^0$
6	$-3.6115 \times 10^1$	$1.4097 \times 10^1$	$-5.7479 \times 10^0$	$2.2436 \times 10^0$
7	$-3.6115 \times 10^1$	$-1.4097 \times 10^1$	$-5.7479 \times 10^0$	$-2.2436 \times 10^0$
8	$-1.6848 \times 10^1$	$1.0332 \times 10^1$	$-2.6814 \times 10^0$	$1.6444 \times 10^0$
9	$-1.6848 \times 10^1$	$-1.0332 \times 10^1$	$-2.6814 \times 10^0$	$-1.6444 \times 10^0$
10	$-3.4178 \times 10^0$	$6.7701 \times 10^0$	$-5.4397 \times 10^{-1}$	$1.0775 \times 10^0$
11	$-3.4178 \times 10^0$	$-6.7701 \times 10^0$	$-5.4397 \times 10^{-1}$	$-1.0775 \times 10^0$
12	$-6.9978 \times 10^{-2}$	$0.0000 \times 10^0$	$-1.1137 \times 10^{-2}$	$0.0000 \times 10^0$
13	$4.4715 \times 10^{-11}$	$3.5855 \times 10^{-6}$	$7.1167 \times 10^{-12}$	$5.7065 \times 10^{-7}$
14	$4.4715 \times 10^{-11}$	$-3.5855 \times 10^{-6}$	$7.1167 \times 10^{-12}$	$-5.7065 \times 10^{-7}$
15	$1.8037 \times 10^{-11}$	$1.8582 \times 10^{-6}$	$2.8707 \times 10^{-12}$	$2.9574 \times 10^{-7}$
16	$1.8037 \times 10^{-11}$	$-1.8582 \times 10^{-6}$	$2.8707 \times 10^{-12}$	$-2.9574 \times 10^{-7}$
17	$-4.8401 \times 10^{-13}$	$0.0000 \times 10^0$	$-7.7033 \times 10^{-14}$	$0.0000 \times 10^0$
18	$-5.0923 \times 10^{-14}$	$0.0000 \times 10^0$	$-8.1046 \times 10^{-15}$	$0.0000 \times 10^0$

Note: oscillatory roots appear as complex conjugates.

Table B.4: Natural frequency, damping ratio at 10 m/s

No.	Frequency [Hz]	Damping Ratio	Time Constant [s]	Wavelength [s]
1	–	–	$9.3944 \times 10^{-4}$	–
2	–	–	$1.1761 \times 10^{-3}$	–
3	$1.1695 \times 10^1$	$3.6214 \times 10^{-1}$	$3.7579 \times 10^{-2}$	$9.1732 \times 10^{-2}$
4	$1.1695 \times 10^1$	$3.6214 \times 10^{-1}$	$3.7579 \times 10^{-2}$	$9.1732 \times 10^{-2}$
5	–	–	$2.0274 \times 10^{-2}$	–
6	$6.1702 \times 10^0$	$9.3155 \times 10^{-1}$	$2.7689 \times 10^{-2}$	$4.4571 \times 10^{-1}$
7	$6.1702 \times 10^0$	$9.3155 \times 10^{-1}$	$2.7689 \times 10^{-2}$	$4.4571 \times 10^{-1}$
8	$3.1455 \times 10^0$	$8.5246 \times 10^{-1}$	$5.9355 \times 10^{-2}$	$6.0812 \times 10^{-1}$
9	$3.1455 \times 10^0$	$8.5246 \times 10^{-1}$	$5.9355 \times 10^{-2}$	$6.0812 \times 10^{-1}$
10	$1.2070 \times 10^0$	$4.5067 \times 10^{-1}$	$2.9258 \times 10^{-1}$	$9.2808 \times 10^{-1}$
11	$1.2070 \times 10^0$	$4.5067 \times 10^{-1}$	$2.9258 \times 10^{-1}$	$9.2808 \times 10^{-1}$
12	–	–	$1.4290 \times 10^1$	–
13	$5.7065 \times 10^{-7}$	$-1.2471 \times 10^{-5}$	$-2.2364 \times 10^{10}$	$1.7524 \times 10^6$
14	$5.7065 \times 10^{-7}$	$-1.2471 \times 10^{-5}$	$-2.2364 \times 10^{10}$	$1.7524 \times 10^6$
15	$2.9574 \times 10^{-7}$	$-9.7070 \times 10^{-6}$	$-5.5441 \times 10^{10}$	$3.3814 \times 10^6$
16	$2.9574 \times 10^{-7}$	$-9.7070 \times 10^{-6}$	$-5.5441 \times 10^{10}$	$3.3814 \times 10^6$
17	–	–	$2.0661 \times 10^{12}$	–
18	–	–	$1.9638 \times 10^{13}$	–

Notes: a) oscillatory roots are listed twice, b) negative time constants denote unstable roots.

### B.3 Eigenvalues, Natural Frequency, Damping Ratio of Telescopic Front Suspension at 40 m/s

Table B.5: Eigenvalues of telescopic front suspension at 40 m/s

No.	Real [rad/s]	Imaginary [rad/s]	Real [Hz]	Imaginary [Hz]
1	$-2.6686 \times 10^2$	$0.0000 \times 10^0$	$-4.2472 \times 10^1$	$0.0000 \times 10^0$
2	$-2.1256 \times 10^2$	$0.0000 \times 10^0$	$-3.3830 \times 10^1$	$0.0000 \times 10^0$
3	$-2.7355 \times 10^1$	$1.4294 \times 10^2$	$-4.3537 \times 10^0$	$2.2750 \times 10^1$
4	$-2.7355 \times 10^1$	$-1.4294 \times 10^2$	$-4.3537 \times 10^0$	$-2.2750 \times 10^1$
5	$-8.2448 \times 10^{-1}$	$4.1763 \times 10^1$	$-1.3122 \times 10^{-1}$	$6.6468 \times 10^0$
6	$-8.2448 \times 10^{-1}$	$-4.1763 \times 10^1$	$-1.3122 \times 10^{-1}$	$-6.6468 \times 10^0$
7	$-2.9153 \times 10^0$	$2.1610 \times 10^1$	$-4.6399 \times 10^{-1}$	$3.4393 \times 10^0$
8	$-2.9153 \times 10^0$	$-2.1610 \times 10^1$	$-4.6399 \times 10^{-1}$	$-3.4393 \times 10^0$
9	$-1.6679 \times 10^1$	$1.0235 \times 10^1$	$-2.6546 \times 10^0$	$1.6290 \times 10^0$
10	$-1.6679 \times 10^1$	$-1.0235 \times 10^1$	$-2.6546 \times 10^0$	$-1.6290 \times 10^0$
11	$-2.4688 \times 10^1$	$0.0000 \times 10^0$	$-3.9293 \times 10^0$	$0.0000 \times 10^0$
12	$5.3022 \times 10^{-2}$	$0.0000 \times 10^0$	$8.4387 \times 10^{-3}$	$0.0000 \times 10^0$
13	$-7.2048 \times 10^{-10}$	$7.9853 \times 10^{-6}$	$-1.1467 \times 10^{-10}$	$1.2709 \times 10^{-6}$
14	$-7.2048 \times 10^{-10}$	$-7.9853 \times 10^{-6}$	$-1.1467 \times 10^{-10}$	$-1.2709 \times 10^{-6}$
15	$-1.6863 \times 10^{-13}$	$2.9408 \times 10^{-6}$	$-2.6839 \times 10^{-14}$	$4.6804 \times 10^{-7}$
16	$-1.6863 \times 10^{-13}$	$-2.9408 \times 10^{-6}$	$-2.6839 \times 10^{-14}$	$-4.6804 \times 10^{-7}$
17	$2.5974 \times 10^{-14}$	$0.0000 \times 10^0$	$4.1339 \times 10^{-15}$	$0.0000 \times 10^0$
18	$-1.0270 \times 10^{-12}$	$0.0000 \times 10^0$	$-1.6345 \times 10^{-13}$	$0.0000 \times 10^0$

Note: oscillatory roots appear as complex conjugates.

Table B.6: Natural frequency, damping ratio at 40 m/s

No.	Frequency [Hz]	Damping Ratio	Time Constant [s]	Wavelength [s]
1	–	–	$3.7473 \times 10^{-3}$	–
2	–	–	$4.7045 \times 10^{-3}$	–
3	$2.3163 \times 10^1$	$1.8796 \times 10^{-1}$	$3.6556 \times 10^{-2}$	$4.3956 \times 10^{-2}$
4	$2.3163 \times 10^1$	$1.8796 \times 10^{-1}$	$3.6556 \times 10^{-2}$	$4.3956 \times 10^{-2}$
5	$6.6481 \times 10^0$	$1.9738 \times 10^{-2}$	$1.2129 \times 10^0$	$1.5045 \times 10^{-1}$
6	$6.6481 \times 10^0$	$1.9738 \times 10^{-2}$	$1.2129 \times 10^0$	$1.5045 \times 10^{-1}$
7	$3.4705 \times 10^0$	$1.3370 \times 10^{-1}$	$3.4302 \times 10^{-1}$	$2.9075 \times 10^{-1}$
8	$3.4705 \times 10^0$	$1.3370 \times 10^{-1}$	$3.4302 \times 10^{-1}$	$2.9075 \times 10^{-1}$
9	$3.1145 \times 10^0$	$8.5231 \times 10^{-1}$	$5.9955 \times 10^{-2}$	$6.1386 \times 10^{-1}$
10	$3.1145 \times 10^0$	$8.5231 \times 10^{-1}$	$5.9955 \times 10^{-2}$	$6.1386 \times 10^{-1}$
11	–	–	$4.0505 \times 10^{-2}$	–
12	–	–	$-1.8860 \times 10^1$	–
13	$1.2709 \times 10^{-6}$	$9.0226 \times 10^{-5}$	$1.3880 \times 10^9$	$7.8685 \times 10^5$
14	$1.2709 \times 10^{-6}$	$9.0226 \times 10^{-5}$	$1.3880 \times 10^9$	$7.8685 \times 10^5$
15	$4.6804 \times 10^{-7}$	$5.7343 \times 10^{-8}$	$5.9301 \times 10^{12}$	$2.1366 \times 10^6$
16	$4.6804 \times 10^{-7}$	$5.7343 \times 10^{-8}$	$5.9301 \times 10^{12}$	$2.1366 \times 10^6$
17	–	–	$-3.8500 \times 10^{13}$	–
18	–	–	$9.7373 \times 10^{11}$	–

Notes: a) oscillatory roots are listed twice, b) negative time constants denote unstable roots.

## B.4 Eigenvalues, Natural Frequency, Damping Ratio of Multi-link Front Suspension at 5 m/s

Table B.7: Eigenvalues of Multi-link front suspension at 5 m/s

No.	Real [rad/s]	Imaginary [rad/s]	Real [Hz]	Imaginary [Hz]
1	$-2.0466 \times 10^3$	$0.0000 \times 10^0$	$-3.2572 \times 10^2$	$0.0000 \times 10^0$
2	$-1.7036 \times 10^3$	$0.0000 \times 10^0$	$-2.7114 \times 10^2$	$0.0000 \times 10^0$
3	$-1.2027 \times 10^2$	$0.0000 \times 10^0$	$-1.9142 \times 10^1$	$0.0000 \times 10^0$
4	$-9.9683 \times 10^1$	$0.0000 \times 10^0$	$-1.5865 \times 10^1$	$0.0000 \times 10^0$
5	$-2.7897 \times 10^1$	$4.5584 \times 10^1$	$-4.4400 \times 10^0$	$7.2549 \times 10^0$
6	$-2.7897 \times 10^1$	$-4.5584 \times 10^1$	$-4.4400 \times 10^0$	$-7.2549 \times 10^0$
7	$-1.5483 \times 10^1$	$1.2143 \times 10^1$	$-2.4642 \times 10^0$	$1.9326 \times 10^0$
8	$-1.5483 \times 10^1$	$-1.2143 \times 10^1$	$-2.4642 \times 10^0$	$-1.9326 \times 10^0$
9	$-6.8231 \times 10^0$	$1.0699 \times 10^1$	$-1.0859 \times 10^0$	$1.7028 \times 10^0$
10	$-6.8231 \times 10^0$	$-1.0699 \times 10^1$	$-1.0859 \times 10^0$	$-1.7028 \times 10^0$
11	$2.6677 \times 10^0$	$0.0000 \times 10^0$	$4.2458 \times 10^{-1}$	$0.0000 \times 10^0$
12	$-3.5727 \times 10^0$	$0.0000 \times 10^0$	$-5.6862 \times 10^{-1}$	$0.0000 \times 10^0$
13	$-1.5574 \times 10^{-7}$	$0.0000 \times 10^0$	$-2.4787 \times 10^{-8}$	$0.0000 \times 10^0$
14	$4.9254 \times 10^{-7}$	$0.0000 \times 10^0$	$7.8389 \times 10^{-8}$	$0.0000 \times 10^0$
15	$1.5574 \times 10^{-7}$	$0.0000 \times 10^0$	$2.4787 \times 10^{-8}$	$0.0000 \times 10^0$
16	$-4.9254 \times 10^{-7}$	$0.0000 \times 10^0$	$-7.8390 \times 10^{-8}$	$0.0000 \times 10^0$
17	$-1.1471 \times 10^{-12}$	$0.0000 \times 10^0$	$-1.8257 \times 10^{-13}$	$0.0000 \times 10^0$
18	$3.2590 \times 10^{-14}$	$0.0000 \times 10^0$	$5.1868 \times 10^{-15}$	$0.0000 \times 10^0$

Note: oscillatory roots appear as complex conjugates.

Table B.8: Natural frequency, damping ratio at 5 m/s

No.	Frequency [Hz]	Damping Ratio	Time Constant [s]	Wavelength [s]
1	–	–	$4.8862 \times 10^{-4}$	–
2	–	–	$5.8698 \times 10^{-4}$	–
3	–	–	$8.3145 \times 10^{-3}$	–
4	–	–	$1.0032 \times 10^{-2}$	–
5	$8.5057 \times 10^0$	$5.2200 \times 10^{-1}$	$3.5846 \times 10^{-2}$	$1.3784 \times 10^{-1}$
6	$8.5057 \times 10^0$	$5.2200 \times 10^{-1}$	$3.5846 \times 10^{-2}$	$1.3784 \times 10^{-1}$
7	$3.1317 \times 10^0$	$7.8686 \times 10^{-1}$	$6.4587 \times 10^{-2}$	$5.1743 \times 10^{-1}$
8	$3.1317 \times 10^0$	$7.8686 \times 10^{-1}$	$6.4587 \times 10^{-2}$	$5.1743 \times 10^{-1}$
9	$2.0196 \times 10^0$	$5.3770 \times 10^{-1}$	$1.4656 \times 10^{-1}$	$5.8727 \times 10^{-1}$
10	$2.0196 \times 10^0$	$5.3770 \times 10^{-1}$	$1.4656 \times 10^{-1}$	$5.8727 \times 10^{-1}$
11	–	–	$-3.7486 \times 10^{-1}$	–
12	–	–	$2.7990 \times 10^{-1}$	–
13	–	–	$6.4208 \times 10^6$	–
14	–	–	$-2.0303 \times 10^6$	–
15	–	–	$-6.4208 \times 10^6$	–
16	–	–	$2.0303 \times 10^6$	–
17	–	–	$8.7175 \times 10^{11}$	–
18	–	–	$-3.0684 \times 10^{13}$	–

Notes: a) oscillatory roots are listed twice, b) negative time constants denote unstable roots.

## B.5 Eigenvalues, Natural Frequency, Damping Ratio of Multi-link Front Suspension at 10 m/s

Table B.9: Eigenvalues of Multi-link front suspension at 10 m/s

No.	Real [rad/s]	Imaginary [rad/s]	Real [Hz]	Imaginary [Hz]
1	$-1.0236 \times 10^3$	$0.0000 \times 10^0$	$-1.6291 \times 10^2$	$0.0000 \times 10^0$
2	$-8.5189 \times 10^2$	$0.0000 \times 10^0$	$-1.3558 \times 10^2$	$0.0000 \times 10^0$
3	$-2.8007 \times 10^1$	$6.9275 \times 10^1$	$-4.4574 \times 10^0$	$1.1025 \times 10^1$
4	$-2.8007 \times 10^1$	$-6.9275 \times 10^1$	$-4.4574 \times 10^0$	$-1.1025 \times 10^1$
5	$-4.7166 \times 10^1$	$0.0000 \times 10^0$	$-7.5067 \times 10^0$	$0.0000 \times 10^0$
6	$-2.3855 \times 10^1$	$1.2977 \times 10^1$	$-3.7967 \times 10^0$	$2.0654 \times 10^0$
7	$-2.3855 \times 10^1$	$-1.2977 \times 10^1$	$-3.7967 \times 10^0$	$-2.0654 \times 10^0$
8	$-1.5381 \times 10^1$	$1.1886 \times 10^1$	$-2.4479 \times 10^0$	$1.8918 \times 10^0$
9	$-1.5381 \times 10^1$	$-1.1886 \times 10^1$	$-2.4479 \times 10^0$	$-1.8918 \times 10^0$
10	$-1.4315 \times 10^1$	$0.0000 \times 10^0$	$-2.2783 \times 10^0$	$0.0000 \times 10^0$
11	$-9.1893 \times 10^0$	$0.0000 \times 10^0$	$-1.4625 \times 10^0$	$0.0000 \times 10^0$
12	$1.1280 \times 10^0$	$0.0000 \times 10^0$	$1.7953 \times 10^{-1}$	$0.0000 \times 10^0$
13	$-6.5869 \times 10^{-7}$	$0.0000 \times 10^0$	$-1.0483 \times 10^{-7}$	$0.0000 \times 10^0$
14	$-1.1905 \times 10^{-6}$	$0.0000 \times 10^0$	$-1.8948 \times 10^{-7}$	$0.0000 \times 10^0$
15	$6.5869 \times 10^{-7}$	$0.0000 \times 10^0$	$1.0483 \times 10^{-7}$	$0.0000 \times 10^0$
16	$1.1905 \times 10^{-6}$	$0.0000 \times 10^0$	$1.8948 \times 10^{-7}$	$0.0000 \times 10^0$
17	$-2.9884 \times 10^{-13}$	$0.0000 \times 10^0$	$-4.7562 \times 10^{-14}$	$0.0000 \times 10^0$
18	$1.6451 \times 10^{-14}$	$0.0000 \times 10^0$	$2.6182 \times 10^{-15}$	$0.0000 \times 10^0$

Note: oscillatory roots appear as complex conjugates.

Table B.10: Natural frequency, damping ratio at 10 m/s

No.	Frequency [Hz]	Damping Ratio	Time Constant [s]	Wavelength [s]
1	–	–	$9.7696 \times 10^{-4}$	–
2	–	–	$1.1739 \times 10^{-3}$	–
3	$1.1892 \times 10^1$	$3.7481 \times 10^{-1}$	$3.5705 \times 10^{-2}$	$9.0699 \times 10^{-2}$
4	$1.1892 \times 10^1$	$3.7481 \times 10^{-1}$	$3.5705 \times 10^{-2}$	$9.0699 \times 10^{-2}$
5	–	–	$2.1202 \times 10^{-2}$	–
6	$4.3222 \times 10^0$	$8.7843 \times 10^{-1}$	$4.1919 \times 10^{-2}$	$4.8416 \times 10^{-1}$
7	$4.3222 \times 10^0$	$8.7843 \times 10^{-1}$	$4.1919 \times 10^{-2}$	$4.8416 \times 10^{-1}$
8	$3.0937 \times 10^0$	$7.9125 \times 10^{-1}$	$6.5016 \times 10^{-2}$	$5.2860 \times 10^{-1}$
9	$3.0937 \times 10^0$	$7.9125 \times 10^{-1}$	$6.5016 \times 10^{-2}$	$5.2860 \times 10^{-1}$
10	–	–	$6.9855 \times 10^{-2}$	–
11	–	–	$1.0882 \times 10^{-1}$	–
12	–	–	$-8.8649 \times 10^{-1}$	–
13	–	–	$1.5182 \times 10^6$	–
14	–	–	$8.3997 \times 10^5$	–
15	–	–	$-1.5182 \times 10^6$	–
16	–	–	$-8.3997 \times 10^5$	–
17	–	–	$3.3463 \times 10^{12}$	–
18	–	–	$-6.0788 \times 10^{13}$	–

Notes: a) oscillatory roots are listed twice, b) negative time constants denote unstable roots.



## B.6 Eigenvalues, Natural Frequency, Damping Ratio of Multi-link Front Suspension at 40 m/s

Table B.11: Eigenvalues of Multi-link front suspension at 40 m/s

No.	Real [rad/s]	Imaginary [rad/s]	Real [Hz]	Imaginary [Hz]
1	$-2.5581 \times 10^2$	$0.0000 \times 10^0$	$-4.0713 \times 10^1$	$0.0000 \times 10^0$
2	$-2.1300 \times 10^2$	$0.0000 \times 10^0$	$-3.3900 \times 10^1$	$0.0000 \times 10^0$
3	$-2.8408 \times 10^1$	$1.4521 \times 10^2$	$-4.5212 \times 10^0$	$2.3111 \times 10^1$
4	$-2.8408 \times 10^1$	$-1.4521 \times 10^2$	$-4.5212 \times 10^0$	$-2.3111 \times 10^1$
5	$1.1464 \times 10^{-1}$	$4.0527 \times 10^1$	$1.8246 \times 10^{-2}$	$6.4500 \times 10^0$
6	$1.1464 \times 10^{-1}$	$-4.0527 \times 10^1$	$1.8246 \times 10^{-2}$	$-6.4500 \times 10^0$
7	$-2.6246 \times 10^0$	$2.0620 \times 10^1$	$-4.1772 \times 10^{-1}$	$3.2818 \times 10^0$
8	$-2.6246 \times 10^0$	$-2.0620 \times 10^1$	$-4.1772 \times 10^{-1}$	$-3.2818 \times 10^0$
9	$-2.4353 \times 10^1$	$0.0000 \times 10^0$	$-3.8758 \times 10^0$	$0.0000 \times 10^0$
10	$-1.5295 \times 10^1$	$1.1736 \times 10^1$	$-2.4344 \times 10^0$	$1.8678 \times 10^0$
11	$-1.5295 \times 10^1$	$-1.1736 \times 10^1$	$-2.4344 \times 10^0$	$-1.8678 \times 10^0$
12	$-1.2261 \times 10^{-10}$	$4.1418 \times 10^{-6}$	$-1.9514 \times 10^{-11}$	$6.5919 \times 10^{-7}$
13	$-1.2261 \times 10^{-10}$	$-4.1418 \times 10^{-6}$	$-1.9514 \times 10^{-11}$	$-6.5919 \times 10^{-7}$
14	$5.9301 \times 10^{-2}$	$0.0000 \times 10^0$	$9.4381 \times 10^{-3}$	$0.0000 \times 10^0$
15	$-1.9266 \times 10^{-6}$	$0.0000 \times 10^0$	$-3.0663 \times 10^{-7}$	$0.0000 \times 10^0$
16	$1.9266 \times 10^{-6}$	$0.0000 \times 10^0$	$3.0663 \times 10^{-7}$	$0.0000 \times 10^0$
17	$-2.3340 \times 10^{-12}$	$0.0000 \times 10^0$	$-3.7147 \times 10^{-13}$	$0.0000 \times 10^0$
18	$3.0372 \times 10^{-14}$	$0.0000 \times 10^0$	$4.8338 \times 10^{-15}$	$0.0000 \times 10^0$

Note: oscillatory roots appear as complex conjugates.

Table B.12: Natural frequency, damping ratio at 40 m/s

No.	Frequency [Hz]	Damping Ratio	Time Constant [s]	Wavelength [s]
1	–	–	$3.9092 \times 10^{-3}$	–
2	–	–	$4.6948 \times 10^{-3}$	–
3	$2.3549 \times 10^1$	$1.9199 \times 10^{-1}$	$3.5202 \times 10^{-2}$	$4.3269 \times 10^{-2}$
4	$2.3549 \times 10^1$	$1.9199 \times 10^{-1}$	$3.5202 \times 10^{-2}$	$4.3269 \times 10^{-2}$
5	$6.4500 \times 10^0$	$-2.8288 \times 10^{-3}$	$-8.7228 \times 10^0$	$1.5504 \times 10^{-1}$
6	$6.4500 \times 10^0$	$-2.8288 \times 10^{-3}$	$-8.7228 \times 10^0$	$1.5504 \times 10^{-1}$
7	$3.3083 \times 10^0$	$1.2626 \times 10^{-1}$	$3.8101 \times 10^{-1}$	$3.0471 \times 10^{-1}$
8	$3.3083 \times 10^0$	$1.2626 \times 10^{-1}$	$3.8101 \times 10^{-1}$	$3.0471 \times 10^{-1}$
9	–	–	$4.1063 \times 10^{-2}$	–
10	$3.0683 \times 10^0$	$7.9338 \times 10^{-1}$	$6.5379 \times 10^{-2}$	$5.3539 \times 10^{-1}$
11	$3.0683 \times 10^0$	$7.9338 \times 10^{-1}$	$6.5379 \times 10^{-2}$	$5.3539 \times 10^{-1}$
12	$6.5919 \times 10^{-7}$	$2.9604 \times 10^{-5}$	$8.1558 \times 10^9$	$1.5170 \times 10^6$
13	$6.5919 \times 10^{-7}$	$2.9604 \times 10^{-5}$	$8.1558 \times 10^9$	$1.5170 \times 10^6$
14	–	–	$-1.6863 \times 10^1$	–
15	–	–	$5.1904 \times 10^5$	–
16	–	–	$-5.1904 \times 10^5$	–
17	–	–	$4.2845 \times 10^{11}$	–
18	–	–	$-3.2925 \times 10^{13}$	–

Notes: a) oscillatory roots are listed twice, b) negative time constants denote unstable roots.

# Appendix C

## C.1 Braking Simulation Results with 100 Nm Braking Torque

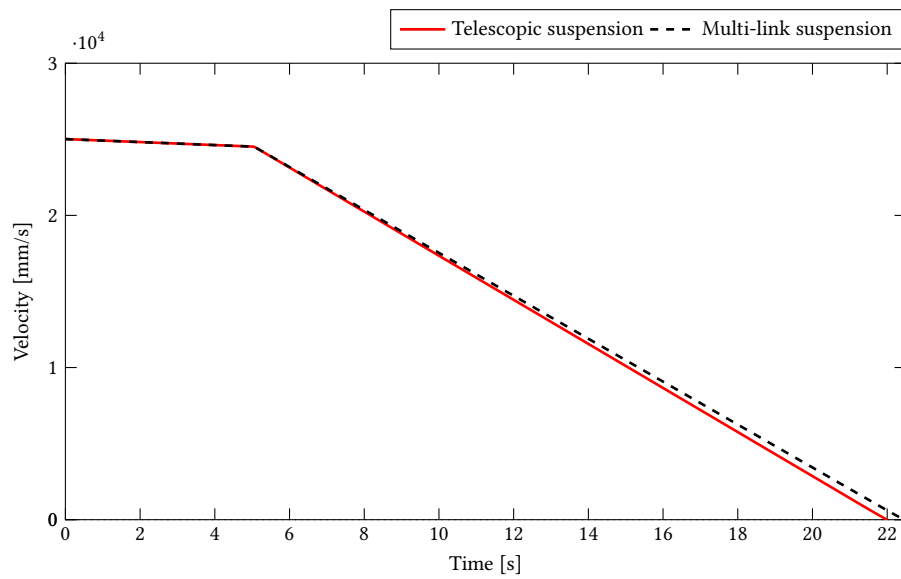


Figure C.1: Forward velocity of both telescopic and multi-link front suspension motorcycles as functions of time, in response to the 100 Nm braking torque, starting from 5 s

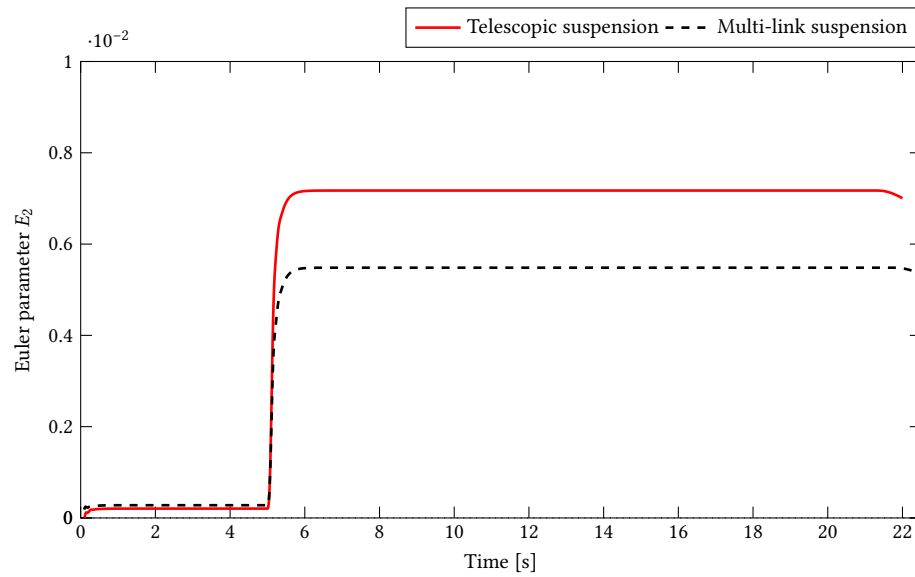


Figure C.2: Euler parameter  $E_2$  of both telescopic and multi-link front suspension motorcycles as functions of time, in response to the 100 Nm braking torque, starting from 5 s

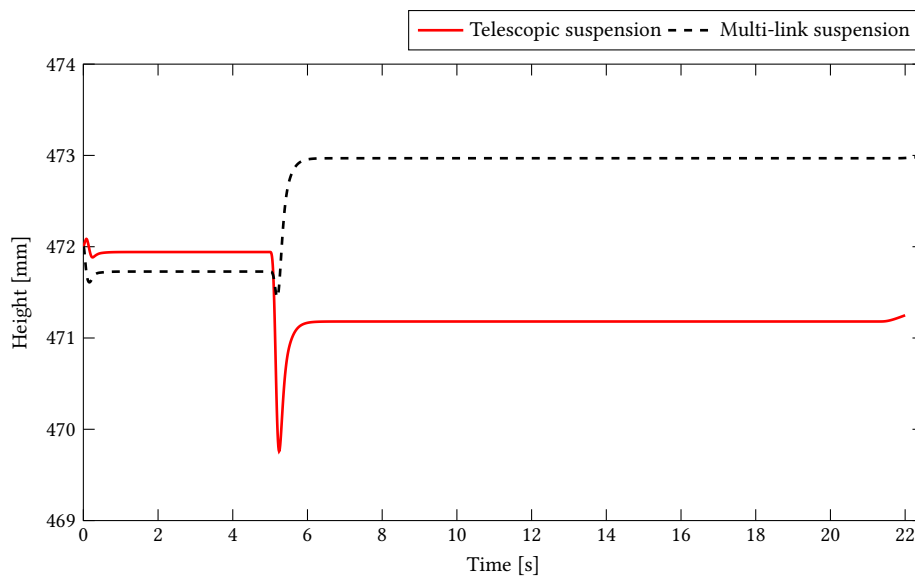


Figure C.3: The height change of both telescopic and multi-link front suspension motorcycles as functions of time, in response to the 100 Nm braking torque, starting from 5 s

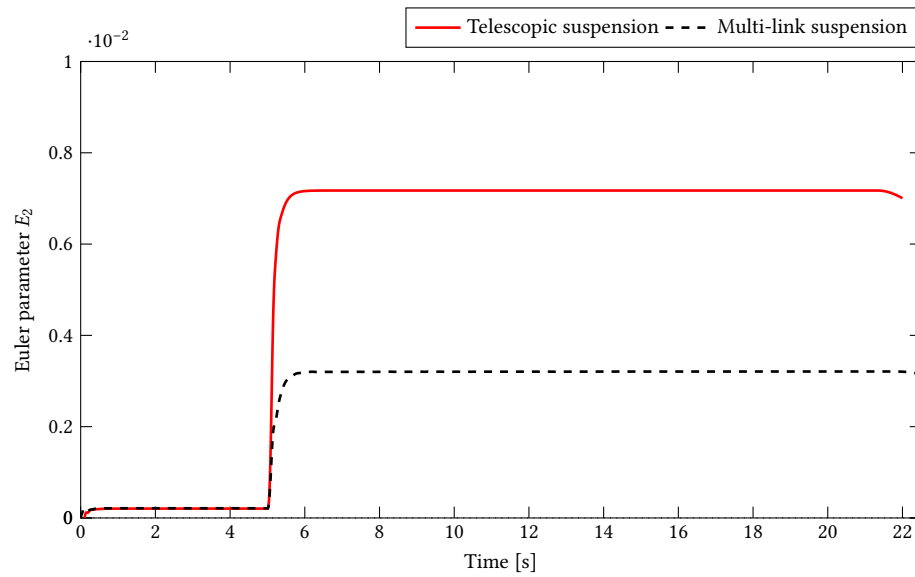


Figure C.4: The Euler parameter  $E_2$  change of steering axis for both telescopic and multi-link front suspension motorcycles as a function of time under 100 Nm braking torque starting from 5 s.

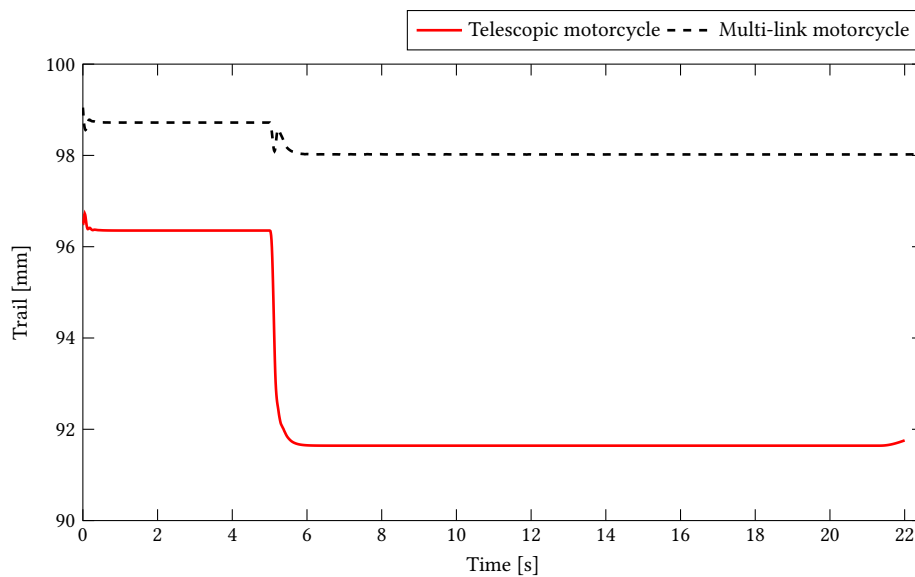


Figure C.5: The trail change of steering axis for both telescopic and multi-link front suspension motorcycles as a function of time, in response to the 100 Nm braking torque, starting from 5 s

## C.2 Braking Simulation Results with 800 Nm Braking Torque

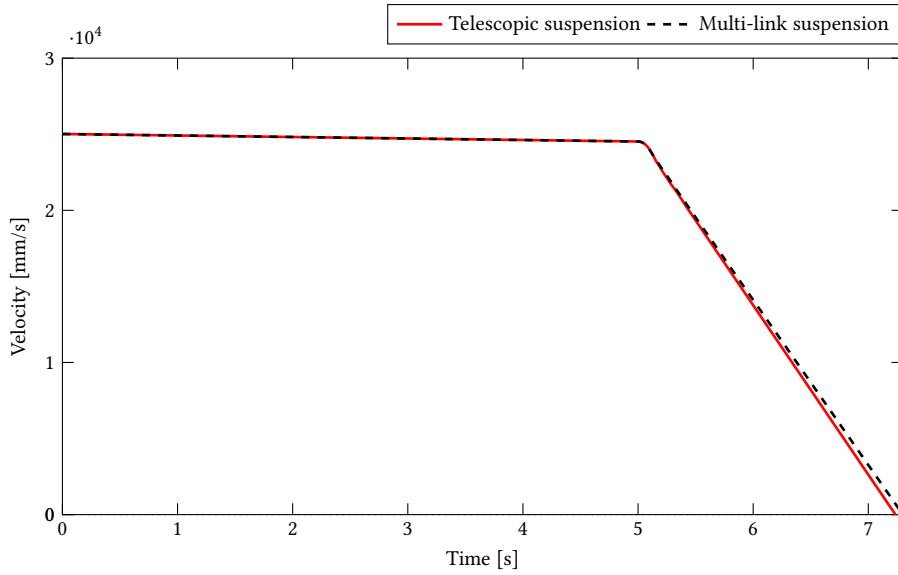


Figure C.6: Forward velocity of both telescopic and multi-link front suspension motorcycles as functions of time, in response to the 800 Nm braking torque, starting from 5 s

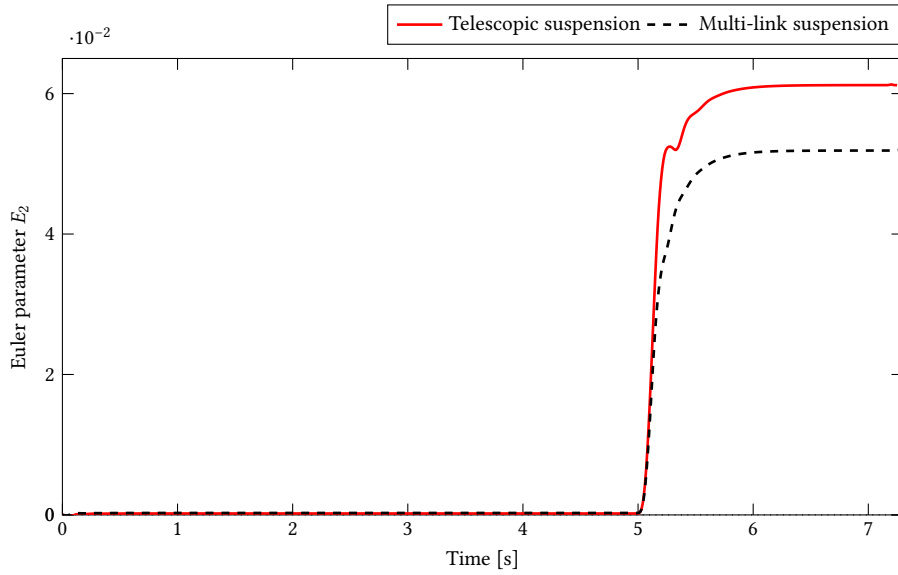


Figure C.7: Euler parameter  $E_2$  of both telescopic and multi-link front suspension motorcycles as functions of time, in response to the 800 Nm braking torque, starting from 5 s

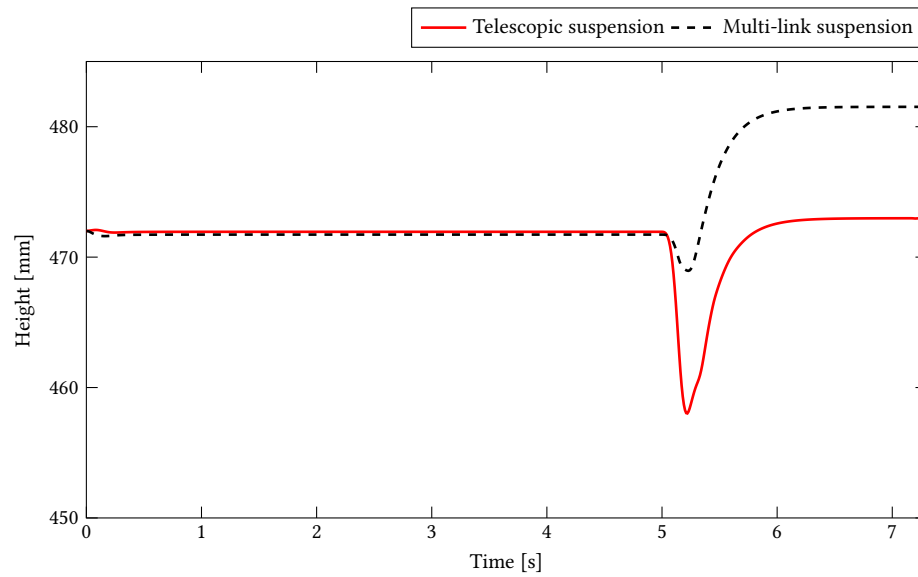


Figure C.8: The height change of both telescopic and multi-link front suspension motorcycles as functions of time, in response to the 800 Nm braking torque, starting from 5 s

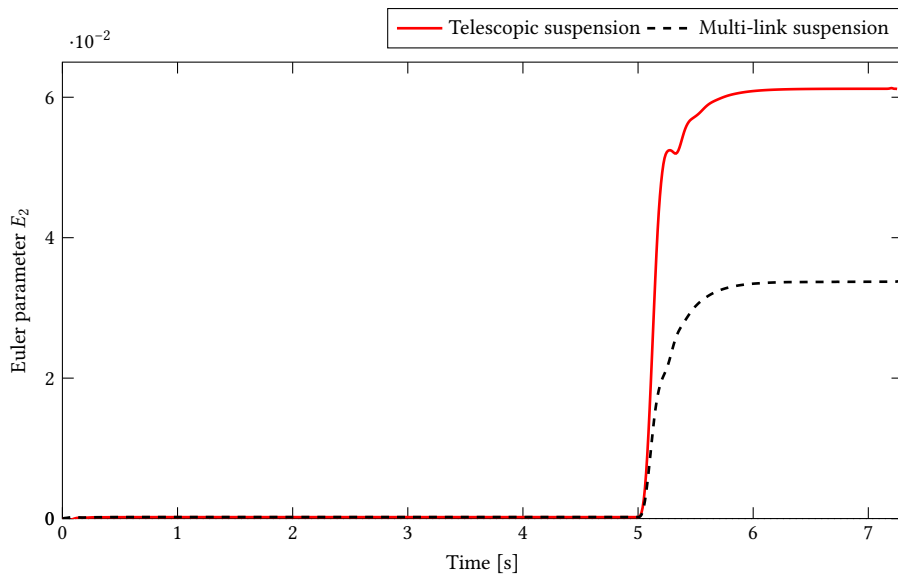


Figure C.9: The Euler parameter  $E_2$  change of steering axis for both telescopic and multi-link front suspension motorcycles as a function of time under 800 Nm braking torque starting from 5 s.

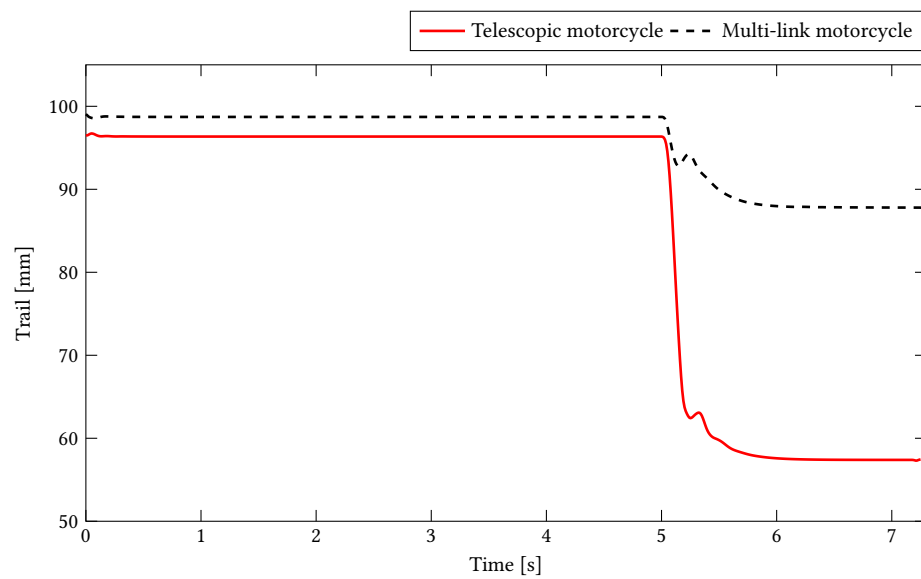


Figure C.10: The trail change of steering axis for both telescopic and multi-link front suspension motorcycles as a function of time, in response to the 800 Nm braking torque, starting from 5 s

## Vita Auctoris

Changdong Liu was born in Urumqi, Xinjiang, China in 1990, but grew up in Beijing, China. He graduated from the Affiliated High School of Beijing Institute of Petroleum in 2008. He then attended the Beijing Institute Of Graphic Communication, where he earned a Bachelor's Degree of Mechanical Engineering and Automatization in 2013. He obtained his Master of Engineering degree at the University of Windsor in 2016 and since that time, he worked under Dr. Minaker. He is presently a candidate for the Master of Applied Science in Mechanical Engineering degree at University of Windsor, and is scheduled to graduate in November, 2017.